NORTH ATLANTIC TREATY ORGANIZATION

SCIENCE AND TECHNOLOGY ORGANIZATION

AC/323(AVT-365)TP/1037

www.sto.nato.int

STO EDUCATIONAL NOTES **EN-AVT-365**

Rotorcraft Flight Simulation Model Fidelity Improvement and Assessment

(Amélioration et évaluation de la fidélité des modèles de simulation du vol à voilure tournante)

Educational Notes for the AVT-365 Lecture Series.

Published October 2021

Distribution and Availability on Back Cover

NORTH ATLANTIC TREATY ORGANIZATION

SCIENCE AND TECHNOLOGY ORGANIZATION

AC/323(AVT-365)TP/1037

www.sto.nato.int

STO EDUCATIONAL NOTES **EN-AVT-365**

Rotorcraft Flight Simulation Model Fidelity Improvement and Assessment

(Amélioration et évaluation de la fidélité des modèles de simulation du vol à voilure tournante)

Educational Notes for the AVT-365 Lecture Series.

The NATO Science and Technology Organization

Science & Technology (S&T) in the NATO context is defined as the selective and rigorous generation and application of state-of-the-art, validated knowledge for defence and security purposes. S&T activities embrace scientific research, technology development, transition, application and field-testing, experimentation and a range of related scientific activities that include systems engineering, operational research and analysis, synthesis, integration and validation of knowledge derived through the scientific method.

In NATO, S&T is addressed using different business models, namely a collaborative business model where NATO provides a forum where NATO Nations and partner Nations elect to use their national resources to define, conduct and promote cooperative research and information exchange, and secondly an in-house delivery business model where S&T activities are conducted in a NATO dedicated executive body, having its own personnel, capabilities and infrastructure.

The mission of the NATO Science & Technology Organization (STO) is to help position the Nations' and NATO's S&T investments as a strategic enabler of the knowledge and technology advantage for the defence and security posture of NATO Nations and partner Nations, by conducting and promoting S&T activities that augment and leverage the capabilities and programmes of the Alliance, of the NATO Nations and the partner Nations, in support of NATO's objectives, and contributing to NATO's ability to enable and influence security and defence related capability development and threat mitigation in NATO Nations and partner Nations, in accordance with NATO policies.

The total spectrum of this collaborative effort is addressed by six Technical Panels who manage a wide range of scientific research activities, a Group specialising in modelling and simulation, plus a Committee dedicated to supporting the information management needs of the organization.

- AVT Applied Vehicle Technology Panel
- HFM Human Factors and Medicine Panel
- IST Information Systems Technology Panel
- NMSG NATO Modelling and Simulation Group
- SAS System Analysis and Studies Panel
- SCI Systems Concepts and Integration Panel
- SET Sensors and Electronics Technology Panel

These Panels and Group are the power-house of the collaborative model and are made up of national representatives as well as recognised world-class scientists, engineers and information specialists. In addition to providing critical technical oversight, they also provide a communication link to military users and other NATO bodies.

The scientific and technological work is carried out by Technical Teams, created under one or more of these eight bodies, for specific research activities which have a defined duration. These research activities can take a variety of forms, including Task Groups, Workshops, Symposia, Specialists' Meetings, Lecture Series and Technical Courses.

The content of this publication has been reproduced directly from material supplied by STO or the authors.

Published October 2021

ISBN 978-92-837-2356-1

Table of Contents

List of Figures

List of Tables

AVT-365 Membership List

LECTURE SERIES DIRECTOR

Dr. Mark WHITE*
The University of Liverpool
United Kingdom
Email: mdw@liverpool.ac.uk

CO-VICE CHAIR

Dr. Mark TISCHLER*
U.S. Army DEVCOM, Retired
UNITED STATES
Email: mrtischler@aol.com

MEMBERS*

Mr. Stefano D'AGOSTO
Leonardo Helicopters
ITALY
Email: stefano.dagosto@leonardocompany.com

Dr. Neil CAMERON*
University of Liverpool
UNITED KINGDOM
Email: ncameron@liverpool.ac.uk

Prof. Steffen GREISER*[1]
University of Applied Science Osnabrück
GERMANY
Email: s.greiser@hs-osnabrueck.de

Mr. Arthur GUBBELS*
National Research Council
CANADA
Email: bill.gubbels@nrc.ca

Dr. Feyyaz GUNER
Georgia Institute of Technology
GERMANY
Email: feyyazguner@gatech.edu

Dr. Chengjian HE*
Advanced Rotorcraft Technology, Inc
UNITED STATES
Email: chengjian.he@flightlab.com

Prof. Joseph HORN
The Pennsylvania State University
UNITED STATES
Email: joehorn@psu.edu

Mr. Kenneth HUI*
National Research Council Canada
CANADA
Email: kenneth.hui@nrc-cnrc.gc.ca

Dr. Michael JONES
DLR Braunschweig
GERMANY
Email: michael.jones@dlr.de

Dr. Ondrej JUHASZ*
United States Naval Academy
UNITED STATES
Email: juhasz@usna.edu

Ms. Olivia LEE
San Jose State University
UNITED STATES
Email: olivia.h.lee@sjsu.edu

Mr. Rhys LEHMANN*
Defence Science and Technology Group
AUSTRALIA
Email: rhys.lehmann@dst.defence.gov.au

*** Lecturer**

[1] Former affiliation was DLR, Germany.

Mr. David G. MILLER*
The Boeing Company
UNITED STATES
Email: david.g.miller@boeing.com

Mr. Vincent MYRAND-LAPIERRE*
CAE
CANADA
Email: vincent.myrandlapierre@cae.com

Mr. Michel NADEAU-BEAULIEU*
CAE
CANADA
Email: michel.nadeaubeaulieu@cae.com

Mr. Samuel NADELL
U.S. Army DEVCOM
UNITED STATES
Email: usarmy.redstone.devcom-avmc.mbx.pao@army.mil

Prof. Gareth PADFIELD*
University of Liverpool
UNITED KINGDOM
Email: Gareth.Padfield@liverpool.ac.uk

Dr. Marilena PAVEL*
Delft University of Technology
NETHERLANDS
Email: M.D.PAVEL@TUDELFT.NL

Prof. Jonnalagadda PRASAD*
Georgia Institute of Technology
UNITED STATES
Email: jvr.prasad@aerospace.gatech.edu

Mr. Andrea RAGAZZI
Leonardo Company
ITALY
Email: andrea.ragazzi@leonardocompany.com

Mr. Sylvain RICHARD
Thales Group
FRANCE
Email: sylvain.richard@thalesgroup.com

Mr. Pavle SCEPANOVIC*
DLR Braunschweig
GERMANY
Email: pavle.scepanovic@dlr.de

Mrs. Susanne SEHER-WEISS*
DLR Braunschweig
GERMANY
Email: susanne.seher-weiss@dlr.de

Mr. Olaf STROOSMA
Delft University of Technology
NETHERLANDS
Email: O.Stroosma@tudelft.nl

Mr. Armin TAGHIZAD*
ONERA
FRANCE
Email: armin.taghizad@onera.fr

Mr. Eric TOBIAS*
U.S. Army DEVCOM
UNITED STATES
Email: usarmy.redstone.devcom-avmc.mbx.pao@army.mil

Dr. Hong XIN*
Sikorsky Aircraft – a Lockheed Martin Company
UNITED STATES
Email: hong.xin@lmco.com

Assoc. Prof. Ilkay YAVRUCUK*
Middle East Technical University
TURKEY
Email: yavrucuk@metu.edu.tr

*** Lecturer**

Rotorcraft Flight Simulation Model Fidelity Improvement and Assessment

(STO-EN-AVT-365)

Executive Summary

Rotorcraft flight dynamics simulation models require high levels of fidelity to be suitable as prime items in support of life cycle practices, particularly vehicle and control design and development, and system and trainer certification. On the civil side, both the FAA (US) and EASA (Europe) have documented criteria (metrics and practices) for assessing model and simulator fidelity as compared to flight-test data, although these have not been updated for several decades. On the military side, the related practices in NATO nations are not harmonised and often only developed for specific applications. Methods to update the models for improved fidelity are mostly ad hoc and lack a rational and methodical approach. Modern rotorcraft system identification (SID) and inverse simulation methods have been developed in recent years that provide new approaches well suited to pilot-in-the-loop fidelity assessment and systematic techniques for updating simulation models to achieve the needed level of fidelity. To coordinate efforts and improve the knowledge in this area, STO Applied Vehicle Technology Panel Research Task Group (STO AVT-296 RTG) was constituted to evaluate update methods used by member nations to find best practices and suitability for different applications including advanced rotorcraft configurations. The proposal of this follow-on Research Lecture Series (STO AVT-365 RLS) is to disseminate the results based on the conclusion of the effort from AVT-296, with the intention to train NATO member nations in these best practices.

An overview of previous rotorcraft simulation fidelity Working Groups is presented, followed by a review of the metrics that have been used in previous studies to quantify the fidelity of a flight model or the overall perceptual fidelity of a simulator. The theoretical foundations of the seven different update methods and a description of the eight flight databases (Bell 412, UH-60, IRIS+, EC135, CH-47, AW139, AW109, and X2, provided by the National Research Council of Canada, US Army, Airbus Helicopters, Boeing, Leonardo Helicopter Division, and Sikorsky) used by the RTG is presented. Both time- and frequency-domain fidelity assessment methods are considered, including those in current use by simulator qualification authorities and those used in the research community. Case studies are used to show the application, utility, and limitations of the update and assessment methods to the flight-test data.

The work of the RTG has shown that time- and frequency-domain SID based metrics are suitable for use for assessing the model fidelity across a wide range of rotorcraft configurations. Gain and time delay update methods work well for well-developed flight dynamics models and can be used for flight control system design, but do not provide physical insights into the sources of errors in a model. Deriving stability and control derivatives from flight-test data using SID and nonlinear simulation models using perturbation extraction methods provides insight into the missing dynamics of the simulation model, which can subsequently be updated using additional forces and moments to significantly improve the fidelity of the model and can be used to update models for flight simulation training application methods. Reduced order model and physics-based correction methods provide large benefits when extrapolating to other flight conditions but does require detailed flight-test data. SID can quickly provide accurate point models, if detailed flight-test data are available, which can be ‘stitched’ together to produce models suitable for real-time piloted simulation and control design applications. However, the dependency on flight-test data means that this method is not suitable for early aircraft development activities.

This documentation of rotorcraft simulation fidelity assessment and model update strategies will benefit NATO nations by allowing for common, agreed-upon best practices and recommendations, ensuring each country's flight dynamics and simulation models are of the highest caliber possible. The collaboration between industry, academia, and government laboratories has been key to the success of this RTG; this cooperation model should be adopted in future research activities. As industries strive to achieve greater efficiency and safety in their products, the fidelity of simulation should match commercial aspirations to ensure that the 'right first time' ethos is fully embedded into industrial best practices. Militaries will be able to use the methods and metrics presented to set criteria that will underpin the use of modeling and simulation in certification to accelerate development and acquisition and reduce the cost of new aircraft systems, e.g., advanced high-speed rotorcraft and legacy system upgrades. The criteria may also set standards for training devices used to support the expansion of synthetic environments for training to offset the high costs of flight hours. The RTG has identified that current flight training simulator standards could be updated to use the flight model and perceptual fidelity metrics presented in this Lecture Series to ensure that models are not 'over-tuned,' and a more rigorous method of subjective simulator assessment is adopted.

Amélioration et évaluation de la fidélité des modèles de simulation du vol à voilure tournante

(STO-EN-AVT-365)

Synthèse

Les modèles de simulation de la dynamique du vol à voilure tournante doivent avoir un niveau de fidélité élevé pour servir d'éléments principaux étayant les pratiques du cycle de vie, en particulier la conception et la mise au point des véhicules et des commandes et la certification du système et du simulateur. Dans le domaine civil, tant la FAA (États-Unis) que l'AESA (Europe) ont documenté des critères (indicateurs et pratiques) d'évaluation de la fidélité des modèles et simulateurs aux données d'essai en vol, même si ces critères n'ont pas été mis à jour depuis des décennies. Dans le domaine militaire, les pratiques correspondantes dans les pays de l'OTAN ne sont pas harmonisées et ne sont souvent élaborées que pour des applications bien précises. Les méthodes de mise à jour des modèles pour en améliorer la fidélité sont principalement ad hoc et manquent d'une approche rationnelle et méthodique. Des méthodes modernes d'identification des systèmes (SID) d'aéronefs à voilure tournante et de simulation inverse ont été mises au point ces dernières années. Elles constituent de nouvelles approches bien adaptées à l'évaluation de la fidélité avec pilote dans la boucle et aux techniques systématiques de mise à jour des modèles de simulation pour atteindre le niveau de fidélité nécessaire. Dans le but de coordonner les travaux et améliorer les connaissances dans ce domaine, le groupe de recherche de la Commission sur la technologie appliquée aux véhicules de la STO (RTG STO AVT-296) a été constitué afin d'évaluer les méthodes de mise à jour qu'emploient les pays membres, de trouver les meilleures pratiques et d'évaluer leur adéquation aux différentes applications, notamment les configurations perfectionnées d'aéronef à voilure tournante. La proposition de cette série de conférences de recherche (RLS STO AVT-365) est de diffuser les résultats en fonction de la conclusion des travaux de l'AVT-296, dans l'intention de former les pays membres de l'OTAN à ces nouvelles meilleures pratiques.

Le présent document donne une vue d'ensemble des groupes de travail précédents portant sur la fidélité de la simulation des aéronefs à voilure tournante, puis passe en revue les indicateurs qui ont été utilisés dans les précédentes études pour quantifier la fidélité d'un modèle de vol ou la fidélité perceptive générale d'un simulateur. Nous exposons les fondements théoriques des sept méthodes de mise à jour et décrivons les huit bases de données de vol (Bell 412, UH-60, IRIS+, EC135, CH-47, AW139, AW109 et X2, fournies par le Conseil national de recherches Canada, l'Armée de terre des États-Unis, Airbus Helicopters, Boeing, Leonardo Helicopter Division et Sikorsky) utilisées par le RTG. Des méthodes d'évaluation de la fidélité du domaine temporel et fréquentiel sont étudiées, y compris celles actuellement appliquées par les autorités de qualification des simulateurs et celles utilisées dans la communauté de la recherche. Des études de cas montrent l'application, l'utilité et les limites de la mise à jour et des méthodes d'évaluation des données d'essai en vol.

Le travail du RTG montre que les indicateurs basés sur le SID du domaine temporel et fréquentiel sont adaptés à l'évaluation de la fidélité du modèle dans une large gamme de configurations d'aéronefs à voilure tournante. Les méthodes de mise à jour du gain et de la temporisation fonctionnent bien pour les modèles de dynamique de vol bien développés et peuvent servir à concevoir des systèmes de commande de vol, mais elles ne fournissent pas d'informations physiques sur les sources d'erreur d'un modèle. La déduction des dérivées de stabilité et de commande à partir de données d'essai en vol utilisant le SID et de modèles de simulation non linéaires utilisant des méthodes d'extraction des perturbations fournit un aperçu

de la dynamique manquante du modèle de simulation, lequel peut ensuite être mis à jour avec des forces et moments supplémentaires pour améliorer sensiblement la fidélité du modèle et peut servir à actualiser les modèles des méthodes applicatives de formation par simulation de vol. Les méthodes de correction basées sur la physique et les modèles réduits offrent de grands avantages lors de l'extrapolation à d'autres conditions de vol, mais nécessitent des données détaillées d'essai en vol. Le SID peut fournir rapidement des modèles de point exacts, si des données détaillées d'essai en vol sont disponibles, lesquels peuvent être « assemblés » pour produire des modèles adaptés à la simulation pilotée en temps réel et aux applications de conception des commandes. Cependant, la dépendance aux données d'essai en vol signifie que cette méthode n'est pas adaptée aux activités précoces de mise au point des aéronefs.

Cette documentation de l'évaluation de la fidélité de simulation des aéronefs à voilure tournante et des stratégies de mise à jour des modèles bénéficiera aux pays de l'OTAN en leur permettant de convenir des meilleures pratiques et des recommandations communes, qui garantiront le niveau le plus élevé possible des modèles de simulation et de dynamique de vol de chaque pays. La collaboration entre l'industrie, le monde universitaire et les laboratoires publics a été la clé de la réussite de ce RTG. Ce modèle de coopération devrait être adopté dans les futures activités de recherche. Alors que les industries s'efforcent d'atteindre une plus grande efficacité et une meilleure sécurité de leurs produits, la fidélité de la simulation devrait correspondre aux aspirations commerciales, afin que la philosophie de « réussite du premier coup » soit pleinement intégrée dans les meilleures pratiques industrielles. Les militaires pourront utiliser les méthodes et indicateurs présentés pour établir des critères qui étaieront l'utilisation de la modélisation et simulation dans la certification, afin d'accélérer la mise au point et l'acquisition et de réduire le coût des nouveaux systèmes d'aéronefs, par exemple les aéronefs à voilure tournante à grande vitesse et les systèmes hérités modernisés. Ces critères peuvent également établir des normes pour les appareils de formation servant à soutenir le développement des environnements synthétiques dans l'entraînement, afin de contrebalancer le coût élevé des heures de vol. Le RTG a déterminé que les normes actuelles des simulateurs d'entraînement au vol pourraient être mises à jour pour utiliser le modèle de vol et les indicateurs de fidélité perceptive présentés dans cette série de conférences, afin de s'assurer que les modèles ne sont pas adaptés de manière excessive et qu'une méthode plus rigoureuse d'évaluation subjective des simulateurs est adoptée.

Chapter 1 – INTRODUCTION

ABSTRACT

The Lecture Series is introduced and motivated. An overview of the Lecture Series is also presented, highlighting aircraft and methods that will be presented later.

1.1 INTRODUCTION

Aircraft and rotorcraft flight dynamics simulation models require high levels of fidelity to be suitable as prime tools to support life cycle practises, particularly in vehicle and control design and development, and system and trainer certification. On the civil side, both the FAA (US) and EASA (Europe) have documented criteria (metrics and practises) for assessing model and simulator fidelity as compared to flight-test data, although these have not been updated for several decades. On the military side, the related practises in NATO nations are not harmonized and are often only developed for specific applications. Methods to update the models for improved fidelity are mostly ad hoc and lack a rational and methodical approach. More rigorous and systematic practises for fidelity assessment and enhancement could pay huge dividends in reducing early life cycle costs for both military and civil rotorcraft acquisitions [1].

Modern system identification (SID) and inverse simulation methods have been developed in recent years (e.g., Refs. [2], [3], [4], [5], [6], [7], [8]) that provide new approaches well suited to pilot-in-the-loop fidelity assessment and systematic techniques for updating simulation models to achieve the needed level of fidelity. Previous NATO Science and Technology Organization (STO) activities (AGARD) by NATO partner countries developed and compared time- and frequency-domain system identification (SID) methodologies to extract accurate models of three different rotorcraft – the AH-64, Bo-105, and SA-330 – from flight-test maneuvres [2]. Flight identified models from each country were compared to each other but not to physics-based nonlinear simulation math models. Since this original AGARD activity, member nations have independently made considerable progress using system identification and inverse simulation methods to update their physics-based flight models using flight-test data. The model updates used by each nation vary greatly in terms of methodology, complexity, and associated technical effort/cost (e.g., Refs. [3], [4], [5], [6], [7], [8]). These research activities demonstrate different update methodologies that provide significant improvements in model fidelity and demonstrate how rotorcraft SID has advanced since the seminal work reported in Hamel et al. [2].

Under the STO Applied Vehicle Technology *(*AVT*)* Panel (STO AVT-296) Research Task Group (RTG), each member nation has refined and documented their own particular methodology, as well as methods from other nations using their unique flight-test databases. Comparisons between update methods have been investigated to find best practises and suitability for different applications including advanced rotorcraft configurations. This Lecture Series highlights work accomplished during the STO AVT-296 work.

1.2 OBJECTIVES

The primary goal of Lecture Series is to apply and compare flight simulation model update and fidelity assessment methods based on flight-test case studies. First, the adoption of model fidelity metrics that will be used throughout the rest of the presentations is discussed. Sample cases studies from STO AVT-296 have been chosen to demonstrate the update methods. The methods are applied to a subset of the aircraft available in the RTG report.

Making such update methods, metrics, and practises more accessible and standardized for industrial and government use was a strong motivation for the RTG and this Lecture Series. The documentation of

simulation fidelity assessment and model update strategies will benefit NATO nations by allowing for common, agreed-upon best practises and recommendations, ensuring each country's flight dynamics and simulation models are of the highest calibre possible. Militaries will be able to use the methods and metrics presented to set criteria that will underpin the use of modeling and simulation in certification to accelerate development and acquisition and reduce the cost of new aircraft systems and legacy system upgrades. The criteria may also set standards for training devices used to support the expansion of synthetic environments for training to offset the high costs of flight hours.

1.3 LECTURE SERIES OVERVIEW AND ORGANIZATION

First, an overview is given of the past several decades of technical work in simulation fidelity and model assessment from the perspectives of researchers, Original Equipment Manufacturer (OEM) engineers, academics, and simulator developers. As the complexity of future rotorcraft designs continues to increase, this work serves as a launching point for model validation efforts and is a snapshot of the current state-of-the-art methods used to improve model fidelity. From an organizational standpoint, references are given at the end of each section or chapter in the Notes to assist the reader in quickly finding additional technical content. The overall structure of the Lecture Series is as follows:

- Overview of group members, the timeline, and technical meetings held. The motivation for each participant is then covered. Brief summaries of the methods each organization are currently employing for math model update, and the end application of the models they develop (simulation, engineering design, control law development, etc.). Current areas of research in model fidelity improvement and past work in system identification and modeling are discussed.
- Various quantitative and qualitative simulation model fidelity metrics are presented. Rotorcraft flight dynamics simulation models serve a variety of purposes and are evaluated by different metrics based on the end application. The metrics and their backgrounds are discussed to give the participant an impression of how models can be evaluated. Many metrics are introduced, and several are down-selected and later used to evaluate an update method's efficacy.
- Model update methods are broadly categorized in terms of complexity and level of technical effort required. Methods range from gross empirical corrections to more complicated methods that require detailed knowledge of rotorcraft dynamics and aerodynamics.
- Databases are presented for the rotorcraft to which simulation update methods are applied in this study. Information provided includes aircraft configuration, flight-test data available, flight simulation modeling tools, system identification methods and results for model fidelity assessment and update. Effort was taken to include a large variety of rotorcraft configurations: legacy to advanced high-speed configurations, partial-authority to full-authority flight control system considerations, and piloted vs UAVs. This large range of rotorcraft configurations provides insight into the modeling nuances of each and to give an impression of deficiencies that may be encountered in new designs.
- Model update case studies organized are presented. The same method is generally applied to multiple aircraft by researchers from different organizations to give a variety of perspectives on each method. Conciseness of each case study is emphasized to allow the reader to grasp the concepts of each method. Additional technical details are left to the AVT-296 report and cited technical papers available in the literature. A concise summary of the update methods and case studies is presented in Figure 1-1.
- Various viewpoints are next presented from simulation companies, OEMs, and flight controls researchers on the applicability of each update method to their industry and how and when to use each method. Recommendations are made regarding the current simulator certification process and how it may be improved based on the results in this report. Finally, the Lecture Series key findings are summarized.

Flight Simulation Model Update Methods

- Method 1: Gain/Time Delay Corrections for Key Responses
- Method 2: "Black Box" Input and Output Filters
- Method 3: Force and Moment Increments Based on Stability Derivatives
- Method 4: Reduced Order Models and Physics-Based Corrections
- Method 5: Simulation Model Parameter Adjustment
- Method 6: Parameter Identification of Key Simulation Constants
- Method 7: Stitched Simulation from Point ID Models and Trim Data

Flight Test Database	Method 1 (Section 7.1)	Method 2 (Section 7.2)	Method 3 (Section 7.3)	Method 4 (Section 7.4)	Method 5 (Section 7.5)	Method 6 (Section 7.6)	Method 7 (Section 7.7)	Quantitative Fidelity	Perceptual Fidelity
412 (NRC)		DLR	UoL, CAE		CAE		NRC	X	UoL
UH-60 (USNA)	USNA			ART, GT, SAC	PSU		TDD	X	
EC135 (DLR)		DLR	METU		Thales/ONERA		DLR	X	
CH-47 (Boeing/DSTG)	DSTG	CAE		GT, Boeing, DSTG	DSTG, CAE			X	
AW139 (Thales/ONERA)			Thales/ONERA					X	
AW109 (LH)				LH				X	
X2 (SAC)				SAC, USNA		USNA		X	
Iris+ (TDD)							TDD	X	

Figure 1-1: AVT-296 Flight Simulation Model Update Methods and Flight-Test Databases.

1.4 REFERENCES

[1] Cooper, J., Padfield, G.D., Abdelal, G., Cameron, N. Fisher, M., Forrest, J. Georgiou, G., Hon, K.K.B., Jump, M., Robotham, A.J., Shao, F., Webster, M., and White, M.D. (2011), Virtual Engineering Centre – Examples of Virtual Prototyping and Multidisciplinary Design Optimization, NATO RTO-MP-AVT-173, Paper NBR1-29, October 2011.

[2] Hamel, P.G. (1991), "Rotorcraft System Identification", AGARD AR-280, Sept. 1991.

[3] Tischler, M.B., Blanken, C.L., Cheung, K.K., Swei, S.S.M., Sahasrabudhe, V., and Faynberg, A. (2004), "Optimization and Flight Test Results of Modern Control Laws for the UH-60 Black Hawk", Presented at the AHS 4th Decennial Specialists' Conference on Aeromechanics, San Francisco, CA, January 2004.

[4] Lu, L., Padfield, G.D., White, M.D., and Perfect P. (2011), "Fidelity Enhancement of a Rotorcraft Simulation Model Through System Identification", *The Aeronautical Journal*, Vol. 115, No. 1170, August 2011.

[5] Tischler, M.B., and Remple, R.K. (2012), *Aircraft and Rotorcraft System Identification: Engineering Methods with Flight Test Examples*, AIAA, Second Edition, Reston, VA.

[6] Morelli, E.A., and Cooper, J. (2014), "Frequency-Domain Method for Automated Simulation Updates Based on Flight Data", Presented at AIAA SciTech Modeling and Simulation Technologies Conference, National Harbor, MD, January 2014.

[7] Greiser, S., and von Grünhagen, W. (2016), "Improving System Identification Results: Combining a Physics-Based Stitched Model with Transfer Function Models Obtained Through Inverse Simulation", Presented at the 72nd Annual Forum of the American Helicopter Society, West Palm Beach, FL, May 2016.

[8] Fegely, C., Xin, H., Juhasz, O., and Tischler, M.B. (2016), “Flight Dynamics and Control Modeling with System Identification Validation of the Sikorsky X2 Technology Demonstrator”, Presented at the 72nd Annual Forum of the American Helicopter Society, West Palm Beach, FL, May 2016.

Chapter 2 – GROUP OVERVIEW

ABSTRACT

This chapter provides an overview of the composition of the AVT-296 group, the manner in which the group operated and the key outcomes from the partner meetings.

2.1 PARTNERS

In AVT-296, partners were drawn from industry (6), government research laboratories (5), and academia (9) with 31 people contributing. Table 2-1 lists the partners' affiliations. The initials in brackets are used to identify participants in the figures that follow.

Table 2-1: Participants.

Organization Type	Organization	Name
Industry	CAE, Canada	Vincent Myrand-Lapierre (VML) Michel Nadeau-Beaulieu (MNB)
	Thales, France	Sylvain Richard (SR)
	Leonardo Helicopters, Italy	Andrea Ragazzi (AR) Stefano D'Agosto (SDA)
	Advanced Rotorcraft Technology, USA	Chengjian He (CH)
	Boeing, USA	David Miller (DM)
	Sikorsky, a Lockheed Martin Company, USA	Hong Xin (HX)
Government Laboratories	Australian Department of Defence, Defence Science and Technology Group (DSTG)	Rhys Lehmann (RL)
	National Research Council, Canada	Bill Gubbels (BG) Ken Hui (KH)
	ONERA, France	Armin Taghizad (AT)
	DLR, Institute of Flight Systems, Germany	Michael Jones (MJ) Pavle Scepanovic (PS) Susanne Seher-Weiss (SSW)
	U.S. Army Combat Capabilities Development Command Aviation & Missile Center, USA	Mark Tischler (MT) Eric Tobias (ET)
	Contractor, U.S. Army Combat Capabilities Development Command Aviation & Missile Center, USA	Jonathan Soong (JS)

Organization Type	Organization	Name
Academia	Osnabrück University of Applied Sciences, Germany	Steffen Greiser (SG)[1]
	Delft University of Technology, Netherlands	Marilena Pavel (MP) Olaf Stroosma (OS)
	Middle East Technical University, Turkey	Ilkay Yavrucuk (IY)
	University of Liverpool, UK	Mark D White (MDW) Gareth D Padfield (GDP) Neil Cameron (NC)
	Georgia Institute of Technology, USA	JVR Prasad (JVR) Feyyaz Guner (FG)
	Naval Academy, USA	Ondrej Juhasz (OJ)
	Pennsylvania State University, USA	Joseph Horn (JH)
	Universities Space Research Association, USA	Samuel Nadell (SN)[2]
	San Jose State University, USA	Olivia Lee (OL)

2.2 SUMMARY OF ACTIVITIES

Two meetings per year were scheduled at different partner facilities, 3 in North America (Georgia Tech, NRC Ottawa and US Naval Academy) and 3 in Europe (University of Liverpool, DLR Braunschweig, ONERA (Salon)). Three-day meetings were planned to allow sufficient time for planning, presentation of results and development of the final report. The meetings also provided an opportunity to see the partners' facilities and how they going to be used in the AVT-296 activity. Unfortunately, due to COVID restrictions, the face-to-face meetings at the US Naval Academy and ONERA had to be replaced with online meetings instead. Additional meetings were held during the Vertical Flight Society Annual Fora and midterm teleconferences were also held. Progress reports were provided to the NATO Panel Board Meetings.

2.2.1 Meeting 1, 13 – 15 March 2018: University of Liverpool, Liverpool, UK

The kick-off meeting was hosted by the Flight Science and Technology research group at the University of Liverpool. 20 participants, representing 14 organizations from 7 NATO countries attended. Meetings during the first day (13 March) covered introductions by the RTG members, with each presenting a 30-min overview of their activities relevant to this RTG. During the second day, the RTG self-organized around 9 flight-test databases and 7 methods for model updates. The Point Of Contact (POC) for each database summarized the key aspects of their database (e.g., flight condition, etc.) and activities by RTG team members that would use their databases. A structure of the final report was proposed with team members offering suggestions for refinements and lead authorship of the various sections. The participants toured the University of Liverpool flight simulator facilities. On the third day, the POC for each database reported final plans for use of their database and the various collaboration opportunities that were identified.

[1] Former affiliation was DLR, Germany.

[2] This work was also supported by the National Aeronautics and Space Administration (NASA) under award number NNA16BD14C for NASA Academic Mission Services (NAMS).

Figure 2-1: Meeting 1 Group Photo at The University of Liverpool's Flight Simulator.

2.2.2 Meeting 2, 16 – 18 October 2018: Georgia Institute of Technology, Atlanta, USA

19 Participants, representing 16 organizations from 8 countries attended the meeting. The started with a status update of the specific action items as consolidated since the previous meeting in Liverpool. Next, reports were presented concerning the 'Overarching Methods' that span the AVT-296 activity: 1) Common flight-test database template; 2) Quantitative fidelity metrics and associated automated scripts; and 3) Perceptual fidelity methods. The following 1.5 days of the meeting were organized by flight-test database (e.g., 412, UH-60, etc.). Each database was organized, and efforts coordinated by a 'database coordinator.' Methodology coordinators and initial summaries of the update methods were drafted. During these 1.5 days, database organization details and availability on the NATO Science Connect website were summarized, and work by each of the participants using the databases was presented. In depth discussions were held among the database teams to coordinate future efforts. During the second day, the participants toured the Georgia Tech flight simulator facilities. On the third day, the final report structure was reviewed, and the organization was approved by the AVT membership. The overall time schedule for AVT-286 was reviewed and the urgency to complete all technical results by Fall 2019 was emphasized.

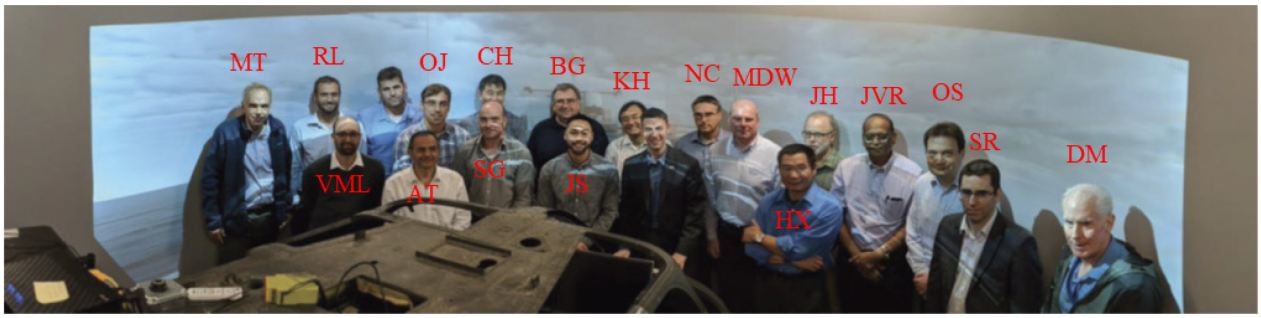

Figure 2-2: Meeting 2 Group Photo at the Georgia Tech Flight Simulator.

2.2.3 Meeting 3, 26 – 28 March 2019: DLR, Braunschweig, Germany

At this meeting, there were 27 participants, representing 17 organizations from 9 countries. The RTG welcomed a new member nation, Turkey, with participation from Dr. Ilkay Yavrucuk. Additionally, a visiting guest from Airbus Helicopters, Dr. Tobias Ries, was invited by the DLR to give an overview of his organization's simulation activities.

The meeting started with a discussion on the overarching methods, including quantitative and perceptual model fidelity evaluation methods and 7 methods of model updates based on flight-test system identification. The next section covered a review of the 8 flight-test databases (reduced from 9 from the previous meeting), ranging from conventional single-rotor helicopter to tandem and a UAV. Each participant briefed their progress using their chosen update methods on their organization's models. A tour was given of the DLR research aircraft hangar and flight simulator. The next period of the meeting was dedicated to individual group discussions organized by aircraft databases to coordinate activities among contributors. Key databases (e.g., Bell 412 and UH-60) chose a common flight condition (hover) across methods to assess the relative effectiveness of each model update method. The final section of the meeting was dedicated to reviewing and updating the proposed report structure outline.

Figure 2-3: Meeting 3 Group Photo in the DLR Hangar.

2.2.4 Meeting 4, 22 – 24 October 2019: National Research Council, Ottawa, Canada

At this meeting, there were 22 participants, representing 17 organizations from 9 countries. The RTG welcomed a new member with participation from Mr. Eric Tobias from the U.S. Army Combat Capabilities Development Command Aviation and Missile Center.

The meeting started with a review of the draft material on the overarching methods, including quantitative and perceptual model fidelity evaluation methods. The next section covered a review of the 8 flight-test databases with each organization providing their technical progress and near-completion of various update methods. A single point of contact was established for each chapter and update methods, with members working in small groups to organize their writing sections. The leads presented a summary report with their current draft status and future plans. A consensus was reached on a common set of frequency and time-domain simulation assessment and update criteria, as well as a common report formatting and style.

The follow-on Research Lecture Series was reviewed, with the initial concept of 4 locations within 2 weeks in March 2021. The locations would be 2 in Europe (Northern and Southern Europe) and 2 in North America (East and West Coast). Location POCs have been established to explore the details and arrangement of the lecture series. A first draft of the speakers was proposed, with a recognition that speakers may vary due to travel availability.

A tour was given of the NRC aircraft hangar with Mr. Bill Gubbels showing their fleet and latest research activities. The meeting concluded with an informal deadline to complete report drafts by the midterm teleconference meeting in January 2020.

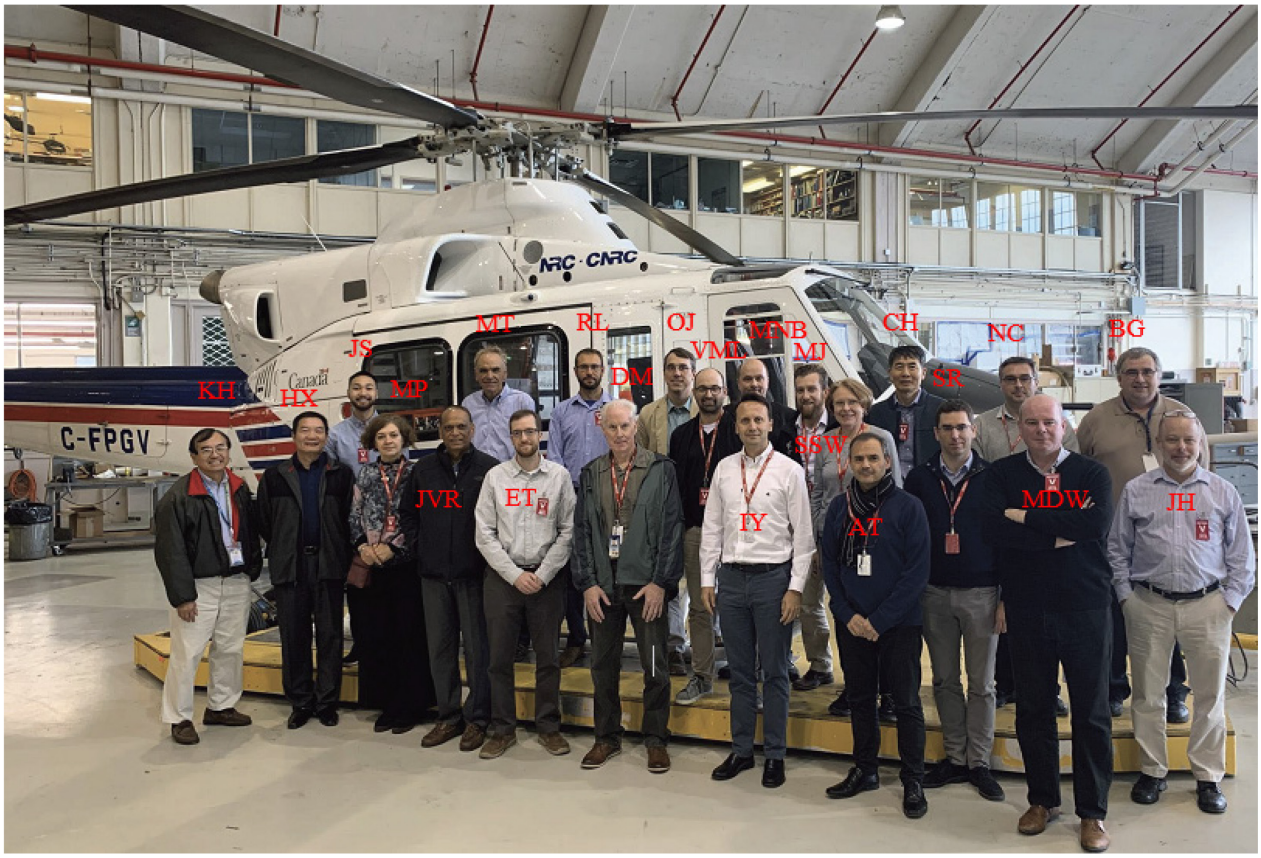

Figure 2-4: Meeting 4 Group Photo in the NRC's Hangar.

2.2.5 Meeting 5, 22 – 26 June 2020: Online

Due to restrictions caused by the COVID-19 pandemic, the in-person meeting that was originally planned to be held in March 2020 at ONERA's research laboratories in Salon-en-Provence were postponed until June to try and facilitate a face-to-face meeting. However, this was not possible, and an online meeting was held instead 22 – 26 June. The meeting spanned 7 time zones, and 27 members of the group, from 18 organizations participated.

The meeting commenced with a review of the report outline and updates were provided for each chapter to produce a final version of the methods and databases matrices. On each day, there was an initial full-group meeting held prior to the team splitting into sub-group meetings to discuss and write material for each chapter.

Internal reviewers were identified for each chapter together with an external reviewer who was not directly involved in the production of the chapter material. It was agreed to try and provide chapter reviews by 15 September to allow sufficient time for chapter leads to incorporate changes by the next formal meeting which was planned for 12 – 16 October hosted by the United States Naval Academy in Annapolis.

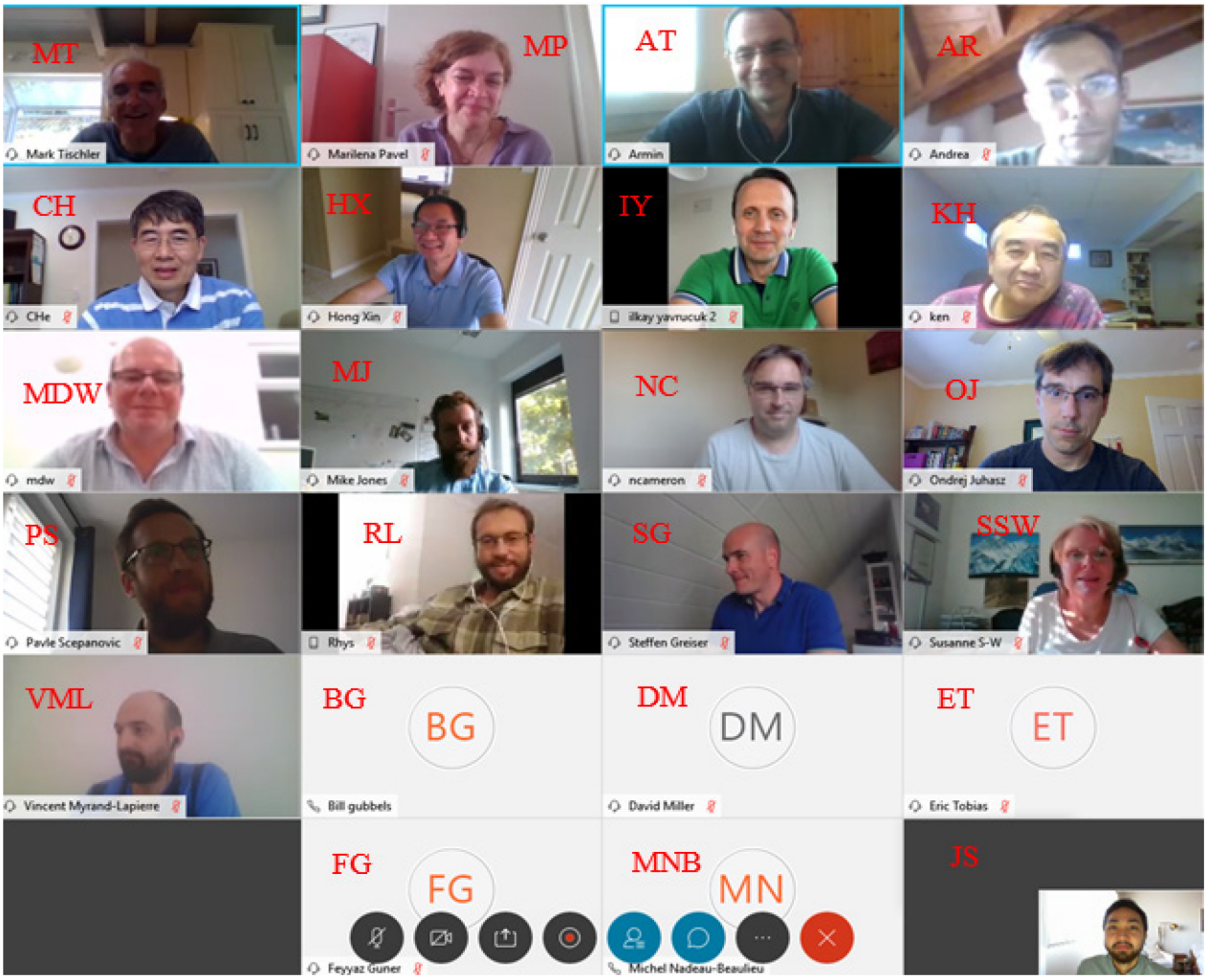

Figure 2-5: Meeting 5 Online Meeting Group Photo.

2.2.6 Meeting 6, 12 – 16 October 2020: Online

The sixth biannual meeting of the NATO AVT-296 Research Task Group on Rotorcraft Flight Simulation Model Fidelity Improvement and Assessment was held virtually and was attended by 29 participants from 20 organizations and 9 countries.

Each day, a team meeting was held starting at 7 am Pacific Time for 1 – 3 hours and side meetings were organized as needed by the lead authors of each chapter. After each team meeting, action items and a chart package with updated status and meeting schedule were sent to focus the efforts of the group.

The first 3 days focused on producing a final rough draft ready for formatting and final review in NATO report form, which will be submitted to NATO at the end of 2020. On Monday, 12 October, the team meeting covered welcome, introduction, meeting agenda, round table discussion of the status of each chapter, and path forward. On Tuesday, 13 October, a brief team meeting was held to check in on the status of each chapter of the report, and most of the day was allocated for finalizing chapter drafts. On Wednesday, 14 October, the team meeting was held to assess the status of the NATO report and determine final actions for its completion. The last 2 days focused on developing charts and discussing plans for the Research Lecture Series (RLS). Due to COVID restrictions it was decided to host the RLS virtually from 1 – 3 June 2021 in Europe and 8 – 10 June 2021 in North America. On Thursday, 15 October, work was begun to outline and determine presenters/aircraft databases for each chapter of the lecture series and a group photo was taken. Friday, 16 October, involved round table discussion of the lecture series status for each chapter, path forward, and meeting wrap up and conclusions.

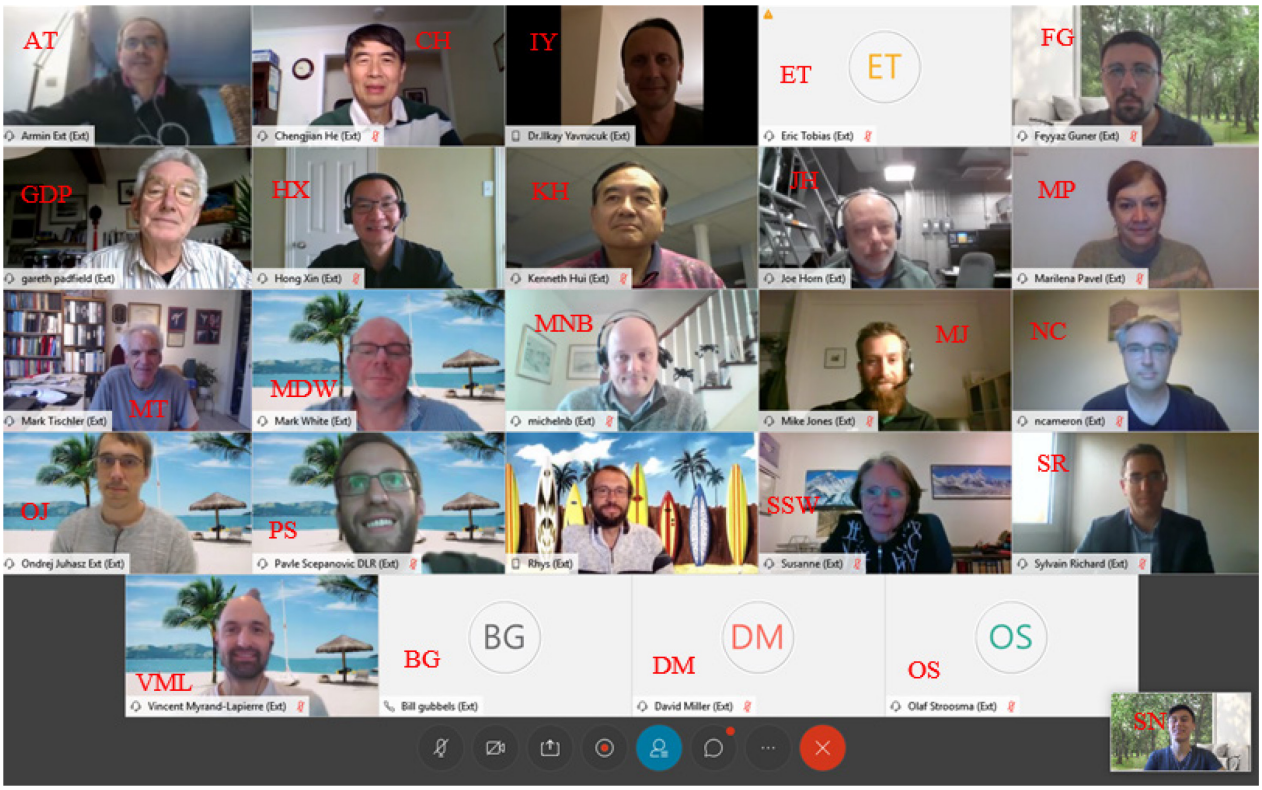

Figure 2-6: Meeting 6 Online Meeting Group Photo.

After the meeting all publication-ready chapters will be submitted to the Research Task Group leadership. The group's technical writer will compile and format the report to comply with NATO guidelines. A final technical review will be performed by the group's leadership and publication authorization will be obtained for each organization, as necessary. A 1-day midterm meeting is being scheduled for the first week of December and will cover final review/discussion of the report by the group. The final report will be submitted to NATO for publication at the end of 2020.

Chapter 3 – REVIEW OF RECENT FIDELITY ASSESSMENT AND MODEL UPDATE ACTIVITIES

ABSTRACT

This chapter of the Lecture Series gives an overview of some of past and recent activities in fidelity assessment and model update. First, a review of industry best practices will be presented before reporting some activities carried out in previous AGARD and GARTEUR Groups.

3.1 INTRODUCTION

The need for unified model fidelity metrics has already been discussed by several AGARD and GARTEUR groups and has been the topic of workshops at the Vertical Flight Society (formerly the American Helicopter Society) Forums in previous years. This research activity also highlights that the fidelity of models used for different purposes may be best captured by different metrics.

The primary goal of this 3-year RTG was to apply and compare flight simulation model update and fidelity assessment methods based on flight-test case studies. The RTG presents methods and results and documents best practices for application to system design, certification, and pilot training. These methods can be carried forward to align flight control system design and simulation certification standards across the nations. The RTG report gives a thorough background and description of each model update method and gives sample results for various rotorcraft test cases.

Table 3-1 summarizes the methods and the case studies investigated.

Table 3-1: Summary of Methods and Case Studies.

Seven Improvement Methods Investigated

- Method 1: Gain/Time Delay Corrections for Key Responses
- Method 2: “Black Box” Input and Output Filters
- Method 3: Force and Moment Increments Based on Stability Derivatives
- Method 4: Reduced Order Models and Physics-Based Corrections
- Method 5: Simulation Model Parameter Adjustment
- Method 6: Parameter Identification of Key Simulation Constants
- Method 7: Stitched Simulation from Point ID Models and Trim Data

Six Assessment Methods Reviewed

- Bounds of Maximum Unnoticeable Added Dynamics (MUAD)
- Model/Flight Data Mismatch and Integrated Cost Functions
- VALCrit and AEE Criterion
- Phase/Gain Errors in Motion Cues
- Simulation Fidelity Rating Scale (SFR)
- QTG, FAA Part 60, and Others Described

Improvement Methods vs Case Studies

	Method 1	Method 2	Method 3	Method 4	Method 5	Method 6	Method 7
412 (NRC)	USNA	DLR	UoL, CAE		CAE		NRC
UH-60 (USNA)	USNA			ART, GT, SAC	PSU		TDD
EC135 (DLR)		DLR	METU		Thales/ONERA		DLR
CH-47 (Boeing/DSTG)	DSTG	CAE		GT, Boeing, DSTG	DSTG, CAE		
AW139 (Thales/ONERA)			Thales/ONERA				
AW109 (LH)				LH			
X2 (SAC)				SAC, USNA		USNA	
Iris+ (TDD)							TDD

This chapter of the Lecture Series gives an overview of some of past and recent activities in this area. First, a review of industry best practices will be presented before reporting some activities carried out in previous AGARD and GARTEUR Groups.

3.2 Industry Best Practices

Flight simulation training devices (FSTD) and rotorcraft flight simulators, in general, can be categorized in two primary groups. One is used for pilot flying skill training, such as those specified by FAA 14 Part 60 and EASA CS-FSTD (H) in various levels of fidelity, including Level 5, 6, 7 (see Ref. [1]), Sections 4.5, 4.6 and 8.3 for more details). The other group of flight simulators is more diverse and mainly used in engineering applications in support of aircraft design, development, and certification as well as research. A survey was conducted on simulation modeling and calibration practices, and the survey responses were received from both rotorcraft and FSTD manufacturers, research, and engineering organizations. The survey covers flight simulation modeling practices for single main rotor helicopter, tiltrotor, and compound rotorcraft. This section summarizes the survey results on modeling practice, model fidelity calibration methods, and metrics used.

3.2.1 Modeling Methods

1) **Main rotor:** Although there may be some difference in implementation details, blade-element methods are used for main rotors in all surveyed. The blade segment airfoil tables are derived from wind tunnel tests or CFD. Rotor CFD solver analysis is also adopted in some applications to supply additional information as needed. Rotor induced inflow is resolved using 3-state dynamic inflow model of either Pitt-Peters or Peters-He. Most consider rigid blade dynamics with hub retention degrees of freedom, such as flap and lead-lag dynamics. Elastic blade models are adopted in some applications as well.

2) **Tail rotor:** Analytical Bailey rotor model is used in most surveyed. More advanced blade-element modeling is also used in some simulations. Specific modeling method is used for Fenestron, including modeling of the fan, duct, diffusor, etc.

3) **Fuselage airloads:** All adopt table look-up or equations describing aerodynamic forces and moments with respect to fuselage angle of attack (AoA) and angle of sideslip. The tables or equations are extracted from wind tunnel tests or CFD solution. In the calculation of flow variables (e.g., AoA), most also consider the effect of rotor induced interference with empirical approach.

4) **Aerodynamic Surfaces:** Table look-up or equations describing aerodynamic forces and moments are used for horizontal surfaces and vertical fins. The table data are derived from wind tunnel tests or CFD simulation.

5) **Aerodynamic Interference:** Parametric models or empirical table look-up are used in modeling rotor or fuselage interference. The data are mostly generated from wind tunnel measurements, comprehensive analysis (vortex wake, viscous vortex particle method, etc.) or CFD.

3.2.2 Application of System Identification Method

System identification methods are used in: 1) Physical modeling parameter extraction; 2) Control law development; and 3) Simulation model validation and calibration.

3.2.3 Simulation Model Fidelity Calibration

The simulation model calibration methods include: 1) Modeling parameter adjustment; 2) System identified dynamic/control derivative based adjustment; and 3) Subject matter expert/pilot based model adjustment.

3.2.4 Simulation Model Fidelity Metrics

FSTD manufacturers use FAA 14 Part 60 or EASA CS-FSTD (H) Qualification Test Guide (QTG) specifications in time-domain with quantitative criteria for simulation model acceptance. Frequency domain is also used for training simulator model development validation. On the other hand, research and engineering simulators mostly adopt self-specified criteria which emphasize match of the variation trend.

3.3 AGARD AND GARTEUR ACTIVITIES IN FIDELITY ASSESSMENT AND MODEL UPDATE

3.3.1 AGARD Activities

During several decades, the mission of AGARD (Advisory Group for Aerospace Research and Development) was to bring together the leading personalities of the NATO nations in the field of science and technology relating to aerospace for the following purposes:

- Exchanging of scientific and technical information.
- Continuously stimulating advances in the aerospace science.
- Improving the cooperation among member nations.
- Providing scientific and technical assistance to the Military Committee.
- Recommending effective ways for the member nations to use their research and development capabilities for the common benefit of the NATO community.

Among the topics supported by AGARD, simulation fidelity has been the subject of several symposiums (lecture series) with the objective of providing an up-to-date description of the progress in this field and of the state-of-the-art achieved.

In 1987 AGARD set up a Working Group (WG) 18 comprising a wide range of research specialists and industry representatives, tasked with exploring and reporting on the topic of Rotorcraft System Identification. WG 18 activity led to a Lecture Series in 1991.

The Working Group had to main objectives:

1) Evaluate the different approaches in System Identification (SID) techniques and develop guidelines for SID applications.
2) Define an integrated and coordinated methodology for application of system identification.

The Working Group was provided with a common flight-test data base for three different helicopter types:

- The Attack helicopter MDHC AH-64 (Apache): MDHC provided data from flight tests at 130 kn.
- The DLR small transport helicopter MBB BO-105: DLR provided data from flight tests at 80 kn.
- The RAE medium size transport helicopter Aerospatiale SA-330 (PUMA): RAE provided flight data at 60, 80 and 100 kn.

The Lecture Series presented the Quad-M requirements of rotorcraft system identification as described below (see Figure 3-1):

- Importance of the control input shape in order to excite all modes of the vehicle dynamic **motions**.
- Type of rotorcraft under investigation in order to define the structure of possible mathematical **models**.
- Selection of instrumentation and filters for high accuracy **measurements**.
- Quality of data analysis by selecting most suitable time or frequency-domain identification **methods**.

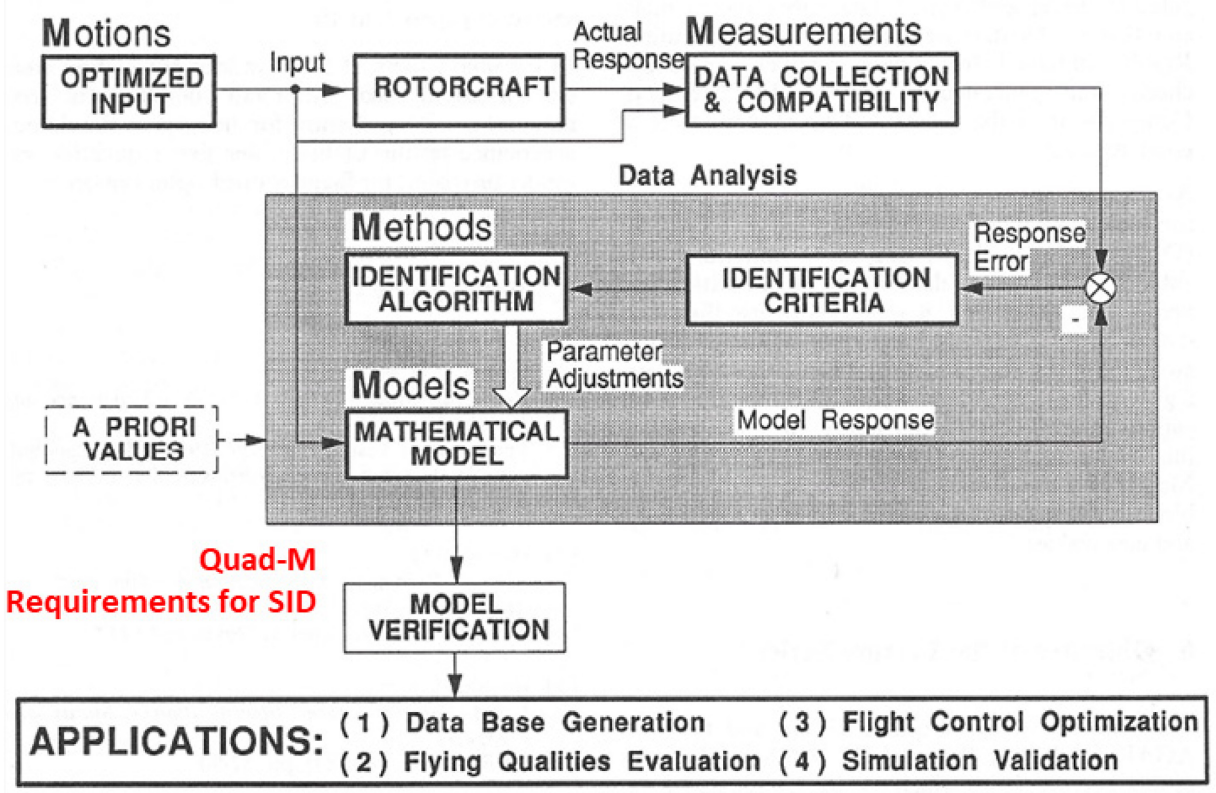

Figure 3-1: Quad-M Requirements for System Identification.

The Lecture Series also discussed the following application areas of SID:

- Rotorcraft development risk reduction;
- Data gathering for helicopter simulators (Figure 3-2);
- Acceptance testing of helicopter flying qualities (Figure 3-3);
- Model provision for flight control optimization (Figure 3-4).

Reporting the progress in helicopters aeromechanics modeling, the AGARD Lecture Series N° 139 (AGARD (AG) Helicopter Aeromechanics (1985)) provided a review of flight-test techniques and test data interpretation methods for helicopter performance and flying qualities analysis. The distinction was drawn between quasi-steady and dynamic testing.

Performance topics covered steady-state performance in hover and forward flight, flight envelope boundaries, and take-off and landing normal and emergency performance (see Figure 3-5).

Flying qualities mainly addressed the treatment of static stability tests and progress to dynamic stability, control response (see Figure 3-6), system identification, and mission-related evaluation techniques. The specificity of tests for certification, development phases, and research was also addressed. The lecture also discusses the forms in which flight data can be presented and draws a review of data reduction and analysis methods.

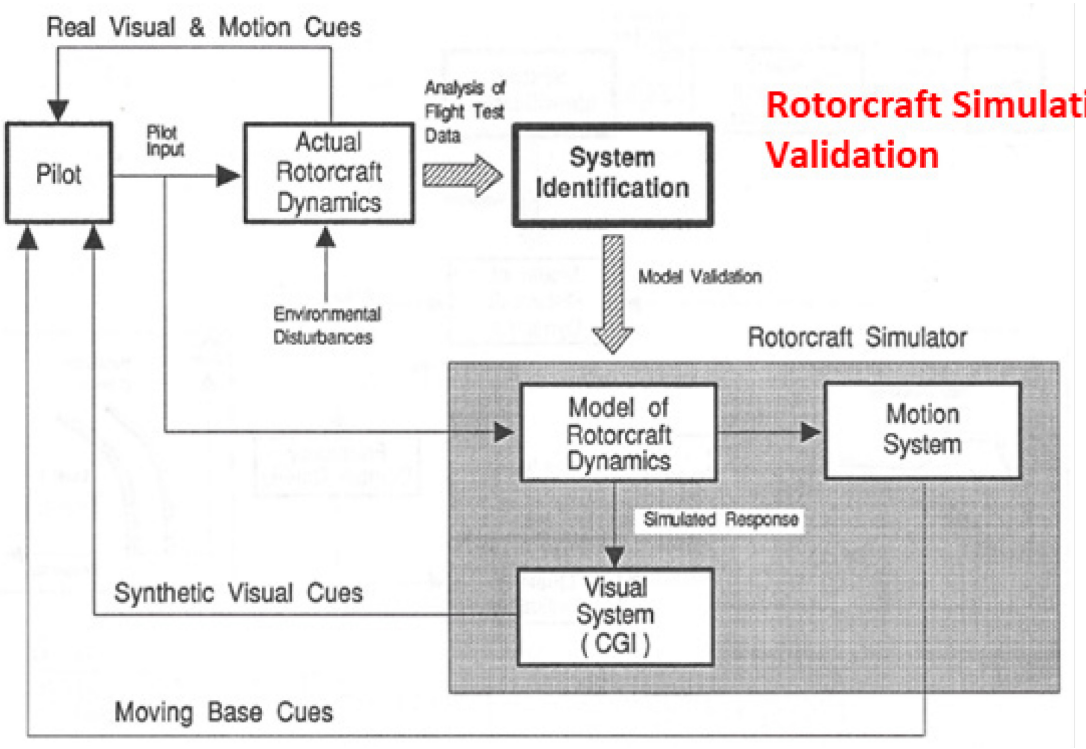

Figure 3-2: System Identification for Rotorcraft Simulation Validation.

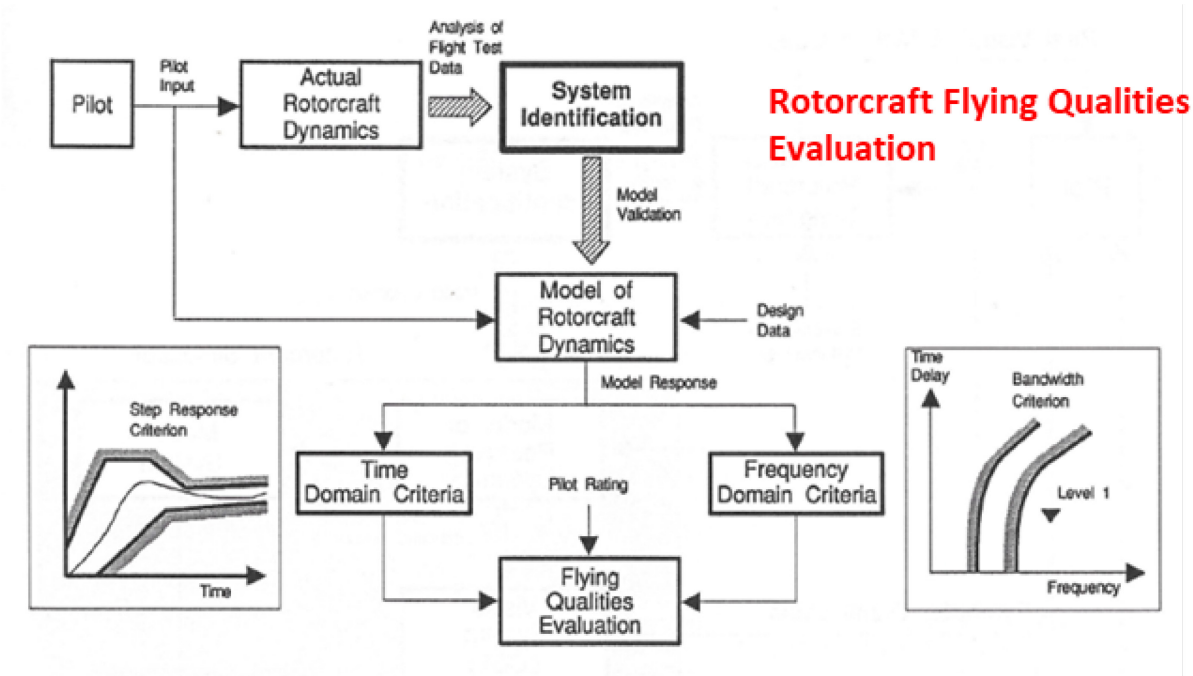

Figure 3-3: System Identification for Rotorcraft Flying Qualities Evaluation.

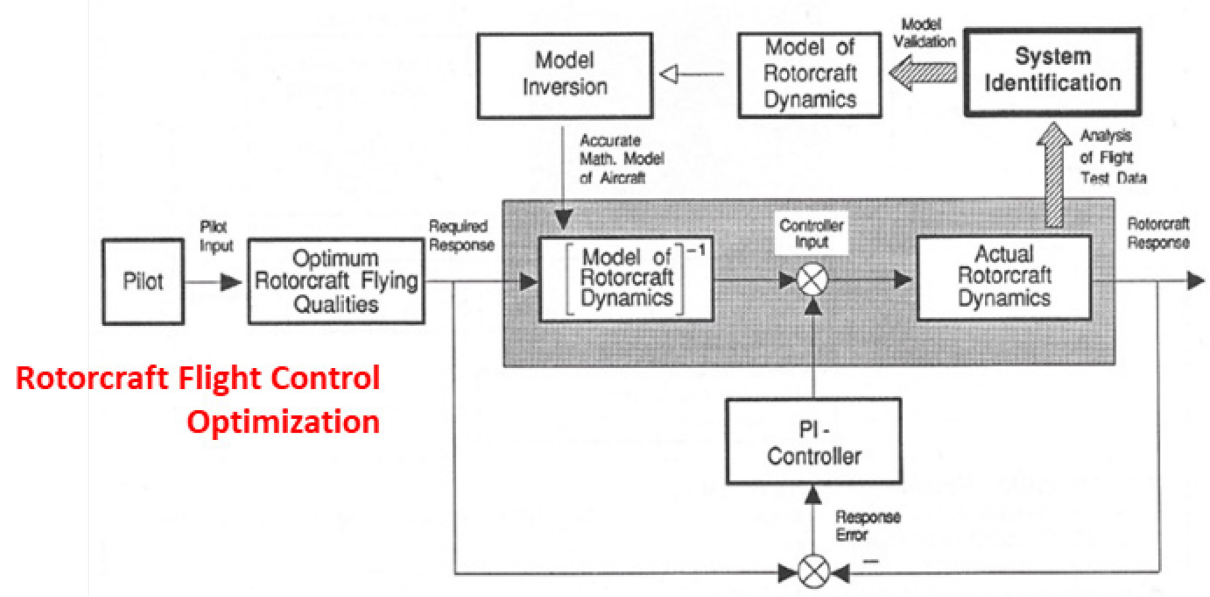

Figure 3-4: System Identification for Rotorcraft Flight Control Optimization.

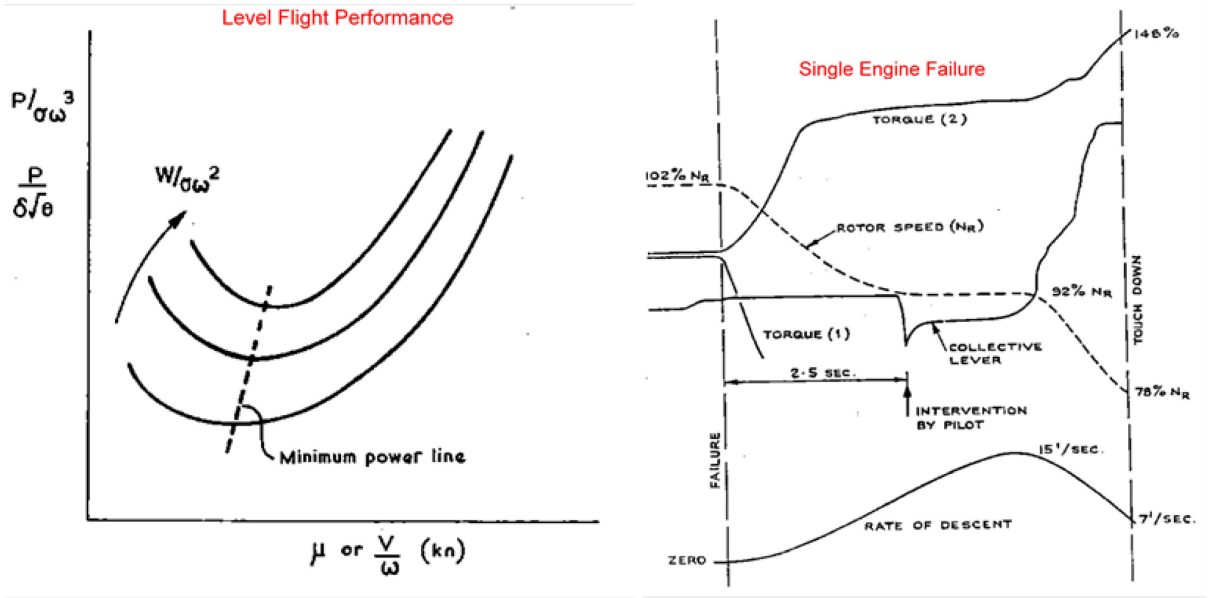

Figure 3-5: Example of Steady-State (Left) and Emergency (Right) Performance Testing Results.

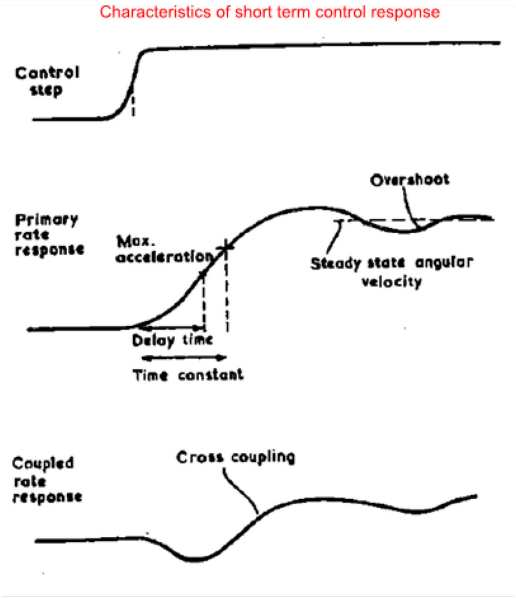

Figure 3-6: Example of Flying Qualities Testing Result.

3.4 GARTEUR ACTIVITIES

The Group for Aeronautical Research and Technology in Europe (GARTEUR) has initiated a number of collaborative activities aimed at improving the predictive capability of rotorcraft modeling since early 1980s. In early 1990s, the advent of ADS-33C standards and their set of discerning flying qualities criteria raised between the European partners a common interest to focus on the modeling of rotorcraft flying qualities. This has been the topic of a series of GARTEUR Action Groups (AG) between 1990 and 2005.

The AG-03 (1990) team introduced the common-baseline-model concept for a Bo105 helicopter, that allowed participants (from industry and research labs in the UK, The Netherlands, France, and Germany) to create their own simulation models and identify shortcomings based on test data provided by the DFVLR (now DLR) Braunschweig.

Although the work of AG-03 was not published in the open literature, it provided a basis for the work of AG-06 (1993), where the prediction of Handling Qualities (HQs) was the focus.

AG-09 (1996) extended this work with the exploration of different forms of validation criteria. As a follow-up activity, AG-12 (2001) undertook a review of the criteria contained in the JAR-STD 1H for helicopter flight simulators and identified various areas where improvements to the standards would be beneficial to safety. Recommendations to develop new metrics for fidelity assessments were also proposed within this action group.

Finally, AG-21 (2017) was established to bring together researchers engaged with the theme of rotorcraft simulation fidelity to examine some of the outstanding issues in this area. The research was conducted through several desktop analyses and real-time piloted simulation. The goal was to determine where gaps exist in simulation fidelity research and to identify areas for new research.

3.5 MAIN FINDINGS

3.5.1 Physics-Based Modeling Improvements

Action Group 09 aimed at improving modeling fidelity for the purpose of predicting helicopter flying qualities. The flight mechanics enhancements investigated were the inclusion of dynamic induced velocities, the wake distortion effect due to hub motion and an improved engine torque transmission system. Figure 3-7 shows the benefit brought by Pitt-Peters dynamic inflow at 80 kts on the on-axis and the cross coupling (pitch-to-roll coupling) responses during a pitch up maneuver.

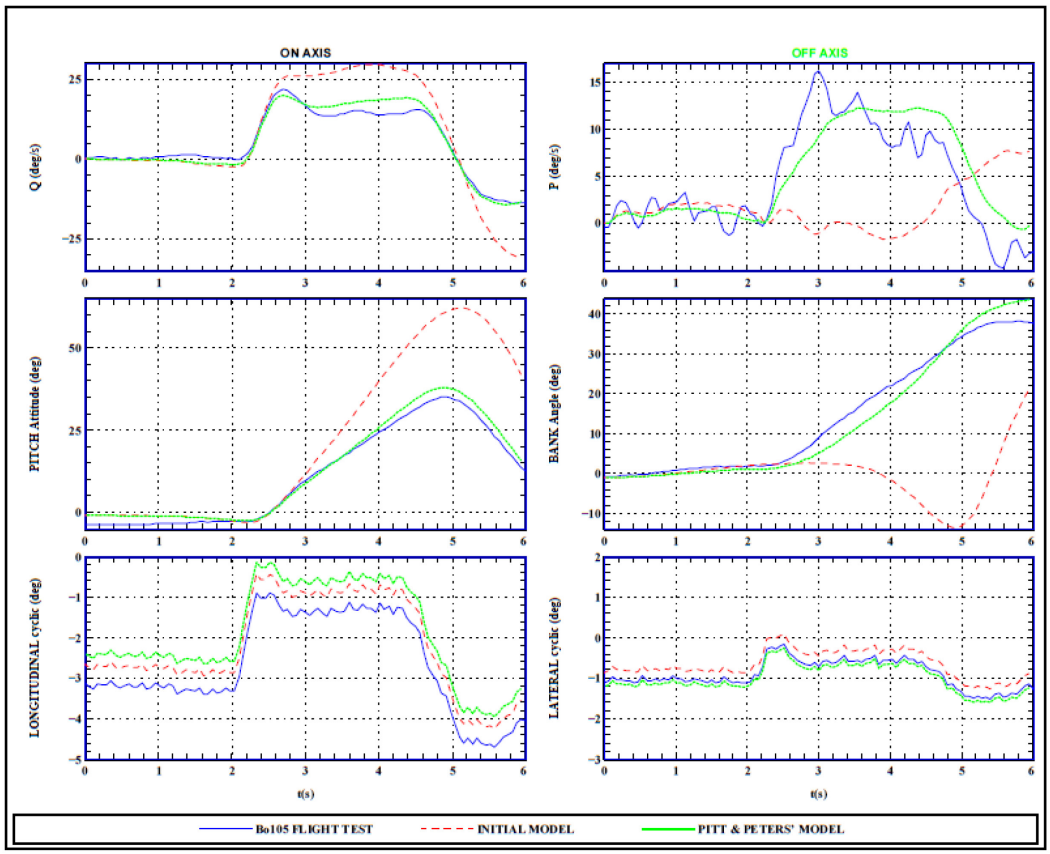

Figure 3-7: Effect of the Dynamic Inflow Model on the Pitch-to-Roll Coupling (80 kts).

If the inclusion of these effects demonstrated a significant enhancement of the physics-based model, they also introduced a new set of parameters which needed to be adjusted to the helicopter type, but also in some cases, to the flight condition. One example is the wake distortion model. Its effect is captured by adding a second term to the inflow model equation. This term is linearly linked to the rotor shaft angular rates $p - \dot{\beta}_s$ *and* $q - \dot{\beta}_c$.

$$[M]\begin{Bmatrix}\dot{\lambda}_0\\ \dot{\lambda}_s\\ \dot{\lambda}_c\end{Bmatrix}+[\hat{L}]^{-1}\begin{Bmatrix}\lambda_0\\ \lambda_s\\ \lambda_c\end{Bmatrix}=\begin{Bmatrix}C_T\\ -C_\ell\\ -C_M\end{Bmatrix}+[\hat{L}]^{-1}\begin{Bmatrix}0\\ K_p\left(p-\dot{\beta}_s\right)\\ K_q\left(q-\dot{\beta}_c\right)\end{Bmatrix} \tag{3-1}$$

Gains *Kp* and *Kq* are the new parameters introduced by this modeling. Figure 3-8 shows their evolution with helicopter forward speed. The use of this model will obviously need an adjustment of these 2 gains to the helicopter type and to the flight speed.

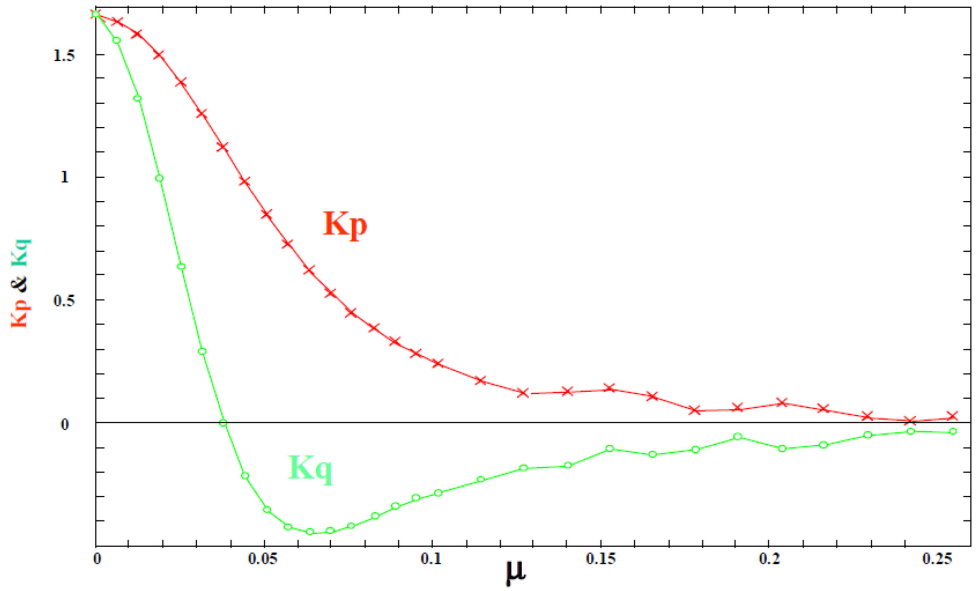

Figure 3-8: Effect of Forward Speed on Wake Distortion Parameters.

3.5.2 Validation Criteria

Another contribution of AG-09 was the extension of the validation criteria as developed in AG-06. A major improvement was obtained by normalizing the criteria, in order to get an unbiased contribution of each parameter in the cost (global error) function.

$$J_T = \frac{1}{N}\sum_{i=1}^{N} Z_T^2(t_i) \tag{3-2}$$

$$Z_T^2(t_i) = \frac{1}{p}\left[\vec{x}(t_i) - \vec{x}_{model}(t_i) - x_{bias}\right]^T X^{-1}(t_i)\left[\vec{x}(t_i) - \vec{x}_{model}(t_i) - x_{bias}\right] \tag{3-3}$$

$\vec{x}$ being the p-dimensional state vector, obtained from measurements, xbias is a bias correction that may be applied and $\vec{x}_{model}$ is the output state from the model prediction. The matrix X allows for (time varying) weighting of the difference between model and measurements.

The scalar J_T can be regarded as the ratio of the model error variance and the allowed inaccuracy of the data when X equals the measurement inaccuracy. Z_T can be assimilated to a normal variate, with zero mean and unit variance. It could be seen as a closeness-of-fit criterion.

The Action Group also investigated a first approach to use the frequency content of the model prediction error. A frequency-domain criterion was developed and partially assessed. The criterion uses the gain and phase errors between the model and the test data, as presented below:

$$J_F = \frac{1}{N}\sum_{i=1}^{N} Z_F^2(\omega_i) \tag{3-4}$$

$$Z_F^2(\omega_i) = \frac{1}{2p}\left[\vec{g}(\omega_i) - \vec{g}_{\text{model}}(\omega_i) - \vec{g}_{\text{bias}}\right] X_g^{-1}(\omega_i)\left[\vec{g}(\omega_i) - \vec{g}_{\text{model}}(\omega_i) - \vec{g}_{\text{bias}}\right] + \frac{1}{2p}\left[\vec{\phi}(\omega_i) - \vec{\phi}_{\text{model}}(\omega_i) - \vec{\phi}_{\text{bias}}\right] X_\phi^{-1}(\omega_i)\left[\vec{\phi}(\omega_i) - \vec{\phi}_{\text{model}}(\omega_i) - \vec{\phi}_{\text{bias}}\right] \tag{3-5}$$

$\vec{g}$ and $\vec{\phi}$ are respectively gain and phase p-dimensional vectors of the frequency response, p being the number of measured parameters. They are calculated for both the model and the real aircraft, based on the available flight tests. Again matrices X_g and X_ϕ allows for weighting the parameters effects between each other.

In order to define statistical boundaries, the probability of χ^2 law (Chi-squared) variates is used. J_F and J_T are related to χ^2 through the following relation, $J_{F,T} = \frac{1}{Np}\chi^2(Np)$, N being the number of samples and p the number of parameters measured. For defined values of probabilities of exceedance (α), the corresponding values for J_F and J_T can be derived.

For Z_T and Z_F the values are based on two-tailed probabilities. Based on these probabilities, Quality-of-Fit indicators are defined using the probability of exceedance values of α.

This approach was applied to some test cases during the AG-09 activities. Figure 3-9 shows the case of a left cyclic pulse maneuver, where both time-domain and frequency-domain criteria were applied to assess the model ability to follow the flight tests bank angle and roll rate.

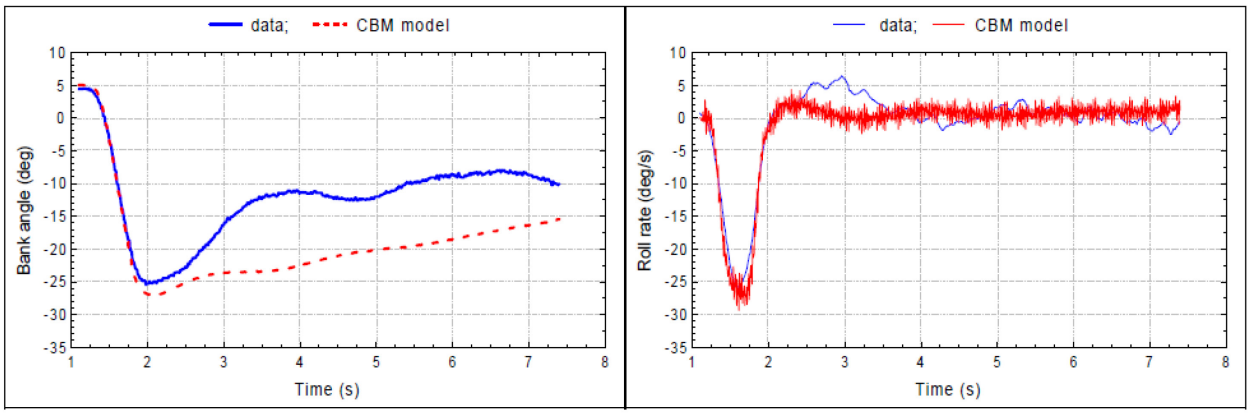

Figure 3-9: Left Cyclic Pulse Response for Bank Angle and Roll Rate vs Time.

The frequency responses of both parameters are presented in Figure 3-10.

Figure 3-11 shows the criteria evolution in time and frequency domains. In frequency domain a maximum allowable error of 10% of the gain and 20 degrees in phase angle was applied. It corresponded to the 95th percentile of the data which was converted to the standard deviation.

One important conclusion of this work was that all the criteria (both in time and frequency domains) were sensitive to the control input types. The control inputs were principally doublets, steps, pulses, and 3-2-1-1. Figure 3-12 shows the sensitivity of the mean value of the time-domain global criteria (J_T) to the input types.

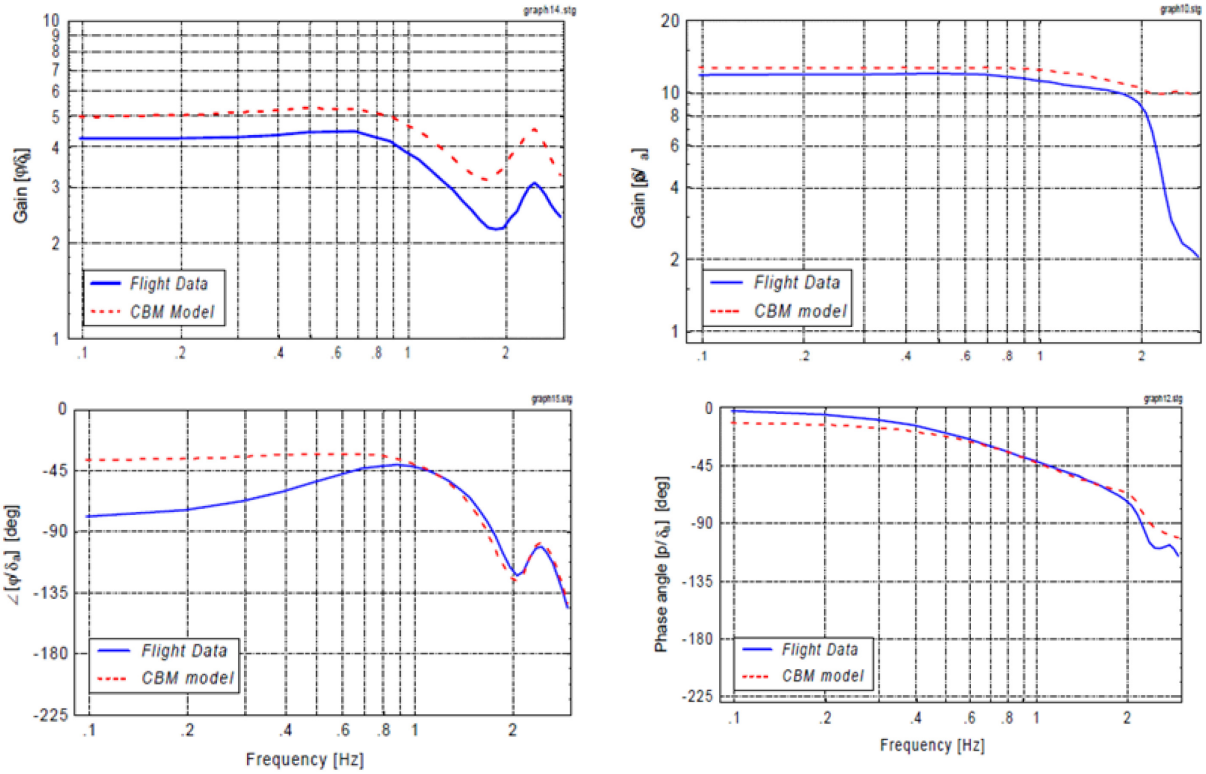

Figure 3-10: Frequency Responses of Bank_Angle/Lat_Cyclic and Roll_Rate/Lat_Cyclic.

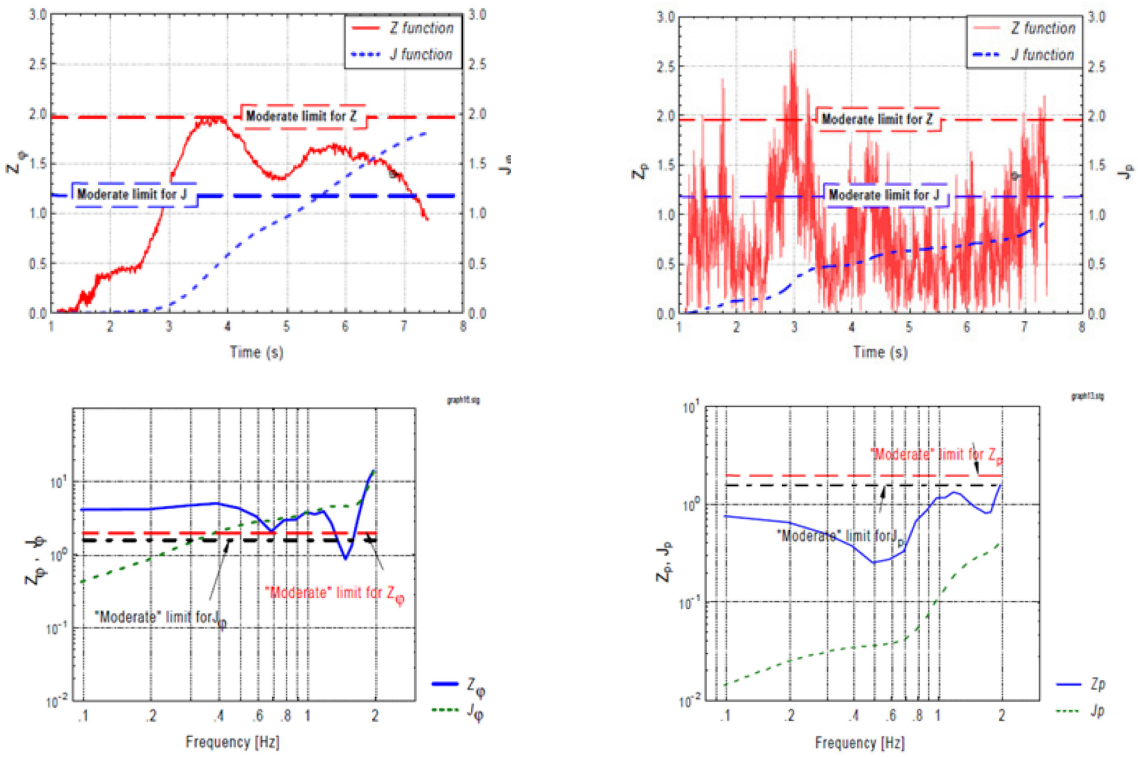

Figure 3-11: "Local" Z and "Total" J Values for Bank Angle (left) or Roll Rate (Right) as Function of Time (Up) and Frequency (Down).

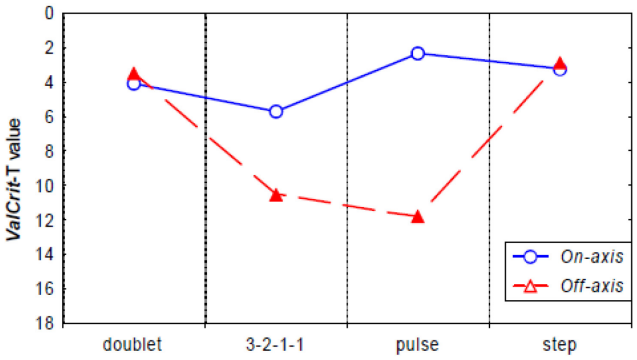

Figure 3-12: Effect of Control Input Type on J_T.

This sensitivity finds its origin in the frequency content of each input. Figure 3-13 shows a comparison of spectral densities of a lateral pulse input versus a lateral doublet. One can see that the energy of the input is differently spread in frequency between the 2 inputs. This shows that the model, but also the real helicopter in flight, will be excited differently whether we use a pulse input or a doublet. Or said otherwise, a good prediction of the model for a pulse input would not guarantee a good predictability for a doublet. The fidelity should be assessed on the full frequency range of the inputs.

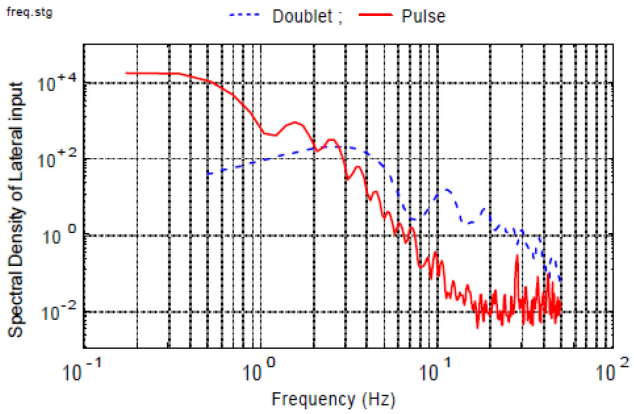

Figure 3-13: Spectral Densities of Lateral Pulse vs Lateral Doublet.

3.5.3 Existing Certification Standards: JAR-STD 1H

As presented above, the first Action Groups (3, 6 and 9), were mainly focusing on modeling support to design and development, and addressed the approaches used to enhance the fidelity of rotorcraft simulations and the criteria to validate the model upgrades. GARTEUR Action Group AG-12 has refocused on real-time simulation models for flight simulators. One main question addressed was whether the tolerances set in the (JARSTD) standard were fine enough that they lead to only minor changes in (ADS-33) handling qualities.

A review of the tolerances and criteria used revealed that the source is largely that developed for fixed-wing applications. The appropriateness to civil or military helicopter missions was, therefore, questionable. Initial industry experience with JAR-STD 1H has been generally positive but has required the development of a comprehensive model (physical) tuning and (non-physical) adjustment process. The physical tuning can achieve a fit, in a general sense, within 80% of the JAR tolerances. The adjustment process is more challenging and can lead to distortions in the model behavior in areas not checked by the JAR criteria.

In JAR-STD 1H, the fidelity of the flight model is assessed, in part, by proof of match time-histories comparing flight and simulation data; the model is deemed 'acceptable' if the model response 'matches' FT within certain tolerances e.g., a match of angular attitudes and velocities within ±10% following a step control input. The work conducted by HC/AG-12 reported that the response metrics in the standards should be re-assessed as there is no historical validation evidence indicating: 1) How they were derived; or 2) Demonstrating relationships between fidelity and the tolerances. AG-12 showed that the relationship is a complex one and sensitive to the nature of the maneuver flown. New metrics derived from the Dynamic Response Criteria (DRC) contained with ADS-33E-PRF were proposed to address some of the shortcomings in the JAR fidelity metrics. To illustrate this, a linear model of a Bo105 in hover was developed and the response to a lateral control input in hover examined. To investigate the sensitivity of the JAR boundaries to changes in the model, parameters in the state matrix 'A' were varied (e.g., the partial derivative of the pitch acceleration with respect to roll acceleration, (element A(11,10)) until the response approached a tolerance boundary. Figure 3-14 shows that changing this cross coupling from its initial value of 1.82 to -5.09 allows the model to just satisfy the JAR fidelity requirements.

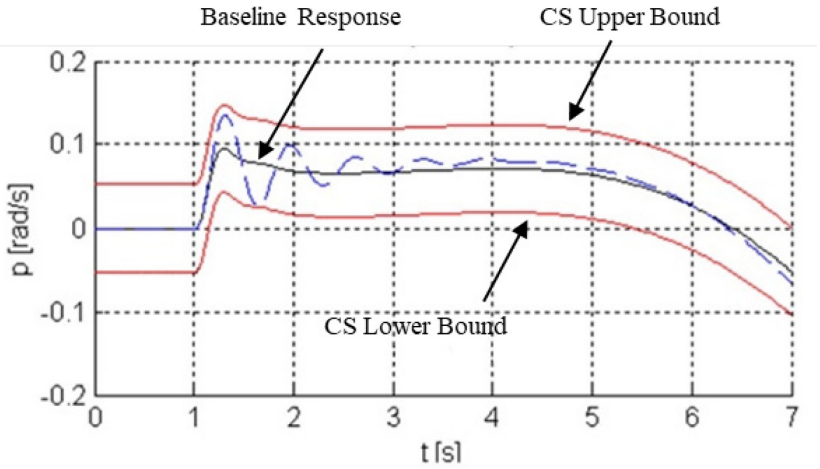

Figure 3-14: Response to Lateral Cyclic Input; Comparison of Baseline Bo105 with Modified Model.

If the model is now examined using the ADS-33E-PRF DRC attitude quickness parameters, the same variations produce a significant change HQs, degrading from Level 1 to Level 3 (see Figure 3-15). Such HQ changes are likely to have a major influence on a pilot's experience of the fidelity of the model and calls into question the validity of the CS boundaries.

These kinds of comparisons are important because they highlight the shortcomings alluded to but also point towards new forms of metric that provide for better fidelity assessment.

The ratio of simulation to flight hours in training is increasing. With more substantiated validation evidence, this trend can continue with confidence and safety and be extended into the LOC-I areas – but only with proven fidelity.

As a conclusion on the tolerances prescribed by JAR-STD 1H, the Action Group highlighted that:

- The relationship between the fidelity and the tolerances is sensitive to the nature of the maneuver performed and the errors in the simulation model. When validating complex and long running maneuver (e.g., the landing maneuver in JAR-STD), the errors introduced by modeling, or the value of discretization used in the control inputs from flight tests, can be very high, making the task of meeting the Level D requirements difficult.

- While there is a general equivalence between the JAR tolerances and handling qualities, in some cases, an aircraft response that ranges across the tolerances can result in quite different ADS-33 handling qualities.

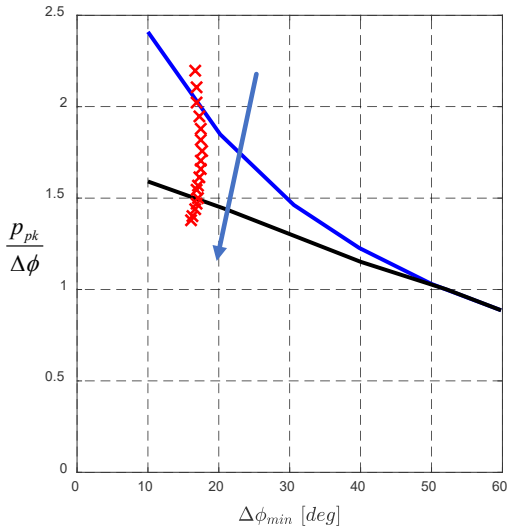

Figure 3-15: Roll Attitude Quickness Criterion for Changes in Element A(11,10), Between Upper and Lower CS Limits.

The Action Group also recommended the use of models of the pilot or aircraft-pilot combination, as a useful source of metrics for measuring simulation fidelity. In one example, the pilot model parameters reflected the errors between flight and simulator. In another, the parameters reflected components of guidance and stabilization control strategy, for which equivalence between flight and simulation is important for high fidelity.

The use of the ADS-33 handling metrics and maneuvers as a supplement to JAR-STD 1H was also suggested as more substantiated framework for model response fidelity.

The sensitivity analyses conducted by the GARTEUR AG have highlighted the need for more substantiation of the criteria and qualification procedures.

3.5.4 Visual Systems – Motion Cueing

Quantifying ‘How good is good enough?’ is key to the assessment of predictive fidelity. AG-12 demonstrated that the current simulator standards would benefit from a review of the tolerances used in defining the acceptable match between flight and simulation. ValCrit-T was found to be a useful metric for quantifying and comparing the relative statistical significance of errors between two models. However, it is not an absolute metric of model quality but could be used to place bounds on acceptable data noise amplitude. The topic of fidelity metrics is ongoing should feature in future research efforts.

The topic of immersion and presence, and their effect on human operations in virtual environments, is a complicated one and extends into different training domains. While there has been significant fundamental research in this area, the findings from this work have not been adopted into defining fidelity requirements in flight simulation environments.

For example, the rotorcraft simulation standard, JAR-STD 1H, states:

> *When evaluating Functions and Subjective Tests, the fidelity of simulation required for the highest Level of Qualification should be very close to the aircraft. However, for the lower Levels of Qualification the degree of fidelity may be reduced in accordance with the criteria contained (within the document).*

This requirement is poorly defined and open to interpretation by the operator and qualifying body. It is suggested that this existing requirement for the subjective aspect of simulator qualification is unsatisfactory and should be improved and that further research is conducted to develop a new methodology to include measures of immersion in the overall fidelity assessment of flight simulators.

Motion cueing research remains an area for debate, new research, and development of fidelity metrics. In AG-21, it was shown that high fidelity motion cueing, judged subjectively by pilots, is achievable with a short stroke motion platform with careful selection of motion algorithm parameters. Steps have been made to rationalize the subjective evaluation process and ratings scales used to provide consistency across experiments. However, there are still challenges to be overcome regarding the design of experiments to show the benefit of motion cueing.

While pilots in one study seemed able to recognize a large degradation in both rotorcraft dynamics and motion, degrading either one of these characteristics yielded less conclusive results. Pilot comments in support of the awarded ratings suggest that pilots are able to perceive and identify crucial characteristics of deficiencies in the simulated environment. However, the awarded pilot ratings and supporting comments were not always found to be in agreement with one another. This suggests further work is required to ensure that the test protocols deliver coherent results and where there are differences.

3.6 REFERENCES

[1] Tischler, M.B., White, M.D., Cameron, N., D'Agosto, S., Greiser, S., Gubbels, A., Guner, F., He, C., Horn, J., Hui., K., Jones, M., Juhasz, O., Lee, O., Lehmann, R., Miller, D., Myrand-Lapierre, V., Nadeau-Beaulieu, M., Nadell, S., Padfield, G., Pavel, M., Prasad, J., Ragazzi, A., Richard, S., Scepanovic, P., Seher-Weiß, S., Soong, J., Stroosma, O., Taghizad, A., Tobias, E., Xin, H., and Yavrucuk, I. (2021), "Rotorcraft Flight Simulation Model Fidelity Improvement and Assessment," NATO STO AVT-296 Technical Report.

Chapter 4 –MODEL FIDELITY ASSESSMENT METHODS AND METRICS

ABSTRACT

Throughout the life cycle of any rotorcraft, flight dynamics simulation models are developed and used for different purposes such as: aircraft design analysis, control system design and development, and trainer certification. Simulation fidelity of such models remains the key for success in application as this ensures: 1) Increased confidence in predictions of aircraft behavior to inform the design processes; 2) Increased efficiency and safety of flight envelope expansion during development process (including through life support); 3) Cost and time savings during qualification and certification processes; and 4) More effective and efficient pilot, crew, and mission training.

This lecture concerns the methods and metrics used for model quality evaluation. Questions will be answered such as, what is model fidelity? and why is this needed? how to measure simulation fidelity? and what are common metrics? what is the process of qualifying the fidelity of helicopter simulators? how to assess the simulator motion cueing fidelity? and what is predicted and perceived simulator fidelity and how can be this assessed?

4.1 INTRODUCTION

Today, simulation is becoming the primary tool for crucial decision-making processes during engineering design, test and evaluation of new systems, safety-critical systems, and the training of people operating these systems. With increasing reliance on simulation results, it is important to know the validity and credibility of simulation results, or in other words, the simulation fidelity. Indeed, fidelity is one of the most important concepts of any model or simulation development, and it is also one of the main cost-drivers of aircraft development. As a general rule, the higher the fidelity the more time and resource consuming the simulation development is. Thus, being able to state what level of fidelity is exactly required avoids unnecessary investments, superfluous simulation components, and unusable simulation.

4.2 MAXIMUM UNNOTICEABLE ADDED DYNAMICS (MUAD) AND ALLOWABLE ERROR ENVELOPES (AEE)

4.2.1 Maximum Unnoticeable Added Dynamics (MUAD)

The overlay of flight-test and simulation frequency responses is a direct and efficient means to validate model fidelity and assess model improvements. After making modifications to the simulation model, the comparison is repeated to determine whether the validity of the model has been improved. The simulation model accuracy for each frequency-response pair can also be characterized in terms of the error response function $\varepsilon_{\text{model}}(f)$ defined as:

$$\varepsilon_{\text{model}}(f) \equiv T(f)/\hat{T}_{\text{c}}(f) \tag{4-1}$$

where the frequency response for simulation denoted as T, and the associated flight-test data frequency response is denoted as $\hat{T}_{\text{c}}$ [1]. In terms of the magnitude (dB) and phase (deg) responses,

$$\text{Mag}_{\text{err}}(f) = (|T| - |\hat{T}_{\text{c}}|) \tag{4-2}$$

$$\text{Phase}_{\text{err}}(f) = (\angle T - \angle \hat{T}_{\text{c}}) \tag{4-3}$$

where an error function with 0-dB magnitude and 0-deg phase indicates perfect tracking of the flight and simulation results. The magnitude and phase of the error response functions for the XV-15 GTR simulation model in cruise are shown as the dashed curves in Figure 4-1 from Tischler and Remple [1]. Also shown in the figure as the solid curves are boundaries that correspond to limits on MUAD, beyond which a pilot will detect a deviation in the aircraft model compared to flight [2], [3]. These boundaries are used in the fixed-wing handling qualities criteria of the USAF MIL-STD-1797B [4] to evaluate the mismatch between an actual aircraft response and a Lower-Order Equivalent System (LOES) model. The equations for the MUAD boundaries [2] are shown in the figure. If the error functions fall within these boundaries, then the simulation model response would be judged by a pilot as being indistinguishable from the actual flight response, thereby providing a good basis for simulation model fidelity assessment. Tischler [5] first proposed the use of the MUAD boundaries for simulation model fidelity assessment and FAA Level D simulation fidelity criteria. The same approach of mismatch boundaries in the frequency domain was also independently proposed and applied by DLR researchers to detect the effects of unnoticeable dynamics in the case of helicopters [6] and for evaluating the fidelity of in-flight simulation [7]. A good overview on low-order equivalent systems was presented by Hodgkinson et al. [8]. More recent research by Mitchell et al. [9] supports these boundaries as useful for evaluating rotorcraft simulation fidelity as well.

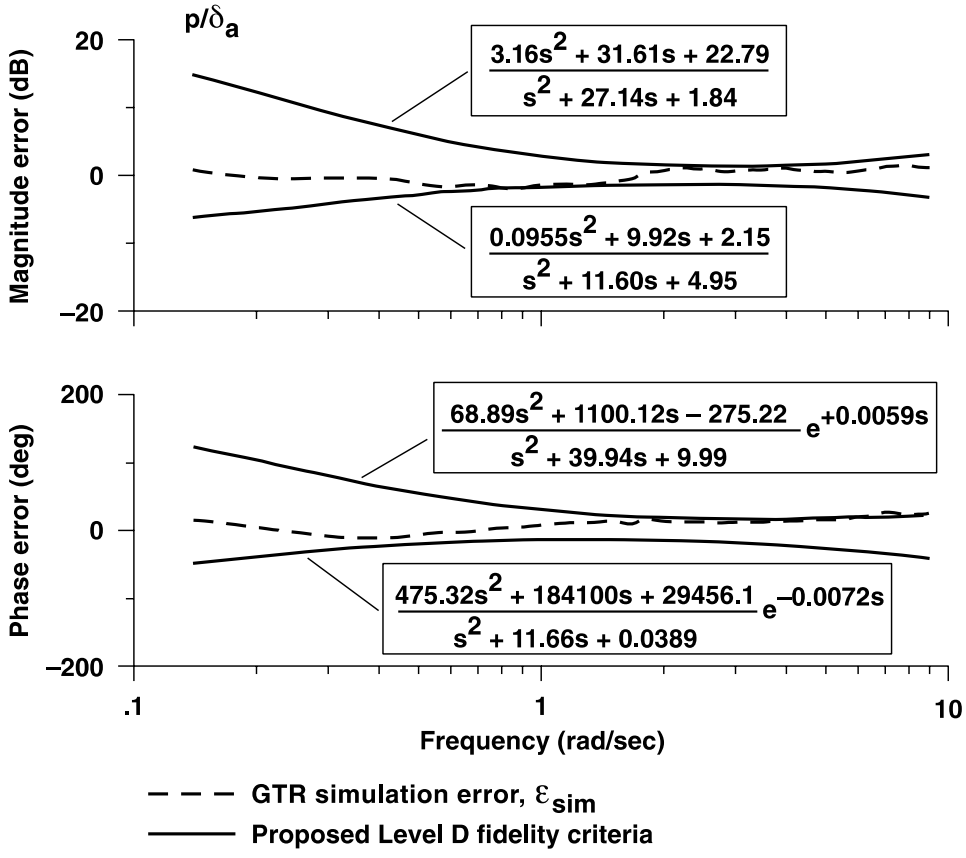

Figure 4-1: XV-15 Cruise Error Functions and MUAD Bounds [2].

4.2.2 Allowable Error Envelopes (AEE)

In 2006 Mitchell et al. [10] verified the application of MUAD to military simulators certification. The MUAD envelopes, as described previously, were developed to define limits on unnoticeable added dynamics from a fixed-wing airplane database. Given that the envelopes have been proposed for simulation validation, Mitchell et al. [10] applied MUAD for validation of military helicopter simulators. It was concluded that the

concept of MUAD and added dynamics should be carefully implemented in the case of helicopter simulator validation. The envelopes describing Maximum Unnoticeable Added Dynamics although still generally ubiquitous when applied to simulation validation, in the case of helicopter roll tasks, added dynamics were still unnoticeable to the pilot. The new goal of Mitchell et al. [10] was thus to identify a set of frequency-domain envelopes defining the boundary between unnoticeable and noticeable dynamics. These envelopes are referred to as 'Allowable Error Envelopes' (AEE), to distinguish them from the MUAD envelopes, and to more accurately reflect their ultimate purpose, i.e., to define the allowable errors in simulation validation.

Based on MUAD envelopes for simulation validation, Mitchell et al. [10] developed the so-called 'Allowable Error Envelopes (AEE)' defined as 'boundaries between unnoticeable and noticeable dynamics.' The idea was that, as pilots cannot evaluate what they cannot see, variations of parameters that caused change in frequency response within envelope could not be meaningfully evaluated. The AEE envelopes could be used to:

- Determine whether the mathematical simulation model is adequate; or
- Determine whether a simulation facility is adequate to accomplish proposed evaluations.

It was foreseen that the AEE envelopes would probably be larger for fixed-base simulators than for moving-base simulators and that the smallest envelopes were to be expected for in-flight simulator. Therefore, AEE should be developed separately for fixed-base piloted simulations, moving-base piloted simulations and for in-flight piloted simulations.

Figure 4-2 shows some AEE proposed boundaries plotted against the MUAD boundaries.

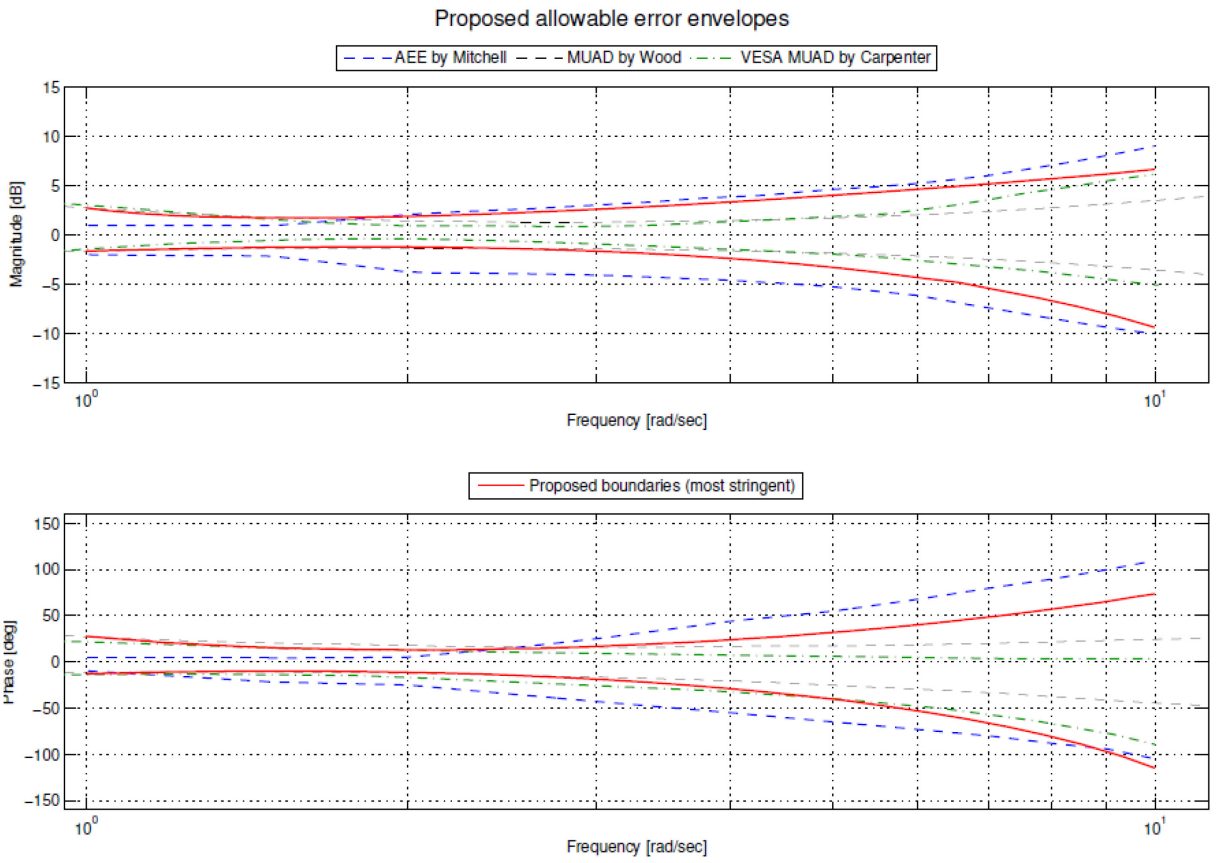

Figure 4-2: Allowable Error Envelope as proposed by Mitchell et al. [11] (Blue) and in Penn [12] (Red), MUAD envelope as proposed by Wood et al. [13] (black dotted line) and VESA MUAD envelope as proposed by Carpenter et al. [14] (green).

4.3 MODEL/FLIGHT DATA MISMATCH AND INTEGRATED COST FUNCTIONS

Single integrated metrics are useful measures of the overall precision of the simulation model. The frequency domain metric J_{ave} indicates the overall integrated cost function based on the comparison of the simulation model and flight-test frequency responses. The time-domain metric J_{rms} indicates the overall integrated cost function for responses to a control input.

4.3.1 Frequency-Domain Integrated Cost Function, J_{ave}

A frequency-domain metric useful for assessing the fidelity of a simulation model frequency response as compared to flight data for a Single Input/Single-Output (SISO) frequency-response pair (e.g., p/δ_{a}, q/δ_{e}, etc.) at a particular flight condition was originally proposed by Hodgkinson and fully covered in Ref. [2] based on the weighted sum of magnitude and phase squared errors:

$$J = \frac{20}{n_\omega} \sum_{\omega_1}^{\omega_{n_\omega}} W_\gamma [W_{\text{g}} (|\hat{T}_{\text{c}}| - |T|)^2 + W_{\text{p}} (\angle \hat{T}_{\text{c}} - \angle T)^2] \tag{4-4}$$

where:

$\|\ \|$	=	magnitude (dB) at each frequency ω.
$\angle$	=	phase (deg) at each frequency ω.
n_ω	=	number of frequency points (typically selected as $n_\omega = 20$).
ω_1 and ω_{n_ω}	=	starting and ending frequencies of fidelity assessment (typically covering 1 – 2 decades).

By selecting the n_ω frequency points ω_1, ω_2, …, ω_{n_ω} with a uniform spacing on a log-frequency scale (rad/s), the fidelity metric or cost (J) well reflects the error as displayed on the Bode plot.

W_{g} and W_{p} are the relative weights for magnitude and phase squared errors. The normal convention from USAF MIL-STD-1797B [4] is to use the values $W_{\text{g}} = 1.0$ and $W_{\text{p}} = 0.01745$. This choice of weighting means that a 1-dB magnitude error is comparable with a 7.57-deg phase error. However, the fidelity metric is largely insensitive to the exact choice of these weighting values.

Tischler and Remple [1] also included function W_γ to weight the fidelity metric more heavily when the flight data is more reliable as determined from the coherence function at each frequency ω:

$$W_\gamma(\omega) = [1.58(1 - e^{-\gamma_{xy}^2})]^2 J = \frac{20}{n_\omega} \sum_{\omega_1}^{\omega_{n_\omega}} W_\gamma [W_{\text{g}} (|\hat{T}_{\text{c}}| - |T|)^2 + W_{\text{p}} (\angle \hat{T}_{\text{c}} - \angle T)^2] \tag{4-5}$$

For a coherence of $\gamma_{xy}^2 = 0.6$, this function reduces the weight on the squared errors by 50%. As a guideline for simulation fidelity and based on extensive experience, Tischler and Remple [1] proposes that a cost function of

$$\textit{Guideline: } J \leq 100 \tag{4-6}$$

generally, reflects an acceptable level of accuracy for flight-dynamics modeling and reflects a good simulation model response for rotorcraft. A cost function of $J \leq 50$ can be expected to produce a model that is nearly indistinguishable from the flight data in the frequency domain and time domain.

Tischler and Remple [1] generalized the SISO cost function for a Multi-Input/Multi-Output (MIMO) matrix of output/input frequency-response pairs for the simulation model $T(s)$ and flight data $\hat{T}_c$. The associated overall fidelity metric at the same flight condition is a direct extension of the SISO formulation of Equation 4-4 and is now simply the summed cost for the n_{TF} transfer functions:

$$J = \sum_{l=1}^{n_{TF}} \left\{ \frac{20}{n_\omega} \sum_{\omega_1}^{\omega_{n_\omega}} W_\gamma [W_g (|\hat{T}_c| - |T|)^2 + W_p (\angle \hat{T}_c - \angle T)^2] \right\}_l \tag{4-7}$$

In most cases, the matrix of flight-test responses will not have good data for several of the theoretically possible input-to-output combinations, as indicated by poor coherence for the entire frequency range of interest. Such responses are dropped entirely from the cost function. So only a subset n_{TF} of the frequency-response pairs will be included in the cost function. The frequency-response pairs retained in the identification are denoted by T_l, l = 1, 2, 3, …, n_{TF}. The choice of frequency range (ω_1, ω_{n_ω}) is made separately for each response pair T_l, corresponding that pair's range of acceptable coherence.

The accuracy of the identified model is best characterized by the average overall cost function or *integrated cost function*:

$$J_{ave} = \frac{J}{n_{TF}} \tag{4-8}$$

The weighting functions W_γ, W_g, and W_p all retain the same definitions as in the SISO formulation and are evaluated at each frequency point (ω_1, ω_2, …, ω_{n_ω}) for each frequency-response pair T_l.

The interpretation of the MIMO fidelity metric extends directly from the SISO case, where an overall average cost function that achieves

$$\textit{Guideline:} J_{ave} \leq 100 \tag{4-9}$$

generally, reflects an acceptable level of accuracy for flight-dynamics modeling and is typical of rotorcraft. Some of the individual cost functions, especially for the off-axis responses, can reach the guideline of

$$\textit{Guideline:} J_l \leq 150 \text{ to } 200 \tag{4-10}$$

without resulting in a noticeable loss of overall predictive accuracy.

4.3.2 Time-Domain Integrated Cost Function, J_{rms}

The time-domain integrated cost function J_{rms} is useful for assessing the predictive accuracy for a short-term doublet input, typically about 5 sec. The simulation response is determined from direct numerical integration of the equations of motion of the simulation model using measured control inputs from the flight data. The simulation model outputs are compared with the flight-data measurements and should not include reconstructed signals. The integrated time-domain cost function is determined from Tischler and Remple [1]:

$$J_{rms} = \sqrt{\left(\frac{1}{n_t \cdot n_o}\right) \sum_{i=1}^{n_t} [(y_{data} - y)^T (y_{data} - y)]} \tag{4-11}$$

where:

y_{data} = time-history measurement vector from the flight data.

y = simulation model time-history response vector.

n_{t} = number of time-history points in the time history data record.

n_{o} = number of outputs (measurement signals) in the time history vector, y.

A good rule of thumb is to select the units of the measurement vector for SI units as

$$\text{deg, deg/sec, m/sec, m/sec}^2 \tag{4-12}$$

and for English units as

$$\text{deg, deg/sec, ft/sec, ft/s}^2 \tag{4-13}$$

Experience shows that a J_{rms} value in the range of [1]

$$J_{\text{rms}} \leq 1.0 \text{ to } 2.0 \tag{4-14}$$

which generally reflects an acceptable level of accuracy for flight-dynamics modeling when the error function is calculated based on the units of Equation 4-12 or Equation 4-13.

4.4 SIMULATOR FIDELITY

When trying to define the fidelity in the context of simulation, it appears that there is a wide variety of definitions for the term fidelity. Almost every paper provides its own definition for several or all the following fidelity related terms: accuracy, error, granularity, resolution, precision, tolerance, validity, model, and simulation. Additionally, many connotations for the term fidelity are encountered in literature, such as functional fidelity, physical fidelity, attribute fidelity, abstract fidelity, and concrete fidelity. This variety of terms illustrates that there still does not exist a clear practical and common agreed terminology for fidelity as well as other modeling and simulation terms in general.

Fidelity in piloted simulation according to the NASA's ad hoc Advisory Subcommittee on Avionics, Controls, and Human Factors (1979) [15] is defined as 'the degree to which characteristics of perceivable states induce realistic pilot psychomotor and cognitive behavior for a given task and environment.' Fidelity in this sense relates primarily to the effect upon the pilot – not to the effective aircraft dynamics – although both aspects are necessarily involved.

Using the fidelity concept as applied to the simulator device, Heffley et al. [16] defined fidelity as 'the simulator's ability to induce the pilot trainee to output those behaviors known to be essential to control and operation of the actual aircraft in performance of a specific task.'

According to Hays (1989), fidelity should be defined in terms of domain of interest, relative to something and in a measurable form. A training simulation domain-oriented definition for fidelity is 'the degree of similarity between the training situation and the operational situation, which is simulated'. Fidelity is presented here as a 2-dimensional measurement in physical and functional characteristics. Physical characteristics address aspects like look and feel while functional characteristics address aspects such as the informational, operational knowledge and stimulus and response options. Fidelity is thus characterized as a summarizing descriptor of the overall training device characteristics and trained scenarios.

Lane (1992) defines fidelity as an engineering concept referring to 'the physical correspondence of the simulator's hardware and software to that of the actual equipment being simulated.' He remarks that implementing 'all you can afford' levels of fidelity in a simulation are not always the most correct and cost-effective approach to address the problem of how much fidelity is required for a specific purpose.

Pace (2015) definition for fidelity dating back to his work on fidelity in 1992 is 'the degree of exactness of a model or simulation representation when compared to the real world.' According to Pace, simulation fidelity is an absolute concept while simulation validity is a relative concept, dependent upon the simulation application.

Fidelity is defined by Gross (1997) as "the extent to which a model reproduces the referent along one or more of its interests" (N.A. referent is an authoritative description of reality in the context of high-level architecture simulation). To characterize fidelity, Gross uses three classifications: 1) Existence (which object of the referent exists in the model); 2) Attributes (which object attributes of the referent exist in the model); and 3) Behavior (what object behavior of the referent is included in the model).

McDonald (1998) defines fidelity as 'the accuracy of representation when compared to the real world.' This fidelity has two major parts: the extent to which the simulation models each aspect of the real world and the agreement between the performance of each modeled aspect and the real performance.

Meyer's (1998) perspective on fidelity definition is to outline four terms for describing simulation goodness, i.e.: 1) Detail describing the measure of the completeness/complexity of the model w.r.t. the observable characteristics of the physical entity; 2) Accuracy as related to the exactness of the model w.r.t. the observable characteristics and behaviors of the physical entity; 3) Resolution defined as a measure of the minimum degree to which the accuracy and detail of the constituent models must coincide with the required level of fidelity of the simulation; and 4) Fidelity as related to the agreement of a simulation with perceived reality.

Roza (2005) proposed a unified fidelity framework in which a formal mathematical definition for fidelity is formulated as 'the inverse difference between the reality and simulated reality.' Concluding, fidelity is 'an intrinsic element of any simulation system, one that all simulation developers and users have to deal with one way or the other'.

This lecture will use the concept of fidelity as related to simulator's fidelity. In this sense, fidelity is the simulator's ability to mimic the vehicle's flight. Figure 4-3 presents the concept of fidelity as related to the simulator. In the real world, the pilot assesses the vehicle orientation by using his/her visual, vestibular, tactile, and aural sensors, integrating all the signals into his/her central nervous system, and using his/her hands, feet, posture, and voice as motor mechanisms to finally control the vehicle.

In the simulated world, likewise, for a certain task assigned, the pilot used the simulator cueing elements (ex. visual, motion, control loading cueing) and the vehicle model to mimic the vehicle's flight and achieve a task performance. Fidelity in the simulated world refers to: 1) Objective fidelity (also called predictive fidelity and physical fidelity) involving a series of 'predictive' metrics for flight model fidelity (physical fidelity) but also for other simulator's components; and 2) Subjective fidelity (also called perceptual or behavioral fidelity) involving the subjective opinion of the assessing pilot, which is always a combination of the complete system.

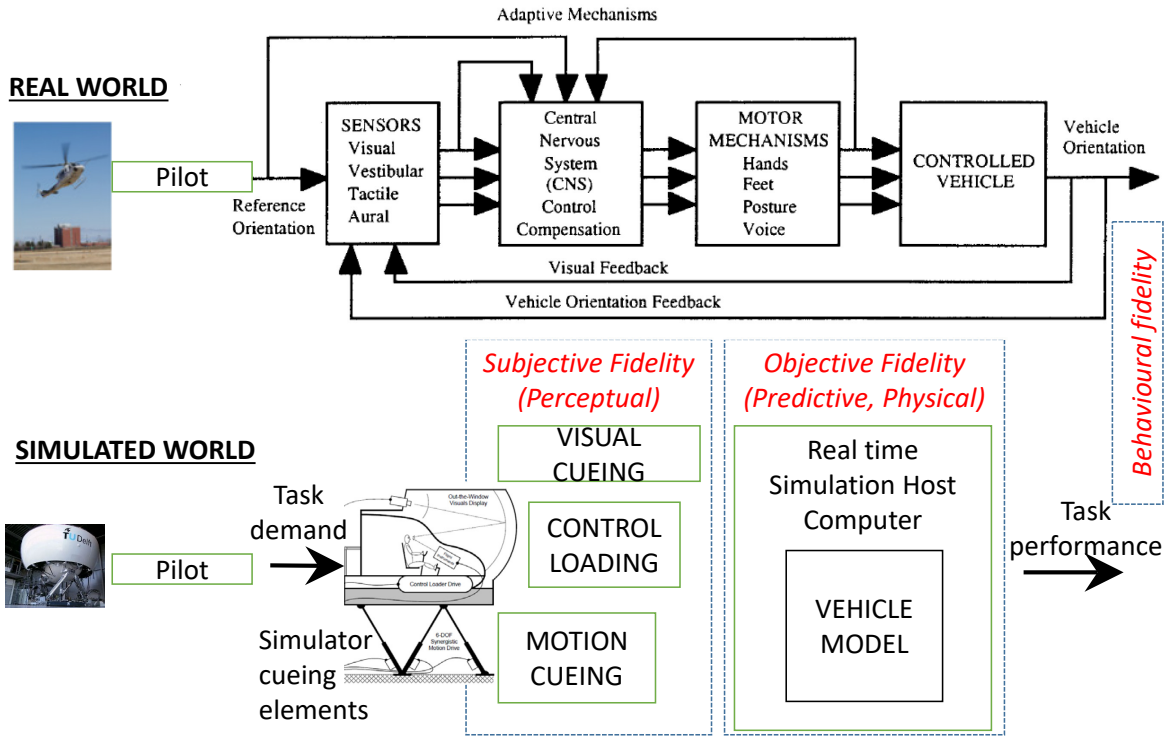

Figure 4-3: Fidelity Concept as Related to the Simulator Device.

4.5 MOTION PERCEPTION, CUEING, TUNING, AND EVALUATION

If a helicopter simulation model is not only used for analysis, but also in a pilot-in-the-loop simulator, any model fidelity deficiencies might be masked or exacerbated by the simulator's cueing systems. While outside visual, instrument, and force feel cueing systems usually distort the helicopter's dynamics with little more than a time delay, a simulator's motion system can introduce more elaborate distortions of the perceived helicopter dynamics. This is caused by the inherently limited motion space of a ground-based simulator and the motion cueing algorithms that are necessarily deployed to transform the model's motion cues into physical motions of the simulator.

In general, a human pilot's vestibular system is sensitive to the specific forces and rotational rates or accelerations of the helicopter. Similar to an accelerometer, a human directly perceives the aerodynamic, engine, and landing gear forces acting on the helicopter. These cues play a number of roles in a piloted simulation: Motion cues help create an immersive virtual environment that elicit realistic pilot behavior.

The motion base's cueing algorithm that converts the simulated vehicle's cues to simulator motions, must achieve two competing goals:

- Provide realistic cues to the pilot; and
- Keep the simulator in the available motion space.

A wide range of motion algorithms and cueing methods exist. A standard method is to employ **high-pass** filters, both in rotational and translational axes. This means that for frequencies that the filter (starts to) attenuates the motion, a phase **lead** is present. The parameters used in the motion cueing algorithm (which essentially define the phase and gain cueing) can significantly affect the simulator's motion fidelity. The freedom is, of course, limited by the available motion envelope of the platform (governed by design and size), and the detrimental effects of false cues inherent to the algorithm.

Despite the continued use of motion in flight simulation, there is no consensus regarding the correct tuning methodology. A combination of objective and subjective techniques is used to assess the fidelity of simulator's motion system as a whole. The application of assessment techniques varies based upon the application, predominantly for regulatory or research purposes. In both Europe (EASA) and the USA (FAA) specific requirements are given to assess the suitability of simulation devices for pilot training aspects (European Aviation Safety Agency [17], Federal Aviation Administration [18]). Taking the example of the EASA guidance, for helicopters, these cover three broad areas; hardware and software capablilities (through robotic tests), repeatability, and vibrations. However, it is acknowledged that the current test pracitises do not explicitly show the capability of the system to adequate cue the pilot. It is stated, 'until there is an objective procedure for determination of the motion cues necessary to support pilot tasks and stimulate the pilot response that occurs in an aircraft for the same tasks, motion systems should continue to be "tuned" subjectively' [17]. Considering the high quality of modern motion base hardware, the largest phase and gain errors in the perceived motion cues are now caused by these unregulated algorithms, which leaves the motion cueing errors largely outside of regulatory control.

A number of additional techniques to objectively quantify motion cueing quality have been proposed from various research efforts. Here an overview of some of the methods often used is given, supplemented with some recent work to illustrate directions of research currently being explored. A more elaborate overview is provided by Jones [20]. These include gain and phase motion requirements developed by Sinacori and Schroeder in the 1970s and 1990s, respectively. More recently, these principles have been extended through observation across the operational frequencies of the motion platform through the development of the Objective Motion Cueing Test (OMCT) [21]. Figure 4-4 shows an example of the fidelity boundaries for the roll axes. Efforts are ongoing to further validate these boundaries both for fixed and rotary-winged aircraft.

Studies reported in Refs. [22], [23] and [24] suggested large differences between perceived motion fidelity and current objective fidelity using Sinacori/Schroeder boundaries. Both studies found beneficial and representative motion was attained when performing typical mission task elements performed by rotorcraft. It was found that large discrepancies exist between OMCT and Schroeder fidelity boundaries. As a result of these discrepancies, further research is required in this area prior to the adoption of OMCT as an objective method to assess rotorcraft training simulators.

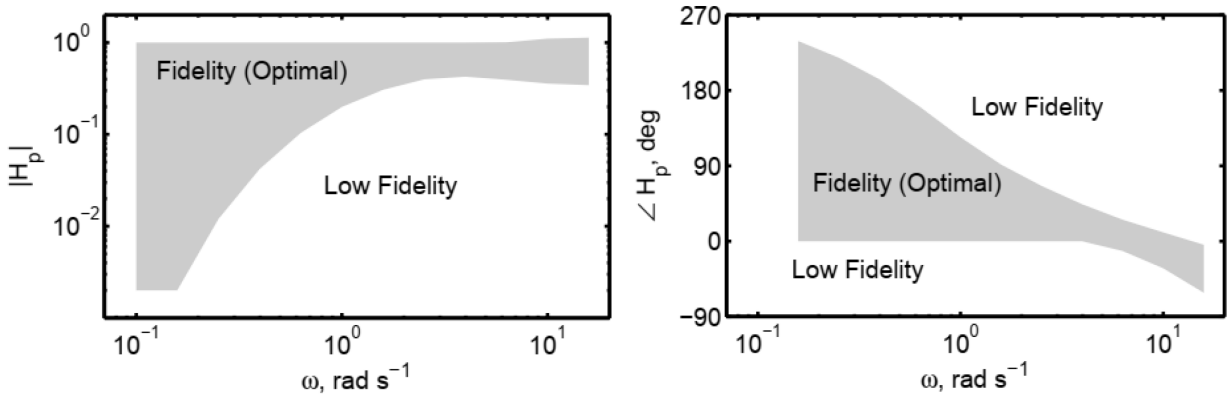

Figure 4-4: Example of OMCT Fidelity Boundaries, Roll Motion Gain and Phase [21].

As stated above, particularly for training simulators and from the view of the regulator, there is a reliance upon subjective opinion. To assure acceptability of a flight simulator for either engineering or training purposes, the end user's subjective assessment of its fidelity cannot be ignored. In addition, many of the objective motion cueing quality metrics have been validated by expert pilot opinion with varying levels of success. Pilot opinion still remains the standard against which motion cueing quality is measured.

To standardize and streamline subjective assessments, a number of techniques have been proposed. These range from simple classification, linear scales, and decision trees. The use of the subjective assessment scale depends on the intended outcome and information required. As with the objective fidelity, there is no consensus on the best method to use.

One way to look at the severity of model gain and phase errors is the concept of MUADS/AEE, discussed previously. The noticeability of model errors by a pilot might change depending on the characteristics of the simulator used, the flying task, pilot strategy, or some feature of the baseline model. It is highly likely that at least some of the differences he found in the MUAD boundaries between the simulators, can be attributed to the influence of the presence of motion cueing on the SRS.

The lack of consensus regarding the objective motion boundaries and methods leads to difficultly both tuning and establishing a baseline for 'good' motion cueing. Whilst early methods are well established and easy to apply, they do not capture characteristics of modern motion systems. Particularly the visual cueing offers 'motion cues' far surpassing those used to define original criteria. Recent efforts have sought to bridge this gap, however there is significant work still to perform to achieve acceptable motion boundaries for rotorcraft.

4.6 INTEGRATING PREDICTED AND PERCEIVED SIMULATOR FIDELITY ASSESSMENT. SIMULATION FIDELITY RATING SCALE

The evaluation of the fidelity of a simulation device for flight training typically includes a series of quantitative requirements contained within simulator qualification documents such as EASA CS-FSTD(H) [17] or FAA 14 Part 60 [25]. These quantitative requirements examine the response or behavior of the individual elements of a simulation device – the visual system, the motion platform (if so equipped), the flight dynamics model, etc. – to a set of predetermined inputs. The results of these tests are typically termed 'engineering fidelity' and only partially serve to characterize the utility of a simulator. The implicit assumption in tests of engineering fidelity is that a strong quantitative match of simulator component systems with the flight vehicle will assure a high degree of simulator utility. Experience has shown that this assumption is not always valid, and that tests of engineering fidelity are insufficient to guarantee a sufficiently accurate simulation. Hence, the qualification standards require a piloted, subjective assessment of the simulation in addition to the quantitative elements. Hence, the Simulation Fidelity Rating (SFR) [26] was developed at the University of Liverpool in collaboration with the National Research Council of Canada to provide a repeatable, prescriptive method for the subjective assessment of fidelity into the overall qualification process.

The SFR scale should be used to complement and augment the existing simulator evaluation processes of CS-FSTD(H) and other applicable simulator qualification processes. It is proposed that the SFR scale may be used as part of a fidelity evaluation methodology based on the use of engineering metrics for both the prediction of the fidelity of the individual simulator components (flight model, motion platform, visual system, etc.) [26] and the assessment of the perceptual fidelity of the integrated simulation system, as experienced by the pilot.

The SFR scale employs several key concepts that are considered fundamental to the utility of a simulation device. They are as follows:

- Transfer of Training (ToT) – the degree to which behaviors learned in a simulator are appropriate to flight.
- Comparative Task Performance (CTP) – comparison of the precision with which a task is completed in-flight and simulator.
- Task Strategy Adaptation (TSA) – the degree to which the pilot is required to modify their behaviors when transferring from simulator to flight and vice versa.

The relationship between task performance and strategy adaptation is similar to that between performance and compensation in a handling qualities evaluation. In the Handling Qualities Rating (HQR) scale [26], the expectation is that the pilot's perception of deteriorating performance will stimulate higher levels of compensation, indicative of worsening Handling Qualities (HQ). While this correlation can be expected in measuring HQ, in the context of fidelity assessment task performance and adaptation will not necessarily change in correlation with each other but will instead depend on the nature of the fidelity deficiencies present in a simulator.

A matrix presenting all possible combinations of comparative performance and task strategy adaptation was constructed (Figure 4-5); this was used to form the basic structure of the SFR scale (Figure 4-6).

Each of the ratings SFR=1 to SFR=9 corresponds to a region in the fidelity matrix. An SFR=10 rating indicates a simulation that is entirely inappropriate for the purpose, and so comparisons with flight cannot be made. As with the HQR scale, boundaries have been defined between the potential combinations of comparative performance and adaptation, reflecting value judgements on levels of fidelity. As the SFR worsens through each level, it can be seen that the individual comparative performance and adaptation measures may not degrade in a progressive manner. However, the intention is that the overall 'experience' of the simulation fidelity degrades progressively as the SFR worsens.

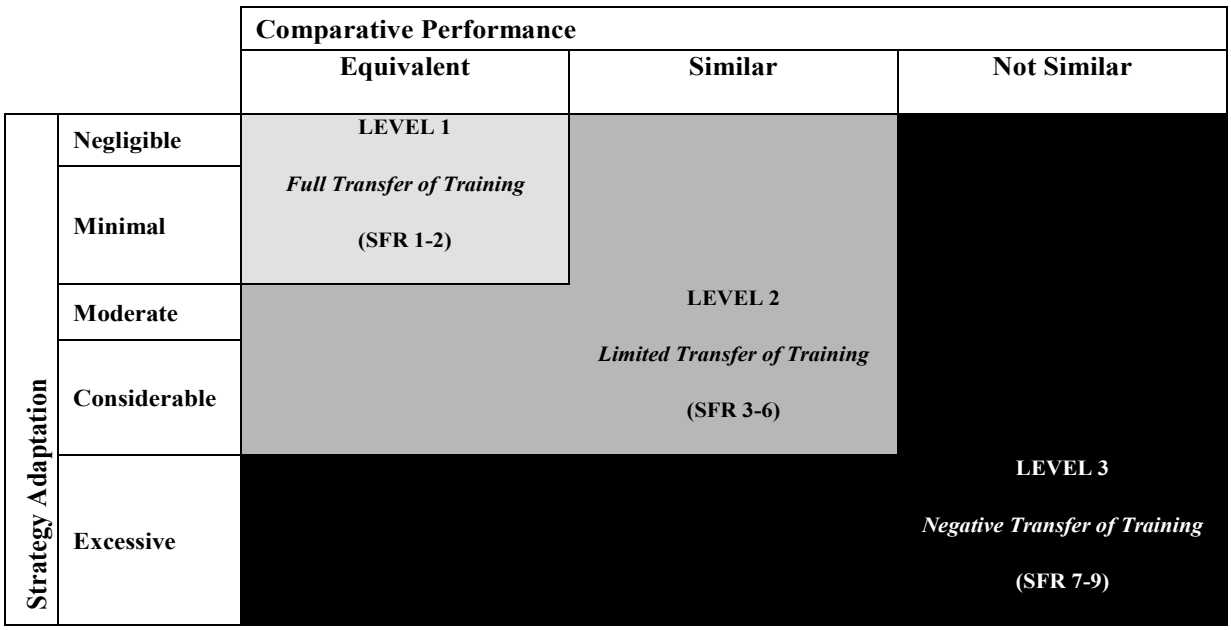

Figure 4-5: SFR Fidelity Matrix [26].

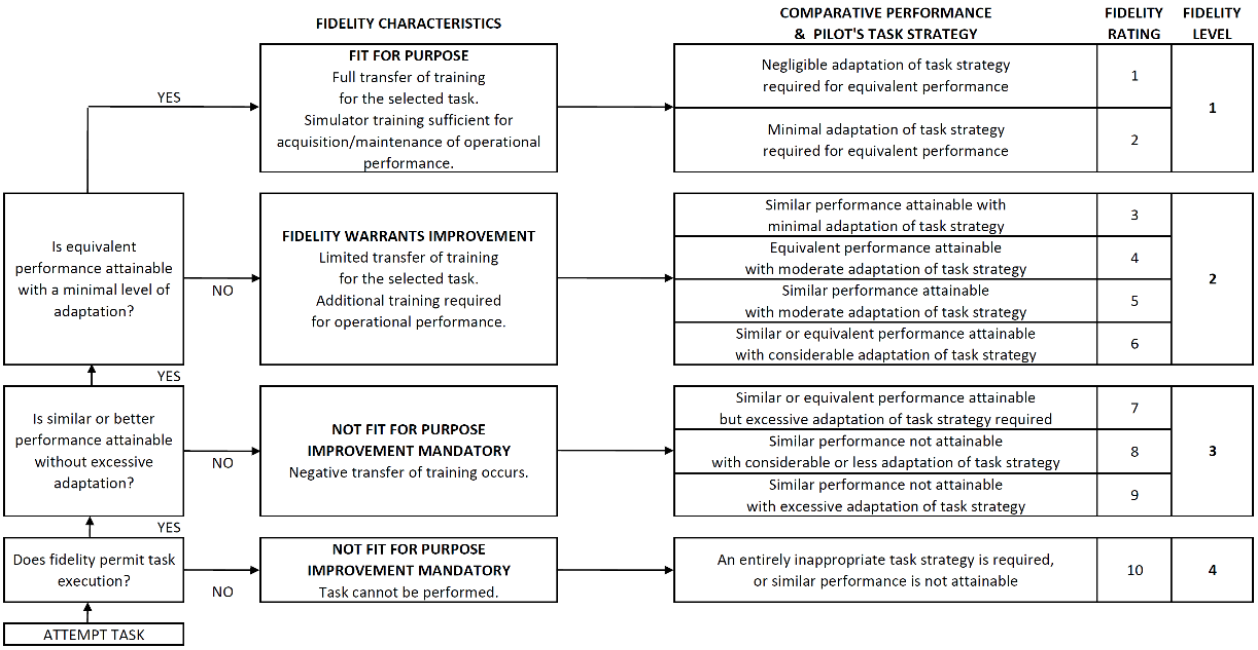

Figure 4-6: Simulation Fidelity Rating Scale [26].

4.7 SIMULATOR QUALIFICATION – QUALIFICATION TEST GUIDE QTG

Helicopter training simulators need to provide high-fidelity immersive environment for pilots in order to obtain a Level D qualification, which is the highest level of simulator qualification defined by the Federal Aviation Administration (FAA), [25], and the European Aviation Safety Agency (EASA) [17]. They are the regulatory authorities responsible for the acceptance of Full Flight Simulators (FFS) and formalize the qualifying criteria and procedures needed for approval for each of the major components of a Level D helicopter simulator. A Level D qualification process allows the replacement of most of the flight hours required for a pilot's type rating or recurrent training by simulator hours. A Level D training simulator is made of many sub-system models related to the vehicle dynamics (flight dynamics, engines autopilot, and flight controls), vehicles systems (avionics, ancillaries, etc.) and simulator immersive cueing environment (motion sound, visual, weather, airport environment, etc.). Each of these sub-systems must meet qualitative and quantitative validation criteria for the specific aircraft type to meet Level D simulator requirements.

Both the FAA and EASA are using a functional performance standard called Qualification Test Guide (QTG). The QTG is a document designed to assess and validate that the performance and handling qualities of a simulator are within prescribed limits of those of the aircraft and that all applicable regulatory requirements have been met. The QTG includes both the helicopter flight-test data and simulator data used to support the validation. A flight-test data package must contain more than one hundred individual events to meet the minimum Level D validation requirements. The qualifying criteria of the mathematical model are formulated by using 'tolerances' and it includes an evaluation based on the comparison between reference flight-test data and results of identical tests computed on a simulator. Also, subjective validation requirements comprise a series of training tasks and abnormal conditions that are normally spot checked during the final assessment to ensure that there are no discontinuities between simulated fight regimes. The combination of objective and subjective testing is meant to guarantee that the fully integrated simulator is sufficiently representative of the aircraft.

QTG maneuvers (Figure 4-7) can be separated in three test categories: snapshot test, dynamics tests, and trajectories tests. Snapshot tests are used when a steady state condition exists in the flight-test data at the instant of time captured. Dynamics tests involve a pre-defined control input perturbation at a trim condition. Trajectories tests are highly non-linear maneuver that will go through multiple flight regimes.

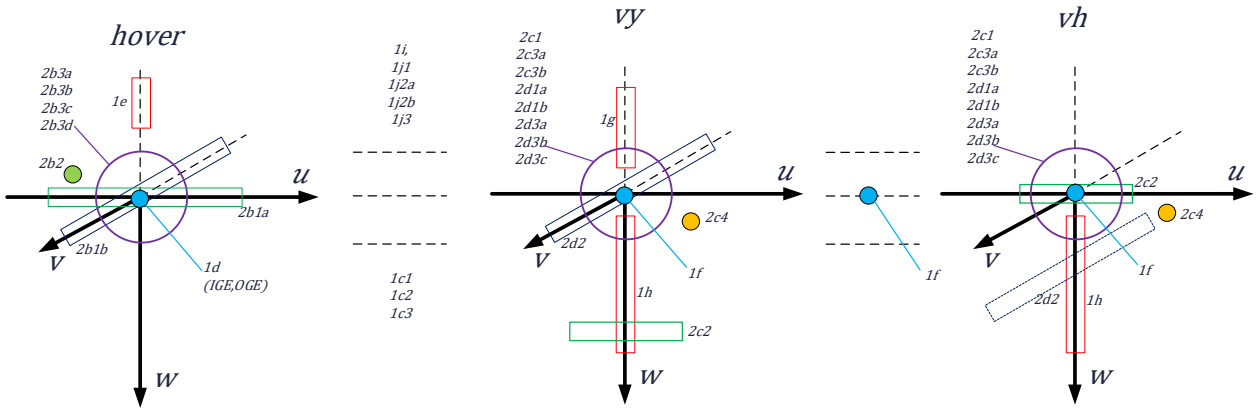

Figure 4-7: Distribution of QTG Throughout the Flight Envelope.

Table 4-1 shows examples of tolerances of the objective test cases required for qualification related to low airspeed handling qualities. It should be noted that Table 4-1 is a summary of the different regulatory authorities' tolerances for each QTG and should not be only used as an official document. It can be found that for low airspeed handling qualities, FAA [Table C2A in FAA 14 Part 60 [25] and SUBPART C in EASA CS-FSTD(H) [17] require for longitudinal cyclic input cases a tolerance of ±10% or 2 deg/sec (whichever is the highest) on the pitch rate response and of ±1.5 degrees on the pitch attitude change following a control input. For lateral cyclic input cases, a tolerance of ±10% or 3 deg/sec (whichever is the highest) on the roll rate response and of ±3 degrees on the roll attitude change following a control input are required. Also, for all cases, the off-axis response must show correct trend for un-augmented cases.

Table 4-1: Low Airspeed Handling Qualities QTG.

Test Entry Number	Test Title	Tolerances	Speed Regime	Flight Condition	Type
2.b.3	Low Airspeed Handling Qualities, Control Response (Longitudinal, Lateral, Directional, Vertical). AFCS ON and OFF	Angular velocities ±10% or ± [a] [b] [c], attitudes change ±10% or ± [g] [h] [i], normal acceleration ± [j]	Low Airspeed	Hover	Dynamic

[a] roll rate ±3 deg/s, [b] pitch rate ±2 deg/s, [c] yaw rate ±2 deg/s, [d] roll attitude ±2 deg, [e] pitch attitude ±1.5 deg, [f] heading ±2 deg, [g] roll attitude change ± 3deg, [h] pitch attitude change ± 1.5 deg, [i] heading change ±2 deg, [j] normal acceleration ±0.1 g.

4.8 CONCLUSIONS

Fidelity should be addressed from a multidisciplinary view, combining ideas from:

- Experienced simulation developers/engineers;
- Statistical experts;
- Analysis specialist/modelers;
- Theoreticians concerned with fidelity and validation; and
- Simulator users.

Fidelity in simulation needs to be addressed quantitatively, otherwise design and development decisions based upon simulation results have significant potential for performance risks. Frequency-domain and Time-domain Integrated Cost Functions are useful metrics for assessing the predictive accuracy of the simulation model. In current practice, to achieve the certification levels of fidelity it is necessary to modify parameters of the simulation through both physical and non-physical tuning. Efforts have been made to establish an engineering basis for this tuning, for example the boundaries established on 'Maximum Unnoticeable Added Dynamics (MUAD)' and 'Allowable Error Envelopes' AEE. FAA/EASA simulator standards reveal shortcomings: for example, the simulation could lie in a different handling qualities level to the aircraft and still meet the fidelity standards. The certification standards address elements of both predictive fidelity (the metrics and tolerances) and perceptual fidelity (pilot opinion).

On motion cueing, the following conclusions may be derived:

1) Vestibular motion cues consist of specific forces and rotational rates.
2) Motion cues can help a pilot close the control loop, both in the simulator, as well as in the real helicopter.
3) Due to the limited motion platform envelope, filtering is normally required. Usually this is achieved through high-pass filter, causing phase lead at lower frequencies.
4) Both amplitude attenuation and phase lead and lag can cause distortion and disorientation if not correctly tuned.
5) Fidelity assessment is performed in the frequency domain; however, no objective boundaries are available. Tools such as OMCT can give some insight.
6) Simulation Fidelity Rating (SFR) scale aim to create the foundation on which predictive, and perceptual fidelity can be tackled together in order to enhance the realism of the integrated simulated pilot experience.

4.9 REFERENCES

[1] Tischler, M.B., and Remple, R.K. (2012), *Aircraft and Rotorcraft System Identification: Engineering Methods with Flight-Test Examples*, 2nd Edition, AIAA Educational Series, November.

[2] Hodgkinson, J. (1998), *Aircraft Handling Qualities*, AIAA Educational Series, AIAA, Reston, VA.

[3] Smith, R.E., Hodgkinson, J., and Snyder, R.C. (1981), "Equivalent System Verification and Evaluation of Augmentation Effects on Fighter Approach and Landing Flying Qualities," U.S. Air Force, Wright Aeronautical Lab., AFWAL-TR-81-3116, Vol. 2, Wright-Patterson Air Force Base, OH.

[4] MIL-STD-1797B (2006), "Flying Qualities of Piloted Aircraft," Department of Defense Interface Standard.

[5] Tischler, M.B. (1995), "System Identification Methods for Aircraft Flight Control Development and Validation," NASA Technical Memorandum 110369.

[6] Hamel, P.G., and Jategaonkar, R.V. (1996), "The Evolution of Flight Vehicle System Identification," *Journal of Aircraft*, 33(1), pp. 10-28, Jan.

[7] Buchholz, J.J., Bauschat, J.M., Hahn, K.U., and Pausder, H.J. (1996), "ATTAS & ATTHeS In-Flight Simulators: Recent Application Experiences and Future Programs," AGARD-CP577, Paper no. 31, April.

[8] Hodgkinson, J. (2005), "History of Low-Order Equivalent Systems for Aircraft Flying Qualities," *Journal of Guidance, Control, and Dynamics*, July-August, 28(4), pp. 577-583.

[9] Mitchell, D.G., Nicoll, T.K., Klyde, D.H., and Schulze, C. (2009), "Effects of Time Varying Rotorcraft Dynamics on Pilot Control," AIAA Atmospheric Flight Mechanics Conference, AIAA 2009-6055, Aug.

[10] Mitchell, D.G., Hoh, R.H., He, C., and Strope, K. (2006b), "Development of an Aeronautical Design Standard for Validation of Military Helicopter Simulators," 62nd Annual Forum of the American Helicopter Society, Phoenix, AZ.

[11] Mitchell, D.G., He, C., and Strope, K. (2006a), "Determination of Maximum Unnoticeable Added Dynamics," AIAA Atmospheric Flight Mechanics Conference and Exhibit Keystone, Colorado, AIAA 2006-6492.

[12] Penn, H. (2013), "Investigating the Feasibility of applying MUAD to Helicopter Simulator Model Validation: An Analysis of the Effect of Multiple Simulators on Allowable Error Envelopes Using Multiple Pilots," Unpublished M.Sc. thesis, Delft University of Technology, July.

[13] Wood, J.R., and Hodgkinson, J. (1980), "Definition of Acceptable Levels of Mismatch for Equivalent Systems of Augmented CTOL Aircraft," Technical Report Number, 1600, A6792, McDonnell Douglas Corp.

[14] Carpenter, C.G., and Hodgkinson, J. (1980), "V/STOL Equivalent Systems Analysis," Technical Report NADC-79141-60, McDonnell Aircraft Co.

[15] Advisory Subcommittee on Avionics, Controls, and Human Factors (1979).

[16] Heffley, R.K., Clement, W.F., Ringland, R.F., and Jewell, W.F. (1981), "Determination of Motion and Visual System Requirements for Flight Training Simulators," Systems Technology Inc., Technical Report No. 546, August.

[17] EASA CS-FSTD(H) (2012), "Certification Specifications for Helicopter Flight Simulation Training Devices," European Aviation Safety Agency EASA CS-FSTD(H), June, https://www.easa.europa.eu/certification-specifications/cs-fstdh-helicopter-flight-simulation-training-devices, Retrieved on June 4th, 2020.

[18] FAA-AC-120-63 (1994), "Advisory Circular on Helicopter Simulator Qualification," Federal Aviation Administration, FAA-AC-120-63, https://www.faa.gov/regulations_policies/advisory_circulars/index.cfm/go/document.information/documentID/23203, Retrieved on June 4th, 2020.

[19] European Aviation Safety Agency, Anon (2012)

[20] Jones, M. (2017), "Motion Cueing Optimisation Applied to Rotorcraft Flight Simulation," CEAS Aeronautical Journal, 8(523), pp. 523-539, https://doi.org/10.1007/s13272-017-0256-1.

[21] Advani, S.K., and Hosman, R.J.A.W. (2006), "Revising Civil Simulator Standards – An Opportunity for Technological Pull," AIAA Modeling and Simulation Technologies Conference and Exhibit, Paper No. AIAA-2006-6248.

[22] Hodge, S.J., Perfect, P., Padfield, G.D. and White, M.D. (2015a), "Optimising the Yaw Motion Cues Available from a Short Stroke Hexapod Motion Platform," *The Aeronautical Journal*, January, 119(1211), pp. 1-21.

[23] Hodge, S.J., Perfect, P., Padfield, G.D. and White, M.D. (2015b), "Optimising the Roll-Sway Motion Cues Available from a Short Stroke Hexapod Motion Platform," *The Aeronautical Journal*, January, 119(1211), pp. 23-44.

[24] Jones, M., White, M., Fell, T., and Barnett, M. (2017), "Analysis of Motion Parameter Variations for Rotorcraft Flight Simulators," Proceedings of the 73rd AHS Annual Forum & Technology Display, Fort Worth, Texas, USA, May 9-11.

[25] FAA 14 Part 60 (2016), "Flight Simulation Training Device Initial and Continuing Qualification and Use," FAA 14 Part 60 Appendix C to Part 60-Qualification Performance Standards for Helicopter Full Flight Simulators.

[26] Perfect, P., Timson E., White, M.D., Padfield, G.D., Erdos, R., and Gubbels, A.W. (2014), "A Rating Scale for the Subjective Assessment of Simulation Fidelity," *The Aeronautical Journal*, August, 118(1206), pp. 953-974.

Chapter 5 – MODEL FIDELITY IMPROVEMENT METHODS

ABSTRACT

Seven different methods for improving a baseline simulation method are presented in this chapter, namely:

1) *Gain/Time-Delay Corrections for Key Responses;*
2) *'Black-Box' Input and Output Filter Corrections;*
3) *Force and Moment Increments Based on Stability Derivatives;*
4) *Reduced Order Models and Physics-Based Corrections;*
5) *Simulation Model Parameter Adjustment;*
6) *Parameter Identification of Key Simulation Constants; and*
7) *Stitched Simulation from Point ID Models and Trim Data.*

The methods are ordered by complexity, starting from the simplest method, and ending with the most complex. The first two methods do not modify the baseline model but apply corrections to the external structure of the model. The next four methods apply corrections to the baseline model, and the last method replaces the baseline model by stitching together linear models at different anchor points. For all seven methods, the methodology is explained, and the advantages and limitations are given.

5.1 GAIN/TIME-DELAY CORRECTIONS FOR KEY RESPONSES

5.1.1 Methodology

In this method, the truth data in the form of frequency responses collected from flight test and system identification are used to evaluate and correct the quantitative response of the simulation model, for key on-axis responses. Bare-airframe frequency responses from flight test and the corresponding frequency responses of the simulation model (e.g., from linearization or frequency-sweep testing) for the key motions are required.

The truth bare-airframe frequency responses are 'divided' by the model responses (in the frequency domain) to obtain the error responses $\epsilon(s)$. A gain (k) and time-delay (τ) model structure $y(s) = ke^{-\tau s}$ is identified from the error response over the frequency range of interest. The gain and time-delay corrections are identified and tabulated for each key output/input response.

The gain and time-delay corrections are then applied to the simulation model. The gain corrections are implemented as a gain on each of the control inputs of the simulation model. Time-delay corrections are implemented as transport delays. These transport delays may be applied to the inputs of the simulation model or alternatively may be placed in the feedback path of the control system if the total closed-loop time delay is excessive (e.g., when accounting for other simulation processing/visual delays).

5.1.2 Applications

The gain/time-delay method is particularly well-suited to:

- Applying small adjustments to high-fidelity models to correct for unknown elements in the simulation model (e.g., vehicle inertia, control system rigging, and unattributed time delays). This is frequently used to correct broken-loop responses for control system optimization as discussed in Refs. [1], [2], [3], [4], and [5].

- Applying corrections to lower-order models to account for higher-order dynamics (actuators, rotor dynamics, processing delays, etc.) [6].
- Accounting for additional delays introduced by the simulation environment [7].

5.1.3 Advantages and Limitations

This method provides a simple, easily implemented, method for applying corrections to a flight simulation model using 'truth' responses from flight-test data.

The primary limitation of the gain/time-delay method is that it is not necessarily physically representative. For cases where the underlying physics of the system being modeled are not captured within the model structure, it is unlikely that the gain/time-delay method will improve the model response. Similarly, where the physics are represented in the model but occur at different frequencies, this method will likely not lead to improvement. The notable exception is the case of an equivalent time-delay used to represent higher-order dynamics, where an improvement will be attained if the frequency range of interest is much lower than the frequency of the un-modeled higher-order dynamics.

5.2 'BLACK-BOX' INPUT AND OUTPUT FILTERS

5.2.1 Methodology

This method aims at improving the fidelity of an existing helicopter baseline model by adding low-order correction models. As these correction models are not physics -based, these are called 'black-box' corrections.

In principle, such correction models can be added at the input side (input filter), in parallel to the baseline model, and at the output side (output filter), see Figure 5-1. If the correction model is in parallel or on the output side, care has to be taken to retain physical relationships, e.g., if the yaw rate has to be improved, the Euler angles have to be recalculated consistently. To avoid this problem, the use of a correction model at the input side is usually preferred. Input and output filters can be combined in such a way that an input filter is first designed to correct the main deficiencies of the baseline model and any remaining deficiencies are then corrected by output filters.

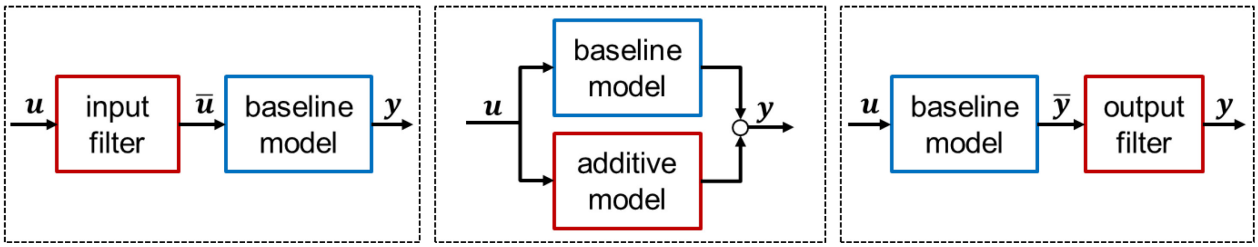

Figure 5-1: Possible "Black-Box" Update Models.

5.2.1.1 Single-Input Single-Output (SISO) Systems

SISO systems are driven by one single input and provide one output signal. For SISO systems, input and output filters are equivalent and the 'black-box' filter method is basically an extension of the gain/time-delay approach to higher-order corrections. Again, errors of Bode magnitude (dB) and Bode phase (deg) are extracted by dividing the frequency responses of flight-test data and the baseline model. The error is then modeled by a transfer function using system identification in the frequency domain as implemented in tools such as CIFER [2] or FitlabGui [8]. To get the updated response, the baseline response is multiplied with the identified error model.

Several examples exist to extract black-box filters from SISO transfer functions. One of the most prominent examples is the modeling of regressive lead-lag dynamics [2], [9]. Another application example is the modeling of the rotor-on-rotor interference for the CH-47 database [10].

5.2.1.2 Multiple-Input Multiple-Output (MIMO) Systems

Possible modeling procedures to design the input filter for MIMO systems are shown in Figure 5-2. The first two procedures (columns) focus in a first step on the derivation of the modified inputs $\bar{u}$ using inverse simulation. These are the inputs that are required so that the baseline model yields the correct (i.e., measured) outputs y. In a second step, the input correction model (filter) is determined based on measured inputs u and modified inverse simulated inputs $\bar{u}$. For this second step, either time-domain or frequency-domain system identification can be used. For the third procedure (column), system identification is used to produce a high-fidelity state-space model $u(t) \rightarrow y(t)$. The input filter can then be determined from this identified model and the baseline model through simple algebraic equations.

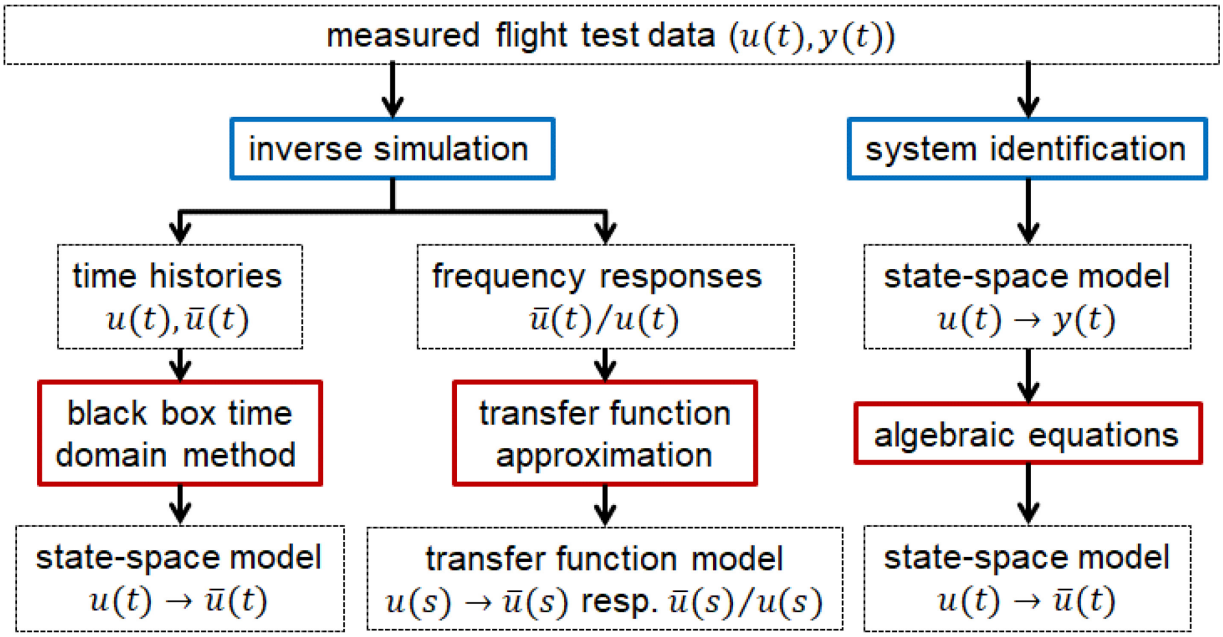

Figure 5-2: Overview of Methodologies to Derive "Black-Box" Input Model Updates.

Several methods can be used for the inverse simulation:

- Nonlinear Inversion;
- Linear Dynamic Inversion in the Time Domain; and
- Approximate Inversion.

Details of the different methods are given in Tischler et al. [1].

Once the inverse simulated inputs $\bar{u}(t)$ have been generated, several options exist for deriving the input filter model in a second step for the first two procedures in Figure 5-2:

- A black-box time-domain identification method, such as the optimized predictor-based subspace identification (PBSIDopt) method [11], can be used to derive the input filter directly from the time histories for $u(t)$ and $\bar{u}(t)$.

- If frequency responses for $\bar{u}(j\omega)/u(j\omega)$ can be generated, they can be approximated by transfer functions $\bar{u}(s)/u(s)$ using frequency-domain system identification. The generated input filter consists of a matrix of transfer functions which can optionally be transferred into a state-space model.

The third procedure in Figure 5-2 features the algebraic inversion which involves system identification in a first step to produce a high-fidelity model of the measured responses. In a second step, the existing linear baseline model (numerically linearized, identified or extracted from literature) is inverted and multiplied by the high-fidelity model. The input filter is, thus, simply given by

$$\text{input filter} = (\text{Baseline Linear Model})^{-1} \times (\text{Helicopter SysID Model})$$

To be able to apply this approach, both models have first to be reduced to a 4x4 system by selecting the same set of output variables because a quadratic system is a prerequisite for an algebraic inversion. This procedure, thus, directly produces the linear input model and is presented in more detail by Grünhagen et al. [12] and Seher-Weiß et al. [13]. Due to the way in which the filter is determined, the updated model yields an exact match with the identified model for those output variables that were selected for the algebraic inversion.

A schematic description of the algebraic approach is given in Figure 5-3.

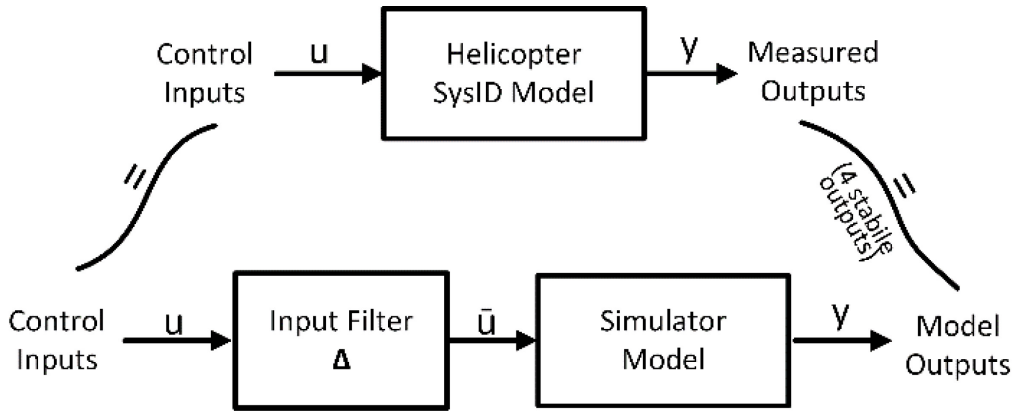

Figure 5-3: Schematic Representation of the Algebraic Approach.

More details about the technical implementation of the inverse simulation, and the resulting input filters can be found in Tischler et al. [1], Greiser [14], and Greiser and Grünhagen [15].

5.2.2 Applications

The 'black-box' method can be applied to both training simulators and engineering simulation. Input and output filters can be combined in such a way that an input filter is first designed to correct the main deficiencies of the baseline model, and any remaining deficiencies are then corrected by output filters.

5.2.3 Advantages and Limitations

The 'black-box' method for the SISO is easy to apply and implement. Unlike for the methods presented in the following sections, no understanding of the physical nature of the deficits that are to be corrected is necessary. Also, the baseline simulation remains unchanged, corrections are only applied to the outside of the model.

However, as the derived corrections are not physics-based, they do not necessarily allow for interpolation or extrapolation. Regarding the implementation, particular care has to be taken for the baseline model's right half-plane invariant zeros. Any right-half plane zero becomes an unstable eigenvalue in the input filter. For (piloted) simulation, the time-to-double of unstable eigenvalues of the input filter should not exceed 1.5 sec. The inverse simulation for the MIMO case requires expertise.

5.3 FORCE AND MOMENT INCREMENTS BASED ON STABILITY DERIVATIVES

5.3.1 Methodology

Deficiencies in the fidelity of the nonlinear model can be corrected with incremental forces and moments as 'delta' derivatives as summarized in Figure 5-4.

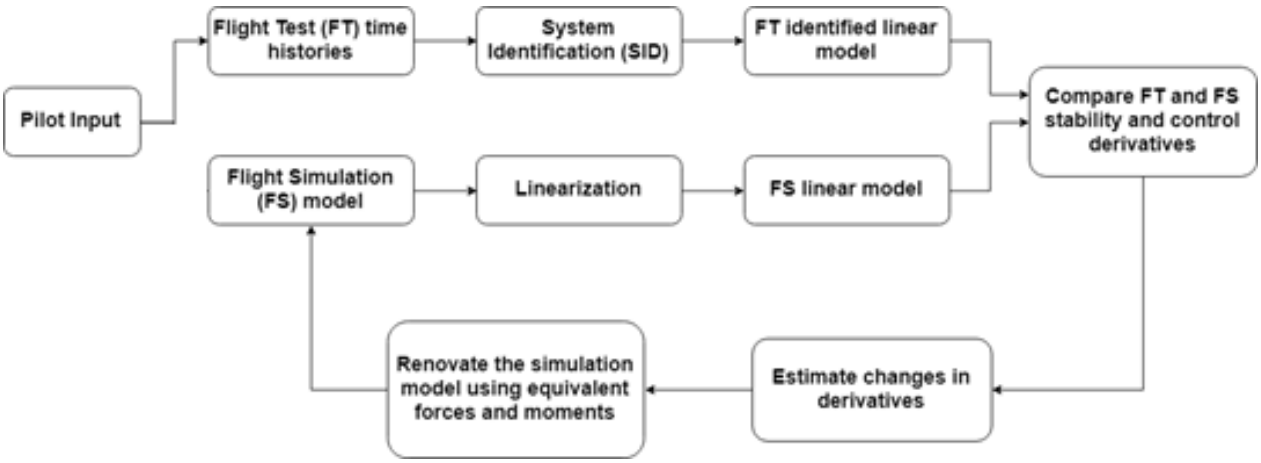

Figure 5-4: Force and Moment Increment Method Flow Chart.

Frequency sweeps or multi-step, e.g., 3211 or 2311 type, inputs are used for generating the Flight-Test (FT) data required for derivative determination through system identification. The identification can either be performed in the frequency domain (frequency response or Maximum Likelihood Method, see Tischler and Remple [2] or FitlabGui [8], or in the time domain with methods such as Maximum Likelihood [16], [17], Additive System Identification (ASID), or Linear Parameter Identification Using Adaptive Learning. The last two methods are described in detail in Tischler et al. [1].

The same inputs and identification methods can be used to generate the derivatives from the simulation model. However, linearization tools are usually available within the flight dynamics codes which simplify this process.

A comparison of FT identified and Flight Simulation (FS) linear model derivatives is then made to compute residual forces and moments. This requires that the same linear model structure be used for the flight and simulation data for quantifying the delta derivatives. Selection of the derivatives to renovate will depend on the nature of the model fidelity shortfall. Applications can range from identifying deficiencies in all axes to renovating a selected axis, mode, or derivative(s). The derivative selection can be achieved either by carrying out a sensitivity calculation or through a physics-based study. Another approach for selecting the derivative deltas for renovation is to identify those that have a quantified impact on a user-defined cost function [18].

The difference between the flight-test Identified (ID) derivatives and those derived from the linearized flight simulation (lin) yields the force and moment increments., e.g., for the rolling moment

$$\Delta L = I_{xx}\left[\left(L_{p\_ID} - L_{p\_lin}\right)p + \left(L_{v\_ID} - L_{v\_lin}\right)v + \left(L_{r\_ID} - L_{r\_lin}\right)r + \left(L_{lat\_ID} - L_{lat\_lin}\right)\delta_{lat} + \left(L_{ped\_ID} - L_{ped\_lin}\right)\delta_{ped}\right]$$

with I_{xx} denoting the helicopter roll moment of inertia.

Finally, the corrected rolling moment $L_{NL-corrected}$ for the nonlinear simulation is given as:

$$L_{NL-corrected} = L_{NL-original} + \Delta L$$

and analogously for the other axes.

5.3.2 Applications

The method is applied in training simulators to complement shortfalls in responses predicted by simulation models, e.g., for the Qualification Test Guide (QTG). For engineering simulation, the method is applied improve model responses and HQs to meet, e.g., CS-FSTD(H) or ADS-33E requirements.

5.3.3 Advantages and Limitations

The force and moment increment method provides insight into model deficiencies through the 'delta' derivatives and points to the potential areas of improvement, but it does not directly identify the root causes of the model's deficiency. The derived force and moment increments can be tabulated e.g., as function of speed and can thus be used throughout the flight envelope. High-quality flight-test data is required to identify a good FT model.

5.4 REDUCED ORDER MODELS AND PHYSICS-BASED CORRECTIONS

5.4.1 Methodology

Although remarkable progress has been made in developing high-fidelity methods for improved prediction of rotorcraft aerodynamics, such as CFD, direct use of such methods in flight simulation is limited by the high computational speed required for real-time flight simulation. Reduced order models can be extracted from high-fidelity models while providing efficient computation. Properly derived reduced order models with physics-based correction of the modeling parameters can retain the simulation accuracy needed for both engineering and real-time flight simulation; and therefore, this provides a practical and effective means of meeting the requirements for both prediction accuracy and computational efficiency. This section covers multiple modeling aspects, including rotor induced inflow dynamics, aerodynamic interference, fuselage aerodynamics, engine/drivetrain dynamics with rotor lead-lag dynamics, and sensor and swashplate actuator dynamics. The following sub-sections describe each of the investigated physics-based reduced order modeling methods.

5.4.1.1 Rotor Induced Inflow Dynamics

The rotor induced inflow model is a vital part of accurate rotor aerodynamics and dynamics modeling that impacts flight simulation in various ways, including performance, stability, and control response. Pitt and Peters [19] and Peters and He [20] inflow models are widely used in most current flight simulations. Both inflow models only address rotor self-induced induced inflow over the rotor plane; and therefore, they lack the capability for predicting rotor interference on other rotors and aerodynamic surfaces. Both inflow models also assume rigid rotor wake geometry, and hence, are limited for modeling the effect of rotor wake distortion that occurs in maneuvering flight. This leads to an erroneous prediction of off-axis response of single main rotor helicopters in hover and low speed flight.

Rotor wake distortion resulting from rotor Tip-Path-Plane (TPP) rotation in maneuvering flight was found to be a cause of erroneous prediction of off-axis response of single main rotor helicopter in hover and low speed flight [21]. As shown in Figure 5-5, the rotor wake experiences noticeable distortion of curvature along with compression on one side while expansion on the other during rotor TPP pitch or roll rotation. The distorted maneuvering wake leads to significant change of rotor induced inflow.

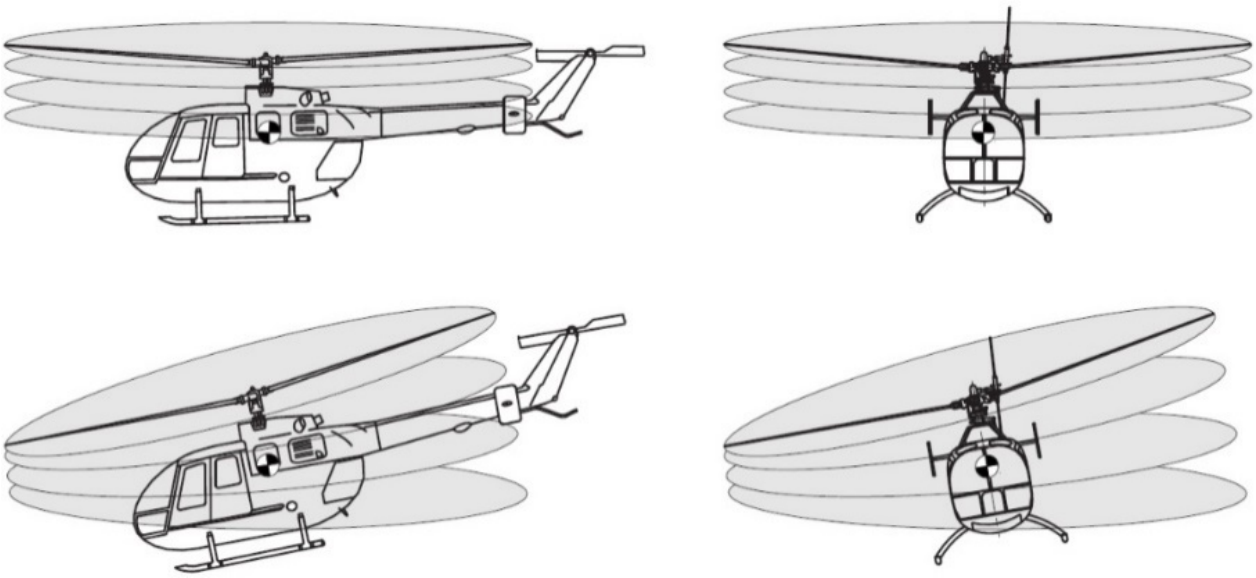

Figure 5-5: Rotor Wake Distortion Due to TPP Rotation.

Different inflow modeling approaches were used by the different partners in the AVT-296 working group.

5.4.1.1.1 Augmented Dynamic Inflow Model for Maneuvering Flight

It was found that the effect of rotor wake distortion involves two dynamic modes. One is the fast mode with rotor induced inflow dynamics that can be addressed by introducing a correction term (so-called Kr parameter [22]) directly into the baseline inflow model. The other is the slower mode that is related to the dynamic change of the curved wake geometry during rotor tip-path plane rotation. One way to model the wake distortion is to derive the wake curvature terms as augmentation to the inflow gain matrix L of the baseline dynamic inflow model [23], [24]. Also, it is important to allow for a dynamic change of the wake geometry while incorporating the wake curvature, as it was found that a quasi-steady wake curvature model could lead to simulation divergence.

5.3.1.1.2 Reduced Order Inflow Model Derived from Viscous Vortex Particle Method (VVPM)

Another approach for the development of a reduced order induced inflow model is to derive it from the first principle-based rotor wake solution, e.g., viscous Vortex Particle Method, (VPM) [25], [26]. By truncating Peters and He's finite state induced inflow model to a dynamic inflow equation of 3 states (i.e., uniform, and cosine, and sine harmonics), it reduces to an equivalent Pitt-Peters inflow model. Both inflow models incur the limitations resulting from their rigid (no distortion) wake geometry and potential flow (non-viscid) assumption. Physics-based inflow model parameter corrections are considered for improved model fidelity through calibration of inflow influence coefficients and interference parameters against high-fidelity models, such as the viscous vortex particle method [27].

5.3.1.1.3 Sikorsky General Helicopter (GenHel) Simulation Model

The GenHel rotor induced inflow dynamic model is based primarily on a downwash distribution prescribed as a function of rotor aerodynamic loading. GenHel calculates total downwash at any point on the rotor as a combination of the three elements below:

1) A basic uniform component which results from generating aerodynamic rotor thrust.
2) First harmonic component derived by cyclic aerodynamic hub moment on the rotor disk.
3) A cosine harmonic component due to rotor wake skew with increasing rotor advance ratio.

The first basic component of rotor downwash in the Howlett GenHel model, which is derived by application of simple momentum theory, is a uniform distribution of induced inflow over the rotor disk, which is calculated as a function of the total rotor aerodynamic thrust. The second component is a first harmonic, or cyclic, inflow distribution, a reaction of the airflow to aerodynamic hub moments [28]. The third component of rotor downwash is the element of wind axis first harmonic longitudinal inflow skew due to wake blowback as modeled by classical Glauert downwash factors. This third component of rotor downwash is due to the tendency of the rotor wake to blowback or skew as wind axis advance ratio increases, resulting in a redistribution of rotor induced downwash along the wind axis across the rotor. This redistribution of downwash over the rotor tends to reduce downwash on the upwind side of the rotor and increase downwash on the downwind side of the rotor.

5.4.1.2 Rotor-on-Rotor Interference

5.3.1.2.1 Tandem Configuration

Pressure Potential Superposition Inflow Model (PPSIM) assumes that flow around the rotor disk is incompressible and inviscid. In PPSIM, the rotors' individual pressure fields are superimposed [29].

Boeing Helicopters Simulation Inflow Modeling Method (BHSimIMM) has a three-state inflow representation similar to the Pitt-Peters inflow model [30]. In BHSimIMM, there is only uniform inflow coupling between the rotors and this coupling comes purely from empirical relations. The first harmonic induced inflow distributions are free from the mutual interference effects of the rotors. BHSimIMM models the first harmonic rotor induced inflow distributions using equations of the form of the GenHel Rotor Induced Inflow Model [31].

5.4.1.2.1 Coaxial Configuration

This method uses system identification to develop a low-order model of the inflow for a coaxial rotor from a free-vortex wake. The inflow dynamics model structure is identical to the Pitt-Peters formulation with the addition of wake distortion and slowly varying "far" wake dynamics [32]. The far wake coupling gives the resulting inflow response a higher-order behavior that has been observed in free-vortex wake results [32], [33], [34], [35]. Time delays on thrust to aerodynamic loading and flapping equations account for computational delays in the stepping between the Maryland Free Wake (MFW) [36] and flight dynamics code for additional dynamics in the MFW that are not accounted for by the model.

The forcing for each rotor's inflow comes from each rotor's aerodynamic thrust as well as pitching and rolling moments. The far wake velocities represent a slowly evolving dynamic wake downstream of the rotor planes and are combined into a single set of equations which contain only sine and cosine components. Finally, the total inflow at each rotor disk is the sum of the self-induced velocity at that rotor and a contribution from the other rotor.

5.4.1.3 Aerodynamic Interference

A rotorcraft involves complicated aerodynamic interference between its rotors, aerodynamic surfaces, and fuselage. Rotorcraft aerodynamic interference modeling remains a very challenging aspect for an accurate flight simulation. Most of existing flight simulation models rely on potential flow-based methods, such as real-time finite state rotor interference models [37] or engineering vortex wake simulation to generate data for table look-up. These potential flow-based methods rely on empirical parameters in order to model the effects of wake distortion and wake vorticity dissipation. The empirical interference model parameters can be derived from first principle-based rotor wake simulation, such as VPM [26] or calibrated against measured data [37]. The aerodynamic interference method applies the rotor interference on aero-surfaces, fuselage, and other rotors. The aerodynamic interference method also addresses the ground effect in hover and low flight speed.

5.4.1.4 Fuselage Aerodynamics

Fuselage aerodynamics covers both fuselage airloads and fuselage interference on aerodynamic surfaces (e.g., horizontal stabilator and vertical fin). Most current simulations use empirical table look-up for estimating fuselage airloads. The empirical data are typically derived from wind tunnel tests or CFD solutions, where only an isolated fuselage is considered without the effect of rotor interference. The interference effect is recovered later in the simulation through simple superposition which often uses only single interference sampling points. The empirical fuselage airloads approach can lack sufficient data to cover the full flight envelope. The fuselage interference effect is not usually as strong as rotors, but sometimes plays a role in both trim and transient response [38].

5.4.1.5 Engine/Drivetrain Dynamics with Rotor Lead-Lag Dynamics

Engine and drivetrain dynamics modeling is important to correctly simulate those flight maneuvers where rotor speed (NR) is not constant in time due to its effect on forces and moments transmitted from the rotor to the fuselage. Maneuvers of this kind are, for example, those involving the use of collective and pedals. The axes which are most involved are typically those of heave and yaw.

The engine modeling consists of the representation of the drivetrain, of the engine thermodynamics, and of the fuel flow control logics. For flight mechanics purposes, the drivetrain can be modeled as a simple inertia-spring-damping model, with equivalent inertia set to guarantee same kinetic energy content and effective spring parameter tuned to capture the dynamics of the lower torsional mode. Engine dynamics can be represented as look-up tables to represent the engine static thermodynamics characteristics and a series of transfer functions to represent engine dynamics and fuel flow control logics.

The engine model structure and interface with the rotorcraft drivetrain used in this report are represented in Figure 5-6.

All the unknown parameters (gain of transfer functions, time delay, and constants) of the engine model can be tuned in order to match the real behavior of the engine to be modeled.

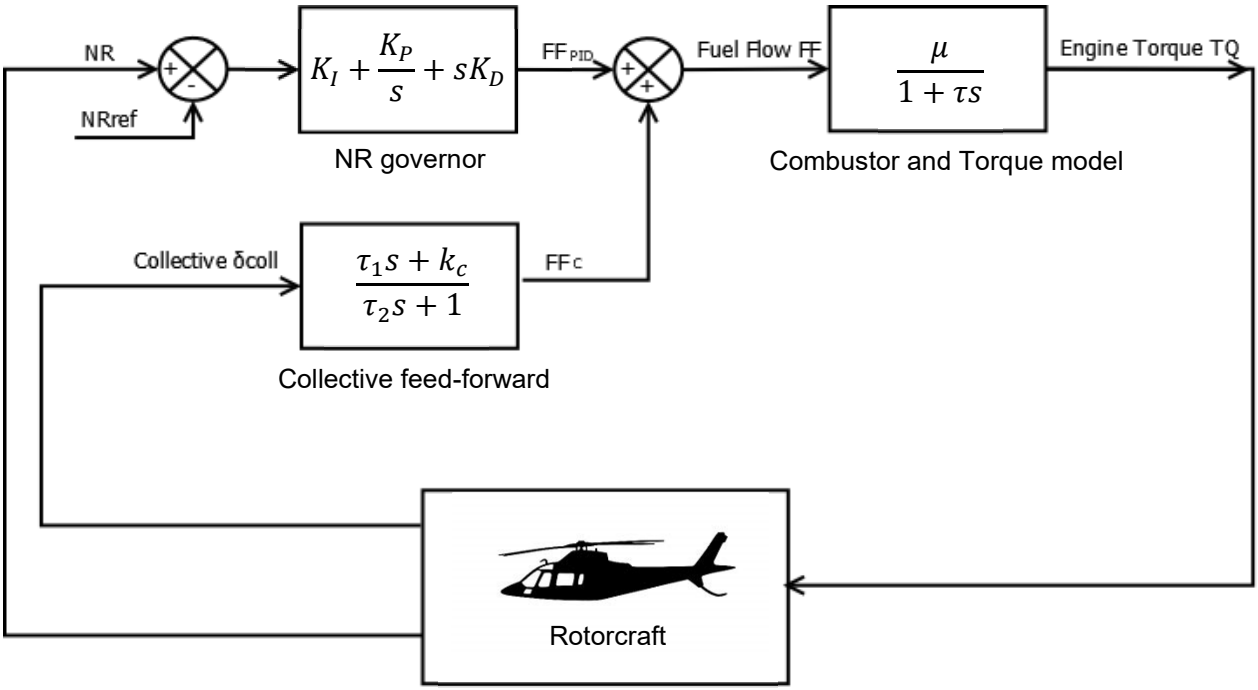

Figure 5-6: Engine Model.

5.4.1.6 Sensor and Swashplate Actuator Dynamics

Methods of sensor and actuator dynamics involve consideration of the effect of sensor dynamics (low-pass frequency) and actuator dynamics on aircraft control response prediction. A sensor is usually described in terms of the type of filter (e.g., Butterworth filter), bandwidth, and computational delay. These pieces of information can be found in the sensor or actuator's data sheet. Actuator's dynamics properties can be derived from the input-output frequency responses function of input displacement that are part of the actuator's qualification test report.

5.4.2 Applications

Reduced order modeling and physics-based corrections are considered for improved rotorcraft flight simulation fidelity. With its physics-based solution, the method is applicable to both engineering simulation for supporting design and analysis, and real-time flight simulation for training simulator applications.

5.4.3 Advantages and Limitations

Physics-based methods allow for extrapolation and improve the root cause of the deficiencies.

The applications of physics-based approaches require good understanding of rotorcraft aerodynamics, dynamics, propulsion, and flight controls for identifying the root cause of the modeling discrepancies and applying the corrections accordingly.

5.5 MODEL PARAMETER ADJUSTMENT FOR PHYSICS-BASED SIMULATIONS

5.5.1 Methodology

Methodologies for physical parameter adjustment vary widely, ranging from comprehensive numerical optimizations using a large number of input parameters to parametric studies involving only one or two parameters. The appropriate method depends largely on the application. Thus, descriptions of update methods below are organized by application.

Model parameter adjustment is justified by the following set of conditions:

- There is significant uncertainty associated with certain key parameters that affect observed discrepancies.
- The model developer can draw a direct physical relationship between the uncertain parameter and the discrepancy in the flight-test data, for example through system identification of linear model terms (e.g., stability and control derivatives) than can then be directly related to the uncertain parameter through well-established theoretical relationships [2].
- Non-linear physics-based models are required for the specific application, such that direct use of identified linear models is not a suitable substitute for the particular application.

5.5.1.1 Parameter Adjustments for Level D Pilot Training Simulator

A modeling/optimization framework is used to determine unknown parameters in a blade-element rotor model to best match the dynamic response of a helicopter following a maneuver [39]. Unknown aeromechanical parameters can include moments of inertia, pitch-flap coupling, aerodynamic phase angle. or rotor blades hinge offsets. Non-aeromechanical parameters, such as main rotor inflow (steady and harmonic components) and helicopter inflow skew angles, skew angle rates rotor-to-rotor interference corrections for dual rotor helicopters, and duct interference for Fenestron tail rotors [40] can also be adjusted by this method.

An optimization objective is used to minimize the residuals between flight-test identified stability and control derivatives obtained by linearization of the blade-element model using numerical approximation at a given trim condition. While manual tuning of these parameters is possible, it is more time-consuming and may not lead to the best overall set of parameters. An alternative method is to adjust parameters to minimize the error in frequency-domain response of the helicopter in terms of magnitude and phase; this requires reference flight data with good sensor correlation and rich frequency content.

5.5.1.2 Parameter Adjustments for Engineering Research Simulations

Physics-based simulations are used for engineering research on rotorcraft handling qualities requirements, vehicle design, and advanced flight control design. Model validation and updates are an important aspect of these efforts, and as discussed above, this is best achieved via a combination of frequency-domain and time-domain identification techniques. Geiger et al. [41], O'Neill [42], and Krishnamurthi and Horn [43] discuss some approaches to systematic tuning of engineering simulation models via parameter adjustment to match flight data. These approaches use frequency-domain system identification to derive low-order models of the dynamics of interest. The discrepancies between identified stability and control derivatives are then used to guide direct parameter adjustment in the non-linear simulation model. Adjustments are made on a small number of uncertain parameters that are known to have direct effect on the observed discrepancies, and parameter sweeps are conducted to optimize these parameters to minimize frequency response mismatch. Time responses are generally checked as well to verify the parameter optimization.

For research simulators, optimization on a large set of parameters is generally avoided since there is often strong correlation between certain physical parameters in terms of their effect on the rotorcraft response. Step-by-step parametric studies on one or two parameters are preferred so that the model developer can gain physical insight as to the input parameters that most likely cause the discrepancy with test data.

5.5.2 Applications

The method can be applied to both training simulators and engineering simulation including blade-element models.

5.5.3 Advantages and Limitations

The physics-based approach of this method indicates the source of the deficits that are to be mitigated.

Model parameter adjustment can be problematic in some cases because certain parameters might be highly correlated in terms of their effect on overall aircraft response. This makes it difficult to isolate which parameter should be updated, and the sheer number of uncertain model parameters can be overwhelming and result in a time-consuming process.

5.6 PARAMETER IDENTIFICATION OF KEY SIMULATION CONSTANTS

5.6.1 Methodology

The equations of motion needed to properly capture a rotorcraft flight dynamics response are well understood. These basic equations include rigid-body, rotor, and inflow degrees of freedom. Higher fidelity simulations may also model engine and drivetrain dynamics, airframe or control system flexibility, and interactional aerodynamics, amongst the dynamic components. Even though the basic modeling requirements are well understood, assumptions may aggregate into an overall mismatch between the model predicted aircraft response and the actual response.

This update method acknowledges that simulation input parameter values may not be known exactly and uses system identification methods, such as in Tischler and Remple [2], to directly identify key flight dynamics parameter values to help align the simulation response to flight data. Key rotorcraft flight dynamics constants can be obtained from analytical flight dynamics equations. To apply this method to a non-linear flight simulation, a linear state-space response is first extracted at a certain flight condition. Various terms of the linear state-space model are replaced by their analytical equivalent, and system identification is used to adjust model parameters to improve model match to flight data. If desired, the identified terms can then be used to update the non-linear flight simulation input data.

5.6.2 Applications

The method can be applied to a nonlinear simulation when there is uncertainty in some physical parameters. The method allows to improve model fidelity for subsequent control design and handling qualities analysis. An application of this methodology for the Sikorsky X2^{TM} Technology Demonstrator is demonstrated in Fegley et al. [44].

5.6.3 Advantages and Limitations

The method allows to directly determine physical parameters in a nonlinear simulation. Due to the physics-based nature of the method, extrapolation to other flight conditions is possible.

This update methodology identifies changes in modeling parameters that are required to improve a model fit to flight data. The choice of parameters to be identified is left to the user to determine. If poor choices of parameters to be identified are made or multiple parameters are correlated with each other, then the identification procedure can produce incorrect results. Moreover, if the model is missing key dynamics that show up in the flight data, this method will lump the net impact of those dynamics into the identified parameters.

5.7 STITCHED SIMULATION FROM POINT ID MODELS AND TRIM DATA

5.7.1 Methodology

Model stitching is the technique of combining or 'stitching' together individual linear models and trim data for discrete flight conditions to produce a continuous, full flight-envelope simulation model. In this technique, the stability and control derivatives and trim data for each discrete point model are stored as a function of key parameters, such as airspeed and altitude. The look-up of trim and derivatives is combined with nonlinear components to produce a continuous, quasi-nonlinear, *stitched* simulation model. Additional nonlinear dynamics may be included to cover complex or edge-of-the-flight-envelope maneuvers, e.g., autorotation.

Application of the model stitching technique using rotorcraft flight-test data was pioneered by NRC, TDD, and DLR. Hui et al. [45] built a Level D simulator model from flight-identified point models of the Bell 427. Zivan and Tischler [46] refined the stitching technique and produced a stitched model of the Bell 206 helicopter from seven flight-identified point models. Greiser and Seher-Weiß [47] developed a stitched model of the EC135 from five flight-identified higher-order models, which included rotor flapping, inflow, and lead-lag effects. Tischler and Remple [2] elaborate on the theoretical approach of the model stitching technique for applications to fixed-wing and rotary-wing aircraft. Tobias and Tischler [48] apply the theoretical concept of the model stitching technique to develop a model stitching simulation architecture, which incorporates extrapolation methods for the simulation of off-nominal aircraft weight, inertia, and CG.

The key requirement for model stitching is a series of state-space point models and associated trim data of the states and controls for point flight conditions or 'anchor' points. Additional, more finely-spaced 'trim shot' data, which capture the variation in trim states and controls over the full airspeed range, are recommended. The dimensional stability and control derivatives are extracted from the anchor point models and stored in lookup tables. The trim data of the states and controls are typically first fitted with splines before being stored in lookup tables. The lookup tables are combined with the nonlinear equations of motion and other simulation elements to yield the model stitching simulation architecture as shown in Figure 5-7. The key elements of this figure are briefly discussed below. For a more detailed discussion, see Tobias and Tischler [48].

State and Control Perturbations ① and ②: Given the current x-body airspeed U, lookups are performed to find the vectors of trim aircraft states and controls, $X_0|_U$ and $U_0|_U$. With the current aircraft state vector X and current control vector U, the state perturbation vector Δx and control perturbation vector Δu are calculated.

Aerodynamic Perturbation Forces and Moments ③: Aerodynamic perturbation forces and moments are calculated based on the dimensional stability and control derivative matrices A_{aero} and B_{aero} at the current airspeed, as stored in the corresponding lookup tables and the state and control perturbation vectors Δx and Δu. The dimensional mass matrix M, which is comprised of the flight-test values of aircraft mass and inertia tensor, is multiplied into the matrix of stability derivatives A_{aero} and the state perturbation vector Δx to yield a vector of aerodynamic dimensional perturbation forces and moments. Likewise, the mass matrix is multiplied into B_{aero} and control perturbation vector Δu to produce a vector of dimensional perturbation control forces and moments.

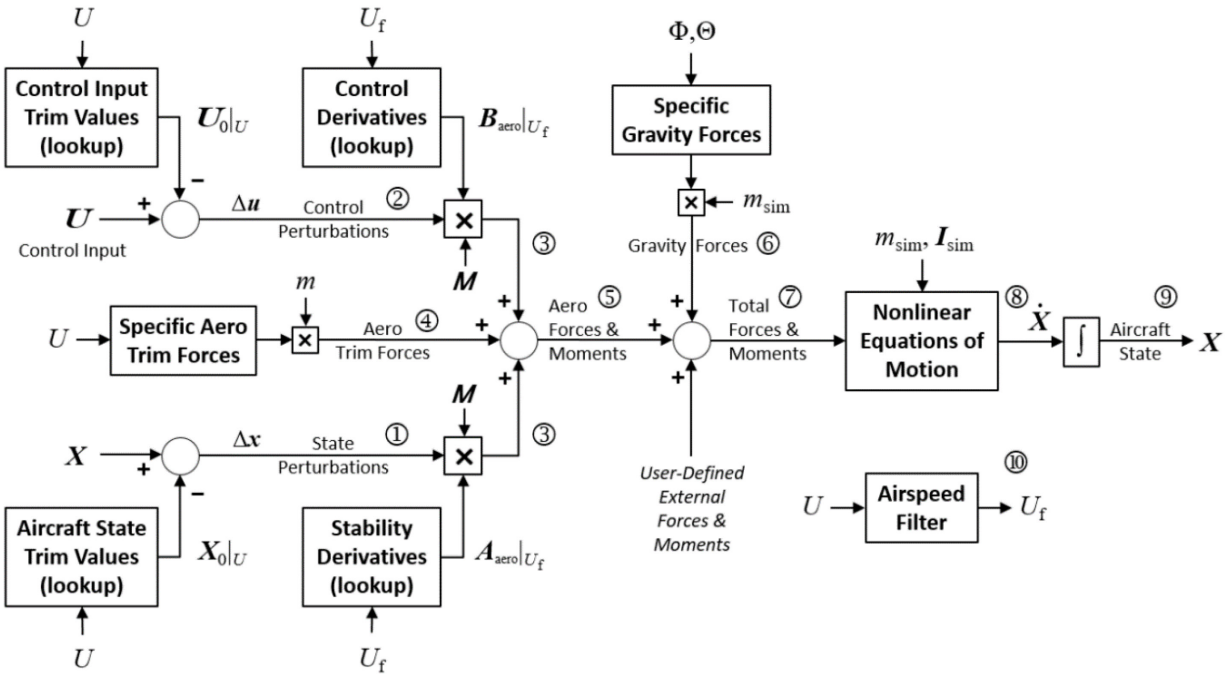

Figure 5-7: Model Stitching Simulation Architecture – Top Level Schematic.

Aerodynamic Trim Forces ④: The *specific* aerodynamic trim forces are computed based on lookups of the trim aircraft pitch and roll attitude at the current airspeed, $\Theta_0|_U$ and $\Phi_0|_U$, and acceleration due to gravity. The specific aerodynamic trim forces are multiplied by aircraft mass m to obtain the dimensional aerodynamic trim forces.

Total Aerodynamic Forces and Moments ⑤: The aerodynamic dimensional perturbation forces and moments are summed with the dimensional aerodynamic trim forces to yield the total aerodynamic forces and moments.

Nonlinear Gravitational Forces ⑥: The stitching architecture incorporates nonlinear kinematics, i.e., small angle approximations are not made. The *specific* gravity forces acting at the aircraft CG are nonlinear with respect to the current, instantaneous values of the aircraft pitch attitude Θ and roll attitude Φ; no look-up of trim data is performed. The specific gravity forces are then multiplied by the current simulation value of aircraft mass m_{sim} to obtain the dimensional gravity forces.

Total Forces and Moments ⑦: The aerodynamic forces and moments are summed with the gravity forces to yield the total external, dimensional forces and moments acting at the CG. These may be augmented with user-specified forces and moments for the simulation of additional modeling components (e.g., landing gear).

Nonlinear Equations of Motion ⑧: Given the total forces and moments of the aircraft CG and the simulation values of mass and inertia, m_{sim} and $\boldsymbol{I}_{sim}$, the 6-DOF body-axes nonlinear representation of Newton's equations of motion are used to obtain the state-dot vector $\dot{X}$. The equations of motion contain the nonlinear Euler equations, which include the cross-coupling inertial and Coriolis terms in full nonlinear form.

Integration ⑨: The state-dot vector is integrated to obtain the updated aircraft state vector X. For a 6-DOF model, the state vector consists of $[U\ V\ W\ P\ Q\ R\ \Phi\ \Theta\ \Psi]^T$. Higher-order states may also be included.

Airspeed Filter ⑩: A first-order low-pass filtered airspeed U_f is used for look-up of the stability and control derivatives. Applying the filter ensures that the derivative values remain constant for short-term motion; thereby, accurate dynamic responses are retained at the anchor points.

When preparing to collect a set of anchor point models and trim data, as identified from flight testing or derived from a non-real-time model, for example, important best practices are as follows.

- Identification point models are typically valid over ±20 kn from the ID airspeed, so a 40-kn spacing is recommended for the identification of anchor point models. Anchor point derivatives should change reasonably and may be linearly or piecewise cubic interpolated.
- More finely-spaced trim data are recommended. Trim data should be collected in straight and level flight at a fine increment around hover and low speed forward flight (a 3 – 5 kn speed increment is recommended up to 20 – 30 kn), and thereafter, a 10-kn increment up to cruise airspeed is recommended to ensure the capture of key trim trends. The collected data should be fit to a fine grid to extract trim gradients correctly; anchor point derivatives may be kept in a coarser grid.
- Additional validation data are helpful for proof-of-match of static stability, extrapolated loading configuration, and maneuvering flight time-history data.

5.7.2 Applications

The stitching method allows to develop wide-envelope simulation models up to Level D quality from flight-identified models. The method can also be used to extract a real-time simulation from a non-real-time high-fidelity model. Stitched models can be sued for hardware-in the-loop simulations.

Variation of aircraft mass and inertia allow to simulate off-nominal loading conditions. Model stitching allows to quickly build a wide-envelope simulation for an unconventional aircraft where a first-principles model is not available.

5.7.3 Advantages and Limitations

A key advantage of this method is that is does not require a baseline model. Even though model stitching is based on linear models, the stitched model can be augmented by higher-order effects to cover edge-of-the-envelope maneuvers. Any of the other update methods can be used to improve the stitched model.

There are some key limitations of the model stitching technique:

- A collection of point-wise linear models, as identified from flight-test data or obtained by linearizing a nonlinear or non-real-time simulation model, are required. The model structure and included states must be consistent among the point models.
- The quantity and spacing of the anchor points must sufficiently capture the dynamics and trim data trends over the flight envelope of interest. The data should vary smoothly or first be processed with piecewise cubic interpolation.
- For higher-order point models, trim data of the higher-order states must be included. If these higher-order state trim data are not collected in flight, the data must be calculated and tabulated in processing.
- The stitched model is a quasi-nonlinear flight dynamics simulation model with linear, time-varying aerodynamics. The stitched model is accurate over the nominal flight envelope but does not, by default, include certain nonlinearities or edge-of-the-envelope dynamics, such as stall or autorotation. Nonlinear components can be incorporated into the stitched model but require additional flight-test data and modeling efforts.

5.8 REFERENCES

[1] Tischler, M.B., White, M.D., Cameron, N., D'Agosto, S., Greiser, S., Gubbels, A., Guner, F., He, C., Horn, J., Hui., K., Jones, M., Juhasz, O., Lee, O., Lehmann, R., Miller, D., Myrand-Lapierre, V., Nadeau-Beaulieu, M., Nadell, S., Padfield, G., Pavel, M., Prasad, J., Ragazzi, A., Richard, S., Scepanovic, P., Seher-Weiß, S., Soong, J., Stroosma, O., Taghizad, A., Tobias, E., Xin, H., and Yavrucuk, I. (2021), "Rotorcraft Flight Simulation Model Fidelity Improvement and Assessment," NATO STO AVT-296 Technical Report.

[2] Tischler, M.B., and Remple, R.K. (2012), *Aircraft and Rotorcraft System Identification: Engineering Methods with Flight Test Examples*, 2nd ed. American Institute of Aeronautics and Astronautics, Reston, VA.

[3] Tischler, M.B., Fletcher, J.W., Morris, P.M., and Tucker, G.T. (1989), "Applications of Flight Control System Methods to an Advanced Combat Rotorcraft," NASA Technical Memorandum 101054, 1989.

[4] Tischler, M.B., Berger, T., Ivler, C.M., Mansur, M.H., Cheung, K.K., and Soong, J.Y. (2017), Practical Methods for Aircraft and Rotorcraft Flight Control Design: An Optimization-Based Approach, AIAA, April.

[5] Tischler, M.B. Blanken, C.L., Cheung, K.K., Swei, S.M., Sahasrabudhe, V., and Faynberg, A. (2004), "Optimization and Flight Test Results of Modern Control Laws for the UH-60 Black Hawk," Proceedings to AHS 4th Decennial Specialists' Conference on Aeromechanics, San Francisco, CA, 21 – 23 January 2004.

[6] Fu, K.H., and Kaletka, J. (1990), "Frequency-Domain Identification of Bo 105 Derivative Models with Rotor Degrees of Freedom," Proceedings of the 16th European Rotorcraft Forum, Glasgow, UK, 1990.

[7] Takahashi, M.D., Fletcher, J.W., and Tischler, M.B. (1995), "Development of a Model Following Control Law for Flight Simulation Using Analytical and Identified Models," USAATCOM Technical Report 95-A-007, 1995.

[8] Seher-Weiß (2016), "FitlabGui – A Versatile Tool for Data Analysis, System Identification and Helicopter Handling Qualities Analysis," 42nd European Rotorcraft Forum, Sep. 5 – 8, Lille, France.

[9] Seher-Weiss, S., and von Gruenhagen, W. (2012), "Development of EC 135 Turbulence Models via System Identification," *Aerospace Science and Technology*, Vol. 23, p. 43-52.

[10] Myrand-Lapierre, V., Tischler, M.B., Pavel, M.D., Nadeau Beaulieu, M., Stroosma, O., Gubbels, B., and White, M.D. (2020), "Bell 412 Modeling and Model Fidelity Assessment for Level-D Training Simulators," Vertical Flight Society Forum 76, Virtual, Oct 5 – 8.

[11] Wartmann, J. (2017), "Closed-Loop Rotorcraft System Identification Using Generalized Binary Noise," American Helicopter Society 73rd Annual Forum, Fort Worth, TX, May 9 – 11.

[12] Grünhagen, W. von, Bouwer, G., Pausder, H.J., Henschel, F., and Kaletka, J. (1994), "A High Bandwidth Control System for the Helicopter In-flight Simulator ATTHeS – Modelling, Performance and Applications," *International Journal of Contro*l, 59 (1).

[13] Seher-Weiß, S., Tischler, M.B., Scepanovic, P., and Gubbels, A. (2021), "Bell 412 System Identification and Model Fidelity Assessment for Hover and Forward Flight," *Journal of American Helicopter Society*, Vol. 66, 012004, Jan.

[14] Greiser, S. (2019), "High-fidelity rotorcraft simulation model: analyzing and improving linear operating point models," *CEAS Aeronautical Journal*, 10 (3), pp. 687-702, DOI 10.1007/s13272-018-0345-9.

[15] Greiser, S., and von Grünhagen, W. (2013), "Analysis of Model Uncertainties Using Inverse Simulation," American Helicopter Society 69th Annual Forum, Phoenix, AZ, May 21 – 23.

[16] Jategaonkar, R.V. (2015), *Flight Vehicle System Identification: A Time-Domain Methodology*, American Institute of Aeronautics and Astronautics, Inc.

[17] Klein, V., and Morelli, E.A. (2016), *Aircraft System Identification: Theory and Practice,* 2nd Ed. Sunflyte Enterprises Williamsburg, VA.

[18] Lu, L., Padfield, G.D., White, M.D., and Perfect, P. (2011), "Fidelity Enhancement of a Rotorcraft Simulation Model Through System Identification," *The Aeronautical Journal*, Volume 115, No. 1170, pp. 453-470 August.

[19] Pitt, D., and Peters, D.A. (1981), "Dynamic Inflow for Practical Applications," *Vertica*, Vol. 5, No. 1.

[20] Peters, D.A., and He, C. (1991), "Correlation of Measured Induced Velocities with a Finite State Wake Model," *Journal of American Helicopter Society*, Vol. 37, No. 3, Jul.

[21] Rosen, A., and Isser, M. (1994), "A New Model of Rotor Dynamics During Pitch and Roll of a Hovering Helicopter," AHS 49th Annual Forum, Washington, D.C. May.

[22] Keller, J.D., and Curtiss, H.C. (1998), "A Critical Examination of the Methods to Improve the Off-Axis Response Prediction of Helicopters," AHS 54th Annual Forum, Washington D.C., May.

[23] Krothapalli, K.R., Prasad, J.V.R., and Peters, D.A. (2001), "Helicopter Rotor Dynamic Inflow Modeling for Maneuvering Flight," *Journal of the American Helicopter Society*, Vol. 46, No. 2.

[24] Zhao, J., Prasad, J.V.R., and Peters, D.A. (2004), "Rotor Dynamic Wake Distortion Model for Helicopter Manoeuvring Flight," *Journal of the American Helicopter Society*, Vol. 49, No. 4, October, pp. 414-424.

[25] He, C., and Zhao, J. (2008), "A Real Time Finite State Induced Flow Model Augmented with High Fidelity Viscous Vortex Particle Simulation," AHS 64th Annual Forum, Montreal, Quebec, Canada, April- May

[26] He, C., and Zhao, J. (2009), "Modeling Rotor Wake Dynamics with Viscous Vortex Particle Method," AIAA Journal, Vol. 47, No. 4, April.

[27] He, C., Gladfelter, M., Chang, C., Tischler, M.B., and Juhasz, O. (2019), "VPM-Derived State Space Inflow Model for Multi-Rotor Air Vehicle Modeling and Simulation," VFS 75th.Annual Forum, Philadelphia, PA, May.

[28] Howlett, J. (1981b), "UH-60A Black Hawk Engineering Simulation Program: Volume II – Background Report," NASA CR-166310, December.

[29] Guner, F., Kong, Y.B, Prasad, J.V.R., Peters, D.A., and He, C. (2018), "Development of Finite State Inflow Models for Multi-Rotor Configurations using Analytical Approach," in Proceedings of the AHS 74th Annual Forum, Phoenix, AZ, May.

[30] Hackett, W.E., Garnett, T.S., and Borek, B.V. (1983), "Mathematical Model of the CH-47B Helicopter Capable of Real-Time Simulation of the Full Flight Envelope," Vol.1, NASA CR-166458, July.

[31] Howlett, J. (1981a), "UH-60A Black Hawk Engineering Simulation Program: Volume I – Mathematical Model," NASA CR- 166309, December.

[32] Keller, J., McKillip, R., Wachspress, D., Tischler, M.B., and Juhasz, O, (2019), "Linear Inflow and Interference Models from High Fidelity Free Wake Analysis for Modern Rotorcraft Configurations," AHS 75th Annual Forum, Philadelphia, PA, May.

[33] Rand, O., Khromov, V., Hersey, S, Celi, R., Juhasz, O., and Tischler, M.B. (2015), "Linear Inflow Model Extraction from High-Fidelity Aerodynamic Models for Flight Dynamics Applications," AHS 71st Annual Forum, Virginia Beach, VA, May.

[34] Hersey, S. Celi, R. Juhasz, O., and Tischler, M.B. (2018), "Accurate State Space Inflow Modeling for Flight Dynamics and Control of a Coaxial-Pusher Rotorcraft," AHS 74th Annual Forum, Phoenix, AZ, May.

[35] Juhasz, O., Xin, H., and Tischler, M.B. (2020), "Inflow Based Flight Dynamics Modeling Improvements for the Sikorsky X2 Technology™ Demonstrator," VFS 76th Annual Forum, Virtual, Oct 5 – 8.

[36] Leishman, J. G., Bhagwat, M. J., and Bagai, A. (2002), "Free Vortex Filament Methods for the Analysis of Helicopter Rotor Wake," *Journal of Aircraft*, Vol.39(5), Sept-Oct., pp.759-775.

[37] He, C., Xin, H., and Bhagwat, M. (2004), "Advanced Rotor Wake Interference Modeling for Multiple Aircraft Shipboard Landing Simulation," AHS 59th Annual Forum, Baltimore, MD.

[38] Xin, H., Zhang, C., and Driscoll, J. (2019), "Enhancement of an Engineering Simulation Model to Improve the Correlation with Flight Test Data in Climb/Descent and Autorotations," AHS 75th Annual Forum, Philadelphia, PA, May.

[39] Spira, D., Myrand-Lapierre, V., and Soucy, O. (2012), "Reducing Blade Element Model Configuration Data Requirements Using System Identification and Optimization," American Helicopter Society 68th Annual Forum, Fort Worth Texas, May.

[40] Basset, P.M., and Brocard, M. (2004), "Fenestron Model for Improving the Helicopter Yaw dynamics flight simulation," 30th European Rotorcraft Forum, Marseille, France.

[41] Geiger, B.R., Piasecki, F.W., Horn, J.F., Schifferle, P., and Lotterio, M. (2010), "Challenges of Flight Control in a Compound Helicopter," Proceedings of the International Powered Lift Conference, Philadelphia, PA, October 5 – 7.

[42] O'Neill, E. (2011), *Modeling and Control of Trailing Edge Flaps for Gust Alleviation and Handling Qualities*, M.S. Thesis, The Pennsylvania State University, May.

[43] Krishnamurthi, J., and Horn, J.F. (2015), "Helicopter Slung Load Control Using Lagged Cable Angle Feedback," *Journal of the American Helicopter Society*, Vol. 60 (2), April.

[44] Fegely, C., Juhasz, O., Xin, H., and Tischler, M.B. (2016), "Flight Dynamics and Control Modeling with System Identification Validation of the Sikorsky X2TM-Technology Demonstrator," Proceedings of the 72nd Annual AHS Forum, West Palm Beach, FL, May 17 – 19.

[45] Hui, K., Lambert, E., and Seto, J. (2006), "Bell M427 Flight Test Data Gathering and Level-D Simulator Model Development," ICAS 25th Congress, Hamburg, Germany, September.

[46] Zivan, L., and Tischler, M.B. (2010), "Development of a Full Flight Envelope Helicopter Simulation Using System Identification," *Journal of the American Helicopter Society*, Vol. 55, (022003), pp. 1-15.

[47] Greiser, S., and Seher-Weiß, S. (2014), "A contribution to the development of a full flight envelope quasi-nonlinear helicopter simulation," *CEAS Aeronautical Journal*, Vol. 5, (1), pp. 53-66.

[48] Tobias, E.L., and Tischler, M.B. (2016), "A Model Stitching Architecture for Continuous Full FlightEnvelope Simulation of Fixed-Wing Aircraft and Rotorcraft from Discrete-Point Linear Models," U.S. Army AMRDEC Special Report RDMR-AF-16-01, April.

Chapter 6 – AIRCRAFT DATABASES LECTURE SERIES NOTES

ABSTRACT

To support the case studies described in this report, comprehensive sets of flight-test data were required from a variety of different aircraft. Ideally, multiple aircraft configurations would be represented so that the various model update methods could be applied to more than just single main rotor helicopters. For this reason, the eight aircraft databases described in this chapter include not only conventional configurations, but also a tandem rotor helicopter, a Fenestron equipped helicopter, a co-axial rotor helicopter, and a quadcopter. Each aircraft is presented along with its basic weight and balance information, rotor characteristics, a list of instrumented parameters from the flight test, and a summary of the configuration and flight-test data available for modeling purposes. Each section also describes the modeling activities and baseline aircraft models to which the update methods were applied.

6.1 NRC BELL 412 ASRA

6.1.1 Basic Data Overview

Basic Information:

Type:	**Manufacturer:**	**Class:**
Bell 412 HP	Bell (formerly Bell Helicopter)	Conventional single main rotor
Role:	**Accommodation:**	**Registration**
Medium Utility	15, including one or two pilots	Canadian C-FPGV sn 36034

Weights:

Empty:	**Maximum Takeoff:**	**Useful Load:**
6,838 lb	11,900 lb	5,111 lb
Cargo Hook Limit:	**Internal Volume:**	**Max Fuel Load:**
4,500 lb	358 cubic ft	2,150 lb

Performance:

Cruise Speed:	**VNE:**	**Range:**
125 kn	140 kn	330 nm
Endurance:	**Max Sideward Velocity:**	**Max Rearward Velocity:**
3.7 hrs	35 kn	30 kn

6.1.2 Summary of Available Modeling Data

Approximately 40 hours of flight testing were performed to acquire the following data.

Configuration Data	Main rotor cyclic blade angle ranges
	Main rotor collective blade angle ranges
	Tail rotor collective blade angle ranges
	Tail rotor delta-3
	Main rotor mass and stiffness data
	Horizontal stabilizer dimensions and airfoil
	Horizontal stabilizer spring properties (stab is spring-loaded)
	Vertical stabilizer dimensions and airfoil
	Main rotor 3D scanned model (step file)
	Fuselage 3D scanned model (step file)
Flight-Test Data	Trim points 30, 60, 90, 120 kn
	Climbs and descents at 60, 75, 90, 105 kn and 500, 1000, 1500, 2000 ft/min
	RUDR at 5, 10, 15, 20, 25, 30 kn at 30 degree azimuths
	Beta sweeps at 60 and 90 kn
	Autorotation at 60, 90, 120 kn
	Frequency sweep at hover, 30, 60, 90, Vh kn
	2311 at hover, 30, 60, 90, 120 kn
	2311 in climbs and descents at 60 and 90 kn, 1000 ft/min
	ADS33 Acel/Decel, sidestep and bob-up
	Hover at 5, 10, 20, 30, 40, 50 ft in turbulence behind a hangar

Instrumented Parameter List:

Control Positions	Pilot stick positions (pre SAS)
	Control positions (post SAS)
Inertial	Body axis rates
	Body axis accelerations
	Attitude
	WGS-84 position and height
	Velocity (3 components)
	Radar altitude
	Laser altitude
Air Data	Static and Dynamic pressure (raw and PEC)
	Airspeed
	Altitude
	Angle of attack
	Sideslip
	Total temperature
	Wind direction
	Wind speed
	Fuselage pressure measurements at 200+ locations
Drivetrain	Mast torque
	Engine 1 and 2 torque
	Rotor speed
	Power turbine 1 and 2 speed
	Gas generator 1 and 2 speed
Rotor States	Individual blade flap
	Individual blade lag
	Coning
	Lateral tilt
	Longitudinal tilt
	Lateral lag
	Longitudinal lag
	Blue blade beam bending at station 36
	Blue blade chord bending at station 36
	Blue blade beam bending at station 132
	Blue blade chord bending at station 132

6.1.3 Modeling Activities and Baseline Models

Organization	NRC	CAE	DLR	U of Liverpool
Model Type	6-DOF time domain	SysID in frequency- and time-domain-based models are used as stepping-stones to support the development of the final BERM model used in the simulator.	Linear models 8-20 states time domain followed by physics-based 6-DOF plus rotor states and engine states frequency domain	Physics-based flight lab
Update Methods	7-Stitched model from point ID	5-Model parameter adjustments 3-Force and moment increments Based on: 7- Stitched model from point ID	2-Black box corrections (inverse simulation)	3-Force and moment increments 4-Pysics based corrections 6-Parameter ID of key constants
Primary Deficiencies to be Addressed with Update Method		Cross-coupling		
Primary End-Use(s)	Training simulator	Training simulator	Engineering simulator	Engineering simulator

6.1.3.1 Identified Models in Forward Flight

Three baseline Bell 412 models were developed using the flight-test database for the 90 kn flight condition. These models are standard 6 degree of freedom linear models plus added time delays in all control inputs. The NRC model was developed using the maximum likelihood estimator time-domain method, and no model reduction was performed on the results. The DLR model used Fitlab's frequency response method, and derivatives with high uncertainty levels were eliminated from the model structure as long as this elimination did not cause a significant degradation in model accuracy. The CAE model was developed using the output error method in the frequency domain, and CAE also eliminated several derivatives from the model structure while restricting all speed stability derivatives.

6.1.3.2 Identified Models in Hover

Two baseline Bell 412 models were developed using the flight-test database for the hover flight condition. The ADD model was developed using the CIFER tool in the frequency domain. This state-space model was comprised of the standard 6-DOF equations-of-motion augmented with inflow and coning equations and a simple Padé engine model.

The NRC model was developed using the MLE tool in the time domain. This state-space model was comprised of the standard 6-DOF equations-of-motion. The NRC hover model stability and control derivatives are provided in the following tables:

6.1.3.3 University of Liverpool Physics-Based Model

The description of the FLIGHTLAB Bell 412 (F-B412) begins with the main rotor. A centre-spring rigid-blade model has been developed which has the added benefit of simplifying greatly the modeling. The spring strengths and locations were chosen to match the first flap and lag frequency estimated from measurements on the NRC ASRA. A blade-element model is used where the blade aerodynamic segments are defined based on the equal annuli area approach. The quasi-steady aerodynamic loads are calculated by treating the blade sections as two-dimensional panels. The 2D aerofoil table includes lift, drag and pitch moment coefficients as functions of angle of attack and Mach number. The inflow model used is the enhanced Peters-He finite three state dynamic inflow model which is augmented with dynamic wake distortion to correct the often poorly predicted off-axis roll/pitch response in low-speed transient maneuvers.

The tail rotor is modeled using the FLIGHTLAB's Bailey rotor component. Fuselage aerodynamics are included as a table look-up where the lift, drag and pitching moment coefficients are supplied as functions of angle of attack and sideslip angle and inertias provided by NRC. Each horizontal stabilizer is represented as one aerofoil section with inverted Clark-Y aerofoil with Gurney flap fitted on the trailing edge. The stabilizers and fin are represented as 2D aerodynamic lookup tables with one and 3 sections, respectively. In addition, the spring-loaded stabilizer angle is determined by the aerodynamic pitching moment.

6.2 US ARMY ADD UH-60 RASCAL

6.2.1 Basic Data Overview

Basic Information:

Type:	**Manufacturer:**	**Class:**
JUH-60A	Sikorsky	Conventional single main rotor
Role:	**Accommodation:**	**Registration:**
Medium Utility	15, including two pilots	Army S/N 78-23012

Weights:

Empty:	**Maximum Takeoff:**	**Useful Load:**
10,260 lb	20,250 lb	
Cargo Hook Limit:	**Internal Volume:**	**Max Fuel Load:**
8,000 lb		362 gallons

Performance:

Cruise Speed:	**VNE:**	**Range:**
150 kts	193 kts	1,380 nm (with external tanks)
Endurance:	**Max Sideward Velocity:**	**Max Rearward Velocity:**
	45 kts	45 kts

6.2.2 Summary of Available Modeling Data

Configuration Data	Available in Howlett Report (NASA CR-166309)
	Mixer identified from US Army RASCAL
	Nominal US Army RASCAL Inertias
Flight-Test Data	Frequency sweeps at hover and 80 kts. Time histories as well as frequency response
	doublets at hover
	2311 at 80 kn

Base Instrumented Parameter List (Hover has many more parameters):

Control Positions	Pilot stick positions (SAS off, so these are control positions)
	Swashplate and tail rotor servo positions
	Stabilator position
Inertial	Body axis angular rates and accelerations
	Body axis linear accelerations
	Attitudes
Air Data	Static pressure
	Differential pressure
	Speed
	Angle of attack
	Angle of sideslip
Drivetrain	Rotor speed

Rotor States	Individual blade flap
	Individual blade lag
	Individual blade pitch
	Rotor azimuth
	Fixed-frame flapping

6.2.3 Modeling Activities and Baseline Models

Organization	USNA	ART	GT
Model Type	GenHel Based linearized blade element model	FLIGHTLAB based blade element model	FLIGHTLAB based blade element model
Update Methods	1-Gain and Time Delay Corrections	4-Reduced Order Models and Physics-based Corrections	4-Reduced Order Models and Physics-based Corrections
Primary Deficiencies to be Addressed with Update Method	Mismatch for key on-axis responses	Off-Axis responses mismatch	Off-axis response mismatch
Primary End-Use(s)	Handling Qualities and Flight Control Design	Training simulator	Engineering Simulator

Organization	SAC	PSU	TDD
Model Type	FLIGHTLAB based blade element model	GenHel based linearized blade element model	GenHel based linearized blade element model
Update Methods	4-Reduced Order Models and Physics-based Corrections	5-Simulation model parameter adjustment	7-Stitched Simulation from Point ID Models and Trim Data
Primary Deficiencies to be Addressed with Update Method	Overall match with flight-test data in trim and dynamic response in variety of flight conditions	General mismatch in frequency responses	Original model is not real-time
Primary End-Use(s)	Engineering simulator	Training simulator	Training Simulator

The UH-60 simulation models used in this report are broadly categorized to originate from two commonly used simulation environments, ones based on GenHel and other using FLIGHTLAB.

6.2.3.1 GenHel Based Model

The first and still widely used UH-60 model is the GenHel nonlinear blade-element simulation originated at Sikorsky Aircraft, which had rigid blades, Glauert harmonic inflow distribution, 2D airfoil tables, and wind

tunnel-based lookup tables for the fuselage. The Ames GenHel model variant used by TDD, USNA, and PSU, incorporated a 3-state Pitt-Peters inflow model and a sophisticated engine/drivetrain model for the 701C engine. Using the simulation equations from GenHel, the University of Maryland and TDD developed the companion tool FORECAST to determine an accurate trim solution (based on periodic balance) and to extract high-order linearized models of varying complexity (up to 54 states) using numerical perturbation methods. Wake curvature effects due to tip-path-plane rate have a first-order effect on the off-axis angular responses in conventional flapping rotors and the on-axis response of stiff hingeless rotors. Wake curvature corrections included in Ames GenHel and FORECAST use a defined lookup table of the aerodynamic phase lag as obtained from system identification results of UH-60 flight data and are used in this study. The user can also select the Keller correction to the Pitt-Peters model, which has been shown to provide an equivalent correction effect. FORECAST linear models have been used extensively for handling qualities and flight dynamics and control applications. The PSU version of the GenHel model (PSU-HeloSim) was derived from the Ames variant of GenHel, but it was re-hosted in the MATLAB/Simulink environment and implemented in state-space form such that high-order linear models can be extracted (41 states).

6.2.3.2 FLIGHTLAB Based Model

The second UH-60 model is obtained from the FLIGHTLAB simulation environment. FLIGHTLAB is a multibody dynamics-based comprehensive rotorcraft modeling and simulation tool used in UH-60 simulation model fidelity improvement method study. The baseline UH-60 simulation model from FLIGHTLAB was built using blade-element modeling option. The blade-element model covers rotor structural dynamics, unsteady airloads, and Peters-He's finite state (truncated to 3-states) induced inflow dynamics. The rotor dynamics model considers geometrically the exact hub articulated retention, both flap and lag hinge dynamics, and rigid blades. The unsteady airloads modeling includes quasi-steady nonlinear airfoil table lookup with respect to blade segment local angle of attack and Mach number plus the effects of yawed flow, unsteady pitch rate, stall delay, and dynamic rotor wake. The fuselage is modeled with nonlinear 6-DOFs and the table lookup of airloads with respect to angle of attack and angle of sideslip of fuselage. Airloads of empennage, both horizontal stabilator and vertical fin, are computed with respect to local angle of attack of aerodynamic segments with the effect of rotor and fuselage interference. The Viscous Vortex Particle Method (VPM) was adopted for improved rotor wake and interference modeling. VPM is a high fidelity first principle-based rotor wake dynamics solver but is computationally very efficient. In the current research, a reduced order rotor inflow dynamics model extracted from VPM simulation is used and integrated with FLIGHTLAB's full flight simulation model for the methodology study.

Sikorsky also developed an engineering simulation model in FLIGHTLAB for the S-70i International Black Hawk helicopter. A blade-element model was applied for both main and tail rotors. The main rotor three-hinge articulation was modeled, including a nonlinear damper with accurate kinematics and validated damping characteristics. The hingeless tail rotor was modeled with an effective hinge offset and a flapping hinge spring to match the measured flatwise bending frequency. The main and tail rotor were modeled with nonlinear quasi-unsteady airloads with stall delay. A 45-state Peters-He inflow model for the main rotor and a 6-state model for the tail rotor provided sufficient inflow fidelity. The inflow L-matrix correction was applied to modeling the effects of the wake distortion in maneuver and the ground vortex in ground effect. Various aerodynamic interference effects were modeled, including the main rotor interference on the fuselage, empennage, tail rotor, the tail rotor interference on the vertical fin, and the fuselage interference on the empennage.

6.3 EC 135

6.3.1 Basic Data Overview

Basic Information:

Type:	**Manufacturer:**	**Class:**
EC 135 T2+	Airbus Helicopters	Conventional single main rotor and Fenestron
Role:	**Accommodation:**	**Registration:**
Light multi-purpose h/c	Max 8 (including flight crew)	

Weights:

Empty:	**Maximum Take-Off:**	**Useful Load:**
1,880 kg	2,910 kg	1,130 kg max cargo
Cargo Hook Limit:	**Internal Volume:**	**Max Fuel Load:**
		568 kg

Performance:

Cruise speed:	**VNE:**	**Range:**
135 kt (fast cruise)	155 kt at MSL	340 nm
Endurance:	**Max sideward Velocity:**	**Max Rearward Velocity:**
3.5 h		

6.3.2 Summary of Available Modeling Data

The DLR conducted flight tests with the EC135 ACT/FHS and gathered data at five operating points from hover to 120 kn. About 1 flight hour per trim speed was required for the basic SysID maneuvers (frequency sweeps and 2311 multistep maneuvers) of the EC135 database. One flight hour was needed for the trim points at different airspeeds (necessary for model stitching) and approximately one additional flight hour was needed to repeat certain test points. Thus, the overall effort is about 7 flight hours. From this database, the hover and 60 kn flight-test data are shared as presented below in the tables.

Flight-Test Data	2311 multistep data at hover and 60 kn (ACT/FHS EC135)
	Sweep data at hover and 60 kn (ACT/FHS EC135)
	Steps at hover and 60 kn (Thales EC135 T2+)
	All SAS off

Instrumented Parameter List:

Control Positions	Cyclic (longitudinal and lateral), directional, collective
Inertial	Load factor (longitudinal, lateral, and vertical)
	Angular rates (pitch, roll, and yaw)
	Attitude (pitch, roll, and heading)
	Ground speed (horizontal, longitudinal, lateral, and vertical)
	Altitude
Air Data	ACT/FHS: side slip, angle of attack, and true airspeed from noseboom Thales: estimated sideslip, and airspeed

6.3.3 Modeling Activities and Baseline Models

Organization	DLR	Thales	Aerotim/METU
Model Type	Physics-based and 11-DOF identified	Physics-based Blade Element Theory (BET) for the main rotor	Physics-based flight model with blade element rotor model for main rotor
Update Methods	2: Black box corrections 7: Stitched model from point ID	5: Model parameter adjustments	3: Force and moment increments
Primary Deficiencies to be Addressed with Update Method	2: include missing high-order dynamics 7: better match with flight-test data	Lateral damping at high frequency	Off-axis response
Primary End-Use(s)	Engineering simulator	Training simulator	Training simulator

6.3.3.1 DLR Physics-Based Simulator Model

DLR's Air Vehicle Simulator (AVES) Centre operates a flight simulator for the Active Control Technology/Flying Helicopter Simulator (ACT/ FHS) rotorcraft. The bare-airframe ACT/FHS helicopter is represented in AVES by a realtime nonlinear flight simulation model in a program system called HeliWorX. It has a classical modular structure dividing the helicopter model into its components (fuselage, horizontal stabilizer, vertical stabilizer, main rotor, tail rotor, etc.), which allows both component-wise validation and simple reconfiguration of single elements. The EC135 configuration data were provided by Eurocopter Deutschland during the ACT/FHS project realization phase. The main rotor is modeled as fully articulated with an equivalent hinge offset and spring restraint in order to represent flapping and lagging natural frequencies. Each main rotor blade is modeled as a rigid blade, and blade element theory is used to calculate the aerodynamic forces and moments. Overall, 10 blade sections are used to model each blade of the main rotor, and the dynamic inflow model of Pitt and Peters is used for the piloted simulation.

6.3.3.2 DLR SysID Models

The system identification database for the EC135 consists of sweeps and 3211-multistep manoeuvres at five operating points (hover, 30, 60, 90, 120 kn). For each operating point, a high-order 11-DOF model was identified that considers the body-fixed velocities (u, v, w – m/s), angular rates (p, q, r – rad/s), flapping (a, b – rad), regressive lead-lag (x_{ll}, y_{ll} – rad), and mean inflow (ν – m/s). The identification was performed using the maximum likelihood method in the frequency domain over a frequency range of 1 – 20 rad/s.

6.3.3.3 Thales

Thales EC135 flight model is a real-time, non-linear, physics-based model, intended to be used in a Flight Simulator Training Device (FSTD) that complies with EASA and FAA FFS Level D requirements. The model has a classical structure, divided into components (including main rotor, tail rotor, fuselage, landing gear, and external loads) and includes the interaction between theses components and with the ground.

The model was developed in the time domain using an extended set of data collected on actual aircraft on ground and in flight, mainly based on validation requirements set out in EASA and FAA standards, which includes static performances, controls inputs (pulses, steps, doublets, etc.), proper modes (phugoid, dutch roll, etc.), trajectories (take-off, landing, autorotation, acceleration and deceleration, etc.), ground handling, and engine operations. Data were gathered at various altitudes and airspeeds and with various weight and CG configurations within the flight envelope.

6.3.3.4 Aerotim/METU

The EC135 baseline model is a nonlinear, physics-based flight model using Aerotim's core model components, intended for the development of flight models for EASA Level D certified full flight simulators. The model employs a Blade Element Rotor Model (BERM) with virtual blades, 2nd order flapping, Pitt-Peters inflow, aerodynamic derivatives for fuselage, vertical tail and horizontal tail, and Fenestron model. Those model components have been used in Level D certified simulators for helicopters of similar class and have been verified with flight tests. All corrections employed are removed, leaving the models with their basic representation as reported in literature. For demonstration purposed for this work, the main rotor wake curvature off-axis corrections are removed.

A time-domain adaptation-based linear model identification is employed to identify the linear system of the helicopter in hover. The 3211 manoeuvre data provided by DLR is used in the process.

6.4 CH-47F CHINOOK DIGITAL AUTOMATIC FLIGHT CONTROL SYSTEM (DAFCS) TEST AIRCRAFT

6.4.1 Basic Data Overview

Basic Information:

Type:	**Manufacturer:**	**Class:**
CH-47F Chinook Multi-Year 1	Boeing	Tandem Rotor Helicopter
Role:	**Accommodation:**	**Registration**
Cargo/Transport Helicopter	3 Crew and 33 – 55 troops	U.S. Army M8003

Weights:

Empty:	**Maximum Takeoff:**	**Useful Load:**
24,578 lb	50,000 lb	24,000 lb
Cargo Hook Limit:	**Internal Volume:**	**Max Fuel Load:**
26,000 lb	1,474 cubic ft	1,030 U.S. Gallons (6,695 lb)

Performance:

Cruise Speed:	**VNE:**	**Range:**
160 KTAS	170 KTAS	400 nm
Endurance:	**Max Sideward Velocity:**	**Max Rearward Velocity:**
3.0 hrs	45 KTAS	40 KCAS

6.4.2 Summary of Available Modeling Data

Configuration Data	Forward rotor cyclic blade angle ranges
	Forward rotor collective blade angle ranges
	Aft rotor cyclic blade angle ranges
	Aft rotor collective blade angle ranges
	Forward rotor inertia and mass moment
	Aft rotor inertia and mass moment
Flight-Test Data	Trim points at hover, and 60 KCAS
	Frequency sweeps at hover, and 60 KCAS

Instrumented Parameter List:

Control Positions	Pilot stick positions
	Integrated Lower Controls Actuator (ILCA) positions
	Differential Airspeed Hold (DASH) Actuator position
	Rotor Longitudinal Cyclic Trim Actuator (LCTA) positions
	Longitudinal, Lateral, and Directional Mixer Commands
	Rotor Upper Boost Actuator (UBA) positions
Inertial	Body axis rates
	Body axis accelerations
	Aircraft Attitudes
	Velocity (3 components)
	Radar altitude
Air Data	Airspeed
	Pressure Altitude
	Outside Air Temperature (OAT)
	Differential Pressure (Sideslip)
Drivetrain	Engine 1 and 2 torque
	Rotor speed
	Power turbine 1 and 2 speed
	Gas generator 1 and 2 speed
Rotor States	None

6.4.3 Modeling Activities and Baseline Models

Organization	DSTG	CAE	Georgia Tech	Boeing
Model Type	FLIGHTLAB – Physics-based flight simulation and analysis model.	CAE Generic Blade Element Rotor Model (BERM) – Physics-based flight simulation model.	FLIGHTLAB – Physics-based flight simulation and analysis model.	Boeing Helicopters Simulation (BHSIM) – Physics-based flight simulation model.
Update Methods	1-Gain/Time Delay Corrections for Key Responses 4-Reduced Order Models and Physics-based Corrections 5-Simulation Model Parameter Adjustment	2-"Black Box" Input and Output Filters 4-Reduced Order Models and Physics-based Corrections 5-Simulation Model Parameter Adjustment	4-Reduced Order Models and Physics-based Corrections	4-Reduced Order Models and Physics-based Corrections 5-Simulation Model Parameter Adjustment
Primary Deficiencies to be Addressed with Update Method	Correlation with Australian CH-47F frequency sweep data.	Correlation with frequency sweep data and state-space models.	Correlation with frequency sweep data and state-space models. Lack of finite-state inflow models for tandem rotor helicopters.	Correlation with lateral axis frequency sweep data and state-space models Underprediction of roll rate damping.
Primary End-Use(s)	Engineering simulator	Training simulator	Engineering simulator	Engineering simulator

6.4.3.1 Baseline System Identification Models

CH-47D frequency response data were identified from flight-test data generated during Aeronautical Design Standard 33 (ADS-33) compliance testing conducted at Edwards Air Force Base (EAFB). The published CH-47D system identification data were collected with the Automatic Flight Control System (AFCS) engaged (AFCS-ON); thus, AFCS OFF frequency response data for the CH-47D are estimated from the system identified AFCS-ON data and the known frequency response characteristics of the CH-47D AFCS. Note that the CH-47D and CH-47F airframe and actuator characteristics are virtually identical although there are significant differences between the Automatic Flight Control Systems implemented on CH-47D and CH-47F Chinooks.

State-space models for the longitudinal/heave dynamics of the CH-47F Chinook in hover were identified from flight-test data during the CH-47F Digital Automatic Flight Control System (DAFCS) program. State-space models for the lateral/directional dynamics of the CH-47F Chinook in hover were also identified from flight-test data generated during the CH-47F DAFCS program.

The inputs to the CH-47F system identified state-space dynamic models are the outputs of the mechanical control mixers that combine pilot mechanical path inputs and AFCS inputs. Control mixer positions were not instrumented during the CH-47F DAFCS flight-test program; therefore, the control mixer positions were

reconstructed using the upstream pilot lower boost servo mechanical path and AFCS Stability Augmentation System (SAS) Integrated Lower Controls Actuator (ILCA) measurements as shown in the Figure 6-1 block diagram.

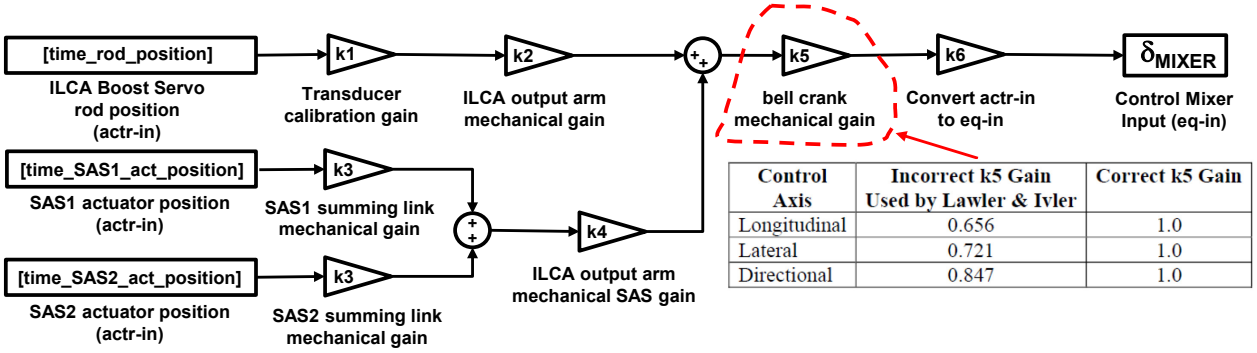

Control Axis	Incorrect k5 Gain Used by Lawler & Ivler	Correct k5 Gain
Longitudinal	0.656	1.0
Lateral	0.721	1.0
Directional	0.847	1.0

Figure 6-1: CH-47 Control Mixer Reconstruction from Upstream Control Positions, Correction to k5 Bell Crank Mechanical Gain.

6.5 AW139 LONG NOSE

6.5.1 Basic Data Overview

Basic Information:

Type:	**Manufacturer:**	**Class:**
AW139	Leonardo Helicopters	Conventional single main rotor
Role:	**Accommodation:**	**Registration:**
Medium multi-purpose h/c	Max 15 passenger + 2 crew	

Weights:

Empty:	**Maximum Take-Off:**	**Useful Load:**
4,250 kg	6,400 kg	
Cargo Hook Limit:	**Internal Volume:**	**Max Fuel Load:**

Performance:

Cruise Speed:	**VNE:**	**Range:**
150 kt	167 kt at MSL	
Endurance:	**Max Sideward Velocity:**	**Max Rearward Velocity:**
5 h 15	See RFM	See RFM

6.5.2 Summary of Available Modeling Data

Flight-Test Data	Collective step at Vy
	Lateral oscillations at Vy
	Lateral step at Vy
	Longitudinal doublet at Vy
	Longitudinal oscillations at Vy
	Longitudinal pulse at Vy
	Longitudinal step at Vy
	Pedals doublet at Vy

Instrumented Parameter List:

Configuration	Gross weight
	Longitudinal CG position
	Lateral CG position
Control Positions	Cyclic longitudinal control position
	Cyclic lateral control position
	Directional control position
	Collective control position
Inertial	Longitudinal load factor
	Lateral load factor
	Vertical load factor
	Roll angular rate

Inertial (cont'd)	Pitch angular rate
	Yaw angular rate
	Bank angle
	Pitch attitude
	Heading
	Horizontal ground speed
	Longitudinal ground speed
	Lateral ground speed
	Vertical speed
	Height
Air Data	Estimated side slip
	Calibrated airspeed
	True airspeed
	Static temperature
	Estimated wind direction
	Estimated wind speed
	Pressure altitude
Drivetrain	Main rotor speed
	Mean engine torque

6.5.3 Modeling Activities and Baseline Models

Organization	**ONERA**
Model Type	Use of Thales Training Simulator model: Nonlinear Flight Mechanics + Blade Element Main Rotor + Aerodynamic interactions
Update Methods	3-Forces and Moments correction terms
Primary Deficiencies to be Addressed with Update Method	Short term response – lateral damping – lateral directional coupling
Primary End-Use(s)	Training Simulator

6.5.3.1 Baseline Model

For this application, ONERA used the Thales Training simulation model of the AW139. It is a real-time, nonlinear, physics-based model, developed for Flight Simulator Training Devices (FSTD). It has a classical structure, divided into components (including main rotor, tail rotor, fuselage, landing gear, and external loads) and includes the interactions between these components and with the ground. Blade elements are used to model the main rotor aerodynamics whereas the tail rotor has an analytical aerodynamic model.

In its certified version, the model is assessed and adjusted in time domain using an extended set of data collected on actual aircraft on ground and in flight, mainly based on validation requirements set out in EASA and FAA standards.

Within AVT-296, the model was used in a degraded version in order to provide a playground for evaluating model improvement Method 3 ('Force and Moment increments'). This version is a step beyond the very initial version of the model (physics-based model configured with the helicopter data package) where some physical parameters are adjusted to comply with the static test points (trim points).

For system identification, a state-space model of lateral axis was used with 4 state variables (p, r, φ, v) and 2 inputs $(\delta_{lat}, \delta_{ped})$.

6.6 AW109 TREKKER

6.6.1 Basic Data Overview

Basic Information:

Type:	**Manufacturer:**	**Class:**
AW109 Trekker	Leonardo	Conventional single main rotor
Role:	**Accommodation:**	**Registration:**
Light utility	1 or 2 pilots with 7 or 6 passengers	

Weights:

Empty:	**Maximum Takeoff:**	**Useful Load:**
	MTOW: 3,175 kg (7,000 lb)	
Cargo Hook Limit:	**Internal Volume:**	**Max Fuel Load:**
1,250 kg		805 liters (213 US gal)

Performance:

Cruise Speed:	**VNE:**	**Range:**
281 km/h 152 kn	281 km/h 152 kn	833 km 450 nm
Endurance:	**Max Sideward Velocity:**	**Max Rearward Velocity:**
4 h 20 min		

6.6.2 Summary of Available Modeling Data

Configuration Data	Main rotor cyclic blade angle ranges
	Main rotor collective blade angle ranges
	Tail rotor collective blade angle ranges
	Tail rotor delta-3
	Main rotor mass and stiffness data
	Horizontal stabilizer dimensions and airfoil
	Vertical stabilizer dimensions and airfoil
Flight-Test Data	Trim points 0, 45, 60, 90, 120, 140 kts
	HD 0, 10000, 18000 ft
	AFCS OFF
	Frequency sweep
	3211
	Doublets

Instrumented Parameter List:

Control Positions	**Pilot Stick Positions**
Inertial	Body axis rates
	Accelerometer measurements
	Attitude
	Rate of climb
	Airspeed
	Altitude
	Angle of attack
	Sideslip
	Total temperature
Drivetrain	Fuel flow
	Engine 1 and 2 torque
	Rotor speed
	Power turbine 1 and 2 speed
	Gas generator 1 and 2 speed

6.6.3 Modeling Activities and Baseline Models

Organization	Leonardo Helicopters
Model Type	Real-time, full non-linear, physic based model developed in FLIGHTLAB.
Update Methods	4-Reduced Order Models and Physics-based Corrections
Primary Deficiencies to be Addressed with Update Method	Main rotor to tail planes interference. Yaw axis response to collective inputs. Roll-off of frequency responses from mid to high frequency.
Primary End-Use(s)	Engineering simulator.

6.6.3.1 Baseline Model

The base line model is a real-time, full non-linear, physic based model developed in FLIGHTLAB featuring:

- Blade element main rotor with rigid blades and quasi-unsteady aerodynamics (alpha at ¾ chord point, yawed flow, dynamic stall due to rotation).
- Peters-He finite state wake (3 states).
- Disk tail rotor.
- Main rotor interference on tail planes (3 states).
- Wind tunnel data for fuselage and tail planes aerodynamics.
- Ideal engine.
- AFCS off.

6.7 SIKORSKY X2 TECHNOLOGY™ DEMONSTRATOR

6.7.1 Basic Data Overview

Basic Information:

Type:	**Manufacturer:**	**Class:**
Sikorsky X2 Technology™ Demonstrator	Sikorsky, a Lockheed Martin (LM) Company	Coaxial rotor compound with pusher propeller
Role:	**Accommodation:**	**Registration**
Technology demonstrator	Two pilots	N525SA

Weights:

Empty:	**Maximum Takeoff:**	**Useful Load:**
5,300 lb	–	–
Cargo Hook Limit:	**Internal Volume:**	**Max Fuel Load:**
N/A	–	–

Performance:

Cruise Speed:	**VNE:**	**Range:**
250 kn	–	–
Endurance:	**Max Sideward Velocity:**	**Max Rearward Velocity:**
–	–	–

6.7.2 Summary of Available Modeling Data

Configuration Data	Upper and lower rotor mass/inertia and stiffness distribution
	Upper and lower rotor chord length, twist, and airfoil distribution
	Airfoil characteristics
	Propeller inertia and aerodynamic properties
	Fuselage inertia and aerodynamic properties
	Empennage geometry and aerodynamic properties
	Fuselage on empennage interference
	Flight control system model
	Drivetrain inertia and stiffness
	Turboshaft engine model
Flight-Test Data	Trim controls, hover through 250 kts
	Hub moments at trim points, hover through 250 kn
	Pitch axis open-loop frequency responses, hover and 200 kn
	Roll axis open-loop frequency responses, hover and 180 kn
	Pitch axis closed-loop frequency responses, hover
	Roll axis closed-loop frequency responses, hover
	Time-domain body response to pitch doublet, 200 kn
	Time-domain body response to roll doublet, 200 kn
	Blade flatwise bending moment at 12.5%R during roll doublet, 200 kn
	Upper/lower rotor blade proximity during roll doublet, 200 kn

Instrumented Parameter List:

Control Positions	Pilot stick positions
	Rotor and propeller Control positions
Inertial	Body axis rates
	Body axis accelerations
	Attitude
	Velocity (3 components)
	Radar altitude
Air Data	Static and Dynamic pressure
	Airspeed
	Altitude
	Angle of attack
	Sideslip
	Total temperature
Drivetrain	Engine torque
	Rotor speed
Rotor States	Blade flatwise bending at various stations
	Blade chordwise bending at various stations
	Blade torsion at various stations
	Blade proximity

6.7.3 Modeling Activities and Baseline Models

Modeling Activities:

Organization	Sikorsky	US Army ADD
Model Type	**State-space GenHel model** Modal elastic blades, nonlinear unsteady airloads, and 3-state dynamic inflow and mutual interference.	**HeliUM model** Modal elastic blades, nonlinear airloads, and 3-state dynamic inflow. Effective interference modeled in hover.
Update Methods	4-Reduced order models and physics-based corrections	4-Reduced order models and physics-based corrections 6-Parameter Identification of Key Simulation Constants
Primary Deficiencies to be Addressed with Update Method	Roll frequency response See Sections 7.4.5 for details	Roll frequency response See Sections 7.4.5 and 7.6.2 for details.
Primary End-Use(s)	Engineering simulation	Engineering simulation

6.7.3.1 X2TD GenHel Simulation Model

GenHel (Generic Helicopter Flight Dynamics Simulation) is a Sikorsky proprietary simulation environment that allows for complete free-flight analysis and real-time simulation of any rotorcraft for which sufficient model data is available. GenHel is capable of modeling the complete air vehicle including engine/fuel control dynamics, flight control systems, elastic airframe deformation, and external load dynamics. GenHel has been developed over many decades at Sikorsky and has been used for the flight dynamic modeling of all current production and development aircraft and various non-Sikorsky aircraft. It has been extensively correlated against a wide variety of flight-test data and updated as appropriate. The State-Space GenHel (SSGH) X2TD model is an engineering simulation model where the coaxial rotors are modeled with elastic blades, nonlinear unsteady airloads, and dynamic inflow with mutual interference. A finite-state rotor interference model has been developed and applied for coaxial rotor modeling. The model uses a finite-state form to model the rotor induced velocity at a circular disk off the rotor. The influence coefficient matrix (L-matrix) and time constants (M-matrix) of the model can be pre-calculated using either a pressure potential model or a free wake model. The full aircraft model includes nonlinear aerodynamics for the fuselage and empennage of which the data maps were derived from the 2012 UTRC Pilot Tunnel Test. The rotor interference on fuselage and empennage is modeled using data maps generated from a CHARM model. The aircraft mass properties are set to be the test aircraft configuration. The flight control system is modeled with SAS gains aligned with the flight test. Estimated control system stiffness is also modeled.

6.7.3.2 X2TD HeliUM Simulation Model

HeliUM is a comprehensive rotorcraft simulation code used primarily for flight dynamics modeling with many flight-test-based validation efforts. HeliUM derives from a high-order single main rotor helicopter model with a dynamic inflow wake model and flexible blades with coupled non-linear flap/lag/torsion dynamics. Blade, wing, and fuselage aerodynamics come from non-linear look-up tables. It has a multibody form to allow for structural flexibility and an arbitrary aircraft configuration with multiple rotors. In the baseline model, the inflow model for each rotor is a 3-state Peters-He dynamic inflow model with inflow coupling between the two rotors. Inflow coupling assumes each rotor is immersed in the uniform component of inflow from the other rotor. Coupling constants are based on analytical velocities above and below an individual rotor's flow fields. The updated HeliUM model is coupled to the Maryland Free Wake (MFW) free-vortex wake method. Tight coupling between HeliUM and MFW allows for time-marching free-flight maneuvers, such as frequency sweeps, to be simulated within the model. However, the MFW is not in ordinary differential equation (ODE) form; therefore, direct linearization of the inflow is not possible. To obtain a linear inflow response, a method for extracting linear inflow models using system identification of the MFW response has been extensively documented. The ODE inflow model extracted from the high fidelity MFW is coupled back into the HeliUM flight dynamics model, and the resulting flight dynamics response are compared with flight data and the baseline coupled dynamic inflow.

6.8 3DR IRIS+ QUADCOPTER

6.8.1 Basic Data Overview

Basic Information:

Type:	**Manufacturer:**	**Class:**
IRIS+	3D Robotics	UAV
Size:	**Accommodation:**	**Registration**
19.75 in diagonally motor-to-motor	N/A	None

Weights:

Empty:	**Typical Flight (W/ Battery):**	**Payload Capacity:**
2.47 lb	3.17 lb	0.9 lb
Heavy Configuration Load:		
0.441 lb (≈50% load capacity)		

Performance:

Max Speed:	**Max Sideward Velocity:**	**Max Rearward Velocity:**
32 kn	32 kn	32 kn
Average Flight Time:		
16 min		

6.8.2 Summary of Available Modeling Data

Flight-Test Data	Frequency sweeps (nominal loading): hover and 17 kn (pitch, roll, yaw, and heave) 10 kn (pitch and roll)
	Frequency sweeps (heavy loading): 10 kn (pitch and roll)
	Trim shot data (trim points), hover – 32 kn
	Doublets, hover and 17 kn
Processed Data	Identified state-space models, hover and 17 kn
	Frequency responses (nominal loading): hover and 17 kn (pitch, roll, yaw, and heave) 10 kn (pitch and roll)
	Frequency responses (heavy loading): 10 kn (pitch and roll)

Instrumented Parameter List:

Control Positions	Pilot stick positions
	Mixer input
Inertial	Body axis rates
	Body axis accelerations
	Attitude
	GPS position and height
	Velocity (3 components)
	Barometric altitude
Motor	Motor PWM
	Motor speed

6.8.3 Modeling Activities and Baseline Models

Organization	**TDD**
Model Type	Full-envelope stitched simulation model
Update Methods	7 – Stitched simulation model from point ID models and trim data
Primary Deficiencies to be Addressed with Update Method	Full-envelope verification maneuver
Primary end-use(s)	Full-envelope simulation

6.8.3.1 Hover

A state-space model for hover was identified from flight-test data using frequency-domain system identification. The model was verified in the time domain with a pulse response not used for identification.

6.8.3.2 Forward Flight

System identification flights in forward flight were conducted using automated frequency sweep inputs. The frequency sweeps were injected just upstream of the mixer to excite the bare airframe directly. With the control system engaged, logging of the total mixer inputs enables identification of the bare-airframe dynamics (e.g., p/δ_{lat}). To ensure a consistent forward-flight velocity, the aircraft pitch attitude was commanded via the transmitter's longitudinal trim. A racetrack pattern was flown to keep the aircraft within line-of-site while in forward flight.

Chapter 7 – ASSESSMENT AND UPDATE CASE STUDIES

This Chapter presents comprehensive case studies of each update method using one or more of the flight test data bases. The full matrix of case studies is given in Figure 7-1 (repeated from Figure 1-1 in Chapter 1).

Flight Simulation Model Update Methods

- Method 1: Gain/Time Delay Corrections for Key Responses
- Method 2: "Black Box" Input and Output Filters
- Method 3: Force and Moment Increments Based on Stability Derivatives
- Method 4: Reduced Order Models and Physics-Based Corrections
- Method 5: Simulation Model Parameter Adjustment
- Method 6: Parameter Identification of Key Simulation Constants
- Method 7: Stitched Simulation from Point ID Models and Trim Data

Flight Test Database	Method 1 (Section 7.1)	Method 2 (Section 7.2)	Method 3 (Section 7.3)	Method 4 (Section 7.4)	Method 5 (Section 7.5)	Method 6 (Section 7.6)	Method 7 (Section 7.7)	Quantitative Fidelity	Perceptual Fidelity
412 (NRC)		DLR	UoL, CAE		CAE		NRC	X	UoL
UH-60 (USNA)	USNA			ART, GT, SAC	PSU		TDD	X	
EC135 (DLR)		DLR	METU		Thales/ONERA		DLR	X	
CH-47 (Boeing/DSTG)	DSTG	CAE		GT, Boeing, DSTG	DSTG, CAE			X	
AW139 (Thales/ONERA)			Thales/ONERA					X	
AW109 (LH)				LH				X	
X2 (SAC)				SAC, USNA		USNA		X	
Iris+ (TDD)							TDD	X	

Figure 7-1: AVT-296 Flight Simulation Model Update Methods and Flight-Test Databases, Repeated from Figure 1-1 in Chapter 1.

Chapter 7.1 – GAIN/TIME DELAY CORRECTIONS

ABSTRACT

In this chapter two case studies are presented for the gain/time delay method, featuring the CH-47F and UH60A for both the longitudinal and lateral axes in hover. The case studies demonstrate that where the underlying physics of the model are well represented, the gain/time delay approach can be quite effective. This is contrasted with the CH-47F longitudinal axis case, where the rigid body dynamics were not well captured in the baseline model and the corresponding correction resulted in only a modest improvement in model cost. The key advantages and limitations of the gain/time delay method are highlighted in the following sections.

7.1.1 Method Overview

The gain/time delay method provides a simple method for adjusting a model response, which can be quite effective in some cases. Depending on the application of the model, this approach affords an easily implemented correction associated with discrepancies relative to test data without delving into the underlying physical mechanisms within the model. It should be noted that because this correction method may not be underpinned by a physical process, the resulting corrected model responses may not be physically representative. For example, if a gain is applied to a response in hover to account for an inflow or interference effect, this gain might not be appropriate at a different airspeed or flight condition. In essence, this method is best suited when the key underlying physics within the frequency range of interest are already well captured in the model. The following case studies detail a number of applications of the gain/time delay correction method, highlighting the primary advantages and limitations of this approach.

7.1.1.1 CH-47F

When compared with frequency responses extracted from flight-test data, a significant gain offset was evident in the model results, particularly in the lateral and longitudinal results. For the lateral axis, the general shape of the model response very closely reflected the flight-test results; however, the model response was offset upwards by approximately 2.5 dB (see Figure 7.1-1(a)). In the figure, the red (dashed) curve denotes the uncorrected model response. A model correction factor was computed by identifying a gain and time delay for the error response (of the model relative to flight-test data) using the NAVFIT function in CIFER [1]. The resulting correction factors are indicated in Figure 7.1-1(a) (Gain: 0.68, Delay: 0.025 s), and the model response was then corrected using these values as indicated by the blue (solid) curve in the figure. The corrected model response matches the flight-test data considerably better than the initial model (model mismatch cost was reduced from $J = 285$ for the initial model down to $J = 78$ after the correction), indicating that the gain/time delay approach was quite effective in this case. Note that there is a small frequency mismatch in the rigid body mode at 0.4 rad/sec which does not change with the gain/time delay correction approach.

The limitations of the gain/time delay method are more evident when considering the longitudinal hover response, as shown in Figure 7.1-1(b). Here, a similar gain offset to the lateral case is evident; however, a considerable variation in the low frequency rigid body mode at 0.6 rad/sec is also present. A gain/time delay correction factor was computed as detailed in the figure, along with the corrected model response. The corrected response matches the flight data very well above 2 rad/sec, but poorly below 2 rad/sec due to the influence of the rigid body mode. This is reflected in the mismatch cost, which reduced from $J = 354$ to $J = 260$, representing an improvement, but still a significant difference relative to the flight-test data.

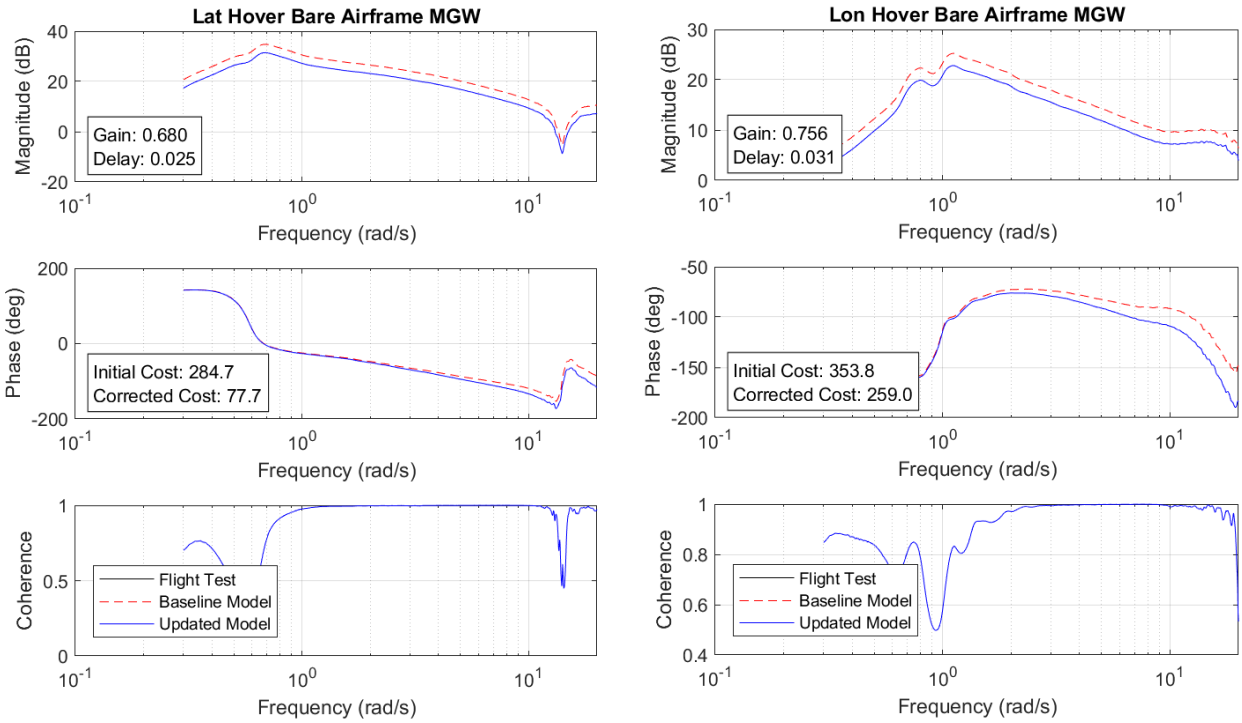

(a) Lateral Axis. **(b) Longitudinal Axis.**

Figure 7.1-1: Gain/Time Delay Corrections for Lateral and Longitudinal Axes in Hover (Flight Data Redacted).

These case studies demonstrate that when the underlying physics of the vehicle are well described in the model for the frequency range of interest, then a gain/time delay correction method can be highly effective at improving the fidelity of the response with minimal effort. When there are differences in the primary dynamics involved within the desired frequency range, then this method is not likely to be particularly effective. It should also be noted that this is a 'non-physical' correction method. It is important to crosscheck with other flight conditions (e.g., different airspeeds, gross weights, etc.) to ensure that correcting the response in one regime does not degrade the performance in another. The baseline and updated cost function values are presented in Table 7.1-1 for hover, showing cost function improvements between 25% and 73%.

Table 7.1-1: Cost Function Comparison for Baseline and Updated Model.

Response	Baseline	Corrected	Improvement (%)
Longitudinal (Hover)	354	259	26.8
Lateral (Hover)	285	78	72.6

The improvements realized in the frequency domain are also realized in the time domain, as demonstrated in Figure 7.1-2(a) and Figure 7.1-2(b) for the lateral and longitudinal axes, respectively. Both plots compare the response to on-axis doublet inputs. As was demonstrated in the frequency domain, the gain correction is the primary driver of model improvement, with the reduced gains resulting in significantly better matches for both axes. For both the lateral and longitudinal axes, the baseline model peak angular rates in response to the doublet inputs were approximately 35% higher than the flight-test results. For the updated model, the peak rates were quite close to the flight-test data. The resulting time-domain cost metrics are demonstrated in Table 7.1-2 for the baseline and updated models. The time-domain cost reduced by approximately 50% in both the lateral and longitudinal axis.

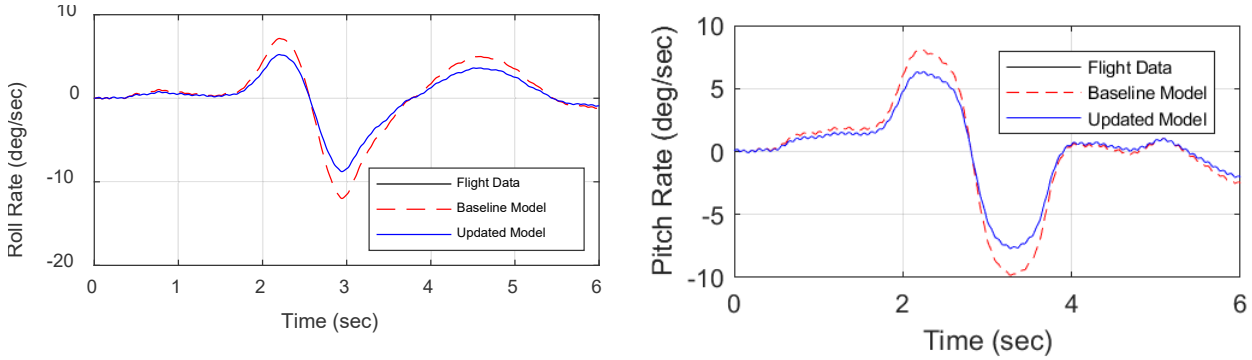

(a) Lateral Axis. **(b) Longitudinal Axis.**

Figure 7.1-2: Time-Domain Comparison for Lateral and Longitudinal Axes in Hover (Flight Data Redacted).

It should be noted that for the frequency-domain comparison the longitudinal axis correction was less effective than the lateral axis because the rigid body falling leaf mode occurred at a different frequency in the model to the flight-test data. This does not appear to be reflected in the time-domain comparison, likely because the length of record for the time-domain comparison was relatively short (corresponding to a frequency of about 1 rad/sec). In other words, a time-domain comparison of this record length tends to suppress model discrepancies in the very low frequency range and highlight differences in the mid-frequencies.

Table 7.1-2: Time-Domain Cost for Baseline and Updated Model.

Axis	Baseline	Updated	Improvement (%)
Longitudinal	1.579	0.798	49.5
Lateral	1.861	1.012	45.6

7.1.1.2 UH-60

The U.S. Army Combat Capabilities Development Command Aviation & Missile Center conducts flight dynamics modeling, control law design, and handling qualities evaluation research to support current and future Army rotorcraft needs. Much of this work has been conducted using the variable stability UH-60A RASCAL helicopter. To support the control law design aspects of its work, an accurate, flight-validated model of the UH-60 is required.

FORECAST has been used to develop flight dynamics models of the UH-60 throughout its flight envelope. Herein, the modeled hover response will be compared with flight data and updated using the gain and time delay method. Modeling capabilities of FORECAST are discussed in detail in Tischler et al. [2], Section 6.2.

The linearized baseline FORECAST model is compared with frequency responses obtained from flight data for the roll and pitch axes in Figure 7.1-3, with the same line type conventions as in Figure 7.1-1(a) and Figure 7.1-1(b). For both axes, the baseline predicted FORECAST response is greater in magnitude than flight data. For the roll axis, the baseline response is at or below the MUAD upper bound (see Tischler et al. [2], Section 4.1) for a large portion of the response, between 0.2 and 15 rad/sec. For the pitch axis, the baseline response is just above the MUAD boundary between 0.2 and 15 rad/sec. Both baseline responses predict the correct shape of the dynamic response but are offset by constant magnitudes. This magnitude shift was next determined using the gain and time delay method.

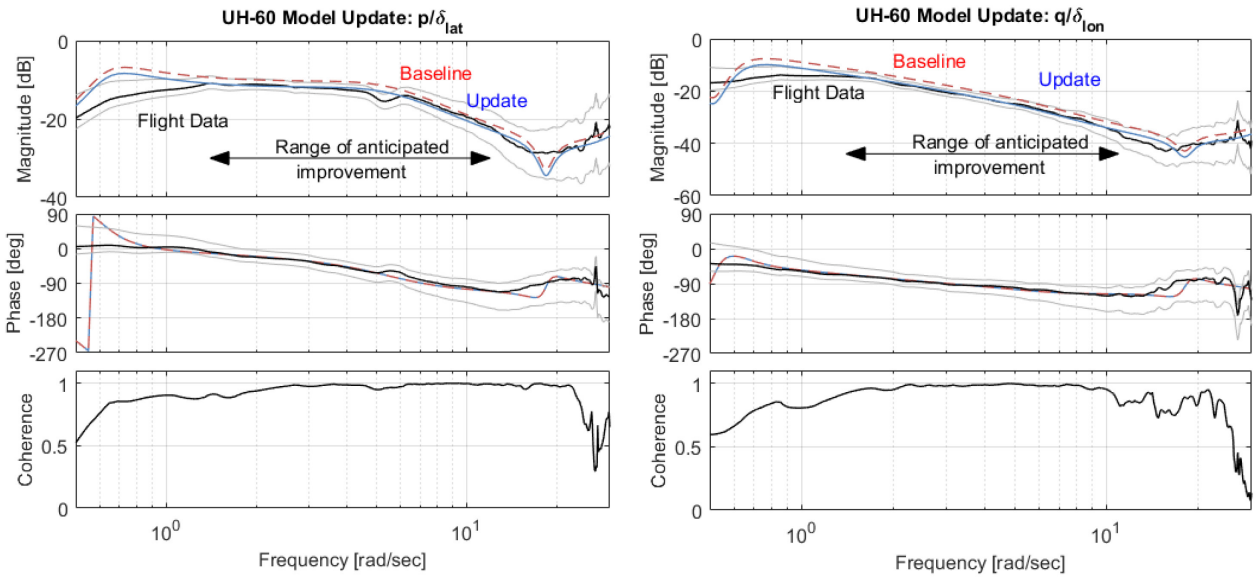

(a) Roll Axis Model Update. **(b) Pitch axis Model Update.**

Figure 7.1-3: UH-60 Hover Response Model Comparisons and Improvements When Compared to Flight Test.

As with the CH-47F example above, a gain and time delay transfer function was identified for the error between the frequency responses obtained from the baseline model and flight data. The frequency range used for the identification was $1.4 \leq \omega \leq 12$ rad/sec for the lateral axis and $1.4 \leq \omega \leq 11$ rad/sec for the longitudinal axes. This is the key frequency range for the piloted response and flight control design. Furthermore, this is the range where the predicted response has a magnitude offset over the flight data. Since this method cannot be used to correct for deficiencies in predicted frequencies of rigid body or rotor modes, its range should only cover where there is a magnitude or phase offset.

For the lateral axis, the model fidelity cost (Tischler et al. [2], Chapter 4.2) was reduced from $J_{baseline} = 67.3$ to $J_{updated} = 21.5$. The identified gain is $K_{lat} = 0.837$, and no time delay was identified. For the longitudinal axis, the cost reduced from $J_{baseline} = 108.9$ to $J_{updated} = 6.14$. The identified gain is $K_{lon} = 0.766$, and again no time delay was required. For both axes, there is a substantial reduction in model fit costs and a much improved response that fit well within the MUAD bounds was produced. The baseline and updated cost function values are summarized in Table 7.1-3.

Table 7.1-3: Cost Function Comparison for Baseline and Updated Model.

Response	Baseline	Corrected	Improvement (%)
Longitudinal	67.3	21.5	68.1
Lateral	108.9	6.14	94.4

7.1.2 Summary

The preceding case studies demonstrate that the gain/time delay method can be highly effective when used for appropriate applications. More specifically, when the underlying physics are well captured in the model for the frequency range of interest, this method can be expected to produce a good correction result. When additional unmodeled dynamics are present or the dynamics are modeled at incorrect frequencies, it is not generally expected that this method will be suitable.

Application of this method requires minimal technical effort, and hence may be considered as a first approach in many circumstances. When correction results are acceptable for a given application, this method can prove to be highly effective due to its simplicity. Care should be exercised when a physically representative system is required since it is difficult to gain insight into the underlying cause of a discrepancy using this method.

7.1.3 References

[1] Tischler, M.B., and Remple, R.K. (2012), *Aircraft and Rotorcraft System Identification: Engineering Methods with Flight Test Examples*, American Institute of Aeronautics and Astronautics, Inc., Reston, VA, 2nd ed.

[2] Tischler, M.B., White, M.D., Cameron, N., D'Agosto, S., Greiser, S., Gubbels, A., Guner, F., He, C., Horn, J., Hui., K., Jones, M., Juhasz, O., Lee, O., Lehmann, R., Miller, D., Myrand-Lapierre, V., Nadeau-Beaulieu, M., Nadell, S., Padfield, G., Pavel, M., Prasad, J., Ragazzi, A., Richard, S., Scepanovic, P., Seher-Weiß, S., Soong, J., Stroosma, O., Taghizad, A., Tobias, E., Xin, H., and Yavrucuk, I. (2021), "Rotorcraft Flight Simulation Model Fidelity Improvement and Assessment," NATO STO AVT-296 Technical Report.

Chapter 7.2 – 'BLACK BOX' INPUT AND OUTPUT FILTERS

ABSTRACT

With this method, a baseline model is improved by a 'black box' (i.e., non-physical) low-order input filter. The framework of the method is presented in Chapter 5 of Tischler et. al. 2021 [1] and the corresponding Lecture Series presentation entitled 'Model Fidelity Improvement Methods'. Several options for deriving the input filter exist. Most of these options are illustrated with examples from the Bell 412, EC135, and CH-47 databases. These educational notes comprise the CH-47 and EC135 examples to give an impression of the presentation material. The respective simulation environments are:

- *Nonlinear Blade Elements Rotor Model (CH-47, CAE, Canada).*
- *Engineering Simulator (EC135, DLR, Germany).*
- *Linear Simulation Models for Flight Control Design (EC135, DLR, Germany).*

NOTATION

J_{ave}, J_{RMS}	cost value in the frequency/time domain	δ_{lon}, δ_{lat}, δ_{ped}, δ_{col}	longitudinal, lateral, pedal, and collective control input
n, d	numerator/denominator coefficients		
$u(t)$	vector of the four controls inputs depending on the time t	$\bar{\delta}_{lon}$, $\bar{\delta}_{lat}$, $\bar{\delta}_{ped}$, $\bar{\delta}_{col}$	inverse simulated control inputs
$\bar{u}(t)$	vector of inverse simulated controls		
u,v,w	rigid-body velocities	Δ	input filter (model in Laplace domain)
p,q,r	rigid-body rates	Φ,θ	roll and pitch attitude

7.2.1 CH-47

The CH-47 database originates from Keller et al. [2] with SAS ON and has been converted to SAS-OFF data using an autopilot system description document provided by Boeing. CAE uses a generic Blade Element Rotor Model (BERM) to simulate twin rotor helicopters. This blade element rotor model simulates the complete helicopter where the blades are divided into 5 segments, and the forces applied on each segment are fully integrated to generate the complete rotors and helicopter response (including flapping, lead-lag, etc.).

This section will concentrate on the pitch and yaw frequency responses in hover. Although the baseline model shows good performance, a certain magnitude dip and sudden change in phase at 7 rad/sec are not covered that well and are to be updated (Figure 7.2-1 and Figure 7.2-2). This dip likely originates from a rotor-on-rotor mode specific to a twin rotor helicopter. This mode is attributed to drive system flexibility in the tandem rotor Chinook, causing a lagging and leading difference between the rotors during high frequency control inputs. These missing dynamics could have been modeled by improving the physical model of the driveshaft between each rotor, but it would have come at a great modeling cost and would not have guaranteed results. In Chapter 7.2 of Tischler et al. [1], this mode was modeled by a filter implemented in the model of the Chinook flight dynamics.

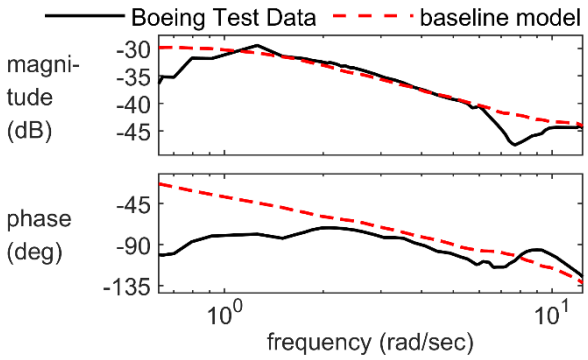

Figure 7.2-1: Boeing Flight-Test Data and CAE Simulation Pitch Responses.

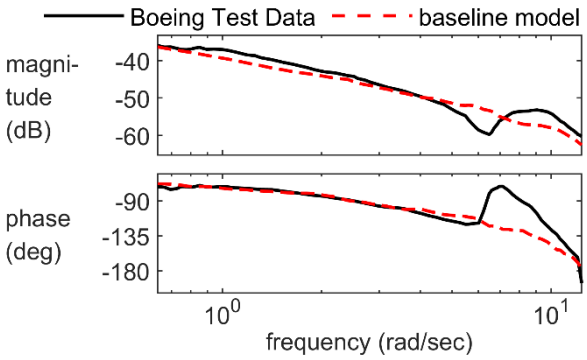

Figure 7.2-2: Boeing Flight-Test Data and CAE Simulation Yaw Responses.

The filter is applied to the inputs of the bare airframe which is inherent to the airframe itself and not a behavior of the control gearing. Figure 7.2-3 shows where in the simulation the filter is applied.

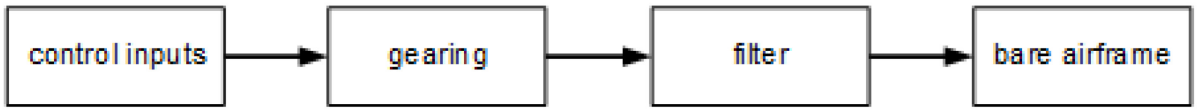

Figure 7.2-3: Filter Implementation in Simulation.

In the pitch axis, the filter was applied directly to the differential collective swashplate blade position. The pitch response of the aircraft is determined by the differential collective between the front and aft rotor, hence placing the filter on the collective swashplate is a direct application to the bare airframe, which is confirmed by the frequency-domain response change. The filter was implemented in the time domain using a z-transform but is given here in the Laplace domain

$$\Delta = R(s) = \frac{\boldsymbol{n_2 s^2 + n_1 s + n_0}}{\boldsymbol{d_2 s^2 + d_1 s + d_0}}$$

The filter coefficients are tuned such that the drop of magnitude and dip in phase are tracked well by the filter. Frequency responses are plotted in Figure 7.2-4 and Figure 7.2-5 in the frequency domain (blue) together with the respective SISO inverse (black). Essentially the black curve is formed by the differences of magnitude and phase between the baseline model and the Boeing flight-test data (i.e., the red-dashed and black curves in Figure 7.2-1 and Figure 7.2-2).

Finally, once the coefficients were determined offline, they were implemented in the BERM simulation and a frequency sweep of the integrated simulation was conducted to generate the actual frequency-domain results shown in Figure 7.2-5 and Figure 7.2-6. It can be seen that the applied filter improved the simulation model to better match the high frequency dip seen in yaw and pitch.

Figure 7.2-6 and Figure 7.2-7 show the model error before and after the SISO transfer function correction on the gearing in comparison to the MUAD bounds. It can be seen in these figures that the model error was significantly reduced in the high frequency range. The original model (dashed red lines) showed a significant increase of the error at about 7 rad/sec for both pitch and yaw. As can be seen from the figures, the SISO transfer function correction on the BERM model allows to reduce the model error at high frequencies within the MUAD boundary, and hence, adds a dynamic aspect that was not previously present in the model.

Table 7.2-1 shows initial and improved frequency-domain cost function values. It can be seen that the cost function for the yaw axis is greatly improved.

So overall, this black-box method, while not physics-based, required minimal implementation efforts to reproduce well the relationship between the pilot's inputs and the response of the helicopter.

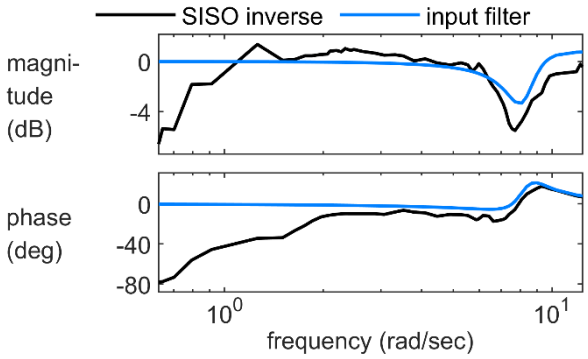

Figure 7.2-4: Pitch Response Error of the Baseline Model and its Model Fit.

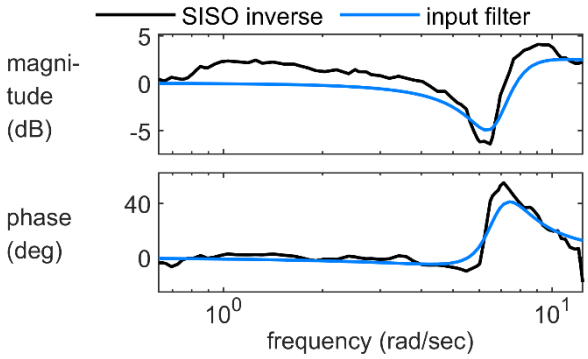

Figure 7.2-5: Yaw response Error of the Baseline Model and its Model Fit.

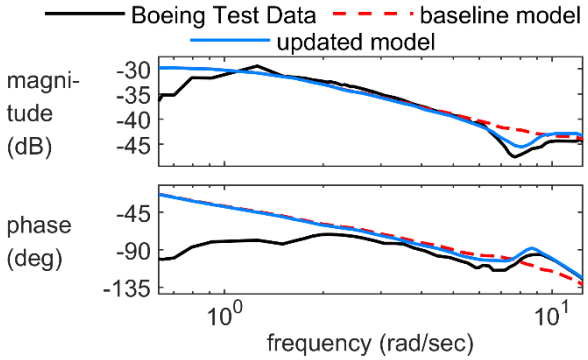

Figure 7.2-6: Pitch Response of the Flight-Test Data Compared to Baseline/Updated Model.

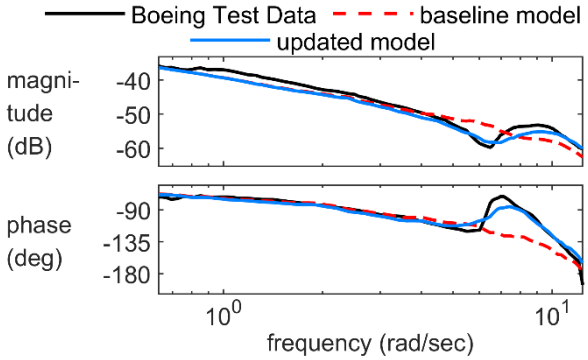

Figure 7.2-7: Yaw Response of the Flight-Test Data Compared to Baseline/Updated Model.

Table 7.2-1: Integrated Frequency Cost Function Values J. (Frequency Range 2-20 rad/s).

Axis	Baseline Model	Updated Model
q/δ_{lon}	78.0	41.5
r/δ_{ped}	297.9	71.0

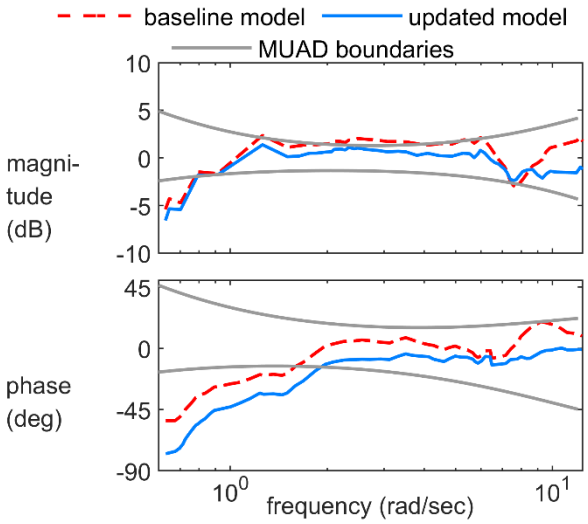

Figure 7.2-8: MUAD Boundaries of the Pitch Axis for the Baseline and Updated Simulation.

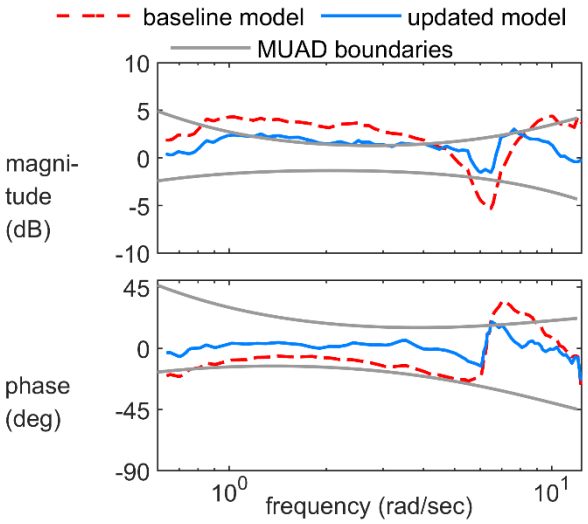

Figure 7.2-9: MUAD Boundaries of the Yaw Axis for the Baseline and Updated Simulation.

7.2.2 EC135

For the EC135, the 'Black-Box' method is applied to flight-test data at 60 knots forward flight as provided within the NATO group. Two baseline models are updated to better match the flight-test data:

1) **11-DOF system identification model:**

   The baseline model is the ACT/FHS 11-DOF model at 60 kn derived by system identification as presented in Chapter 6 of Tischler et al. [1]. This model accounts for the rigid-body states and the higher-order modes of flapping, regressive lead-lag and dynamic inflow and was identified over a frequency range of 0.5-30 rad/s. Although this model already shows high fidelity, some remaining deficits had to be corrected to be able to use the updated model for control system development. These deficits appear mainly in the yaw response in the mid-frequency range (3-7 rad/sec, probably due to missing engine dynamics) and at frequencies above 30 rad/sec. The **frequency-domain approach** (see Chapter 5 of Tischler et al. [1]), i.e., inverse simulation followed by frequency-domain identification of the input filter, is used in this case.

2) **DLR's EC135 engineering simulator model:**

   The baseline model is a nonlinear blade element helicopter model and is described in Chapter 6 of Tischler et al. [1]. This model is updated by the **algebraic approach** (see Chapter 5 of Tischler et al. [1]) using identified models of DLR's simulator and the ACT/FHS EC135. A black-box input filter is derived that updates DLR's simulator and improves simulation fidelity for all axes and especially for off-axis responses.

7.2.2.1 Frequency-Domain Approach

The EC135's baseline 11-DOF model at 60 kn is updated by the frequency-domain approach. First, linear dynamic inversion is applied to compute inverse control signals. Then, frequency responses between measured and inverse control signals are computed to identify transfer functions that are used as input filter for the update of the baseline model. Finally, the updated responses are simulated using the input filter. These three steps are summarized in Figure 7.2-10.

In the first step, the inverse controls $\bar{u} = \left(\bar{\delta}_{lon} \quad \bar{\delta}_{lat} \quad \bar{\delta}_{ped} \quad \bar{\delta}_{col}\right)$ (see Figure 7.2-10) have to be determined using Rynaski's approach for the inverse simulation (Section 5.2 of Tischler et al. (2021)). The linear baseline state-space model is partitioned into the states to be matched $x_1 = (\dot{p}, \dot{q}, r, w)^T$ and remaining states $x_2 = (u, v, p, q, w_h, \phi, \theta, x_{ll}, \dot{x}_{ll}, y_{ll}, \dot{y}_{ll})$. The inverse simulation model is implemented as a state-space model. Inputs to this states-space model are the measured states $y_{\mathrm{m},1} = (\dot{p}, \dot{q}, r, w)^T$ and their derivatives $\dot{y}_{\mathrm{m},1} = (\ddot{p}, \ddot{q}, \dot{r}, \dot{w})^T$. Both are generated by flight path reconstruction so that the integrated $\dot{y}_{\mathrm{m},1}$ perfectly match $y_{\mathrm{m},1}$ which is required to obtain reasonable results. It is important to simulate all outputs, such as forward and lateral speed together with the inverse controls by one state-space model, so that unstable modes such as the phugoid are numerically stabilized. This is especially mandatory if sweep data are analyzed which usually have a long duration.

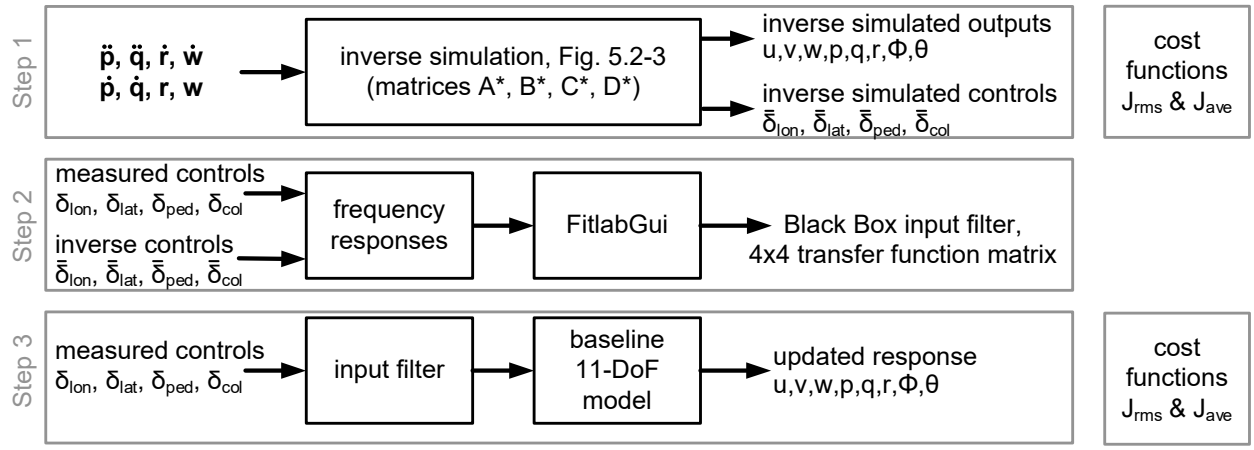

Figure 7.2-10: Steps to Update the Baseline 11-DOF Model.

Figure 7.2-11 shows the inverse simulation result of a collective sweep input from flight test. The climb and yaw rates (w, r) are part of the states to be matched so that measured and inverse simulated signals match exactly (except for measuring noise). The longitudinal speed u is a remaining state which does not match exactly but achieves high fidelity – the RMS error is $J_{\mathrm{rms}} = 0.40$ at 60 knots forward flight. The RMS cost of the x_1-states is zero, and only the remaining states, such as roll and pitch angle, forward and lateral speed, and longitudinal and lateral acceleration, increase the RMS cost. Integrated frequency costs as shown in Table 7.2-2 are averaged costs for all the rigid-body states $(u, v, w, p, q, r, \phi, \theta)$ in the frequency range between 1 and 20 rad/sec. Note that for lateral, longitudinal, and pedal axes, the baseline model has already a high fidelity which is indicated by costs of these axes being well within with guideline of $J \leq 100$. The cost is reduced most for the collective axis so that any black-box filters will most notably improve fidelity for this axis. Figure 7.2-12 shows a detailed frequency response from the inverse simulation and ACT/FHS – frequencies above 40 rad/sec are not matched due to a low-pass filter that reduces measuring noise. As a result, inverse simulated outputs have integrated cost values below $J_{ave} \leq 100$ so that an additional output filter is not needed (see guideline in Section 5.2 of Tischler et al. [1]).

In the second step of Figure 7.2-10 frequency responses between the measured and inverse simulated controls are generated as exemplarily shown in Figure 7.2-13. The frequency responses are plotted for all reference speeds from hover to 120 knots into one diagram – it can be seen that these are very similar, and that all responses are above the guideline of -20 dB so that this axis should be modeled. As all frequency responses $\bar{u}/u$ were mostly independent of reference speed, only one common input filter with stable eigenvalues for the control inputs was extracted by using the tool FitlabGui [3]. It was found that this single input model is sufficient for most operating points.

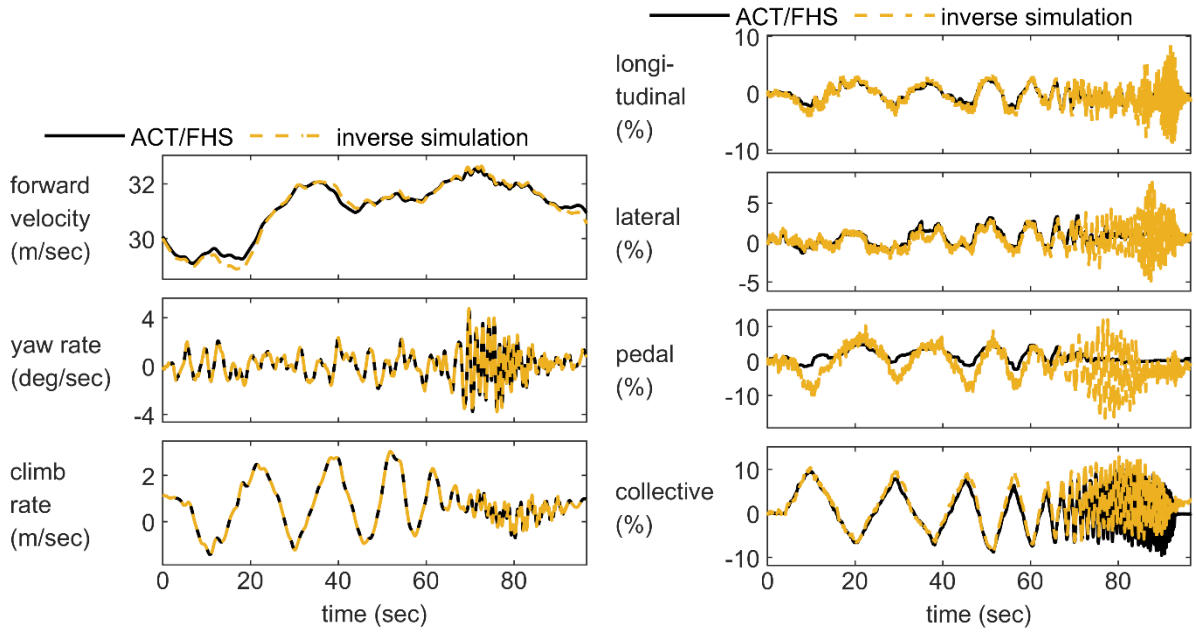

Figure 7.2-11: Inverse Simulation of EC135 ACT/FHS Collective Sweep Data at 60 kn Forward Flight.

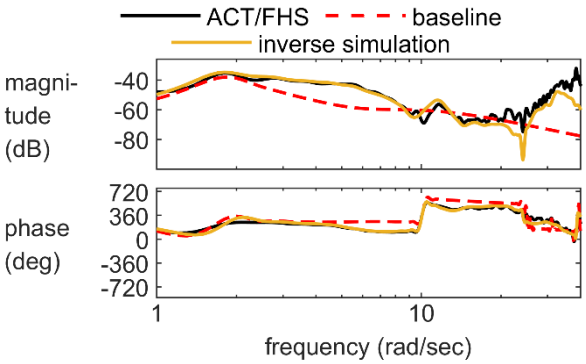

Figure 7.2-12: Frequency Response of the yaw Rate Due to Collective r/δ_{col} at 60 kn.

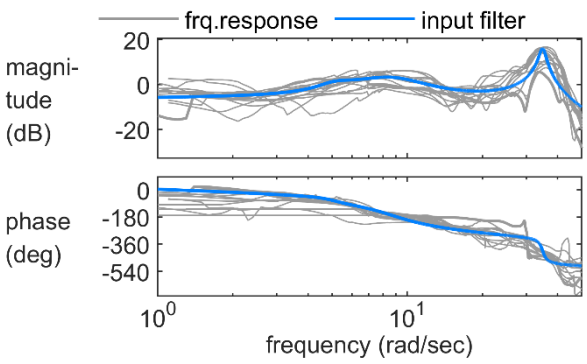

Figure 7.2-13: Frequency Responses and Resulting Input Filter for Inverse Pedal Control Due to Measured Collective.

Table 7.2-2: Integrated Frequency Cost at 60 kn Forward Flight.

	Longitudinal	Lateral	Pedal	Collective
Baseline Model	45.3	66.4	54.8	282.1
Inverse Simulation	44.4	93.2	40.4	50.9

Finally, the updated model is evaluated by RMS and frequency cost functions as indicated by Figure 7.2-10. Figure 7.2-14 shows a step response to collective at 60 knots forward flight – instead of the body rates, the angular accelerations are displayed to better show the updates achieved. The responses in the accelerations are improved with the updated model – especially the off-axis response in yaw achieves a higher fidelity as

frequencies at 3-5 rad/sec are matched better. Another example is shown in Figure 7.2-15 with a longitudinal multistep input. Here, the off-axis response in roll is improved by the updated model. In both cases, oscillations with a frequency of approx. 35 rad/sec are introduced/added by the black box update.

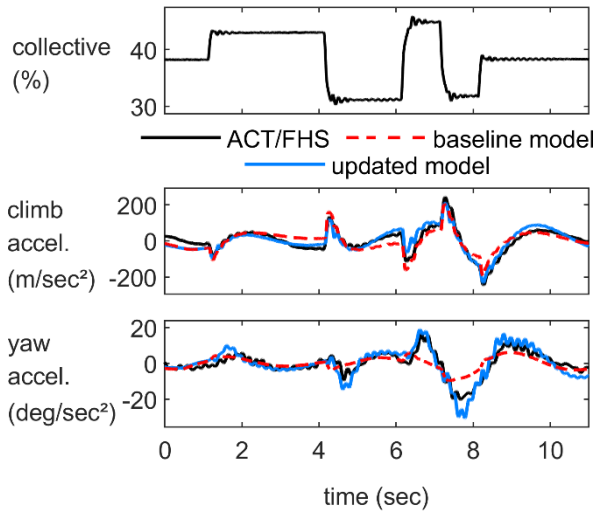

Figure 7.2-14: Collective Multistep Input at 60 kn Forward Flight.

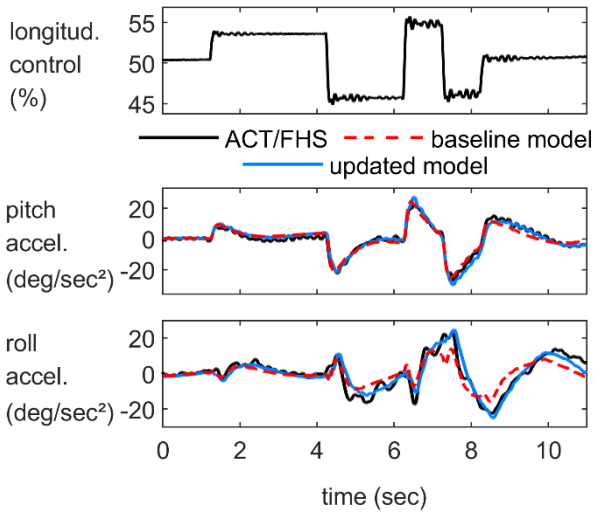

Figure 7.2-15: Longitudinal Multistep Input at 60 kn Forward Flight.

All multistep data are simulated and assessed using the RMS cost function in the time domain with a guideline of $J_{rms} < 2$ for an adequate match. The baseline model is already quite good as shown by the red circles in Figure 7.2-16. The updated model using one input filter for the whole flight envelope achieves a slightly better match in the time domain (blue markers). If separate input models had been determined for each of the five reference speeds, similar cost function values as indicated by the inverse simulation could have been achieved.

Most notably, the input filter addresses the yaw response due to collective. Figure 7.2-17 shows all individual responses of the collective axis to the respective rigid-body states. Frequency costs (calculated for 1 to 10 rad/sec) show that the input model greatly reduces the cost for the yaw rate response r. But not all the states of the updated model achieve a better match with the flight-test data. Note that the input filter is averaged over airspeed so that the black-box filter may not capture all effects at each operating point.

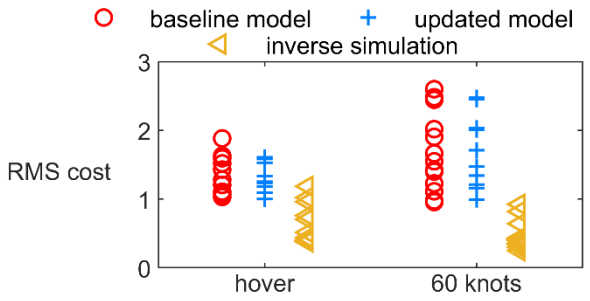

Figure 7.2-16: RMS Cost in the Time Domain.

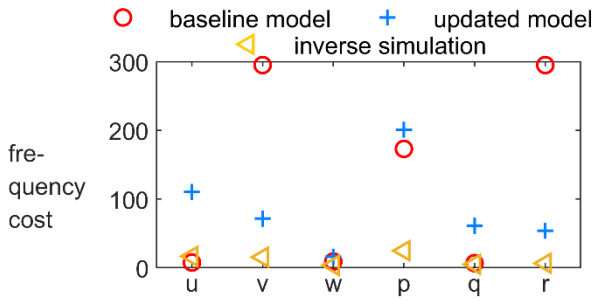

Figure 7.2-17: Frequency Costs for Collective Input at 60 kn Forward Flight.

From a modeling perspective, the additional input model is 'black box' with no physical model structure. This may be regarded as a drawback as it is not known which physical effects are missing in the baseline model. However, by comparing the eigenvalues of the baseline and the augmented model, missing physical effects may be interpreted by flight mechanics experts (see Figure 7.2-18). It is believed that the update filter corrects deficits of the baseline model originating from missing engine dynamics (3-5 rad/sec), tailboom flexible modes (approx. 35 rad/sec) and coning mode (approx. 40 rad/sec).

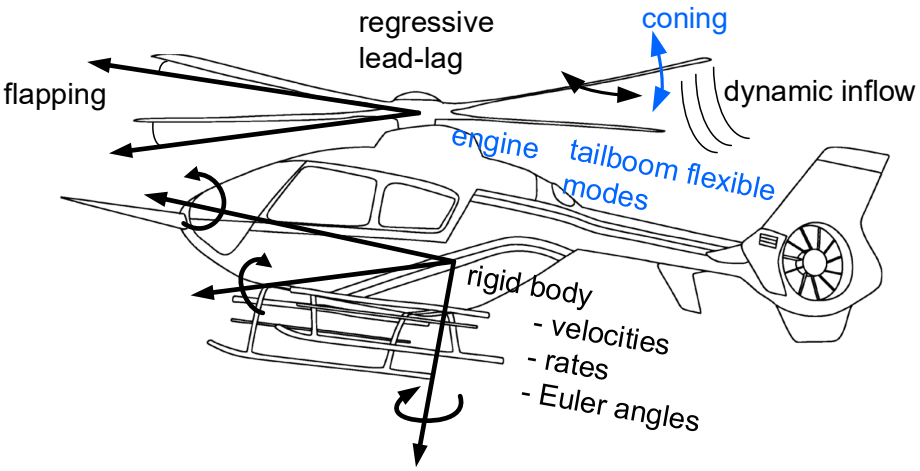

Figure 7.2-18: Physical Effects Regarded by the Baseline Model (Black) and Additional Effects Respected by the Input Filter (Blue).

7.2.2.2 Algebraic Approach

The algebraic approach is applied to DLR's nonlinear flight simulator model. To arrive at a linearized version of the nonlinear simulator model, system identification was used instead of numerical linearization. Thus, sweeps were flown on the simulator and models of different complexity (6-DOF, 11-DOF, and 17th-order) were identified from that data.

The goal is to impose to the simulator the response of the identified models of the EC135 ACT/FHS. The flight-identified models already achieve a high fidelity as presented exemplarily in Section 2.1 for the 11-DOF model – only the collective axis has an integrated frequency cost above the guideline of 100 while the responses of the remaining axes (longitudinal, lateral, and pedal) are almost indistinguishable from flight-test data. Therefore, in the case of the 11-DOF model, the algebraic approach will thus produce a black-box filter that improves the cyclic and pedal axes while the collective axis will still contain deficits.

In order to calculate the input filter, four outputs have to be chosen for both models, i.e., the matrices C and D have to have four rows. The outputs chosen are pitch attitude θ, roll attitude ϕ, yaw rate r, and vertical velocity w. For these outputs, the baseline simulator model has a stable Rosenbrock matrix – in other words, invariant zeros are in the left half-plane – so that the inverse of each baseline model is stable. The product of the inverted baseline model with the flight-identified ACT/FHS model is characterized by the unstable eigenvalues of the flight-identified model. Only the phugoid mode of the identified model is unstable and has a time-to-double of approx. 7 sec so that this input filter can still be piloted in the simulator (see guideline in Section 5.2 of Tischler et al. [1]). The final result is a 4x4 transfer function matrix that is implemented as a filter to the control inputs, just before the mixer inputs in the simulator model.

Figure 7.2-19 shows the time-domain results of the baseline and updated simulator responses at 60 kn. The updated simulator responses are obtained for input filters based on the 17th-order model (blue line). For

the lateral input, almost all quantities are significantly improved – especially the on-axis roll attitude angle and off-axis pitch rate. For the longitudinal input, yaw rate is improved the most while the amplitudes of all rates are predicted more correctly. In both cases, the simulator model was improved by the input filter.

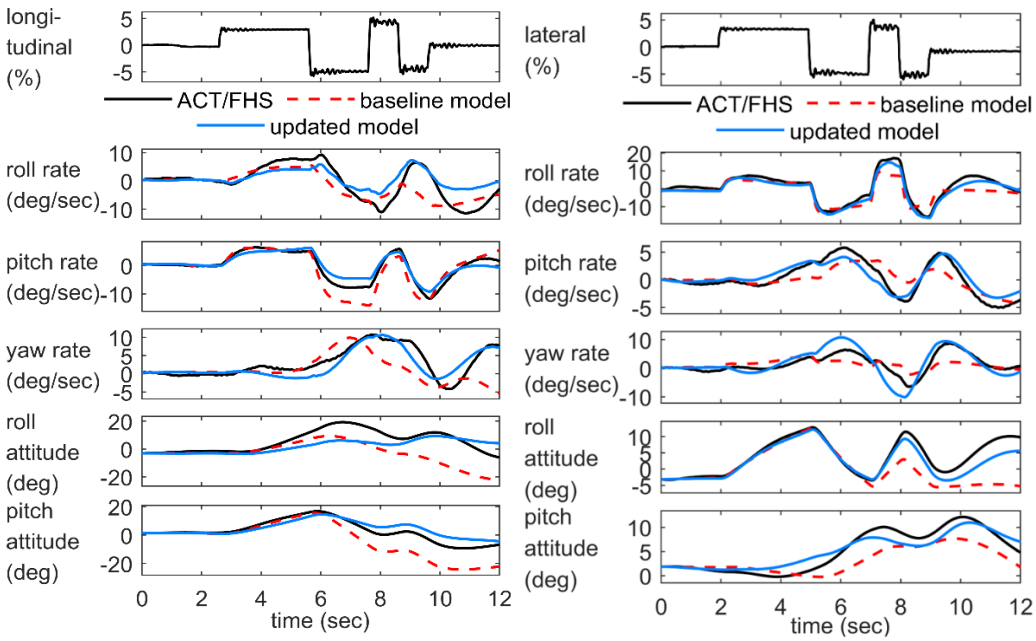

Figure 7.2-19: Results of the Input Filter for 60 kn 3211 Longitudinal (Left) and Lateral (Right) Inputs.

Inverse simulated control inputs together with the original ones are shown in Figure 7.2-20. It can be seen that the high-order (17th-order) filter imposes more energy into the system than the low-order (6-DOF) filter. Both black-box filters exhibit a strong input in pedal (of the same order of magnitude as the main lateral input), indicating missing coupling effects in the baseline model between lateral input and yaw response.

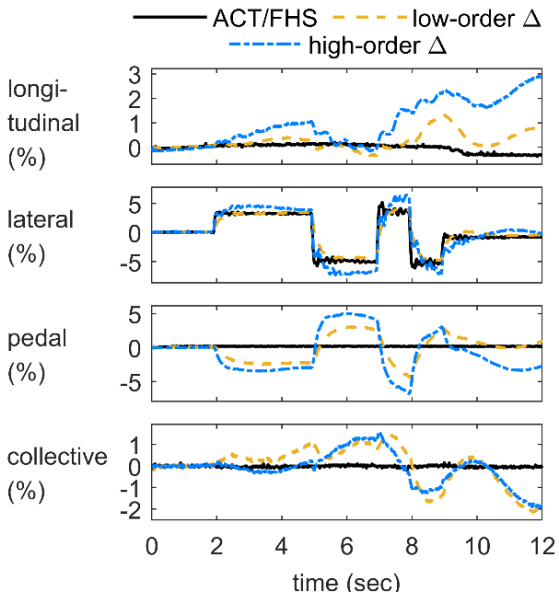

Figure 7.2-20: Inverse Control Inputs Created by the Input Filter for the Lateral Maneuver of Figure 7.2-10.

Figure 7.2-21 shows the RMS values of the baseline simulation and the updated one (using the 17th-order input filter) for all 3211-manoeuvres at 60 kn. It can be seen that the baseline model is above $J_{rms} = 2$ for almost all cases. The updated model shows generally lower RMS values with the greatest improvement in the longitudinal axis. It can be observed that all axes are improved even though the RMS cost function values are still mostly above the $J_{rms} = 2$ guideline.

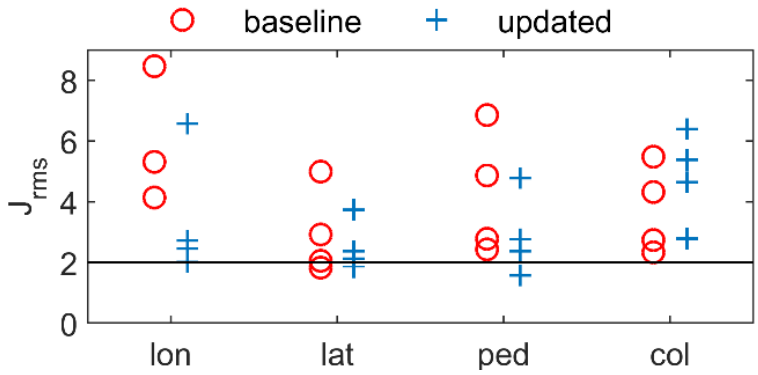

Figure 7.2-21: RMS Cost Function Values for Baseline and Updated Model: 3211 Inputs at 60 kn.

Finally, Figure 7.2-22 and Figure 7.2-23 show the frequency-domain results of the input filter. The off-axis response of the pitch rate due to lateral stick input at 60 kn forward flight is shown in Figure 7.2-22. Most notably, the lower frequency domain (between 1 and 3 rad/sec) is updated and matches the flight-test data of the ACT/FHS. Details of the input filter are highlighted in Figure 7.2-23. Here, the frequency response (grey 'FR' line) is generated by the product of the inverted baseline response and the helicopter response. In addition, the different input filter variants for the off-axis signal from longitudinal to lateral are overlaid. It can be seen that the high-order model (blue) matches best the calculated frequency response (grey). Both filters show a similar behavior at lower frequencies (dip in magnitude at 0.7 rad/sec) and a similar trend at mid-frequencies (between 1.5 and 7 rad/sec); however, they differ at higher frequencies.

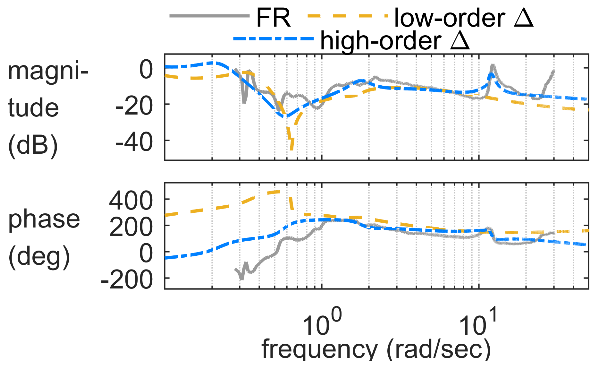

Figure 7.2-22: Frequency Responses of the Pitch Rate Due to Lateral Input at 60 kn.

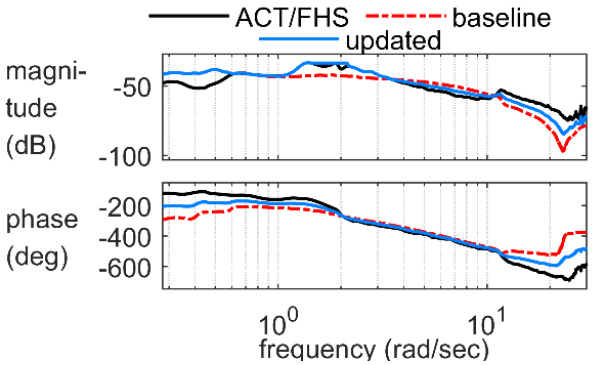

Figure 7.2-23: Off-Axis Response Error and Input Filter of the Modified Longitudinal Control Due to Lateral Stick Input.

7.2.3 Summary

The summary includes statements for all case studies – including the Bell412. This should give the reader of the educational notes more confidence on the range of application.

1) The black-box filter update method can be used to update a baseline simulation model when physics-based modeling of the deficits is impossible or too costly. The range of applicability is from linear to nonlinear models and examples are shown for tandem and single rotor helicopter rotorcraft configurations.
2) Nonlinear helicopter simulation models for the CH-47 training simulator and EC135 engineering simulator have been updated and fidelity metrices are halved – in the case of the CH-47 for selected on-axis focusing on a specific phenomenon and in the case of the EC135 for on- and off-axis.
3) Linear baseline models are available for the Bell 412 (derived by numerical linearization) and EC135 (extracted by system identification). Updated models use input filters added to the baseline models and improve the averaged fidelity for each of the two cases by a factor of 2.
4) Black-box filters are linear models and may not necessarily predict a wider flight envelope. However, these filters are quickly produced and balance well effort and achievable fidelity improvement for flight control, handling qualities, and modeling tasks dominated by linear effects.

7.2.4 References

[1] Tischler, M.B., White, M.D., Cameron, N., D'Agosto, S., Greiser, S., Gubbels, A., Guner, F., He, C., Horn, J., Hui., K., Jones, M., Juhasz, O., Lee, O., Lehmann, R., Miller, D., Myrand-Lapierre, V., Nadeau-Beaulieu, M., Nadell, S., Padfield, G., Pavel, M., Prasad, J., Ragazzi, A., Richard, S., Scepanovic, P., Seher-Weiß, S., Soong, J., Stroosma, O., Taghizad, A., Tobias, E., Xin, H., and Yavrucuk, I. (2021), "Rotorcraft Flight Simulation Model Fidelity Improvement and Assessment," NATO STO AVT-296 Technical Report.

[2] Keller, J.F., Hart, D.C., Shubert, M.W., and Feingold A. (1995), "Handling Qualities Specification Development for Cargo Helicopters," American Helicopter Society 51st Annual Forum.

[3] Seher-Weiß (2016), "FitlabGui – A Versatile Tool for Data Analysis, System Identification and Helicopter Handling Qualities Analysis," 42nd European Rotorcraft Forum, Lille, France, Sep. 5 – 8.

Chapter 7.3 – FORCES AND MOMENT INCREMENTS BASED ON STABILITY DERIVATIVES

ABSTRACT

To improve model responses and Handling Qualities (HQs) to meet, e.g., CS-FSTD(H) (2012) or ADS-33E-PRF (2000) requirements, a method has been developed that adds force and moment increments as delta derivatives to the nonlinear simulation, generating the additional accelerations needed to capture the dynamics lacking in the simulation model.

These delta derivatives are obtained by quantifying differences between stability and control derivatives obtained using System Identification (SID), through Flight Test (FT) and Simulation (FS) responses, in both the time and frequency domains. When the derivative mismatches are identified, the physical source of the low fidelity can be more directly investigated. Examples of the method application to improve the match for lateral-directional responses and for training simulators is presented.

7.3.1 Background

State-space models are widely used to analyze rotorcraft Handling Qualities and dynamic responses. To complement shortfalls in responses predicted by nonlinear simulation models, e.g., for the Qualification Test Guide (QTG), state-space models can be used as a reference basis for nonlinear model updates.

Among the techniques exploiting this approach, the estimation of force and moment increments is a novel approach to complement the lacking dynamics of the nonlinear model. The method makes an efficient use of the derivatives to generate additional accelerations needed to capture the dynamics lacking in the simulation model.

The delta derivatives are obtained by quantifying differences between stability and control derivatives obtained using System IDentification (SID), through Flight Test (FT) and Simulation (FS) responses, in both the time and frequency domains. When the derivative mismatches are identified, the physical source of the low fidelity can be more directly investigated. Figure 7.3-1 shows how the methodology is used to update a model.

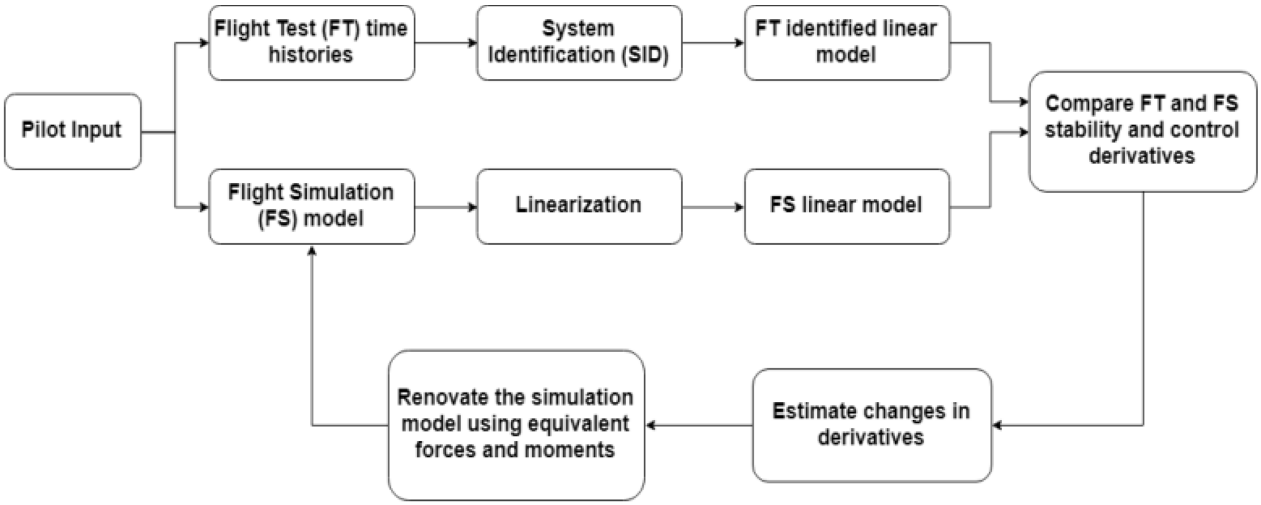

Figure 7.3-1: Force and Moment Increment Method Flow Chart.

Pilot inputs such as frequency sweeps or multi-step, e.g., 3211 or 2311 type, inputs are used for generating the FT data required for derivative identification, using frequency-domain methods such as implemented in CIFER® [1]. Alternatively, the derivatives can also be estimated using classical time-domain identification methods [2], [3]. Derivatives can also be estimated from flight-test data using the Additive System IDentification method reported by Cameron et al. [4] and Agarwal et al. [5] or the Linear Parameter Identification Using Adaptive Learning [6], [7]. Whilst the same inputs and methods can be used to generate the derivatives from the simulation model linearization tools are available within flight dynamics codes that simplify this process.

A comparison of FT identified and FS linear model derivatives is then made to compute residual forces and moments. This requires that the same linear model structure be used for the flight and simulation data for quantifying the delta derivatives. Selection of the derivatives to renovate will depend on the nature of the model fidelity shortfall. The derivative selection can be achieved either by carrying out a sensitivity calculation or through a physics-based study. The differences in the linear models are converted into force and moment derivatives, which can then be used in the update of, e.g., stability and the on-axis or off-axis responses of the helicopter.

The next step in the model updating process is to select the derivative deltas which can enhance the model's capacity to capture the helicopter dynamics.

Next, the force and moment increment method is applied to the states to demonstrate the behavior improvement. The corrective terms for forces and moments are calculated are expressed as linear combinations of individual contributions from state and control derivatives corrections.

Another approach for selecting the derivative deltas for renovation is to identify those that have a quantified impact on a user-defined cost function [8].

This lecture shows how this approach has been used to update models (Bell 412 and AW139) to specifically improve lateral-directional predictions and also for more general applications to enhance models for use in flight training simulators.

7.3.2 Model Enhancement for Lateral-Directional Oscillation Predictions

Predicting the damping of the rotorcraft lateral-directional oscillatory (LDO, aka Dutch roll) mode through modeling and simulation has proved notoriously difficult. Padfield and DuVal [9] and Padfield [10] describe analyses carried out on three helicopters by the AGARD System Identification (SID) working group WG-18 (in the early 1990s) that showed damping predictions were typically double those measured in flight using SID methods. Figure 7.3-2 shows these results and includes the values for the NRC's Bell 412 research aircraft and the nonlinear FLIGHTLAB® (F-B412) simulation model described in Cameron et al. [4]. The LDO frequency (vertical axis) and damping (horizontal axis) are shown in terms of the modal natural frequency (ω_n) and relative damping (ζ).

The qualification/certification requirements for the damping of LDO are set out in the military standard [11] and the European civil standard [12] for flight in Instrument Meteorological Conditions (IMC) (Figure 7.3-2). CS-29 states that the aircraft must (only) be stable for flight in Visual Meteorological Conditions (VMC); this is effectively the vertical, zero damping, line on Figure 7.3-2. The charts define minimum acceptable levels considered appropriate for military and civil operations, respectively. The European Certification Standards replicate the FAA standards [13], which themselves appear to be derived from the early MIL-SPEC 8501 from the 1950s [14].

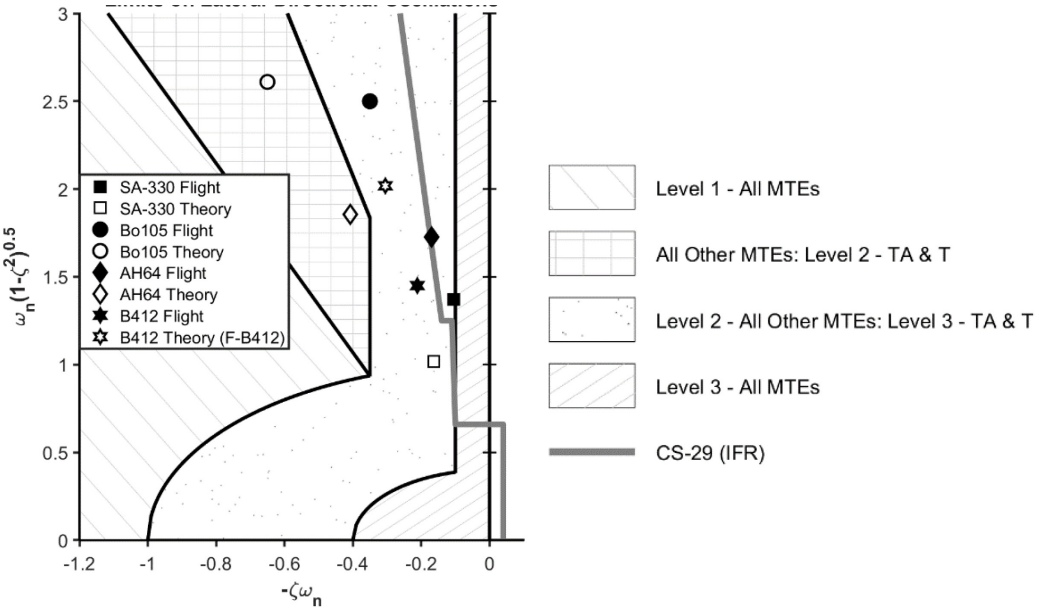

Figure 7.3-2: Comparison of SID Estimates from Flight, and Simulation Predictions of the Lateral-Directional Oscillatory Mode Characteristics [9].

Understanding the sources of modeling deficiencies requires a systematic approach to the comparison of flight and simulation responses and the analysis of any differences and their physical sources. SID provides this, and recent developments have enabled the differences to be transformed into model updates or renovations that reflect the missing physics. The approach is applied to Liverpool's FLIGHTLAB simulation model of the NRC's ASRA Bell 412, designated the F-B412 and ONERA's AW139 model supplied by THALES to improve fidelity of the LDO mode.

7.3.2.1 Bell 412 90kn LDO Study – Frequency-Domain Approach

The model updating, or renovation, approach for Method 3 adopted by Liverpool is summarized in Section 5.3.1.1 of Tischler et al. [15] and described in more detail in Lu et al. [8]. Essentially, deficiencies in the fidelity of the nonlinear F-B412 model, or the mismatch between flight and simulation, are corrected with incremental forces and moments as 'delta' derivatives. These deltas are derived from comparisons of the parameters in the SID and linearized F-B412 derivative models. Derivative deltas that have a sufficiently large quantified impact on the user-defined cost function are selected for use in renovation.

The integrated cost function or value of J function for the identified SID model is $J = 52$. With a guideline for acceptable fidelity of $J \leq 100$, the SID model extracted from the flight-test data well meets this fidelity guideline as expected. The LDO mode eigenvalues derived from the (stability) derivative matrices are shown in Table 7.3-1. Here, the eigenvalues for the 3-DOF model structure are compared with those for the 6-DOF model structure. Significantly, the LDO eigenvalues from Flight-Test (FT) SID obtained using 3-DOFs are within 2% of the 6-DOF SID models. This suggests that the couplings from surge, heave, and pitch have little impact on the key LDO dynamic characteristics of the Bell 412. As expected, the real aircraft is less stable than predicted by the F-B412. The LDO frequency, dominated by the contribution from N_v, are reasonably well predicted by the approximation, but the damping is consistently under-predicted by the F-B412.

Table 7.3-1: LDO Damping (ζ) and Frequency (ω) from FT, 3-DOF, and 6-DOF Models.

Derivatives	Eigenvalues
F-B412 3 DOF	[0.166, 2.1418][1]
FT 3 DOF	-0.207 ± 1.466i
F-B412 6 DOF	-0.354 ± 2.107i
FT 6 DOF	-0.211 ± 1.450i

[1] $[\zeta, \omega_n]$, ω_n in rad/sec

Figure 7.3-3 compares the responses from FT lateral cyclic and pedal inputs with the linear SID model and non-linear F-B412 model; these are the responses of primary interest for examining the lateral-directional motion. The figure shows responses to 2311 control inputs with very little free response after the inputs are returned to trim. With the short time period, the LDO mode is not particularly evident in these responses, but they should contain sufficient information to provide insights into the baseline F-B412 fidelity. First, the linear 3-DOF SID model captures the FT responses reasonably well. Following the lateral cyclic input, the fidelity of the 'baseline' yaw rate is poor F-B412. Following the pedal input, both yaw and roll responses show poor fidelity, exposing a need for on-axis renovation.

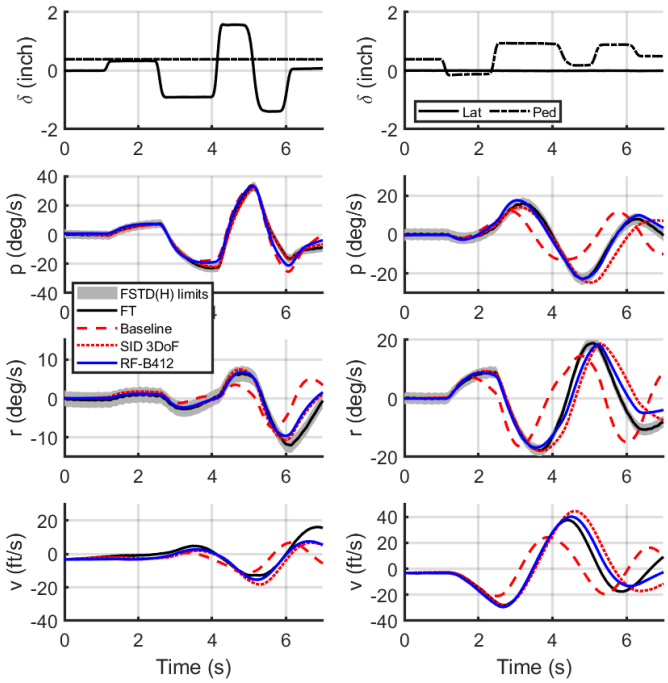

Figure 7.3-3: Comparison of Responses of FT with F-B412 Before (Baseline) and After Renovation (RF-B412); Lateral Cyclic (Left) Pedal (Right) Inputs at 90 kn.

The fidelity of the model can be observed in the magnitude and phase error frequency response functions (FT/model) in Figure 7.3-4 and Figure 7.3-5. These boundaries relate to limits on Maximum Unnoticeable Added Dynamics (MUAD) of Section 4.1.1 in Tischler et al. [15] and verified by Mitchell [16] for rotorcraft simulation fidelity. The integrated cost function or value of J function for the F-B412 model is J = 127 and 215 for p/δ_{ped} and r/δ_{ped} respectively. The fidelity of the baseline physics-based model exceeds this guideline, thus requiring renovation.

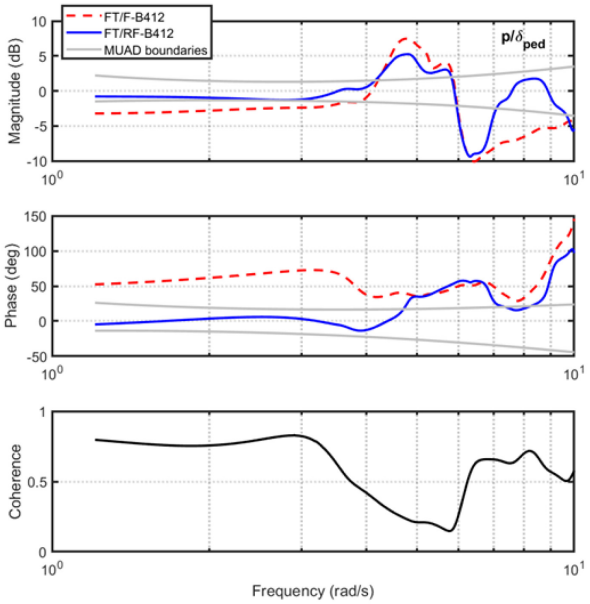

Figure 7.3-4: Error Functions for p from Pedal Frequency Response.

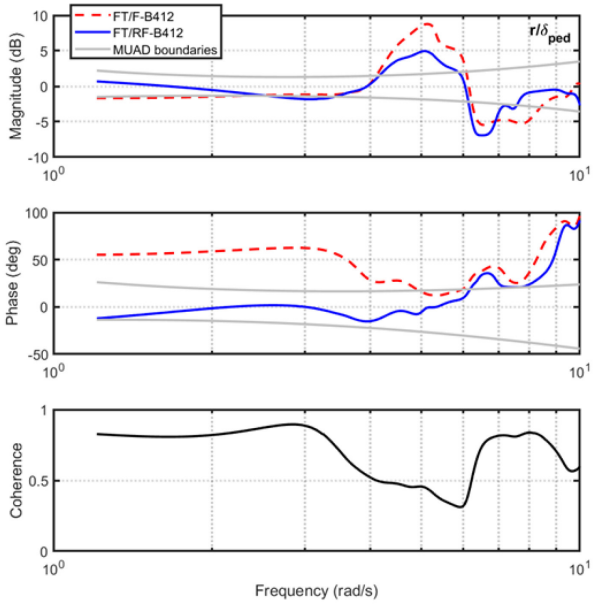

Figure 7.3-5: Error Functions for r from Pedal Frequency Response.

The renovation method selects the derivatives which are effective in improving the match between the FT and the F-B412 response. The required changes in these derivatives (Δs) are estimated by comparing the stability and control derivatives derived from 90kn frequency sweep FT data and perturbation analysis of the F-B412. In view of the dominance of the lateral-directional derivatives in the LDO, the renovation of the F-B412 (RF-B412) has been restricted to the 3-DOF sub-set and is shown in Table 7.3-2. Figure 7.3-5 shows the responses of the RF-B412 to the multi-step control inputs compared with FT, the baseline F-B412, and the 3-DOF SID model. The comparisons confirm the good quality match of the linear SID 3-DOF model with FT, as assessed by the FSTD(H) tolerances, have been preserved in the RF-B412.

Table 7.3-2: Renovation of F-B412.

Derivative	Δ Value Change	% Δ Change
L_v	0.0120	-32.5%
N_v	-0.0164	-69.5%
N_r	0.2227	-21.6%
N_{ped}	0.1178	-17.5%

The LDO mode eigenvalues from renovation are shown in Figure 7.3-3. As before, the F-B412 is more stable than the 'real' aircraft, with a higher mode frequency. The renovated 3-DOF lateral-directional model features a modal damping and frequency mismatch of only 2% relative to the 6-DOF results. The integrated cost function or value of J function for the RF-B412 model is $J = 58$ and 84 for p/δ_{ped} and r/δ_{ped} respectively. The points for the RF-B412 are shown on the eigenvalue chart in Figure 7.3-6, with the 10% box centered on the FT indicating the limits for fidelity from the flight training standards [17], [18].

Table 7.3-3: LDO Damping (ζ) and Frequency (ω) for RF-B412 Model.

Derivatives	ζ	ω
F-B412	-0.3540	2.107
F-B412 ren. N_v, L_v, N_r	-0.2078	1.476
FT 3 DOF	-0.2071	1.466
FT 6 DOF	-0.2113	1.450

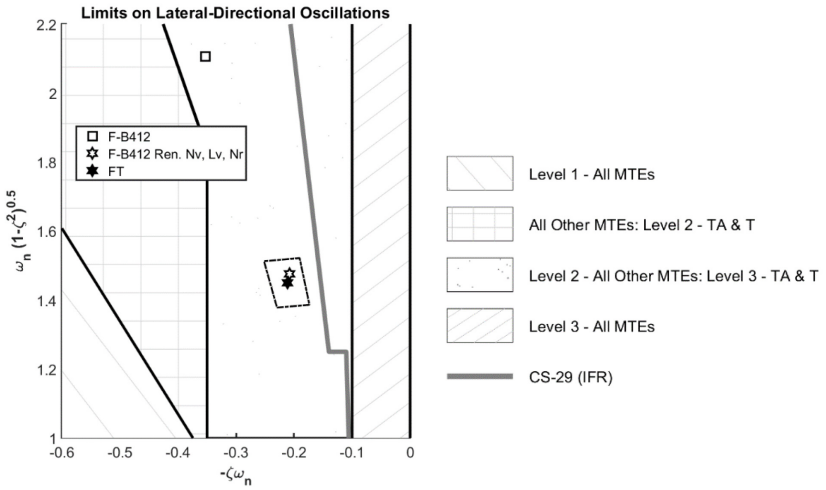

Figure 7.3-6: LDO Characteristics of F-B412 Before and After Renovation Compared with Flight.

7.3.2.2 Bell 412 90kn LDO Study – Time-Domain Approach

The identification approach presented in this section is described as 'Additive System IDentification' (ASID), based on Equation-Error (EE) analysis in the time domain. The method has been developed principally to aid investigations of nonlinear aerodynamic complexities [5]. The ASID method can then be augmented by the force and moment increment method (described earlier in this section) to complete the model update process with delta derivatives or nonlinear force and moment contributions.

In this case, the pedal responses shown in Figure 7.3-7 are used to illustrate how to derive these values.

The ASID method estimates the derivatives in sequence. The time delay $\tau_{X_{p\dot{r}}}$ is estimated to be 0.086 sec by comparing the difference between the pedal input and the yaw acceleration. Following this, the control derivative N_{X_p} is the first derivative chosen for identification since, following the control input, the rotor disk re-orientates rapidly. N_{X_p} is chosen as illustrated in Figure 7.3-8.

N_r is selected as the second derivative, as yaw is the dominant response within the first two seconds. After fixing N_{X_p}, and N_p is selected immediately after N_r arising from the strong yaw/roll inertia coupling (due largely to the non-zero product of inertia, I_{xz}) and the incremental roll moment resulting from tail rotor thrust variation (above CG).

The reduced order 3-DOF LDO model structure provides a good match against FT for the validation responses shown in Figure 7.3-9. The F-B412 renovation follows a similar process to that previously discussed using the frequency-domain results.

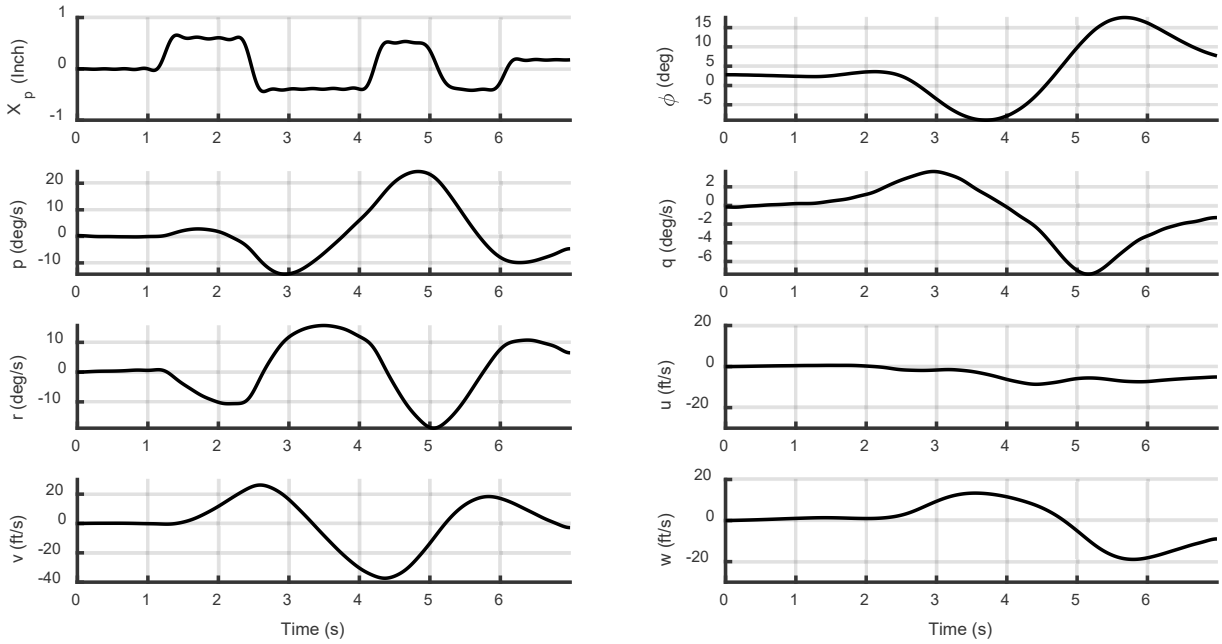

Figure 7.3-7: Responses of B-412 with Pedal Input at 90 kn.

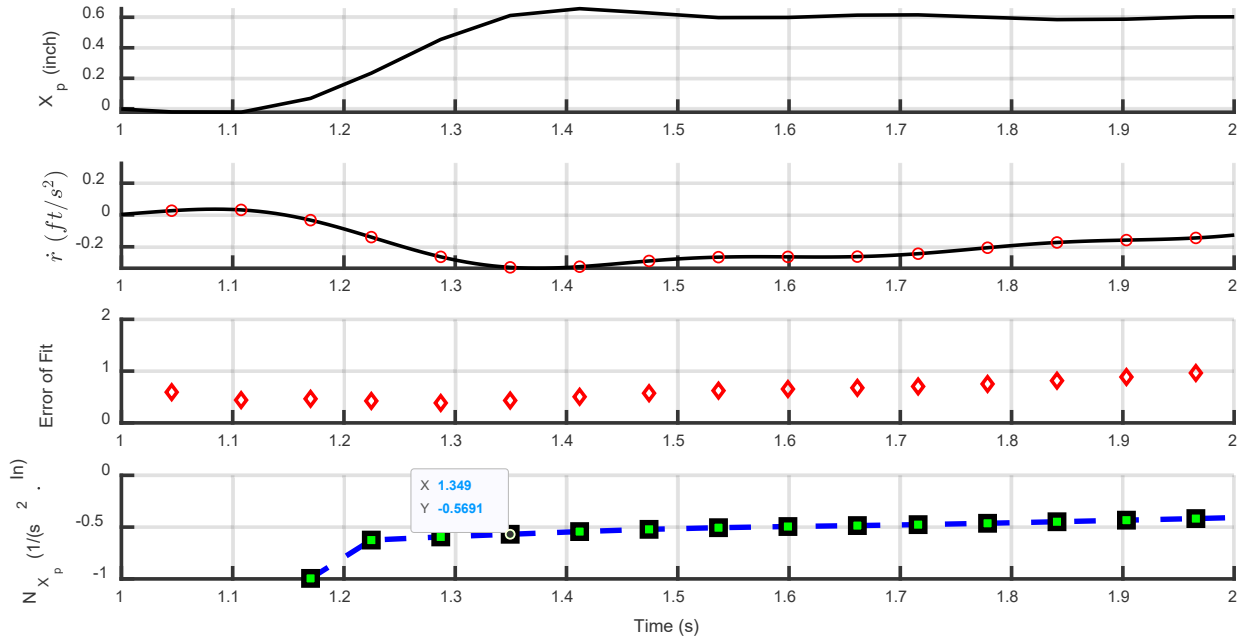

Figure 7.3-8: Estimating N_{X_p} Using the ASID Approach.

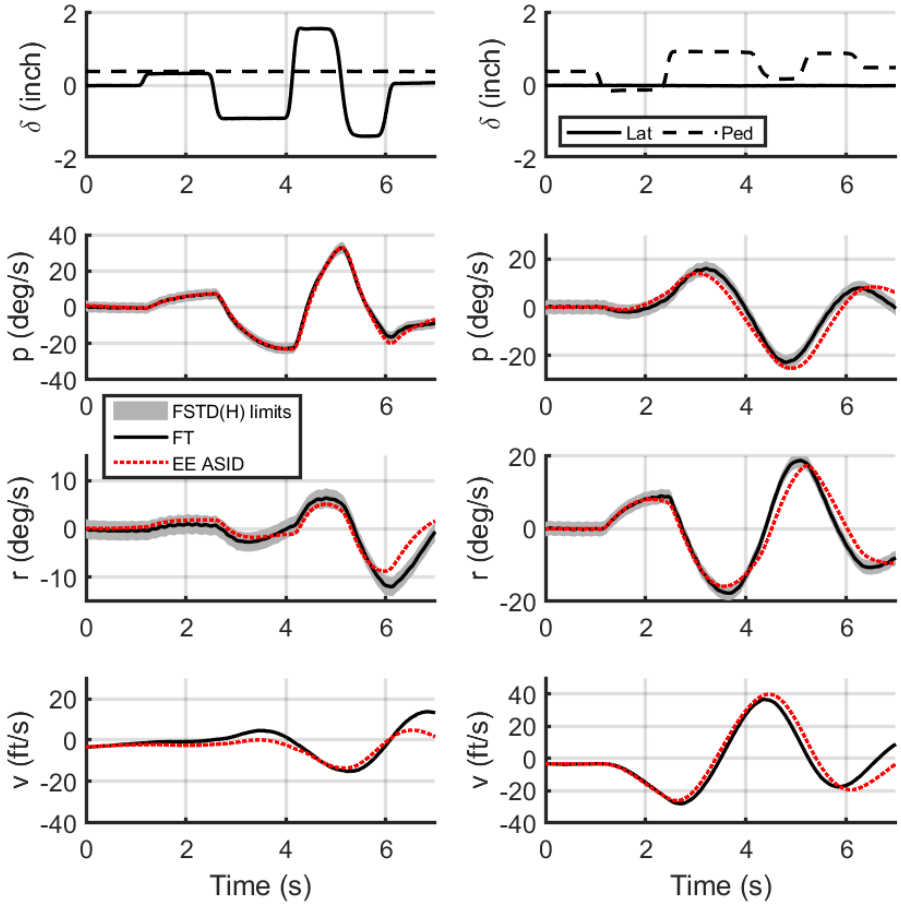

Figure 7.3-9: Validation Study: Comparison of Responses of FT with ASID; Lateral Cyclic (Left) Pedal (Right) Inputs at 90 kn.

7.3.2.3 AW139 75kn LDO Study

As a case study, ONERA applied the renovation method based on corrective force and moment terms to the THALES flight mechanics model of the AW139 helicopter. The application focused on the lateral/directional behavior improvement at V_y (optimal climb speed) which is approximately 75kn for this aircraft. Flight tests were those from the regular QTG tests used for Level D certification of the simulator. These flights did not include frequency sweep tests; therefore, the data were not ideal for frequency-domain system identification of a 6 DOF state-space model. Using the CIFER® software suite [1], a reduced order (3-DOF) lateral-directional model could be identified for this application. The details of obtaining the system identification results using the QTG inputs and CIFER are given in the complementary paper by Taghizad et al. [19]. Overall, a satisfactory lateral-directional model was identified in the mid-frequency range (1 – 10 rad/sec), providing good accuracy in the short-term time response. The SID partial derivatives could be used to complement lateral-directional forces and moments by linear corrective terms. The results of this case study are presented hereafter, with an emphasis on renovation for pilot lateral inputs.

QTG flight tests include lateral and pedal doublet inputs and additional low frequency sweeps in the lateral axis. Due to the low frequency sweeping tests, the identified model was able to better capture the dynamics in response to lateral low frequency inputs. Hence, it was decided to investigate model renovation for pilot lateral inputs. SID achieved good parameter reliability for the decoupled lateral model. Figure 7.3-10 shows an example of the identification results as transfer functions for V_y nil wind conditions.

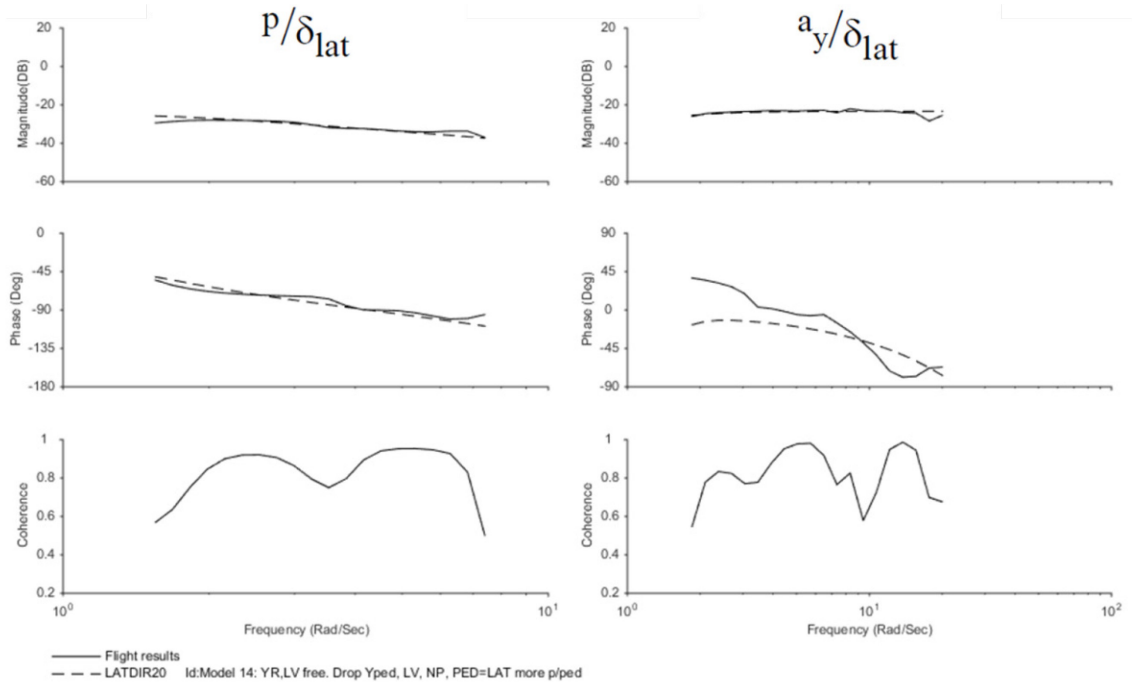

Figure 7.3-10: Transfers from δ_{lat} to Roll Rate (p) and Lateral Acceleration (a_y).

Table 7.3-4 shows partial stability and control derivatives obtained from SID in comparison with those from nonlinear model linearization. Corrective terms were calculated on roll and yaw moments (ΔL and ΔN) and on lateral and vertical forces (ΔY and ΔZ). Not all the derivatives are actively involved in lateral-directional dynamics mechanism. Therefore, the NL model sensitivity to derivatives corrections will not be the same from one derivative to another. Consequently, it is recommended to select a coherent set of derivatives for lateral-directional fidelity enhancement. This work is generally supported by a sensitivity analysis.

In the current application, since the number of parameters is limited, the sensitivity study was performed manually and produced the following outcome:

- L_p, L_r and N_r bring a real improvement.
- Y_{lat} and Z_w bring minor improvements.
- The other derivatives have no impact or, in some cases, negative effects.

It should be noted that of the yaw axis derivatives only Nr was used for contributing to the lateral-directional dynamics simulation renovation. Tests revealed that the nonlinear model output was almost insensitive to other derivatives for this motion. This observation suggests 2 hypotheses: either the physical model does not need any improvement on yaw axis, or the yaw axis exhibits less contribution during this motion. Table 7.3-4 shows that yaw axis derivatives obtained from SID are quite far from those extracted from the physical model. Therefore, the physical model needs also to be improved on this axis.

The most plausible explanation of the low effect of yaw derivatives in this study is that the lateral-directional dynamics could principally be driven by a dominant roll motion. The derivatives selected for linear force and moment corrections were L_p, L_r, N_r, Y_{lat}.

Table 7.3-4: Partial Stability and Control Derivatives from AW139 Model Linearization and SID on FT (*Vy*).

Stability Derivative	FT	Model	Control Derivative	FT	Model
Z_w	- 0.606	*-1.0471*	Y_{lat}	0.06835	*0.0752*
Y_v	0.02552	*-0.135*	Y_{ped}	0*	*0.0746*
Y_p	0*	*-0.198*	L_{lat}	0.1023	*0.7405*
Y_r	0.9209	*0.4355*	L_{ped}	−0.03617	*-0.0335*
L_v	−0.01449	*-0.0748*	N_{lat}	0*	*-0.083*
L_p	−1.214	*-2.2763*	N_{ped}	0.03582	*0.105*
L_r	1.563	*-0.1483*	τ_{lat}	0.06674	
N_v	0.01144	*0.0319*	*τped (=1.0*τlat)*	0.06674	–
N_p	0*	*-0.3114*			
N_r	−0.9458	*-0.7175*			

*: Eliminated during model structure determination.

For all cases tested, a real improvement is brought on the lateral axes responses, namely roll rate and bank angle and as shown in Figure 7.3-11, yaw axes dynamics are also notably improved.

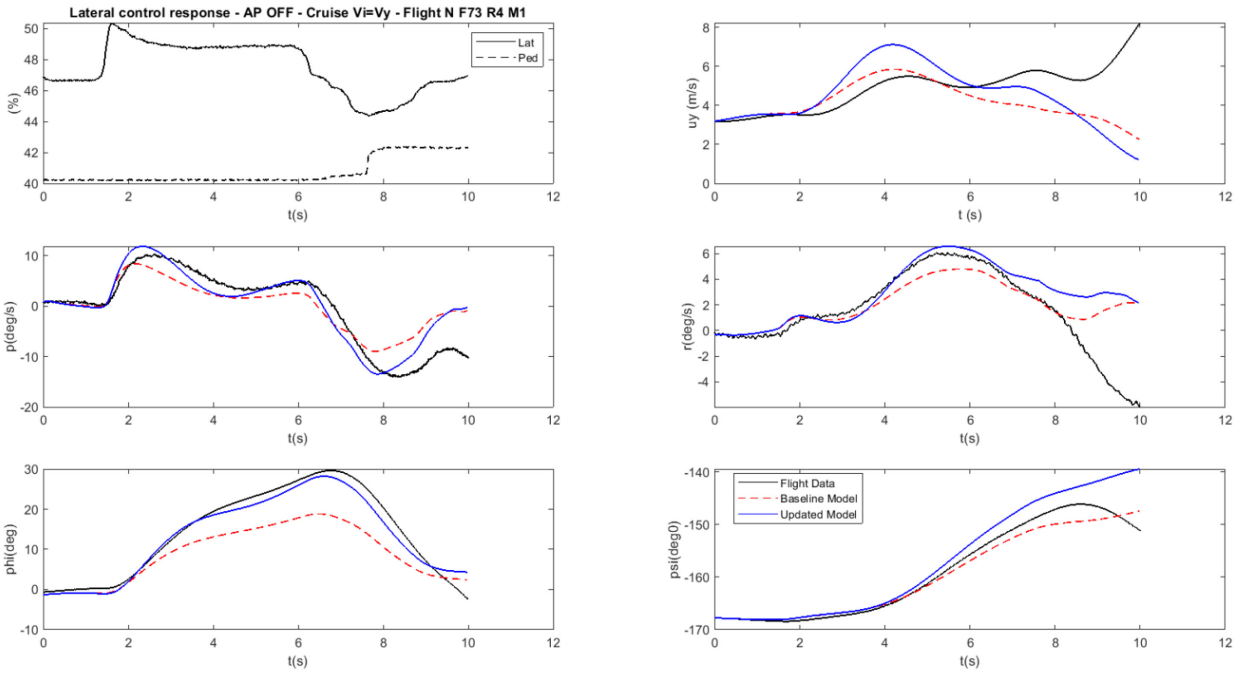

Figure 7.3-11: Flight Case 2 – Comparison with FT, Before and After Force and Moment Corrections.

7.3.3 Model Enhancement for Full Flight Simulator Applications

Helicopter training simulators need to provide high-fidelity immersive environments for pilots in order to obtain a Level D qualification, which is the highest level of simulator qualification defined by the Federal Aviation Administration (FAA) [17], the European Union Aviation Safety Agency (EASA) [18], and the International Civil Aviation Organization (ICAO) [20]. A Level D qualification allows the replacement of most of the flight hours required for a pilot's type rating or recurrent training by simulator hours. A Level D simulator is made of many sub-system models related to the vehicle dynamics (flight dynamics, flight controls, engines, autopilot), vehicles systems (avionics, ancillaries, etc.) and simulator immersive cueing environments (motion, sound, visual, weather, airport environment, etc.). Each of these sub-systems must meet qualitative and quantitative validation criteria for the specific aircraft type to meet Level D simulator requirements.

In all, over 1000 test points and QTG maneuvers are typically collected for simulator model generation and validation. The maneuvers span from maneuvers near the ground (Engine start and shutdown, ground taxi, Hover and low speed, takeoff and landing) to cruise flight performance static stability, dynamic maneuvers, and autorotation. The flight tests may also include a range of operational maneuvers specific to the customer training requirements (CAT A takeoff and landings, slope landings, quick stops or tactical maneuvers, ILS capture and approaches, etc.). The flight-test time can be over 100 hours collected through a period of months. The total number of sorties is about 40. In addition to the parameters required for the aerodynamic model, sound and vibration data are also typically recorded.

In order to comply with the qualification requirements, the flight model is evaluated by comparing the model with flight-test data using time-domain metrics such as flight parameters in trimmed flight conditions (e.g., control positions, Euler angles, torque readings, etc.) and responses to pilot inputs. The majority of handling qualities tests include those associated with the longitudinal long-term response (phugoid), lateral-directional oscillations (Dutch roll), spiral stability, and adverse-proverse yaw. In addition, long flight maneuvers, such as take-off and landing, are compared with the response of the flight model in the simulator. Altogether, more than 100 flight maneuvers are compared. The time-domain metric to measure the simulator accuracy are called tolerance bands. Examples of tolerance bands relevant to the results presented in this paper are shown in Table 7.3-5.

Table 7.3-5: Examples of Time-Domain Metrics Required in a QTG Package.

Maneuver	Tolerance Band	Test Details
Longitudinal input in Hover	Pitch rate: ±10 % or 3 º/sec, Pitch attitude change after the input of ±10 % or 3 º	Record results for a step control input. The off-axis response must show correct trend for the unaugmented cases.
Lateral input in Hover	Roll rate: ±10 % or 3 º/sec, Roll attitude change after the input of ±10 % or 3 º	Record results for a step control input. The off-axis response must show correct trend for the unaugmented cases.

This is the so-called ‘objective’ part of the qualification procedure related to flight dynamics and is presented to the authorities via documentation. The following sections cover case studies of the use of the force and moment corrections to improve the simulator responses for the objective assessment part of the simulator development.

7.3.3.1 Bell 412: Simulation Model Improvements in Hover

The case study in this section will present the different steps leading to a Level D model in hover based on the Bell 412 ASRA airborne research simulator referenced in Gubbels et al. [21] Details and results of the identified model in hover can be found in Seher-Weiß et al. [22]. The hover model was identified using the CIFER® frequency response method detailed in Tischler and Remple [1].

Using small perturbation finite differences, we calculated stability and control derivatives for the Baseline OO-BERM configuration in hover. As seen in Table 7.3-6, static and dynamic derivatives relative errors are > 88%. It should be noted that the dynamic derivatives L_p and M_q have a higher magnitude than the CIFER identified values. This results in a baseline simulation exhibiting an overdamped response to any pilot control or atmospheric perturbation.

Table 7.3-6: CIFER Identified Rolling and Pitching Static/Dynamic Derivatives Compared with Baseline and Updated OO-BERM Calculated Derivatives for the Hover Model.

Par.	CIFER Value	Baseline OO-BERM	Rel. Error [%]	Updated OO-BERM	Rel. Error [%]
L_u	.0311	.0028	91.00	.021	32.48
L_v	-.0216	-.1	362.96	-.032	48.15
L_w	0^a	-.002	-	-.0035	-
L_p	-2.362	-5.28	123.54	-2.35	0.51
L_q	-.274	.05	118.25	-.28	2.19
L_r	0^a	.23	-	.05	-
M_u	.017	.002	88.24	.019	11.76
M_v	.0178	.0005	97.19	.0126	29.21
M_w	0^a	-.0011	-	-.001	-
M_p	-.446	-1.6	258.74	-.43	3.59
M_q	-.528	-1.97	273.11	-.53	0.38
M_r	0^a	-.037	-	.05	-

(u, v, w in ft/s, p, q, r in rad/s, ^{a}eliminated during model structure reduction)

Once the control derivatives have been updated, the dynamic derivatives are implemented in the OO-BERM using body aerodynamic coefficients and interactional aero parameters. Increments of forces and moments are calculated to match the dynamics derivatives (L_p, L_q, etc.). Also, in order to match the Level D requirements for the low-speed trimmed attitude and control positions conditions (Table D2A in 14 Part 60 [17] and SUBPART C in Ref. [18]), trims and changes of control and attitude each side of the trim condition ($\Delta u, \Delta v$) are calculated to match the trim flight-test data points.

Validation is conducted first in the frequency domain to compare on- and off-axis responses. Figure 7.3-12 shows frequency-domain comparison of the Baseline/Updated OO-BERM models with the flight-test data and the identified hover model using CIFER. As expected from the Baseline OO-BERM calculated derivatives in Table 7.3-7, Baseline OO-BERM frequency responses show poor results compared to the flight-test data. The significant control derivatives are too low ($L_{\delta_{lon}}, L_{\delta_{lat}}$ and $M_{\delta_{lon}}$); the on-axis damping terms (L_p, M_q) are too high and almost all the other static and dynamic terms have large errors.

Figure 7.3-12 shows good results for the Updated OO-BERM model compared to the measurements and the identified linear model from CIFER. Indeed, for on- and off- axis pitch and roll frequency-domain responses were the coherence is acceptable (> 0.6), p/δ_{lat}, p/δ_{lon} and q/δ_{lon} responses show good match for both magnitude and phase with the Updated OO-BERM model frequency responses having a difference of phase of 20 degrees at 10 rad/s compared to the Model CIFER frequency responses. Off-axis response q/δ_{lat} show an average maximum offset of 3.3 dB and a drift in the phase.

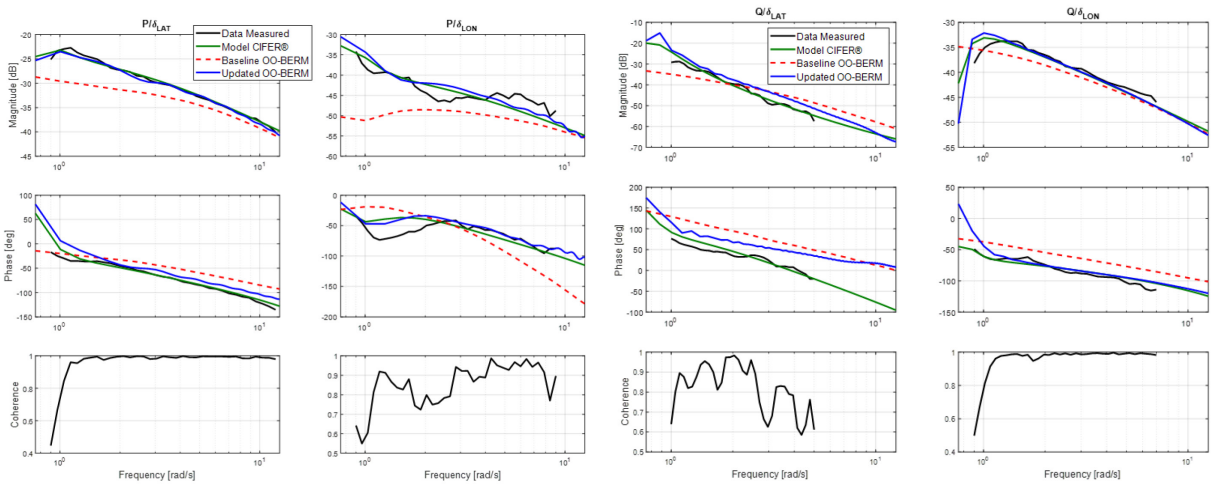

Figure 7.3-12: Frequency Domain Comparison of the Flight Data with Identified CIFER® Hover Model and Baseline/Updated OO-BERM Model.

Table 7.3-7: Frequency-Domain Integrated Cost *J*.

Frequency response	*J* Baseline OO-BERM	*J* Updated OO-BERM
p/δ_{lat}	400.9	64.2
p/δ_{lon}	842.6	118.9
q/δ_{lat}	1111.9	518.7
q/δ_{lon}	258.6	34.5

In hover, the time-domain criteria in both 14 Part 60 Table D2A [17] and CS-FSTD(H) SUBPART C [18], SUBPART C requires for a tolerance of ±10 % or 2 deg/sec (whichever is the highest) longitudinal cyclic input cases on the pitch rate response (q) and of ±1.5 degrees on the pitch attitude change ($\Delta\theta$) following a control input. For lateral cyclic input cases, a tolerance of ±10 % or 3 deg/sec (whichever is the highest) on the roll rate response (p) and of ±3 degrees on the roll attitude change ($\Delta\phi$) following a control input are required. Also, all off-axis parameters need to follow the correct trend and have the correct magnitude. Initial condition adjustment is required because the flight-test data is never perfectly trimmed, and small initial linear and angular accelerations are usually required when starting the simulation run on a maneuver to ensure that the simulation result is in a steady state before the control inputs. It should be noted that the same initial conditions were applied for each case for the Baseline and Updated OO-BERM.

Figure 7.3-13 shows time-domain validation for longitudinal and lateral cyclic input cases of the Baseline and Updated OO-BERM. The grey bands represent the allowable tolerance band. By looking at both frequency and time responses, the Baseline OO-BERM responses are overly damped for the rolling and pitching moments following a pitch input. Roll response due to lateral input is overdamped and pitch response does not follow the trend well. Finally, from Figure 7.3-13, one can conclude that the Updated OO-BERM simulation time-domain responses are within the FAA and EASA tolerance bands for the on-axis control input and has a correct trend and magnitude for off-axis responses within 2x the tolerance bands.

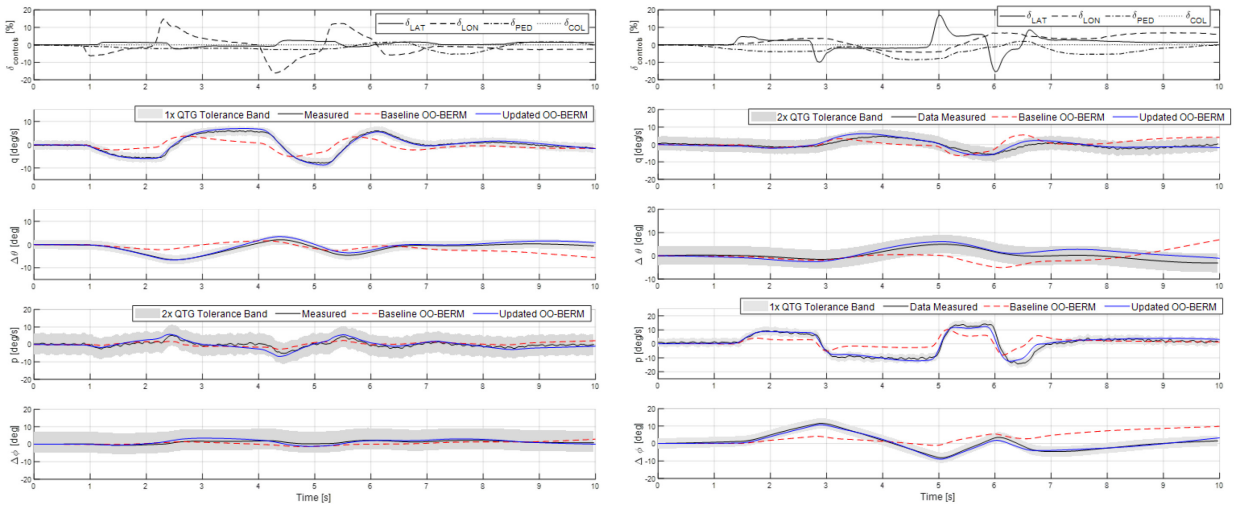

Figure 7.3-13: Time-Domain Validation of the Hover Model OO-BERM Against Flight Data (Left: Longitudinal Cyclic Input, Right: Lateral Cyclic Input).

Two other metrics that are widely used in the piloted simulator community (Tischler and Remple [1] and Seher-Weiß et al. [23]) are calculated for comparison purpose, namely the frequency-domain integrated cost metric J and the mismatch mean square cost function J_{rms}.

From Tischler and Rempel [1], it is found that the acceptable standard value for frequency-domain integrated cost metric model fidelity is $J_{ave} < 100$. It should be noted that J_{ave} is the average cost of all frequency responses. Table 7.3-7 shows the frequency-domain integrated cost of p/δ_{lat}, p/δ_{lon}, q/δ_{lat} and q/δ_{lon}. As expected from previous results, Baseline OO-BERM results for on- ($J > 250$) and off-axis ($J > 400$) show poor frequency domain integrated cost compared to the Updated OO-BERM, where the on-axis frequency responses p/δ_{lat} and q/δ_{lon} are below the acceptable standard ($J < 65$). Off-axis response cost p/δ_{lon} is reasonably low ($J = 118.9$), whereas q/δ_{lat} still has a very high cost ($J = 518.7$).

From Figure 7.3-13, the Updated OO-BERM simulation time-domain responses for the on-axis control input agree with results from Table 7.3-7. Also, off-axis roll time response to longitudinal cyclic input seems to show reasonable behavior as expected. With a very high cost ($J = 518.7$), off-axis pitch time response to lateral cyclic input q/δ_{lat}, one would expect poor results, but the response is within 2x the tolerance bands. This 'apparent' inconsistency is due to the small absolute value of the q/δ_{lat} response in Figure 7.3-13, due to the much higher pitch inertia as compared to roll inertia, while the large of J reflects a large relative error in dB (i.e., %) and phase (deg).

7.3.3.2 EC135: Improving Off-Axis Response Characteristics in Hover

A typical single main rotor helicopter is usually coupled in all axes. Classic blade element rotor models with dynamic inflow and flapping dynamics do not capture this response accurately. Particularly, modeling the roll response to pitch rate and the pitch response to roll rate is a challenge. In fact, the direction of the predicted angular rates in the off-axis are often reversed [24], [25], [26], [27], [28], [29]. Among others, the rotor wake curvature, which is not captured in the classic rotor inflow models, is believed to modify the pressure distribution around the rotor, such that the off-axis response would change direction.

To capture the deficiencies in the off-axis response when dynamic inflows are used, various corrections have been suggested. For instance, Rosen and Isser [30] show rotor wake geometric distortion in a pitch/roll motion in hover using a dynamic rotor model. This wake distortion changes the inflow distribution over the disk causing the off-axis response to change sign. Using a free vortex method, Bagai et al. [31] and Bhagwat and Leishman [32] also show wake distortion in the pitching/rolling motion. Mansur and Tischler [33] and Tischler [34] propose an empirical aerodynamic lag to represent the unsteady nature of the rotor blade section lift and drag forces. In Tischler [34], the off-axis discrepancy is resolved by changing the effective swashplate phasing angle. Theodore and Celi [35] use blade elasticity and rotor wake dynamics to overcome the off-axis discrepancy. In more recent studies, Zhao [28], and Zhao et al. [36], developed the dynamic wake distortion model with four states (wake spacing, wake skew, and wake curvature in lateral and longitudinal axes) and augmented it with the Pitt-Peters dynamic inflow model.

In this section, the off-axis model response of an EC135 helicopter nonlinear model is enhanced by adding moment increments using delta derivatives. These derivatives are obtained by comparing linear models obtained through parameter System IDentification (SID) using DLR's flight-test data and a baseline EC135 nonlinear helicopter model obtained using Aerotim Engineering's core model libraries [37]. The purpose of this enhancement is to improve the model responses that are to be used in flight simulator training devices.

The goal in this section is to improve the off-axis characteristics of a baseline nonlinear helicopter model response with moment increments obtained through SID. First, the baseline nonlinear model is run using 3211 type maneuvers around hover and SID is performed on the data obtained from the baseline simulation. DLR's 3211-type flight-test time history data around hover is used for SID to obtain the aerodynamic stability and control derivatives for the EC135 helicopter. The difference in the relevant aerodynamic derivatives is then added to the baseline nonlinear model as 'delta derivatives' to capture the off-axis response seen in the flight data.

A physics-based nonlinear model of the EC135 twin engine helicopter is built using Aerotim Engineering's core model libraries [37] core model components intended for the development of flight models for EASA Level D certifiable full flight simulators. The model used here has no flight-test data-based corrections and is, therefore, referred to as a 'baseline flight model.' Most components are used as reported in literature: A Blade Element Rotor Model (BERM), 2nd order flapping, Pitt-Peters inflow model, aerodynamic derivatives for fuselage, vertical tail, horizontal tail, Fenestron model, etc. All stability and control augmentation are turned off.

A time-domain based identification method is used based on Model Reference Adaptive Control, where it is shown that the uncertainty arising from the unmodeled dynamics could be linearly parameterized, and the convergence of the adaptive weights around the optimal locations is possible. Moreover, a unique optimal solution exists if the basis of the adaptive element is composed of a minimal representation of the dynamic system [38], [39]. Adaptation is run in sequence for all channels and is repeated until convergence is achieved. At the beginning of each sequence, the adaptive weights, W, and the recorded data stack, Z, are initialized to the values obtained at the end of the previous sequence. Therefore, a continuous update on the adaptive parameters is obtained. All 8 rigid body states and 4 control channels are used in the linear model.

To obtain 'delta' derivatives, the linear models obtained from the identification of the baseline model and the flight-test data are compared numerically. A reduced order (pitch-roll) linear model is used to update the off-axis response. The identified reduced order linear model of the nonlinear baseline model is found to be

$$\begin{bmatrix}\dot{p}\\ \dot{q}\\ \dot{r}\end{bmatrix} = \begin{bmatrix}-4.49 & -4.06 & -0.09\\ 1.10 & -1.01 & 0.01\\ -0.20 & -0.12 & -0.08\end{bmatrix}\begin{bmatrix}p\\ q\\ r\end{bmatrix} + \begin{bmatrix}-0.023 & 0.129 & 0.005\\ 0.047 & 0.0037 & 0.001\\ -0.006 & 0.004 & 0.021\end{bmatrix}\begin{bmatrix}\delta_e\\ \delta_a\\ \delta_p\end{bmatrix} \quad (7.3\text{-}1)$$

while the identification using DLR's flight test data resulted in

$$\begin{bmatrix}\dot{p}\\ \dot{q}\\ \dot{r}\end{bmatrix} = \begin{bmatrix}-3.09 & 1.13 & -0.01\\ -0.69 & -0.92 & -0.02\\ -0.51 & 0.053 & -0.36\end{bmatrix}\begin{bmatrix}p\\ q\\ r\end{bmatrix} + \begin{bmatrix}-0.033 & 0.12 & 0.01\\ 0.037 & 0.0003 & -0.01\\ -0.013 & 0.018 & 0.034\end{bmatrix}\begin{bmatrix}\delta_e\\ \delta_a\\ \delta_p\end{bmatrix} \quad (7.3\text{-}2)$$

Although the on-axis parameters in the system matrices in Equation 7.3-1 and Equation 7.3-2 are close, the sign reversal in the pitch-to-roll and roll-to-pitch off-axis is apparent.

To correct the response of the baseline model, the difference in the identified reduced order models is used. For that, the angular rate equations (p, q, r) along with the longitudinal, lateral, and pedal control input related derivatives are compared. The reduced order linear pairs of the Flight Test (FT) identified model $[A_{FT}, B_{FT}]$ and the nonlinear baseline model (m) $[A_m, B_m]$ are subtracted from each other to obtain the differences that can be used as corrections. The delta differences between the matrix elements of the reduced order models are shown in Table 7.3-8.

Table 7.3-8: Reduced Order 'Delta' Derivatives.

	Delta A (A_{FT}-A_{model})		
	p	q	r
$\dot{p}$	1.40	5.18	0.08
$\dot{q}$	-1.79	0.10	-0.03
$\dot{r}$	-0.31	0.17	0

	Delta B (B_{FT}-B_{model})		
	lat	lon	pedal
$\dot{p}$	-0.010	-0.009	0.006
$\dot{q}$	-0.004	-0.010	-0.010
$\dot{r}$	0.013	-0.007	0.012

The nonlinear model is corrected using the differences in the stability and control derivatives by adding moments increments to the 6-DOF equations of motion of the nonlinear model. Therefore, the moment increments used here are due to the following stability and control derivatives: ΔL_p, ΔL_q, ΔL_r, ΔM_p, ΔM_q ΔM_r, ΔN_p, ΔN_q $\Delta L_{\delta e}$, $\Delta L_{\delta a}$, $\Delta L_{\delta r}$, $\Delta M_{\delta e}$, $\Delta M_{\delta a}$, $\Delta M_{\delta r}$, $\Delta N_{\delta e}$, $\Delta N_{\delta a}$, $\Delta N_{\delta r}$. ΔN_r is not used in the update for off-line corrections.

In Figure 7.3-14 and Figure 7.3-15, step input flight-test response is compared with the non-corrected baseline model, and the corrected model along with the QTG limits [16]. As can be observed, both the on-axis responses as well as the off-axis response are improved from the baseline model.

J_{rms} is a metric to identify accuracy in the time domain. Table 7.3-9 shows the calculated J_{rms} values both for the baseline model response and the corrected model response, when compared with the flight-test data for the maneuvers shown in Figure 7.3-14 and Figure 7.3-15.

The model is improved for step inputs in both the lateral and longitudinal channels.

Table 7.3-9: J_{rms} Comparison for Baseline and Corrected Models.

J_{rms}	Lateral Cyclic Step	Longitudinal Cyclic Step
Baseline	2.68	2.92
Corrected	1.11	2.71

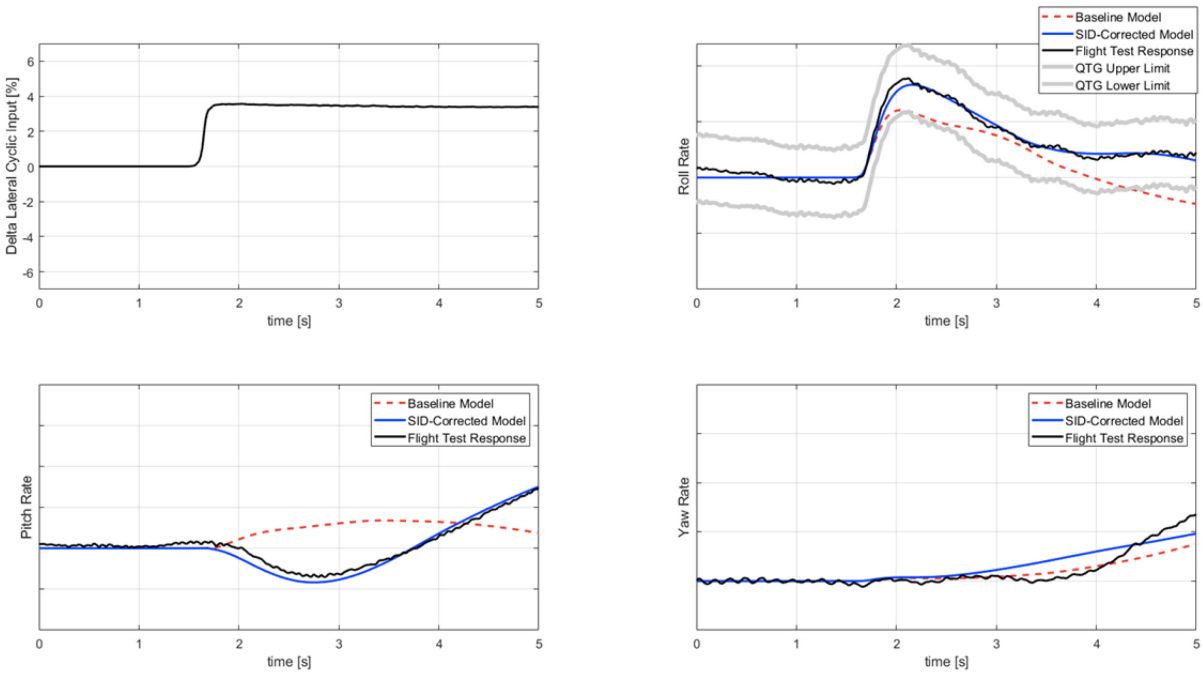

Figure 7.3-14: Response to Right Lateral Cyclic Step Input in Hover.

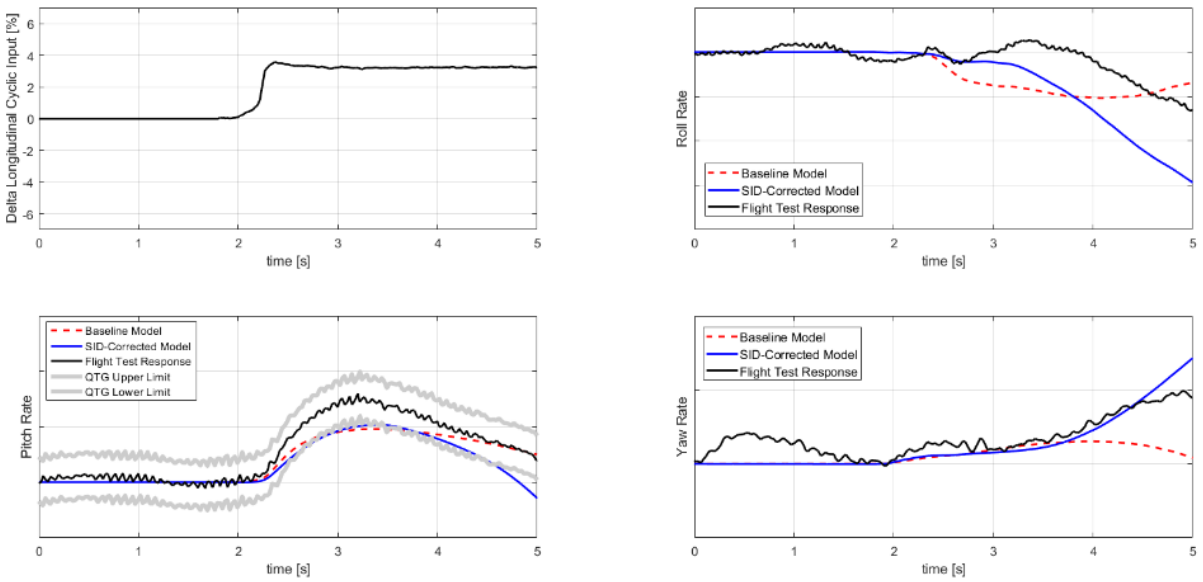

Figure 7.3-15: Response to Aft Longitudinal Step Input in Hover.

J_{rms} is a metric to identify accuracy in the time domain.

Table 7.3-10 shows the calculated J_{rms} values both for the baseline model response and the corrected model response, when compared with the flight-test data for the maneuvers shown in Figure 7.3-14 and Figure 7.3-15.

The model is improved for step inputs in both the lateral and longitudinal channels.

Table 7.3-10: J_{rms} Comparison for Baseline and Corrected Models.

J_{rms}	Lateral Cyclic Step	Longitudinal Cyclic Step
Baseline	2.68	2.92
Corrected	1.11	2.71

A major part of the improvement using delta corrections is the fact that the trend of the off-axis responses now matches the flight-test data. This is of major importance in the handling performance of the model when used in a flight simulator. In fact, for FFS Level D simulator certification, the off-axis response 'must show correct trend' [16]. In the case above, this condition is satisfied for the off-axis. A rule of thumb is to use double the tolerance in the off-axis when compared with the tolerance in the on-axis for a particular maneuver.

7.3.4 Concluding Remarks

This section has applied the forces and moments update method in four case studies and three different aircraft. The principal findings are as follows:

1) Case studies for the Lateral-Directional Oscillation (LDO) of the B412 and AW139 aircraft demonstrate that the poor prediction of the baseline model frequency and damping can be corrected by a selection of lateral-directional subset stability derivatives. For the B412 at 90 kn, a poor prediction of natural frequency was corrected by reduced weathercock stability; this may be caused by the absence of the dynamic pressure reduction at the tail in the baseline model.
2) On the AW139, the LDO was revealed to be a roll-dominant motion. This behavior potentially explains the different derivative candidates for updating identified between the B412 and AW139 studies. For the B412, the relevant stability derivatives were L_v, N_v, N_r and N_{ped}, for AW139 they were mainly associated to lateral axis L_p, L_r, N_r and Y_{lat}. This observation is particularly true for the weathercock stability derivative N_v which played an important role in the B412 LDO damping prediction whereas it was identified as not sufficiently relevant for the AW139. This suggests that different derivative sets should be considered based on the nature the LDO response i.e., *p/r* ratio.
3) A case study conducted on the EC135 suggests that moment updates on three axes using aerodynamic and control derivatives improve the model off-axis response when compared with the flight tests in the pitch and roll channels. In particular, delta derivatives related to the angular velocities are used. By doing so, a corrected sign reversal in the off-axis response was also achieved. Overall, the baseline model is improved significantly, achieving better performance in the QTG tests. The sign reversal in the off-axis response would also significantly improve the handling of the model in a training device.
4) Increments of forces and moments calculated to match static and dynamic derivatives can be artificial, but for training simulators, it is more important to achieve a good handling qualities match with flight test through accurate stability and control characteristics rather than through complex aerodynamic models; this approach is permitted in current training simulator standards.

7.3.5 References

[1] Tischler, M.B., and Remple, R.K. (2012), Aircraft and Rotorcraft System Identification: Engineering Methods with Flight Test Examples, 2nd edition, Reston, VA: American Institute of Aeronautics and Astronautics.

[2] Jategaonkar, R.V., Flight Vehicle System Identification: A Time-Domain Methodology, AIAA, Inc., 2015, Chaps. 4, 6.

[3] Morelli, E.A., and Klein, V., Aircraft System Identification: Theory and Practice, 2nd ed. Sunflyte Enterprises, VA, 2016, Chaps. 4, 5.

[4] Cameron, N., White, M.D., Padfield, G.D., Lu, L., Agarwal, D., and Gubbels, A.W. (2019), "Rotorcraft Modelling Renovation for Improved Fidelity," Vertical Flight Society 75th Annual Forum & Technology Display, Philadelphia, USA, May 13 – 16.

[5] Agarwal D., Lu L., Padfield G.D., Cameron N., White M.D., and Gubbels A.W. (2019), "Rotorcraft Simulation Fidelity for Low Speed Manoeuvring Using 'Additive' System Identification," 45th European Rotorcraft Forum, 17 – 20 September, Warsaw, Poland.

[6] Gursoy, G., and Yavrucuk, I., "Direct Adaptive Limit and Control Margin Estimation with Concurrent Learning," Journal of Guidance, Control, and Dynamics, Vol. 39, No. 6, 2016, pp. 1356-1373.

[7] Yavrucuk, I., and Prasad, J.V.R. (2012), "Online Dynamic Trim and Control Limit Estimation," Journal of Guidance, Control, and Dynamics, Vol. 35, No. 5, 2012, pp. 1647-1656. doi: 10.2514/1.53116.

[8] Lu, L., Padfield, G.D., White, M.D., and Perfect, P. (2011), "Fidelity Enhancement of a Rotorcraft Simulation Model through System Identification," The Aeronautical Journal, Vol. 115, no. 1170, pp 453-470.

[9] Padfield, G., and DuVal, R. (1991), "Application Areas for Rotorcraft System Identification: Simulation Model Validation," AGARD LS-178, pp. 12.1 – 12.39.

[10] Padfield, G.D. (2018), Helicopter Flight Dynamics: Including a Treatment of Tiltrotor Aircraft, Third ed., John Wiley & Sons.

[11] ADS-33, (2000), "ADS-33, Handling Qualities Requirements for Military Rotorcraft," U.S. Army AMCOM, Redstone, AL, (A version 1987, B version 1988, C version 1989, D version, 1994, D-PRF version 1996, E-PRF version).

[12] CS-29 (2019), "Certification Specifications and Acceptable Means of Compliance for Large Rotorcraft CS-29," Amendment 7, EASA 15 July.

[13] CFR 29 (2011), "Airworthiness Standards: Transport Category Rotorcraft," 14 CFR 29, Federal Aviation Administration, Department of Transportation January 1.

[14] MIL-H-8501 (1952), "Military Specification – General Requirements for Helicopter Flying and Ground Handling Qualities," MIL-H-8501A (superseded by MIL-H-8501A, 1961).

[15] Tischler, M.B., White, M. D., Cameron, N., D'Agosto, S., Greiser, S., Gubbels, A., Guner, F., He, C., Horn, J., Hui., K., Jones, M., Juhasz, O., Lee, O., Lehmann, R., Miller, D., Myrand-Lapierre, V., Nadeau-Beaulieu, M., Nadell, S., Padfield, G., Pavel, M., Prasad, J., Ragazzi, A., Richard, S., Scepanovic, P., Seher-Weiß, S., Soong, J., Stroosma, O., Taghizad, A., Tobias, E., Xin, H., and Yavrucuk, I. (2021), "Rotorcraft Flight Simulation Model Fidelity Improvement and Assessment," NATO STO AVT-296 Technical Report.

[16] Mitchell, D.G., Nicoll, T.K., Klyde, D.H., and Schulze, C. (2009), "Effects of Time Varying Rotorcraft Dynamics on Pilot Control," AIAA Atmospheric Flight Mechanics Conference, AIAA 2009-6055, Aug.

[17] FAA (2016), "Federal Aviation Administration," National Simulator Program, 14 CFR Part 60, 2016.

[18] CS-FSTD(H) (2012), "Certification Specifications for Helicopter Flight Simulation Training Devices," CS-FSTD(H), EASA, Initial issue, 26 June.

[19] Taghizad, A., Tischler, M.B., Richard, S., Clark, R.G. (2021), "Extraction of Flight Dynamics Data from Level D Qualification Flight Tests: Application to Training Simulators Model Fidelity Enhancement," VFS Forum 77, May 10 – 14.

[20] ICAO (2012), ICAO 9625 Manual of Criteria for the Qualification of Flight Simulation Training Devices, Volume II - Helicopters, 1st edition.

[21] Gubbels, A.W., Carignan, S., Ellis, K., Dillon, J., Bastian, M., Swail, C. and Wilkinson, C. (2006), "NRC Bell 412 Aircraft Fuselage Pressure and Rotor State Data Collection Flight Test," 32nd European Rotorcraft Forum, Maastricht, Netherlands, September 12 – 14.

[22] Seher-Weiß., S., Tischler, M.B., Scepanovic, J., and Gubbels, A.W. (2019a), "Bell 412 System Identification and Model Fidelity Assessment for Hover and Forward Flight," 8th Asian/Australian Rotorcraft Forum, Ankara, Turkey, Oct. 30 – Nov. 2.

[23] Seher-Weiß. S., Greiser, S. Wartmann, J., Myrand-Lapierre, V., Gubbels, A.W., Ricciardi, J., and Hui, K. (2019b), "Bell 412 System Identification: Comparing Methods and Tools," Vertical Flight Society 75th Annual Forum and Display, Philadelphia, PA, May 13 – 16.

[24] Ballin, M.G., and Dalang-Secre'tan, M.A. (1991), "Validation of the Dynamic Response of a Blade-Element UH-60 Simulation Model in Hovering Flight," Journal of the American Helicopter Society, Vol. 36, No. 4, pp. 77-88.

[25] Chaimovich, M., Rosen A., Rand, O. Mansur, M.H. and Tischler, M.B. (1992), "Investigation of the Flight Mechanics Simulation of a Hovering Helicopter," AHS, 48th Annual Forum, Washington, June 3 – 5.

[26] Tischler, M.B., Driscoll, J.T., Cauffman, M.G., and Freedman, C.J. (1994), "Study of Bearingless Main Rotor Dynamics from Frequency-Response Wind Tunnel Test Data," Aeromechanics Specialists Conference on Aerodynamics, Acoustics and Dynamics, San Francisco, CA.

[27] Harding, J.W., and Bass, S.M. (1990), "Validation of a Flight Simulation Model of the AH-64 Apache Attack Helicopter Against Flight Test Data," AHS, Annual Forum, 46th, Washington May 21 – 23.

[28] Zhao, J. (2005), Dynamic Wake Distortion Model for Helicopter Maneuvering Flight, PhD Thesis, Georgia Institute of Technology.

[29] Eshow, M.M., Orlandi, D., Bonaita, G., and Barbieri, S. (1988), "Results of an A109 Simulation Validation and Handling Qualities Study", 14th European Rotorcraft Forum, Milan, 20 – 23 September.

[30] Rosen, A., and Isser, A. (1995), "A New Model of Rotor Dynamics During Pitch and Roll of a Hovering Helicopter," Journal of the American Helicopter Society, Vol. 40, No. 3, pp. 17-28.

[31] Bagai, A.J., Leishman, G., and Park, J. (1999), "Aerodynamic Analysis of a Helicopter in Steady Maneuvering Flight Using a Free-Vortex Rotor Wake Model," Journal of the American Helicopter Society, Vol. 44, No.2, pp109-120.

[32] Bhagwat, M.J., and Leishman, G.J. (2003), "Rotor Aerodynamics During Maneuvering Flight Using a Time-Accurate Free-Vortex Wake," Journal of the American Helicopter Society, Vol. 48, No. 3, pp. 143-158.

[33] Mansur, M.H., and Tischler, M.B. (1998), "An Empirical Correction for Improving Off-Axes Response in Flight Mechanics Helicopter Models," Journal of the American Helicopter Society, Vol. 43, No. 2 pp. 94-102.

[34] Tischler, M.B. (1999), "Identification of Bearingless Main Rotor Dynamic Characteristics from Frequency-Response Wind-Tunnel Test Data," Journal of the American Helicopter Society, Vol. 44, No. 1, pp. 63-76.

[35] Theodore, C., and Celi, R. (2002), "Helicopter Flight Dynamic Simulation with Refined Aerodynamics and Flexible Blade Modeling," Journal of Aircraft, Vol. 39, No. 4, pp. 577-586.

[36] Zhao, J., Prasad, J.V.R., and Peters, D.A. (2004), "Validation of a Rotor Dynamic Wake Distortion Model for Helicopter Maneuvering Flight Simulation," American Helicopter Society 60th Annual Forum Proceedings, Baltimore, Maryland.

[37] Aerotim Engineering, www.aerotim.com.tr (Accessed October 2020).

[38] Chowdhary, G., Concurrent Learning for Convergence in Adaptive Control Without Persistency of Excitation, PhD. Thesis, Georgia Institute of Technology, 2010.

[39] Chowdhary, G., Yucelen, T., Muhlegg, M., Johnson, E.N., "Concurrent Learning Adaptive Control of Linear Systems with Exponentially Convergent Bounds," International Journal of Adaptive Control and Signal Processing, Vol. 27, No. 4, April 2013, pp. 280-301.

Chapter 7.4 – CASE STUDIES OF REDUCED ORDER MODELS AND PHYSICS-BASED CORRECTION METHOD

ABSTRACT

This section presents the model fidelity improvement and assessment case studies that apply the Reduced Order Models (ROM) and physics-based correction methods. A detailed method description can be found in Tischler et al. [1], Chapter 5.4. This section presents the case study results and discussion. The aircraft selected for the case studies include the UH-60, CH-47, AW109, and X2TD.

7.4.1 UH-60 Case Study

An engineering simulation model developed by Sikorsky [2], [3], is used for the UH-60 helicopter case study. FLIGHTLAB® well satisfies all the technical requirements for rotorcraft modeling and was therefore selected for model development. To investigate the rotor wake distortion effect for the off-axis response in maneuvering flight, two variant simulation models are utilized. One adopts the augmented dynamic inflow model [4] as integrated with the NASA version of GenHel [5] and the other uses a VPM-derived finite state wake model [6] as integrated with a FLIGHTLAB UH-60 blade element simulation model.

7.4.1.1 Baseline Model

The simulation model developed consists of several major subsystems: main rotor, tail rotor, fuselage, empennage, landing gear, flight control system, and propulsion system. Both the main and tail rotors were modeled using a blade element formulation in FLIGHTLAB. In a blade element approach, each blade is divided into multiple segments, and local segment airflow details are used to compute unsteady airloads using airfoil table lookups plus unsteady, stall delay, and yawed flow enhanced modeling. The 3D unsteady rotor induced inflow is considered using the Peters-He finite state dynamic wake model [7] and the rotor interference modeling uses the extended Peters-He finite state model [8]. Engineering data available from the aircraft manufacturer were used for generating the baseline UH-60 simulation [2], [3].

The simulation results were correlated with a broad range of flight-test data from both trim and control response tests. The trim tests included hover (both in- and out-of-ground effect), lateral and longitudinal low-speed flight, level flight, vertical climb, forward climb and descent, and autorotation. The dynamic response tests included longitudinal, lateral, collective, and pedal step and doublet control response tests in both hover and cruise. Detailed descriptions of the flight-test data can be found in Zhang et al. [2] and Xin et al. [3]. With an accurate and complete data set and appropriate selection of modeling parameters, the baseline model correlates well with the flight-test data in most of the test cases, including the trim sweeps in hover and level flight, as well as the on-axis control responses in hover and cruise speed.

7.4.1.2 Model Improvement with Rotor Ground Effect Correction

Discrepancies

Previous research indicates that at small heights above ground, the main rotor power and collective position can increase rather than decrease when entering low-speed flight from hover [2], [3]. For the UH-60 helicopter, this occurs in both rearward flight and sideward flight to the left. With the default ground effect model and constant coefficients, the baseline model is unable to capture the asymmetric increase in collective and power at specific speeds.

Physical Phenomenon

When the helicopter enters low-speed flight from hover at a low height above ground, the rotor is entering the ground vortex at certain speeds, which increases the inflow experienced by the rotor, which in turn increases the power and collective required. This effect is not symmetrical depending on the Tip Path Plane (TPP) angle relative to the ground plane. For the UH-60 helicopter, the tip path plane tilts more flying rearward than flying forward. In sideward flight, the tip path plane tilts more flying to the left than flying to the right. The asymmetric tilt of TPP results in different rotor wake skew, which, in turn, impacts the ground effect on rotor performance and control.

Corrections and Improvements

Most flight dynamics simulation models use a semi-empirical ground effect model to reduce the mean induced velocity as a function of the height above the ground and airspeed. The model improvement results are shown in the final report. With the varying coefficient ground effect model, the predicted rotor power shows the initial increase in the rearward flight and in the flight to the left as seen in the test data. The correlation of the collective stick position compared with test data is also improved to satisfactory level in both longitudinal and lateral flights. The improvement is also reflected in J cost function as listed in the figure caption where the first J value in the brackets is for the left plot (main rotor power), while the 2nd number in the brackets is for the right plot (collective stick position). The large difference between the J values of the left and right plots are due to the difference in units.

7.4.1.3 Model Improvement with Rotor Interference Correction

Discrepancies

In low-speed longitudinal flight, the baseline model is not able to accurately predict the pitch attitude and longitudinal control variation with respect to the forward/rearward speed, Although the model predicts a brief increase in the pitch attitude at a low forward speed, the magnitude of the attitude peak and the corresponding speed disagree with the flight-test data. A similar discrepancy is seen in the variation of the longitudinal control position.

Physical Phenomenon

The brief increase in pitch attitude is due to the main rotor wake impingement on the horizontal stabilator, which has a significant impact on the force moment balance (and resulting attitude change) at this condition. The potential flow-based rotor interference model with rigid wake assumption is unable to accurately predict the wake geometry and strength, which introduces errors in the velocities and airloads of the horizontal stabilator.

Corrections and Improvement

For typical rotorcraft, the rotor wake experiences a roll-up as the airspeed increases. An effective wake skew angle, χ_e, can be used to capture the roll-up effect on the wake geometry. A viscous decay factor can be used to reduce the off-rotor induced velocity magnitude due to the air viscosity. The effective wake skew angle has a large impact on the rotor interference especially during low-speed flight. The adjustment of the effective wake skew angle and the viscous decay factor improves the prediction of the rotor wake interference on the horizontal stabilator. A customized effective wake skew angle map was developed to accurately capture the speed condition and the magnitude of the wake impingement on the stabilator. Details can be found in Zhang et al. [2]. The effective wake skew angle adjustment significantly improves both the pitch attitude and longitudinal control variation compared with the flight-test data.

7.4.1.4 Model Improvement with Fuselage Interference Correction

Discrepancies

Compared to the flight-test data, the baseline model predicted more right pedal position in forward descent. The baseline model also predicted a more nose-down pitch attitude than the test data in forward descent.

Physical Phenomenon

When the helicopter is operating at a high angle of attack condition such as in a high-rate forward descent or an autorotation, the flow separates behind the fuselage and the shed vortices interact with the empennage. When the vertical fin is impacted by the strong unsteady vortices shed from the fuselage, its effectiveness is significantly reduced [9]. This phenomenon of reduced tail surface effectiveness at high AoA has been observed in fixed-wing aircraft flight test [10]. Also, when the flow separates behind the fuselage at high angles of attack, the fuselage wake could induce a strong downwash at the horizontal stabilator, which tends to increase the pitch attitude angle.

Corrections and Improvement

Although the fuselage vortex is not explicitly modeled, a similar impact on the vertical fin can be approximately modeled as a reduction in dynamic pressure. The dynamic pressure reduction factor at the vertical fin due to the fuselage was increased around the fuselage AoA of 25 degrees. It is smoothly transitioned to the baseline value at low and high AoA to localize the impact. The dynamic pressure reduction effect is smoothly phased out as the sideslip angle increases and the vertical fin is eventually cleared of the fuselage wake. The fuselage downwash velocities at the left and right sides of the stabilator were also increased around 25 degrees fuselage AoA. It is transitioned to the baseline value at low and high AoA to localize the impact. An adjustment of the fuselage interference on the vertical fin improves the model-data correlation of the pedal position in both forward descent and autorotation.

7.4.1.5 Model Improvement with Fuselage Aerodynamic Drag Correction

Discrepancies

In high-rate forward descent, the baseline model predicted higher collective position and higher rotor power as compared with the test data. In autorotation, the baseline model underpredicts the rate of descent in the low airspeed range and overpredicts the rate of descent in the high airspeed range.

Physical Phenomenon

At high rates of descent and in autorotation, the fuselage is operating at a high Angle of Attack (AoA). In these conditions, flow separation occurs at the fuselage, causing the fuselage drag to become unsteady and vary nonlinearly. The fuselage drag data was based on wind-tunnel test results that were obtained in a low AoA range and at 90-deg AoA. A curve fitting was applied in between low and high AoA, causing uncertainties in the fuselage drag data in the mid to high AoA range.

Corrections and Improvement

Based on the analysis of the model-data discrepancy in high-rate descent and autorotation, the fuselage drag coefficient was slightly reduced in the mid to high AoA range where the wind-tunnel data was unavailable. To localize the impact, the drag coefficient is smoothly transitioned to the baseline value at both low AoA and 90-deg AoA. Further details can be found in Xin et al. [3].

The enhanced model correlates better with the test data than the baseline, especially at high descent rates. These improvements are due to the adjustment in fuselage drag at high AoA. The final report shows the autorotation rate of descent with respect to varying airspeed. The enhanced model correlates better with the test data than the baseline model over the entire airspeed range. The improvement at high speed is related to the pitch attitude improvement as shown in the final report. The improvement at low speed is attributed to the adjustment in fuselage drag at high angle of attack.

7.4.1.6 Off-Axis Response Due to Rotor Wake Distortion in Maneuvering Flight

Discrepancies

It was not well understood for a while why the baseline simulation predicted the opposite off-axis response compared to flight-test data for a single main rotor helicopter. The erroneous off-axis response prediction was seen in the roll response due to pitch control and pitch response due to roll control, mainly seen in hover or at low-speed flight.

Physical Phenomenon

Rotor wake variation in maneuvering flight exhibits a dynamic wake distortion due to rotor tip path plane rotation, which results in a remarkable wake curvature, and in turn, rotor inflow variation that conventional rotor inflow models do not capture.

Corrections

Correction methods address the problem by enhancing the baseline dynamic inflow [7], [11], models with additional terms as shown in Tischler et al. [1], Chapter 5.4 (Equations 5.4.3.1.1-1 and 5.4.3.1.2-1) to account for the effect of curved wake on the rotor induced flow distribution during a rotor pitch/roll maneuver [4], [6].

The dynamic distortion of rotor wake during the maneuver was confirmed using a physics-based viscous Vortex Particle Method (VPM) simulation [6], and an alternate approach was pursued to extract a reduced order inflow dynamics model from the physics-based VPM simulation using CIFER®, a model parameter identification tool [12]. In this approach, both L- and M-matrix elements used in the Peters-He inflow model [7] are replaced with the VPM-extracted parameters. In addition, the rotor wake distortion effect is also extracted from the VPM rotor wake simulation and used to augment the Peters-He baseline equation with an added inflow forcing term as shown in Tischler et al. [1], Chapter 5.4 (Equation 5.4.3.1.2-1).

Improvement

The improved off-axis time response of the UH-60 helicopter in hover is documented in the final report. As shown there, the baseline model without the wake distortion effect predicted the off-axis (pitch due to lateral doublet) response in the opposite direction as compared to the measured data. The mismatch of the off-axis responses is corrected with the added wake distortion effect without significantly impacting the on-axis response. The impact of wake distortion effect correction parameter (KRe as listed in Tischler et al. [1], Equation 5.4.3.1.1-1) is also studied. As investigated, while the theoretical value of KRe of 1 captures the correct phase of the off-axis response, a KRe of 3.8 is needed in order to match both the phase and magnitude of the off-axis response with the flight-test data. Using the VPM-derived dynamic inflow model with wake distortion effect, the on-axis pitch response shows improved prediction as compared to the baseline Peters-He model as seen from the frequency-response mismatch cost (VPM: 73.4 vs Peters-He: 92.1), which is a measure of the prediction error relative to the measured data. The lower the cost value, the smaller the prediction error is, and in general any value less than 100 indicates a good match [12]. More importantly, the off-axis phase response was correctly predicted by the VPM-derived inflow model. Similar improvement can be seen for the frequency response of both on- and off-axis to lateral control.

7.4.2 CH-47 Case Study

7.4.2.1 CH-47 Simulation Handling Qualities Fidelity Improvement by Physics-Inspired Modeling of Rotor-on-Rotor Dynamic Inflow Interactions

This case study applies the simulation model fidelity improvement method of implementing reduced order models and physics-based corrections to improve handling qualities fidelity of the Boeing CH-47D Chinook flight simulator. The Georgia Institute of Technology and The Boeing Company collaborated to document this case study. Both semi-empirical physics-inspired model corrections, developed by Boeing, and theoretically rigorous model corrections, developed by Georgia Tech, are implemented.

The physics-inspired semi-empirical modeling of rotor-on-rotor dynamic inflow interactions developed by Boeing is referred to as the Boeing Helicopters Simulation Inflow Modeling Method (BHSimIMM). Georgia Tech developed a theoretically rigorous physics-based Pressure Potential Superposition Inflow Model (PPSIM) to account for dynamic rotor-on-rotor interference effects in tandem rotor helicopters. Tandem rotor unique reduced order dynamic inflow models are identified from the full order PPSIM theory and implemented in the Boeing Helicopters Simulation (BHSIM) flight simulation model.

Baseline Model: Boeing Helicopters Simulation (BHSIM) Math Model

As depicted in Figure 7.4-1, BHSIM is a physics-based, nonlinear, full flight envelope, 6-DOF simulation math model. BHSIM is a generic model capable of simulating all types of tandem rotor helicopters. Blade element rotor models are implemented on both rotor heads that represent the nonlinear and coupled flap and lag motion of each individual rotor blade. Rotor dynamic inflow, rotor-on-rotor interference between zeroth harmonic rotor dynamic inflow states, and drive system dynamic coupling are also represented in the BHSIM math model. High fidelity representations of the Chinook's mechanical and hydraulic flight control systems and Automatic Flight Control System (AFCS) are included in the baseline simulation model.

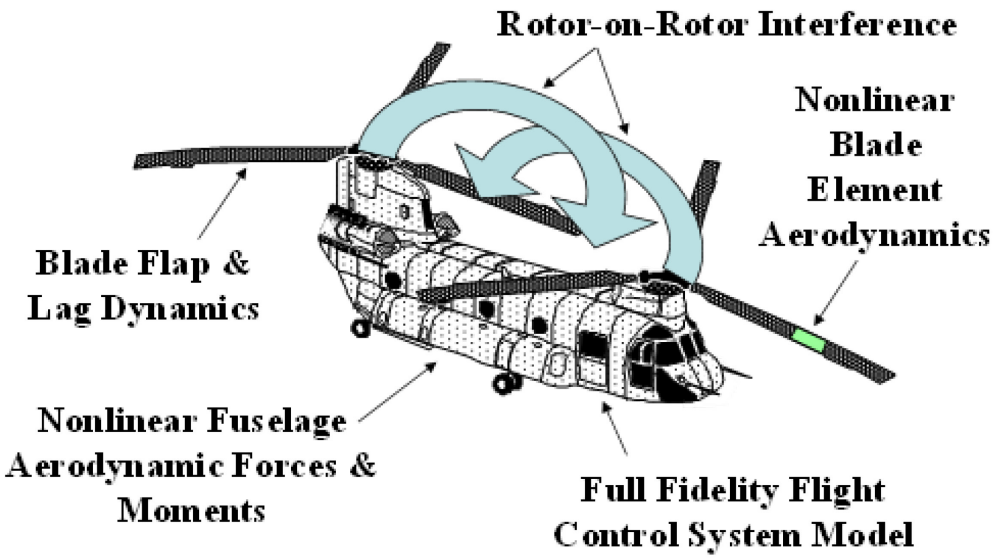

Figure 7.4-1: Boeing Helicopters Simulation (BHSIM) Math Model.

Discrepancies

In this case study, the primary simulation fidelity issue addressed is that test pilots found the hover and low speed lateral axis handling qualities of the Boeing CH-47D Chinook simulator to be degraded with respect to the actual aircraft. Test pilots observed that lateral axis handling qualities were particularly unrealistic in the simulator when the Automatic Flight Control System (AFCS) was selected OFF (AFCS-OFF). Test pilots also noted that lateral axis workload and control response phase loss were exaggerated unrealistically in the simulator when performing ADS-33E Mission Task Elements (MTEs) in the Chinook simulator with the AFCS selected ON (AFCS-ON). Test pilots commented that aircraft roll attitude and roll rate responses in the simulator seemed significantly more out of phase with lateral stick inputs than in the actual Chinook helicopter.

Physical Phenomenon

The influence of cyclic inflow dynamics on total vehicle and control characteristics, and in particular aircraft pitch and roll rate damping stability derivatives, has been well understood since the 1970s when Professor Howard C. 'Pat' Curtiss documented analytical and experimental investigations of the handling qualities of hingeless and bearingless rotor configurations and developed a quasi-static approximation of the effects of rotor first harmonic induced inflow on helicopter control response and angular rate damping known as the 'reduced Lock number' approximation [13], [14]. The reduced Lock number approximation made it clear that first harmonic induced inflow dynamics have a strong effect on helicopter handling qualities in low-speed flight and that neglecting or underestimating the sensitivity of cyclic inflow skew to rotor aerodynamic hub moments can result in overly pessimistic predictions of lateral and longitudinal axis control response bandwidth and rate damping.

Figure 7.4-2 and Figure 7.4-3 illustrate the unique physics and aerodynamics of the tandem rotor configuration that occur when the aircraft undergoes a roll rate perturbation. Rotor-on-rotor interference effects in tandem rotor helicopters increase the influence of rotor aerodynamic hub pitching moments on lateral cyclic first harmonic induced inflow skew well beyond isolated rotor values such as those predicted by Pitt and Peters dynamic inflow theory.

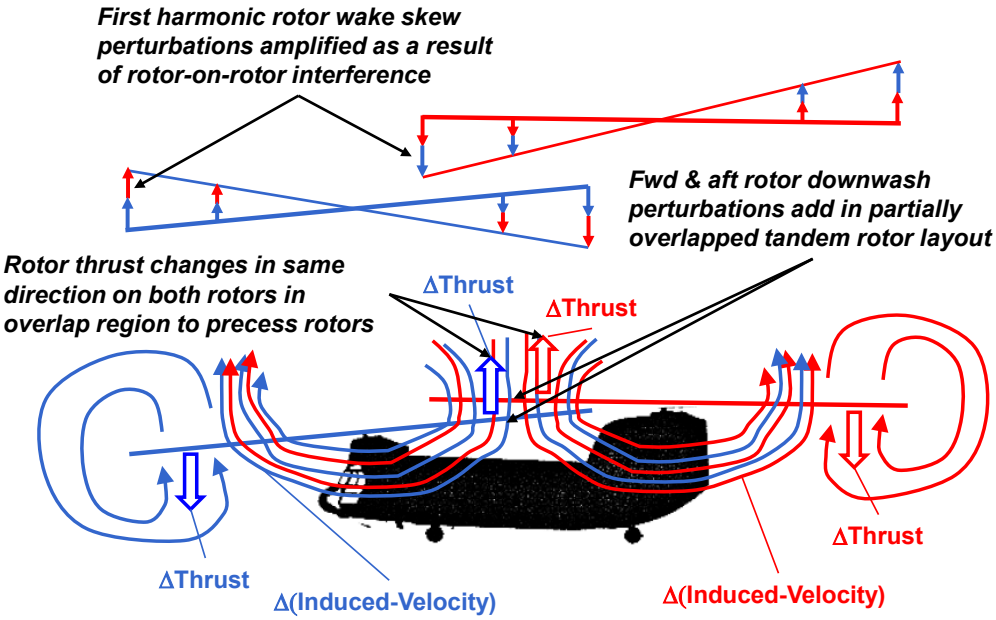

Figure 7.4-2: Tandem Rotor Pitching Moment and Physics-Inspired Notional Downwash Pattern During Steady Left Roll Rate Perturbation.

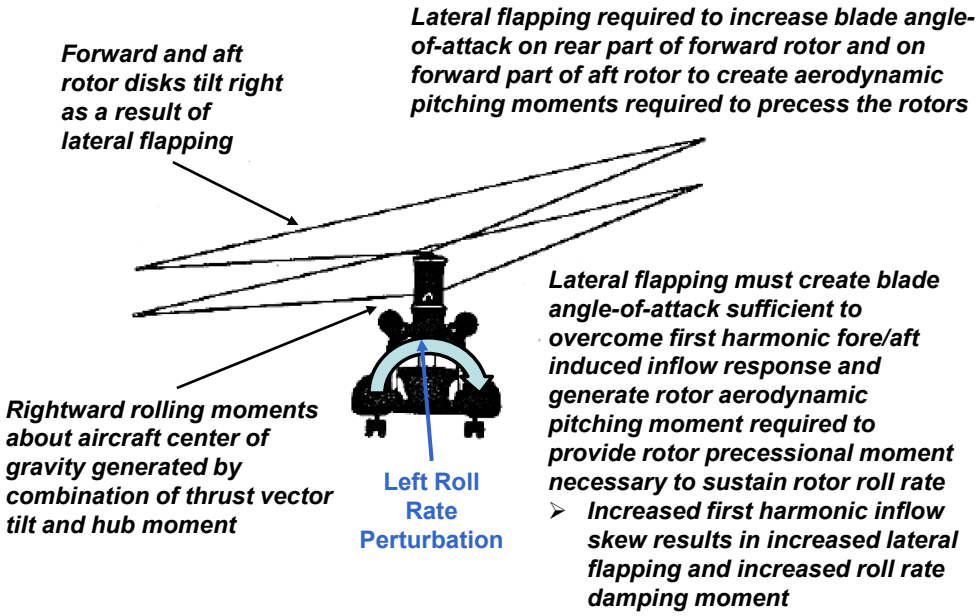

Figure 7.4-3: Tandem Rotor Helicopter Lateral Flapping and Aircraft Rolling Moment During Steady Left Roll Rate Perturbation.

Corrections and Quantitative Improvements

Table 7.4-1 tabulates values of the Model/Flight Data Mismatch Frequency-Domain Integrated Cost Function quantifying the mismatch between flight test and simulation model frequency responses. The semi-empirical Improved BHSIM and BHSIM PPSIM tandem rotor inflow models improve the mismatch cost function metric by 80.6% and 80.4% respectively, while the BHSIM isolated rotor Pitt-Peters model configuration improves the metric by only 29.8% over the original BHSIM simulation configuration with no rotor hub moment induced cyclic inflow effects. Conforming within the MUAD error bound envelopes, as shown in Figure 7.4-4, and comparison of flight test and model ADS-33E handling qualities specification bandwidth and phase delay parameters, as shown in Figure 7.4-5, indicate that the improved BHSIM simulation semi-empirical and PPSIM inflow model configurations provide a realistic representation of the AFCS-OFF handling qualities of the actual CH-47D helicopter.

Table 7.4-1: Model/Flight Data Mismatch Frequency-Domain Integrated Cost Function Metric Values for Roll Attitude to Lateral Control Position Frequency Response, CH-47D, 41,850 lb Gross Weight, Hover, AFCS-OFF.

#	Simulation Inflow Model Configuration	Model/Flight Data Mismatch Frequency-Domain Integrated Cost Function Metric	Reduction (Improvement) in Cost Function Metric Relative to Original Simulation (%)
1	BHSIM, Original	1211.2	0.0
2	BHSIM, Improved	234.5	80.6
3	BHSIM, Pitt-Peters	850.0	29.8
4	BHSIM, PPSIM	237.7	80.4

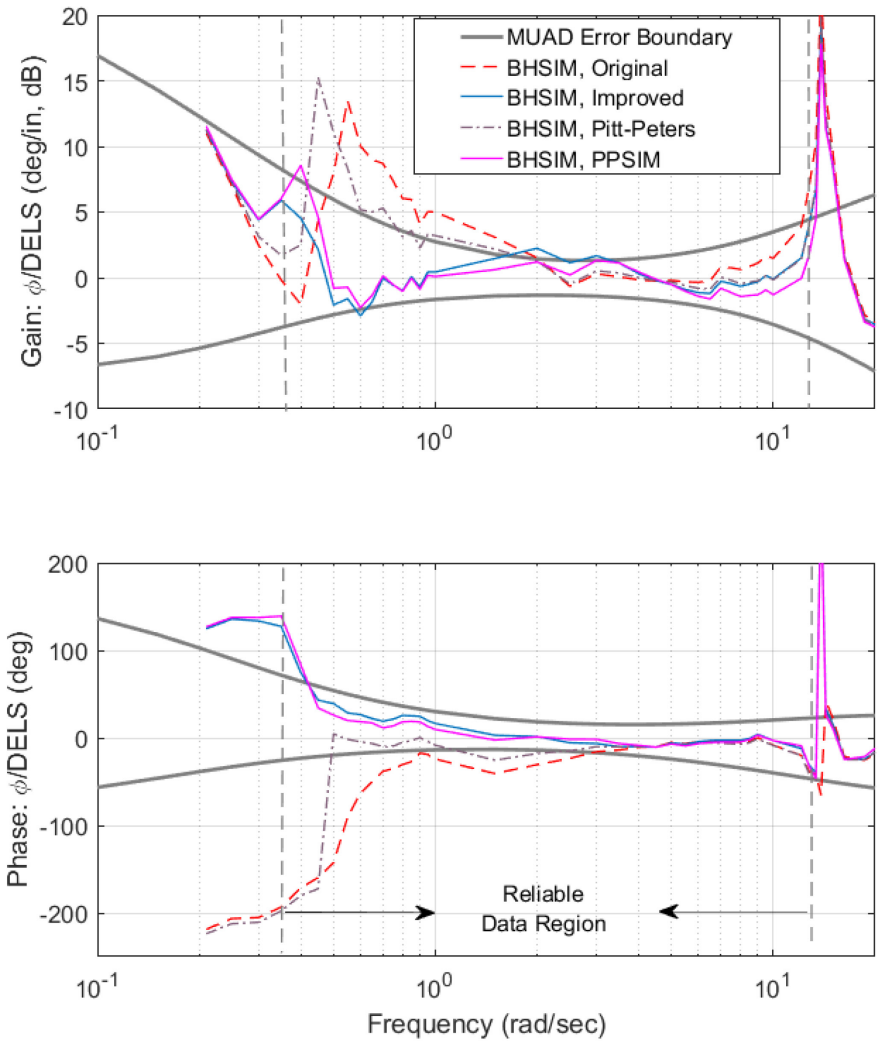

Figure 7.4-4: Maximum Unnoticeable Additional Dynamics (MUAD) Error Bound Envelopes for Roll Attitude to Lateral Control Position Frequency Response, CH-47D, 41,850 lb Gross Weight, Hover, AFCS-OFF.

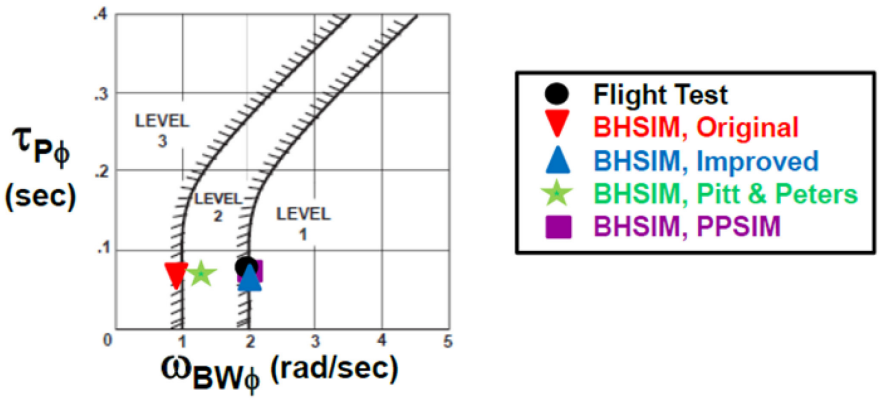

Figure 7.4-5: ADS-33E Lateral Axis Bandwidth and Phase Delay Parameters, Usable Cue Environment (UCE) > 1 and or Divided Attention Operations, CH-47D, 41,850 lb Gross Weight, Hover, AFCS-OFF.

7.4.2.2 Rotor Mutual Interference Models

For the tandem rotorcraft configuration, rotor interference effects play a significant role in the dynamics due to overlapping rotors and changes in wake strength and geometry at different airspeeds. The most pronounced effect is on the longitudinal static stability, which undergoes a sign reversal between the hover/low speed regime and forward flight (typically at about 40 kn) [15]. As speed increases below the sign reversal speed, induced flow from the front rotor reduces the effectiveness of the aft rotor, resulting in a stable longitudinal gradient. Above the sign reversal, the induced velocity of both rotors reduces along with the resultant interference effect on the aft rotor. Consequently, above the sign reversal speed, tandem rotor aircraft exhibit a longitudinal static instability.

The DTSG CH-47F FLIGHTLAB® model incorporates a finite state interference model, which utilizes empirical correction factors for effective wake skew and wake velocity decay, which must be established for a given rotor configuration. Wake skew and velocity decay influence the geometry and strength, respectively. These strongly affect the speed stability (Mu), as indicated in the trim gradient and low frequency hovering cubic mode. The baseline FLIGHTLAB model exhibited significant differences in the longitudinal trim gradient at low speed.

A consistent discrepancy was also present in the low frequency longitudinal dynamic response in hover. The break frequency associated with the speed stability mode was approximately 50% higher in the FLIGHTLAB model than in the flight-test data. Both the trim gradient and dynamic response mismatch are consistent with a higher value of speed stability (Mu), resulting from the influence of the front rotor interference on the aft rotor being over-predicted.

The uniform induced velocity decay (η_0) parameter was varied to adjust the wake strength, which influenced the longitudinal trim gradient throughout the entire speed range, effectively determining the magnitude of overall control variation. The forward flight regime is relatively insensitive to wake geometry (wake structure is fully rolled up with a skew angle close to 90°), meaning that the interference effects in this region are predominantly a function of wake strength. Consequently, the uniform induced velocity decay parameter was established by calibrating against the longitudinal trim data in forward flight. The effect of the wake velocity decay on the trim data was investigated. A value of $\eta_0 = 0.1$ was found to match the high-speed forward flight trim data very well. Also evident from the figure is the poor agreement of the trim data in low-speed flight, indicating that the wake strength alone is unable to account for the entire speed range in this case.

The wake geometry of the finite state interference model as implemented in FLIGHTLAB is achieved using an *effective wake skew*, which accounts for the curvature of the wake far from the rotor plane. The standard effective wake skew is implemented using a correction factor, f_x, as follows [8]:

$$\tan\chi_e = f_x \tan\chi \qquad \text{where } f_x = \frac{\pi^2}{4}$$

In order to reduce the amplitude of the model trim gradient in the low-speed range, the effect of the wake curvature must be delayed increasing the speed at which the front rotor interference on the aft rotor reaches a maximum. This corresponds to a more linear conversion from wake skew at the rotor plane to effective wake skew. The effective wake skew in the modified wake skew curve is considerably lower than the standard wake skew in the 0 – 60° range, delaying the point at which the wake begins to roll up. The right-hand portion of the figure presents the effective wake skew as a function of airspeed, which shows the delay of 10 – 15 kn in the modified wake skew relative to the standard values. The modified wake skew approach presented here is similar to results presented in previous studies [2].

The resultant trim and longitudinal frequency response comparisons are presented in the final report with the velocity decay and wake skew updates included. A significant improvement in model response is evident in both the trim and dynamic response data. As a result of the wake skew update, the cost function reduced from 293 to 141.

The wake skew update also influences the lateral axis response due to the changing structure in the rotor overlap region. The results of the lateral axis frequency-response comparison in hover, before and after the model update, can be found in the final report. The direction of the phase change at the low frequency hovering cubic mode is reversed after the model update, resulting from a small shift of the speed stability poles into the right half plane. Following the model update, the lateral axis frequency response is essentially an exact match ($J = 11$). The baseline and updated frequency-domain cost metrics are presented in Table 7.4-2 for the longitudinal and lateral axes.

Table 7.4-2: Frequency-Domain Cost Metrics for Baseline and Updated Model.

Axis	Baseline	Updated	Improvement (%)
Longitudinal	293	141	51.9
Lateral	26	11	57.7

Improvements observed in the longitudinal frequency response are also evident in the time domain from a comparison of the pitch rate response to a longitudinal doublet, before and after the model update. A 74% time-domain cost reduction was achieved as a result of the model update (the cost reduced from J_{rms}= 2.97 to $J_{\text{rms}} = 0.76$).

7.4.3 AW109 Trekker Case Study

This section presents some examples of physics-based model improvement applied to the AW109 Trekker helicopter. The first section focuses on aerodynamic interference modeling on tail planes, the second on turboshaft engine modeling, and the third on sensor and actuator modeling. The figures show the baseline model (red dashed line), updated model (blue line), and reference flight-test data (black markers). Trim data in level flight have been used for the aerodynamic interference case study and frequency sweeps for the turboshaft engine, sensor, and actuator modeling.

7.4.3.1 Aerodynamic Interference

The beneficial effect of using the VPM approach [16] over a non-empirically tuned Peters-He model is an improved prediction of the longitudinal cyclic position and pitch attitude for the AW109 Trekker helicopter in trimmed straight and level flight. It was found that the VPM model improves the correlation with flight-test data at all speeds but for the highest (possibly due to shortcomings for other components of the model) for both longitudinal stick position and aircraft pitch attitude.

7.4.3.2 Engine and Drivetrain Dynamics

This section presents an example application of the engine tuning process presented in Tischler et al. [1], Section 5.4.3.4. All the unknown parameters (transfer function gains, time delays, and constants) presented in that section will be tuned in order to match the behavior of the PW207C engine installed on the AW109 Trekker helicopter. Each of the three transfer functions are tuned separately by the using the proper frequency responses. Then, both the individual transfer functions and the whole system are validated in the time domain. To accomplish this, reference flight-test data are needed for both dynamics and static performance:

- Trim sweeps at different ambient conditions and/or fuel consumption vs power vector.
- Flight data from the identification campaign. In particular, pedal and collective sweeps and 3211's, with the acquisition at least of the following parameters:
  - Collective and pedal position;
  - Fuel flow;
  - Engine torque; and
  - Rotor speed (NR).

7.4.3.2.1 Tuning of Engine Parameters: Combustor and Torque Model

The engine torque response to fuel flow is represented with a transfer function as illustrated in Figure 7.4-6 which graphically reflects [1], Equation 5.4.3.4-1. The gain and time constant can be tuned by comparing the frequency response of this transfer function with the one computed with CIFER from flight data, via either collective or pedal sweeps (with preference for those with higher coherence).

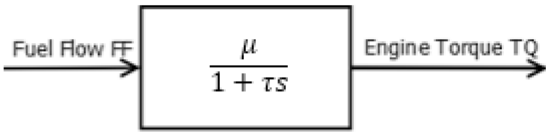

Figure 7.4-6: Fuel Flow to Engine Torque Transfer Function Model.

In Figure 7.4-6, μ corresponds to the static gain between torque and fuel flow and can be derived from static performance data (power vs fuel consumption). This can be checked against the frequency sweeps. Additionally, τ is the time constant of the fuel flow to engine torque dynamics, which can be tuned to match fuel flow to torque frequency responses computed with CIFER® from flight data. An example is presented in the final report that shows a comparison between the Fuel Flow (FF, in lb/hr) to torque (TQ, in %) model frequency response and that computed with CIFER from flight-test data for collective input in hover at Low weight and Low altitude (LL).

7.4.3.2.2 Tuning of Engine Parameters: Rotor Speed Governor

The Fuel Flow (FF) is the sum of the contribution due to the collective feed-forward and that of the rotor speed governor (Equations 5.4.3.4-2, 5.4.3.4-3, and 5.4.3.4-4 in Tischler et al. [1], Chapter 5.4).

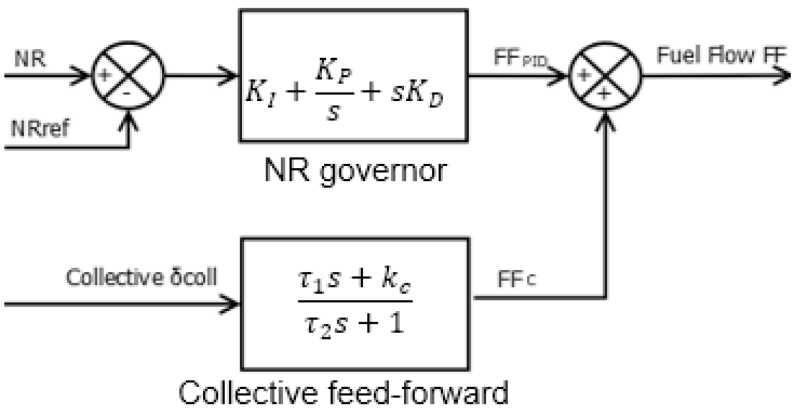

Figure 7.4-7: NR Error to Fuel Flow and Collective to Fuel Flow Transfer Function Models.

The NR governor parameters (K_I, K_P, K_D) can be tuned by comparing the frequency response of the model transfer function (PID) with NR to fuel flow frequency responses computed with CIFER using flight data from pedal sweeps. In fact, pedal sweeps are able to induce variations of NR and torque with the collective fixed. In this way, the contribution of the collective feed-forward is a constant, and the variations in Fuel Flow (FF) are affected only by variations of NR. An example is shown in the final report for comparison between the PID frequency response and the frequency response computed with CIFER in hover at Low weight and Low altitude (LL).

7.4.3.2.3 Tuning of Engine Parameters: Collective Feed-Forward

In order to tune the collective feed-forward block, the signal FF_C (fuel flow contribution due to the collective) is computed as ($FF - FF_{PID}$) where FF is the fuel flow measured during collective sweep performed in flight, and FF_{PID} is computed by simulation, using ($NR - NR_{Ref}$) measured in flight during the same collective sweep as the input to the PID block transfer function (previously validated).

The collective feed-forward parameters (τ_1, τ_2, k_c) can be tuned by comparing the frequency response of the describing transfer function with that of FF_C computed following the process described above. A first guess of k_c can be found by looking at flight data in trim conditions. An example is given in the final report that compares the collective feed-forward describing function with the frequency response computed with CIFER.

Notice that the decrease of the phase at high frequency is caused by a 0.2 seconds of transport delay, due to engine data acquisition system synchronization with the helicopter data set (see Tischler et al. [1], Section 7.4.3.2).

7.4.3.2.4 Drivetrain Modeling

Drivetrain is represented as a spring and inertia model calculated from the elastic and inertial properties of the helicopter drivetrain. Further discussion of the model can be found in Tischler et al. [1], Chapter 5.4.

7.4.3.2.5 Validation of the Engine Model in the Time Domain (Open-Loop)

The validation (open loop) in the time domain of the 'NR error to fuel flow' and 'collective to fuel flow models' involves comparing the main outputs of the engine model (TQ and FF) with flight-test data following inputs of NR and collective measured in flight. The simulated dynamic responses have been initialized with their values at the trim condition.

The fuel flow response result is documented in the final report that compares the fuel flow and torque predicted by the model with the flight-test data following NR and collective 3211 inputs measured in a collective 3211 maneuver. The final report also presents the comparison between the fuel flow and torque predicted by the model and the flight-test data following NR and collective inputs measured in a pedal 3211 maneuver.

7.4.3.2.6 Impact of the Engine Model on Closed-Loop Dynamics (FLIGHTLAB® Model)

To show the improvements produced by this turboshaft model with respect to an ideal engine (perfectly constant NR and infinite available power), The final report presents the frequency responses for yaw rate, rotor speed, engine torque, and body normal loads factor to collective control inputs, which illustrate the significant improvement of simulation using the turboshaft engine model rather than the ideal engine model. The improvement is also reflected in the reduction of the cost function *J* values as listed. The results of the frequency responses for rotor speed (NR), yaw rate, and engine torque, to pedal inputs can be found in the final report. Again, the significant improvement in frequency-response agreement of the model and flight data is reflected in the large reduction of the integrated cost function *J*.

7.4.4 X2TD Case Study

7.4.4.1 Baseline Model

Baseline models using the Sikorsky GenHel and HeliUM [17] simulations were compared with flight-test frequency-response data. Details of these models are discussed in Tischler et al. [1], Section 6.7, for the X2TD database. Both models include wake interference effects, but do not include wake distortion. Additional details on this update methodology are available in Juhasz et al. [18]. The comparisons of the bare-airframe responses in roll and pitch use the total commands for each axis being sent to the mixer. Overall, the HeliUM and GenHel models accurately predict the aircraft response over a broad frequency range.

7.4.4.2 Model Improvement with Inflow Model Identification

7.4.4.2.1 Discrepancies

While the responses align very well in pitch from 1 to 10 rad/sec, there is a small magnitude reduction in the predicted roll response in this frequency range. In roll, HeliUM predicts the hovering cubic in-line with flight data, while GenHel slightly under-predicts it. Both models correctly predict the mode to be unstable in both axes as seen by the positive phase shift at low frequency. Both math models over-predict the frequency of the rotor lead-lag mode at 12 rad/sec and place it closer to 20 rad/sec. This shift in lead-lag dynamics also impacts the prediction of the flapping mode around 30 rad/sec, most easily seen in the roll axis due to the lower inertia in that axis.

7.4.4.2.2 Physical Phenomenon

The baseline inflow models for the X2TD coaxial rotor system did not include wake distortion effects. Wake distortion is caused by a curvature of the rotor wake due to angular rates at the Tip Path Plane (TPP), which affects the airflow around the rotor disk. For an articulated rotor, wake distortion has the largest impact on the off-axis response [4], [19], [20]. For a hingeless rotor system, such as the X2TD, there is an impact in the on-axis response as well. These effects are modeled by adding analytically derived wake distortion factors, as was done in the GenHel case, or by using system identification to extract an inflow model including wake distortion, as was done for the HeliUM case. The next two sections discuss these two methods in more details.

7.4.4.2.3 GenHel Corrections and Improvements

As part of the State-Space GenHel development under the Sikorsky internal funding, the coaxial rotor mutual interference model has been improved by implementing a reduced order model for the wake distortion effect based on the formulation published in Zhao et al. [4]. A set of delta terms are introduced in the L-matrices for the rotor mutual interference. This results in an additional first harmonic rotor interference in response to the TPP angular rate. The model parameters are set to the values recommended in Zhao et al. [4]. As documented in the final report (Tischler et al. [1]), modeling of the wake distortion effect improves the GenHel correlation of the roll response with test data in the frequency range of anticipated improvement, between 1 and 10 rad/sec. Due to the relatively large pitch inertia of the aircraft, the wake distortion impact on the pitch response is minimal. In addition, with the wake distortion effect modeled, the phase variations of both roll and pitch responses at low frequency (< 1 rad/sec) now trend correctly when compared to the test data.

The wake distortion mainly affects the responses in hover and at low speed, and the impact reduces with increasing airspeed. At high speed, the wake distortion only shows a small impact on the roll response. The time-domain response to a roll doublet at 200 knots is slightly improved when the wake distortion effect is modeled.

7.4.4.2.4 HeliUM Corrections

The inflow model of Maryland Free Wake (MFW) was coupled with HeliUM to improve model correlation of the linear aircraft response when compared with frequency responses from flight-test data. A reduced order state-space model of the X2TD inflow dynamics in hover was first extracted from MFW using system identification techniques [12]. The form of the inflow model is based on the work by Keller [21] and is presented in Tischler et al. (2021), Chapter 5.4.3.1 in Equations 5.4.3.1.6-1 to 5.4.3.1.6-6. Additional details about the identification methodology and results can be found in Juhasz et al. [17].

7.4.4.2.5 Inflow Model Identification

The inflow model parameters were identified from MFW [17] using the CIFER® system identification tool [12]. As documented in the final report, the identified linear model is compared to the MFW frequency responses of the upper (λ_(0,U)) and lower (λ_(0,L)) rotor uniform inflow to upper rotor thrust inputs (C_(T,U)). The model aligns very well with the data over the entire frequency range used for identification, up to 20 rad/sec. Further, the model and response show the characteristic first order nature of classical dynamic inflow models. The identified output coupling parameters were identified as H_(UL,0) = 0.56 and H_(LU,0) = 1.07. These are similar in magnitude to the simple momentum theory derived values of 0.86 and 1.13, respectively [22], that were used in the original coaxial HeliUM inflow model.

The lateral cyclic inflow response of the lower ($\lambda_{s,L}$) and upper ($\lambda_{s,U}$) rotor to lower rotor rolling moment inputs ($C_{L,L}$) can be found in the final report. The identified model again very well captures the characteristics of the MFW response as shown by the low overall costs for the curves, as given in Juhasz et al. [18]. The curves show the higher-order behavior of the wake is well captured by the inflow model structure over a very broad frequency range. The identification results show that there is substantial coupling between the upper and lower rotor inflow through the output coupling matrix. The identified output coupling values for cyclic responses had averages of $H_{UL} = 0.17$ and $H_{LU} = 0.73$. The baseline HeliUM implementation of inflow coupling only included uniform inflow output coupling, so these influences were not captured and are likely a key source of the misalignment of the baseline model relative to flight data.

7.4.4.2.6 HeliUM Improvements

The identified X2TD dynamic inflow model was coupled into the HeliUM flight dynamics simulation code. Since the identified model is a perturbation model, the X2TD flight dynamics model was first trimmed with the MFW inflow with the trim values from MFW serving as the baseline inflow values for perturbation used in linearization. The resulting roll and pitch rate frequency responses to on-axis commanded inputs are presented in the final report. Comparisons are given for the updated model against the baseline model, flight data, and bounds of Maximum Unnoticeable Added Dynamics (MUAD). The updated model roll response shows a dramatic improvement in the mid-frequency range, between 1 rad/sec and 10 rad/sec, the most critical region for flight control design and piloted simulation. There is a shift in response magnitude by using the identified inflow model, which brings it into alignment with flight data. The updated model is within the MUAD bounds, meaning that pilots would not notice a difference in the modeled aircraft response compared with flight. The improvement is shown by the substantially reduced frequency-response mismatch cost, *J*, shown in Table 7.4-3, where the error is reduced from $J_{baseline} = 248$ to $J_{update} = 85$. The low frequency phugoid mode in the updated model is predicted to occur at lower frequency than for the baseline model.

The updated inflow model produces only a small effect on the pitch response. Both models track the flight data well and are generally within the MUAD bounds. Impact on the pitch axis is expected to be smaller than the roll axis primarily due to the much larger inertia in the pitch axis as compared to roll. As with the roll response, the longitudinal phugoid mode shifts to lower frequency in the updated model. This reduction in frequency leads to an increase in the mismatch between the model and flight data, which is captured in the cost increase shown in Table 7.4-3 but is still within the guideline ($J \leq 100$).

Table 7.4-3: Mismatch Cost Function Comparisons Between Baseline and Updated Models. Costs Calculated Between 1 Rad/Sec and 12 Rad/Sec.

Response	Baseline Model Cost, J	Updated Model Cost, J	Cost Change, ΔJ
p/δ_{lat}	248	85	-163
q/δ_{lon}	47	91	+44

7.4.4.2.7 Wake Distortion Comparisons

Wake distortion in traditional SMR helicopters has been extensively studied and applied to first-order Pitt-Peters type inflow models; see for example Zhao et al. [4], Keller [20], Tischler [23]. Inclusion of maneuvering wake distortion on an articulated rotor helicopter is required to correctly model the off-axis response. For the hingeless rotor system of the X2TD, there is also an impact in the on-axis response in both the GenHel model update and the HeliUM update. Table 7.4-4 compares the wake distortion analytical value for traditional SMR helicopters in hover [20] with two values obtained from system identification for coaxial rotors (the work herein using MFW and CHARM from Keller et al. [21] and from the GenHel update presented in this section). Both coaxial identification methods used the same higher-order model structure, from equivalent K_R is obtained by assuming the far wake dynamics are quasi-static and simplifying.

$$K_R = \frac{\Omega(K_{N_{avg}} + K_{F_{avg}})}{1 + 2K_{M_{avg}}} \tag{7.4-1}$$

The CHARM and MFW free-wake models give similar wake distortion values that are less than the analytically derived SMR value. All three coaxial values (CHARM, MFW, GenHel) are similar in magnitude.

Table 7.4-4: Comparisons of Wake Distortion, K_R, Constants for Coaxial Rotors from Various Identified Models.

Parameter Source	Parameter Value
Analytical SMR Value (Keller et al. (1998) [20])	1.5
CHARM Coax Sys ID (Keller et al. (2019) [21])	0.86
Present MFW Coaxial Sys ID (Juhasz et al. (2020) [18])	1.0
GenHel Coaxial Wake Distortion (Juhasz et al. (2020) [18])	0.95

7.4.5 References

[1] Tischler, M.B., White, M.D., Cameron, N., D'Agosto, S., Greiser, S., Gubbels, A., Guner, F., He, C., Horn, J., Hui., K., Jones, M., Juhasz, O., Lee, O., Lehmann, R., Miller, D., Myrand-Lapierre, V., Nadeau-Beaulieu, M., Nadell, S., Padfield, G., Pavel, M., Prasad, J., Ragazzi, A., Richard, S., Scepanovic, P., Seher-Weiß, S., Soong, J., Stroosma, O., Taghizad, A., Tobias, E., Xin, H., and Yavrucuk, I. (2021), "Rotorcraft Flight Simulation Model Fidelity Improvement and Assessment," NATO STO AVT-296 Technical Report.

[2] Zhang, C.; Xin, H. and Driscoll, J. (2017), "Development and Validation of an Engineering Simulation Model in FLIGHTLAB with Customized Modeling Enhancements," AHS 73rd Annual Forum, Fort Worth, Texas, May.

[3] Xin, H.; Zhang, C. and Driscoll, J. (2019), "Enhancement of an Engineering Simulation Model to Improve the Correlation with Flight Test Data in Climb/Descent and Autorotations," AHS 75th Annual Forum, Philadelphia, PA, May.

[4] Zhao, J., Prasad, J.V.R., and Peters, D.A. (2004), "Rotor Dynamic Wake Distortion Model for Helicopter Maneuvering Flight," *Journal of the American Helicopter Society*, Vol. 49, No. 4, October, pp. 414-424.

[5] Howlett, J. (1981a), "UH-60A Black Hawk Engineering Simulation Program: Volume I – Mathematical Model," NASA CR- 166309, December.

[6] He, C.; Gladfelter, M.; Chang, C. Tischler, M.B.; and Juhasz, O. (2019), "VPM-Derived State Space Inflow Model for Multi-Rotor Air Vehicle Modeling and Simulation," VFS 75th.Annual Forum, Philadelphia, PA, May.

[7] Peters, D.A. and He, C. (1991), "Correlation of Measured Induced Velocities with a Finite State Wake Model," Journal of American Helicopter Society, Vol. 37, No. 3, Jul.

[8] He, C., Xin, H., Bhagwat, M. (2004), "Advanced Rotor Wake Interference Modeling for Multiple Aircraft Shipboard Landing Simulation," AHS 59th Annual Forum, Baltimore, MD.

[9] Nelson, R. (1989), Flight Stability and Automatic Control, McGraw-Hill.

[10] Napolitano, M.R., and Spagnuolo, J.M. (1993), "Determination of the Stability and Control Derivatives of the NASA F/A-18 HARV Using Flight Data," Technical Report NASA CR-194838, NASA Dryden Flight Research Facility.

[11] Pitt, D. and Peters, D.A. (1981), "Dynamic Inflow for Practical Applications," *Vertica*, Vol. 5, No. 1.

[12] Tischler, M.B., and Remple, R.K. (2012), *Aircraft and Rotorcraft System Identification: Engineering Methods with Flight Test Examples*, AIAA, Second Edition, Reston, VA, 2012.

[13] Quackenbush, T.R., and McKillip, R.M., Jr. (2013), "The Technical Legacy of Prof. Howard C. 'Pat' Curtiss, Jr.," AHS 69th Annual Forum, Phoenix, Arizona, May 2013.

[14] Curtiss, H., Jr. and McKillip, R.M., Jr. (1990), "Coupled Rotor-Body Equations of Motion in Hover Flight," NASA-CR-186710.

[15] Bramwell, A.R.S. (1961), "The Longitudinal Stability and Control of the Tandem-Rotor Helicopter," Ministry of Aviation, R & M No. 3223.

[16] He, C. and Zhao, J. (2009), "Modeling Rotor Wake Dynamics with Viscous Vortex Particle Method," *AIAA Journal*, Vol. 47, No. 4, April 2009.

[17] Juhasz, O., Celi, R., Ivler, C.M., Tischler, M.B., and Berger, T. (2012), "Flight Dynamic Simulation Modeling of Large Flexible Tiltrotor Aircraft," American Helicopter Society 68th Annual Forum, FortWorth, TX, May 2012.

[18] Juhasz, O., Xin, H., and Tischler, M.B. (2020), "Inflow Based Flight Dynamics Modeling Improvements for the Sikorsky X2 Technology™ Demonstrator," VFS 76th Annual Forum, Virginia Beach, VA, Oct.

[19] Rosen, A. and Isser, M. (1994), "A New Model of Rotor Dynamics During Pitch and Roll of a Hovering Helicopter," AHS 49th Annual Forum, Washington, D.C., May.

[20] Keller, J.D., and Curtiss, H.C. (1998), "A Critical Examination of the Methods to Improve the Off-Axis Response Prediction of Helicopters," AHS 54th Annual Forum, Washington D.C., May.

[21] Keller, J., McKillip, R., Wachspress, D., Tischler, M.B., and Juhasz, O, (2019), "Linear Inflow and Interference Models from High Fidelity Free Wake Analysis for Modern Rotorcraft Configurations," AHS 75th Annual Forum, Philadelphia, PA, May.

[22] Juhasz, O., Syal, M., Celi, R., Khromov, V, Rand, O., Ruzicka, G.C., and Strawn, R.C. (2014), "Comparison of Three Coaxial Aerodynamic Prediction Methods Including Validation with Model Test Data", *Journal of the American Helicopter Society*, Vol.59, (3), July 2014.

[23] Tischler, M.B. (1999), "Identification of Bearingless Main Rotor Dynamic Characteristics from Frequency-Response Wind-Tunnel Test Data," *Journal of the American Helicopter Society*, Vol. 44, No. 1, pp. 63-76.

Chapter 7.5 – SIMULATION MODEL PARAMETER ADJUSTMENT

ABSTRACT

This section describes in details case studies investigating model fidelity updates via direct updates to the input parameters of physics-based simulation models. The investigations focus on input parameters that are uncertain and that have known correlation with the observed discrepancies between the models and flight-test data. Those methods can be applied to any physics-based simulation model and are illustrated with examples from the Bell 412 and CH-47 databases. Methodologies vary widely from comprehensive numerical optimizations of many input parameters to parametric studies of a just a few parameters. They can be used to improve fidelity of simulation models used for engineering research and training simulators.

7.5.1 Bell 412 ASRA

The case study in this section is based on the Bell 412 ASRA airborne research simulator [1]. The goal is to demonstrate the steps leading to a Level D physics-based model in hover using flight-test data and configuration data.

Details and results of the identified model in hover can be found in Seher-Weiß et al. [2]. The hover model was identified using the CIFER® frequency response method [3]. Currently, CAE uses a real-time nonlinear simulation platform called 'Object Oriented Blade Element Rotor Model' (OO-BERM) [4]. The OO-BERM is a flight mechanics simulation framework that allows users to compose multibody vehicle models of scalable fidelity at simulation load time using C++ compiled libraries.

For this study, a baseline OO-BERM is set up to simulate a medium twin-engine helicopter. Four rigid blades with flap and lag degrees of freedom are simulated. The anti-torque tail rotor is modeled as an actuator disc based on Bailey's equations [5]. Generic blade, fuselage, horizontal stabilizer, vertical fin, and blade coefficients are used. Using the data and measurement provided in the Bell 412 ASRA data package [1], several parameters are fixed in the simulation: main rotor configuration (diameter, mass of blade, and rotation speed) and flight control gearing (blade angles [deg] vs control inputs [%]). All aerodynamics surfaces and position are approximated using the provided drawings. Simplified flight control gearing model is used, and there is no delay between control input and blade deflection. Finally, the OO-BERM is set up to use a quasi-steady inflow model which includes three inflow states representing the average and the first harmonic induced velocities over the rotor plane in the hub-wind frame.

Using small perturbation finite differences, we calculated the stability and control derivatives for the baseline OO-BERM configuration. As can be seen in Table 7.5-1, control derivatives show relative errors > 10%. It should be noted that control derivatives $L_{\delta_{lat}}$, $L_{\delta_{lon}}$, and $M_{\delta_{lon}}$ have a lower magnitude value than the CIFER identified derivatives. This results in a baseline simulation being under-responsive to cyclic control inputs.

The first step of the OO-BERM model optimization process is to adjust well-established theoretical physical relationships of uncertain parameters of the main rotor to obtain correct control derivatives. Using the algorithm presented in Spira et al. [6], we treated the following rotor design parameters Φ as unknown in the optimization problem: swashplate phase angle offset $\Delta\theta_1$ [deg], rotor blade pitch-flap coupling angle δ_3 [deg] and flap hinge offset e_β [%]. The objective function J (Equation 7.5-1 and 7.5-2) to minimize is defined as a weighted sum of the squared normalized errors of on- and off-axis pitch and roll control derivatives as:

$$\Phi \equiv \left[\Delta\theta_1, \delta_3, e_\beta\right]$$

$$\min_{\Phi} J(\Phi) \ , J(\Phi) = \sum_{i=1}^{4} w_i \left(1 - \frac{g_i^M(\Phi)}{g_i^S}\right)^2 \tag{7.5-1}$$

subject to the physical constraints:

$$0^o \le \Delta\theta_1 \le 30^o$$

$$-30^o \le \delta_3 \le 0^o \tag{7.5-2}$$

$$0\% < e_\beta \le 20^o$$

where g_i^S are the identified control derivatives ($g_1^S = L_{\delta_{lon}}$, $g_2^S = L_{\delta_{lat}}$, $g_3^S = M_{\delta_{lon}}$, and $g_4^S = M_{\delta_{lat}}$) and w_i are weighting factors. The OO-BERM control derivatives $g_i^M(\Phi)$ are calculated using small control perturbation finite differences for pre-defined constrained combination of design variables Φ. The measured aeromechanical parameters and the updated (optimal) solution are presented in Table 7.5-2. The updated solution shows relatively close aeromechanical parameters compared to its associated measured value. Final calculated control derivatives results (controls in %) are presented in Table 7.5-1.

Table 7.5-1: CIFER Identified Rolling and Pitching Control Derivatives Compared with Baseline and Updated OO-BERM Calculated Derivatives for Hover Model.

Par	CIFER Value	Baseline OO-BERM	Rel. error [%]	Updated OO-BERM	Rel. error [%]
$\boldsymbol{L_{\delta_{lon}}}$	**.023**	**.0144**	**37.39**	**.021**	**8.70**
$\boldsymbol{L_{\delta_{lat}}}$	**.131**	**.1144**	**12.67**	**.129**	**1.53**
$L_{\delta_{col}}$	0^a	-.01	-	-.007	-
$L_{\delta_{ped}}$	-.017	-.01	41.18	-.01	41.18
$\boldsymbol{M_{\delta_{lon}}}$	**.032**	**.02856**	**10.75**	**.0323**	**0.94**
$\boldsymbol{M_{\delta_{lat}}}$	**.006**	**-.00208**	**134.67**	**-.0024**	**140**
$M_{\delta_{col}}$	0^a	-.0032	-	-.003	-
$M_{\delta_{ped}}$	0^a	.0003	-	.0003	-
τ_{lon}	.054	0	100	0	100
τ_{lat}	.068	0	100	0	100
τ_{lon}	.021	0	100	0	100
τ_{lon}	.084	0	100	0	100

(controls in %, bold used in objective function for aeromechanical parameters optimization)

Table 7.5-2: Measured Aeromechanical Parameters Optimal Solution.

	$\Delta\theta_1$[deg]	δ_3 [deg]	e_β[%]
Measured/Baseline	13	unknown/0	8
Optimal/Updated Solution	15.4	-7.3	10.3
Rel. error [%]	18.4	N/A	28.8

The updated aeromechanical parameters values found by optimization are consistent with what could be expected based on CAE empirical experience, namely

- Increasing the flap hinge offset e_β has the effect of increasing the on-axis control derivatives ($L_{\delta_{lat}}$ and $M_{\delta_{lon}}$) of the helicopter. Since the Baseline model had lower on-axis derivatives than what was identified by CIFER, it is to be expected that the optimal value of e_β has increased.
- Increasing the swashplate phase angle offset $\Delta\theta_1$ has the effect of increasing the off-axis control derivatives of the helicopter ($M_{\delta_{lat}}$ and $L_{\delta_{lon}}$). Since the baseline model had lower on-axis derivatives than what was identified by CIFER, it is to be expected that the optimal value of $\Delta\theta_1$ has increased.

The pitch-flap coupling δ_3 of the baseline model was assumed with an initial value of zero (Table 7.5-2), this parameter has some influence on all the control derivatives. Optimizing the pitch-flap coupling allowed the solution for the hinge offset and the phase angle offset to converge closer to their physical values. Any vehicle simulation model is an approximation based on a limited number of parameters; it is, therefore, normal that the solution for these parameters is not equal to their measured value.

During early experiments of the optimization, all weighting factor w_i were set to w_i=1, but a lower weight (w_4=0.2) was required to be assigned to $g_4^s(M_{\delta_{lat}})$ to prevent it from driving the other derivatives away from their optimal values. Table 7.5-1 shows that the relative errors are less than 9% for $L_{\delta_{lon}}$, $L_{\delta_{lat}}$, and $M_{\delta_{lon}}$, except for $M_{\delta_{lat}}$ (140%), which had been purposely de-weighted. From CIFER, it can be found that $M_{\delta_{lat}}$ has a higher CR (17.6%) and Insensitivity (4.8%) than the other control derivative. It seems that the final weighting factors w_i values are a close approximation of 1/CR, since the Cramer-Rao bound of $M_{\delta_{lat}}$ (CR = 17.6) is about 5 times higher than the other control derivatives ($L_{\delta_{lat}}$ (CR = 2.7), $L_{\delta_{lon}}$ (CR = 3.8), and $M_{\delta_{lon}}$ (CR = 2.5)). A good practice would be to use 1/CR as initial weighting factors w_i. Finally, magnitude of $M_{\delta_{lat}}$ is much lower than the other control derivatives (4 times lower than the corresponding coupling derivative $L_{\delta_{lon}}$), which means that it has much less impact on the dynamics of the B412 ASRA.

Validation is done in the frequency domain to compare on- and off-axis responses. Figure 7.5-1 and Figure 7.5-2 show frequency-domain comparisons of the Baseline/Updated OO-BERM models with the flight-test data and the identified hover model using CIFER. It should be noted that the stability derivatives are implemented in the OO-BERM for both the baseline and the updated model using body aerodynamic coefficients and interactional aero parameters.

As expected from the baseline OO-BERM calculated derivatives in Table 7.5-1, the frequency responses show different results compared to the flight-test data. This is expected as the significant control derivatives are lower ($L_{\delta_{lon}}$, $L_{\delta_{lat}}$ and $M_{\delta_{lon}}$). There is a difference between the baseline OO-BERM and the updated OO-BERM of approximatively -1 dB for p/δ_{lat}, q/δ_{lon} frequency responses, which is expected from Table 7.5-1 using average relative error of 12% ($20\log_{10}\left(\frac{1}{1.12}\right) \approx -1$). Also, there is difference between

the baseline OO-BERM and the updated OO-BERM of approximatively -3 dB for p/δ_{lon} , which is what is expected from Table 7.5-1 using relative error of 37% ($20\log_{10}\left(\frac{1}{1.37}\right) \approx -3$). q/δ_{lat} has a better match for the baseline OO-BERM, and this is consistent with the error still present for $M_{\delta_{lat}}$ in the updated model (Table 7.5-1).

Finally, the frequency-domain integrated cost metric J [2], [3] is also calculated for comparison purposes. The acceptable standard value for frequency-domain integrated cost metric model fidelity is $J_{ave} < 100$ [3]. It should be noted that J_{ave} is the average cost of all frequency responses. Table 7.5-3 shows the unique frequency-domain integrated cost of p/δ_{lat}, p/δ_{lon}, q/δ_{lat} and q/δ_{lon}. As expected from previous results, baseline OO-BERM results for on- ($J > 85$) and off-axis ($J > 320$) have higher frequency-domain integrated costs compared to the updated OO-BERM with the exception for q/δ_{lat}, which has a lower cost in the baseline OO-BERM ($J = 324.4$ vs $J = 518.7$). The relatively high cost ($J = 518.7$) of the updated model's off-axis pitch response would appear to indicate a poor match between the model and the flight data. However, as mentioned previously, an error in $M_{\delta_{lat}}$ may not have a significant impact on the overall dynamics of the helicopter. This means that the parameters $\Delta\theta_1, \delta_3$ and e_β were not sufficient to match all the control derivatives, and adjustment of another design variable affecting $M_{\delta_{lat}}$would be required. Time-domain validation results presented in Tischler et al. [7], Section 7.3.2, show this behavior.

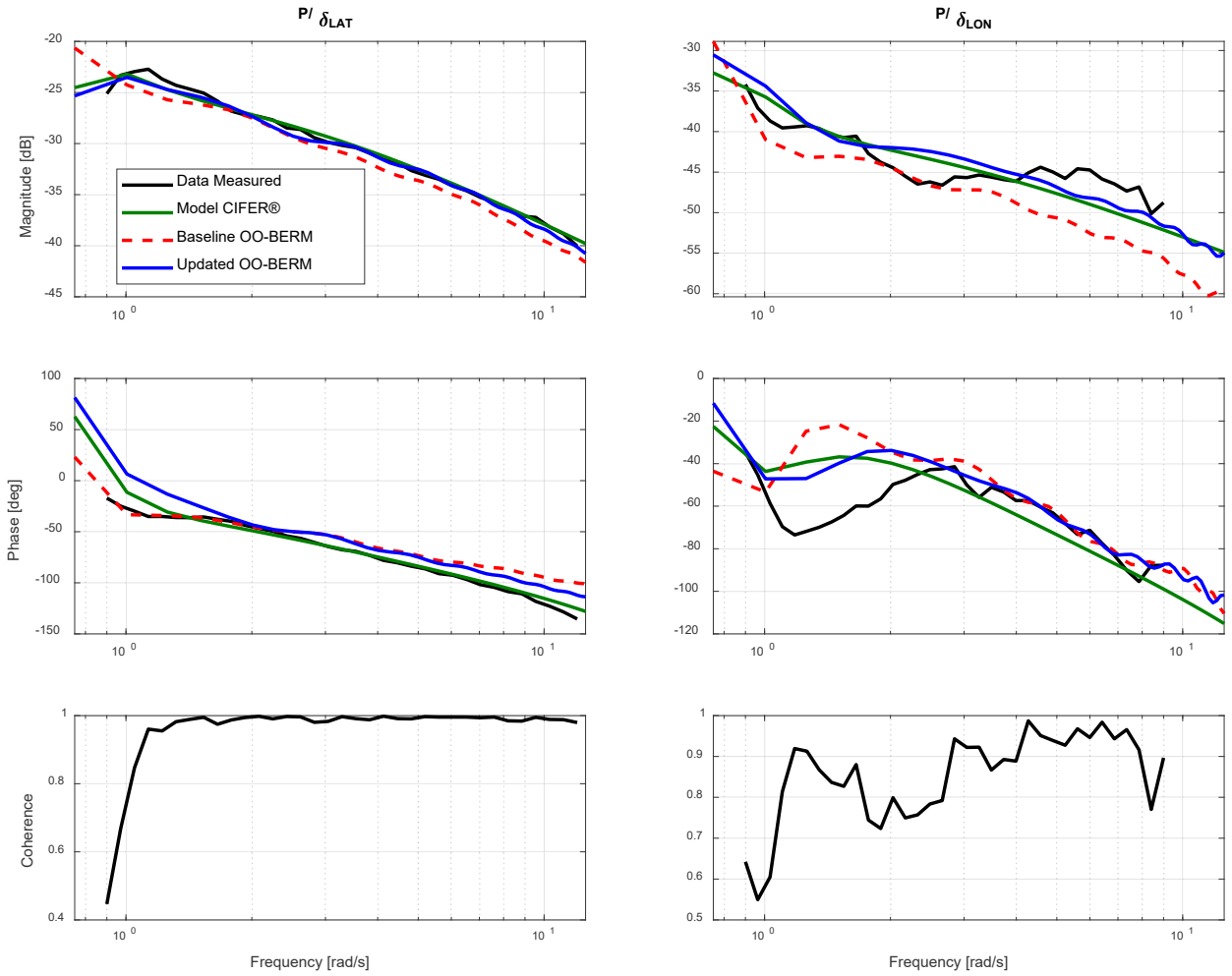

Figure 7.5-1: Frequency-Comparison of the Flight Data Roll Rate Response with Identified CIFER Hover Model and Baseline/Updated OO-BERM Model.

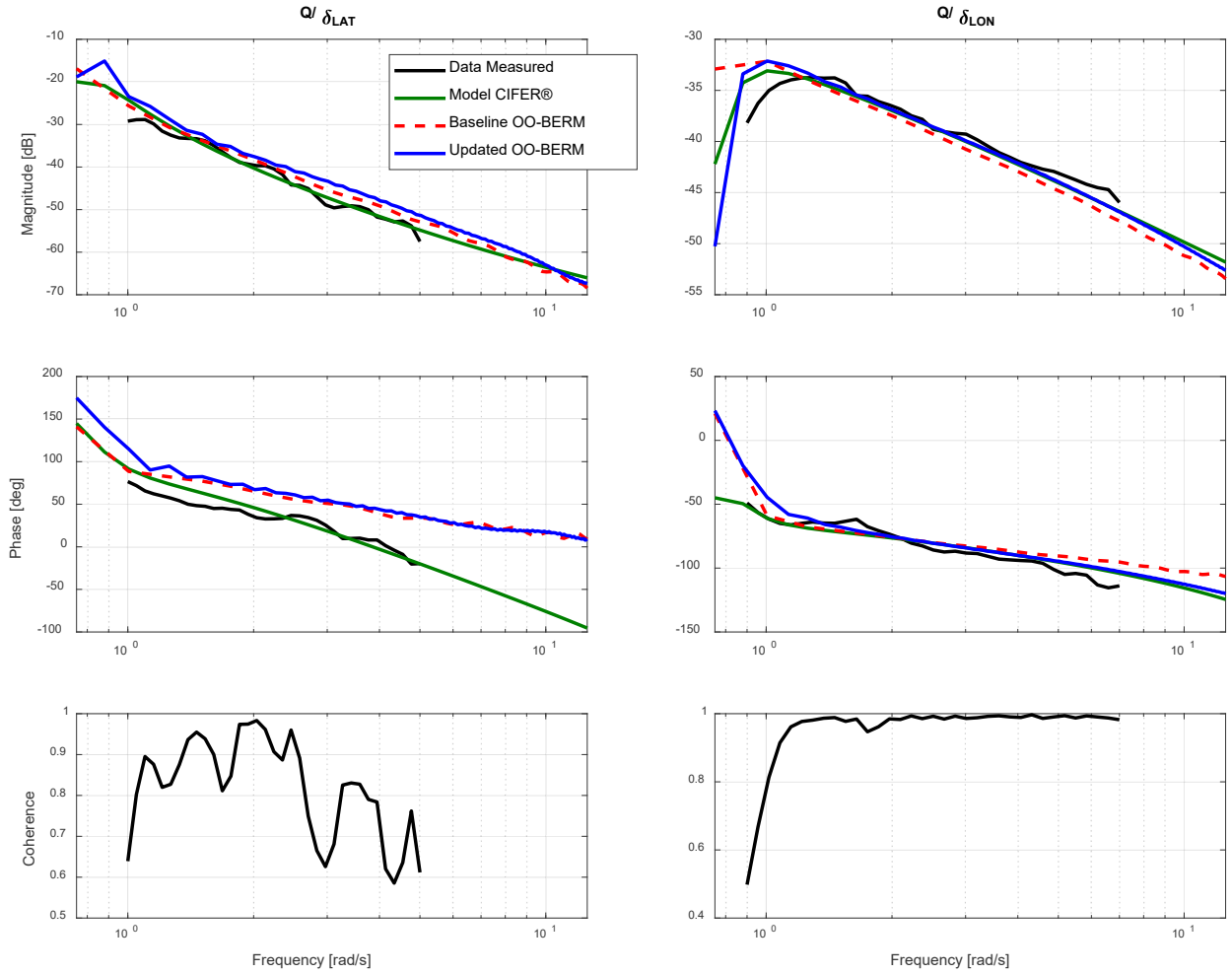

Figure 7.5-2: Frequency-Domain Comparison of the Flight Data Pitch Rate Response with Identified CIFER Hover Model and Baseline/Updated OO-BERM Model.

Table 7.5-3: Frequency-Domain Integrated Cost *J*.

Freq. resp	*J* Baseline OO-BERM	*J* Updated OO-BERM
p/δ_{lat}	146.9	64.2
p/δ_{lon}	526.5	118.9
q/δ_{lat}	324.4	518.7
q/δ_{lon}	86.2	34.5

7.5.2 CAE Updates to CH-147F Model

This section is a case study of a CH-147F model. Improvements are based on hover frequency-domain flight-test data. This section will first describe the CH-147F data used and a description of the CAE's BERM framework. It will then show how the parameters adjustment method can be used to significantly improve the frequency-domain simulation results of a Chinook. This case study also leverages the reduced order rotor

dynamic inflow models encompassed by the simulation model fidelity improvement method of implementing reduced order models and physics-based corrections illustrated in Tischler et al [7], Section 7.4.2 CH-47 case study of the report.

7.5.2.1 Description of the CH-147F Data Used

In the CH-147 model improvement effort, the frequency-domain results of the model were compared against frequency-domain results from flight-test data. The flight-test data used is from Keller's 1995 Chinook flight tests [8] SAS ON data. This data was converted to SAS OFF data using an autopilot system description document provided by Boeing. When using these data, frequencies were restricted with a high coherence (above 0.6) as shown in Figure 7.5-3 and Figure 7.5-4. All subsequent frequency responses are shown with SAS OFF.

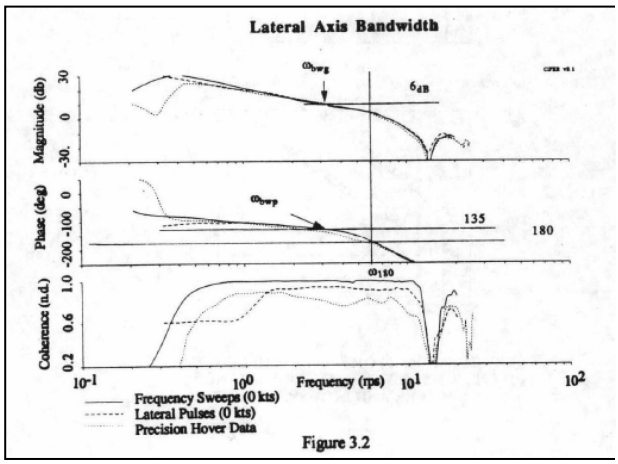

Figure 7.5-3: Keller Lateral Axis Test Data, SAS ON.

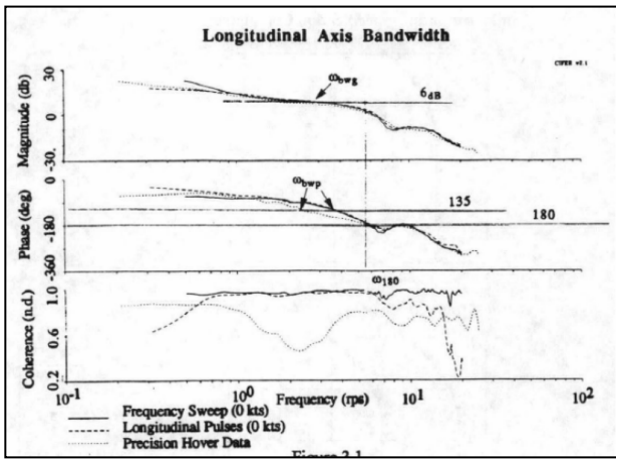

Figure 7.5-4: Keller Longitudinal Axis Test Data, SAS ON.

7.5.2.2 CAE BERM Model Description

CAE uses a generic Blade Element Rotor Model (BERM) to simulate twin rotor helicopters. This model divides each blade of the helicopter into 5 segments, and calculates aerodynamic properties such as lift, drag, induced velocity, forces, and moments for each segment and all other helicopter components. This blade element rotor model takes as inputs the pilot control positions, atmospheric state, and ground reaction, and outputs the resulting helicopter accelerations, attitudes, and rates in time domain.

7.5.2.3 Initial Model Results

Figure 7.5-5, Figure 7.5-6, Figure 7.5-7, Figure 7.5-8 show the initial CAE twin rotor simulation model roll and yaw responses customized using parameters provided by the Boeing on the CH-147F database described in Tischler et al. [7], Section 7.5.4.1, with no modifications or improvements, compared against Keller's experimental data. In these results, the flight-test data have been converted to SAS OFF frequency responses, and the simulation model is also SAS OFF.

The initial simulation results show a significant need for improvement in yaw and roll. In yaw, the magnitude is outside the MUAD below 4 rad/sec. In roll, phase and magnitude are both away from experimental results below 3 and 2 rad/sec, respectively. Also, the simulation fails to model the dip seen at approximately 7 rad/sec in yaw. According to Ivler et al. [9], this dip represents a rotor-on-rotor mode caused by the power transmission from the aft rotor to the front rotor through the main driveshaft. Based on the results, improvement efforts will focus on roll and yaw, which are the furthest from experimental results.

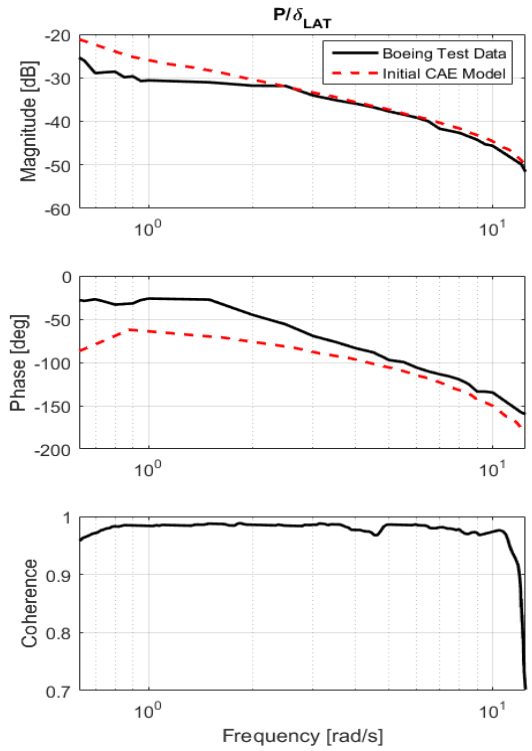

Figure 7.5-5: Initial CAE Simulation Roll Response.

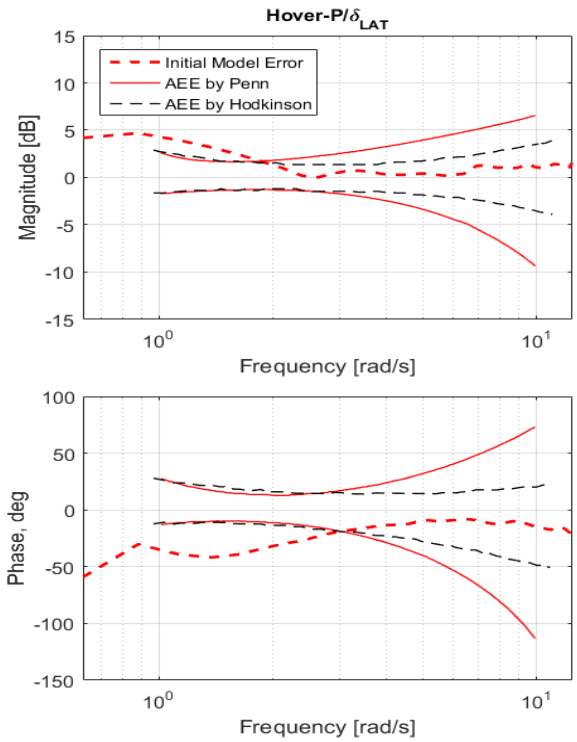

Figure 7.5-6: Initial CAE Simulation Roll MUAD.

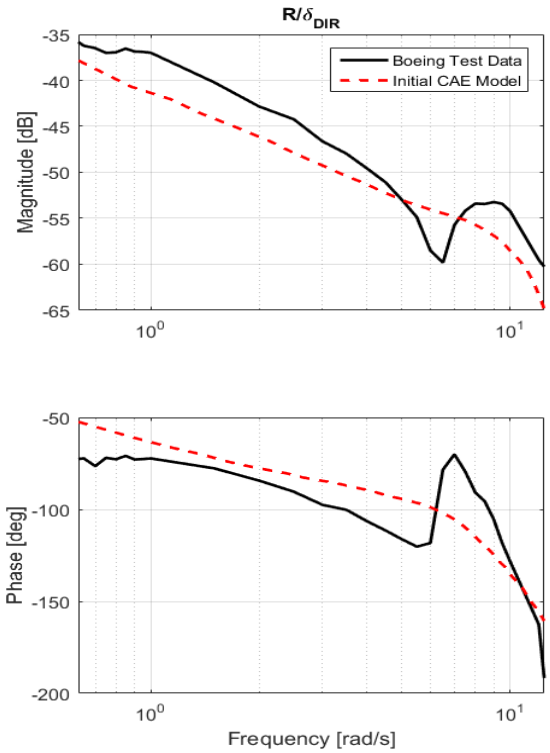

Figure 7.5-7: Initial CAE Simulation Yaw Response.

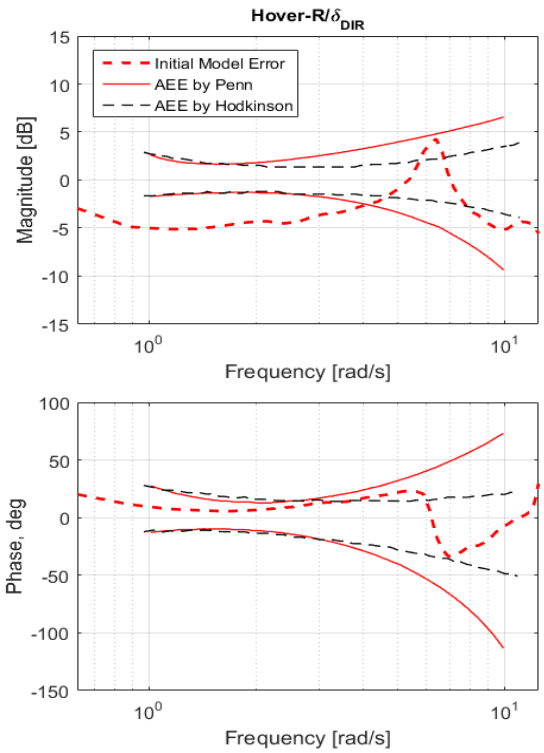

Figure 7.5-8: Initial CAE Simulation Yaw MUAD.

Several methods were used to improve the model performance. In this section a summary of each of these methods is provided. The improved results when applying all methods are shown in Figure 7.5-9 and Figure 7.5-10 and Figure 7.5-12 and Figure 7.5-13 at the end of this document.

7.5.2.4 Tuning of BERM with Components of the BHSIM Inflow Model

To improve low frequency roll response, components from Boeing's BHSIM model as described by Gunner et. al. [10] were implemented. BHSIM is an empirically tuned inflow model for CH147F, tuned to match earlier NASA flight-test data [11]. A detailed description of BHSIM is provided by Gunner et al. [10]. The components added are:

$$\lambda(\bar{r},\psi) = \lambda_0 + \lambda_{1c} * \bar{r}\cos(\psi) + \lambda_{1s} * \bar{r}sin(\psi)$$

where λ_0 is the steady state inflow, $\bar{r}$ is the rotor radial coordinate where the inflow is calculated and ψ is the rotor azimuthal coordinate. λ_{1c} and λ_{1s} capture first harmonic inflow distribution contributions to the total inflow calculated as:

$$\dot{\lambda_{ic}} = \left[\frac{\mu_{TOT}}{\xi}\sqrt{2}\mu_x\right]\dot{\lambda_{io}} + \left[\frac{\mu_{TOT}}{\tau_c\sqrt{\xi}}\sqrt{2}\mu_x\right]\lambda_{io} - \frac{K_{cM}C_{M,aero}}{\tau_c} - \frac{\sqrt{\xi}}{\tau_c}\lambda_{ic}$$

$$\dot{\lambda_{is}} = -\left[\frac{\mu_{TOT}}{\xi}\sqrt{2}\mu_y\right]\dot{\lambda_{io}} - \left[\frac{\mu_{TOT}}{\tau_s\sqrt{\xi}}\sqrt{2}\mu_y\right]\lambda_{io} - \frac{K_{cL}C_{L,aero}}{\tau_s} - \frac{\sqrt{\xi}}{\tau_s}\lambda_{is}$$

The implemented model from the GenHel model [12] and provided to CAE by the Boeing company is similar to the Pitt-Peters model, described theoretically by Pitt and Peters [13] and described for a practical application by Peters and HaQuang [14]. In these equations $[\lambda_0, \lambda_{1c}, \lambda_{1s}]$ are the steady state inflow, μ_{TOT} is the total advance ratio of the rotor disk and ξ is the magnitude of the advance ratio and the main rotor inflow as shown in the following equations:

$$\mu_{TOT} = \sqrt{\mu_x^2 + \mu_y^2}\,,\ \xi = \sqrt{\mu_x^2 + \mu_y^2 + \lambda_{TOT}^2}$$

The parameters, K_{cM} and K_{cL} are tuning handles, which can be used to change the performance of the model. τ_s and τ_c are time constants as defined by BHSIM. The combination of the additional contribution to induced flow and the tuning provided by K_{cM} and K_{cL} improved the roll response of the model at low frequencies. This is shown in Figure 7.5-9. The improvement in the results coming from the BHSIM method is mainly in the low frequency ranges for the roll rate magnitude and phase plots and is shown in Figure 7.5-9 and Figure 7.5-10. We can see from these figures that it is possible to correct the simulation response to be within the MUAD (Maximum Unnoticeable Added Dynamics) band.

7.5.2.5 Force and Moment Tuning Based on Physical Parameters for Hover Yaw Response

Several gains were used as tuning variables on various force and moment calculations to adjust the frequency-domain response of the CH147 model to better match flight-test data. These variables and their effect are described here.

Yaw moment due to differential lateral swashplate angle between rotors was used to adjust yaw response phase as illustrated in Figure 7.5-11. Adjusting yaw moment due to differential lateral swashplate angle cannot be used solely to correct either phase or magnitude as it would increase the error in the other variable. Yaw magnitude can be individually improved by increasing gain on an aerodynamic moment correction term defined as $C_{n,aero} = f(\alpha,\beta)$ in the yaw axis. A combination of the correction term illustrated in Figure 7.5-11 and a direct fuselage moment coefficient in the form $C_{n,aero} = f(\alpha,\beta)$ was therefore used to improve the yaw response of the simulation.

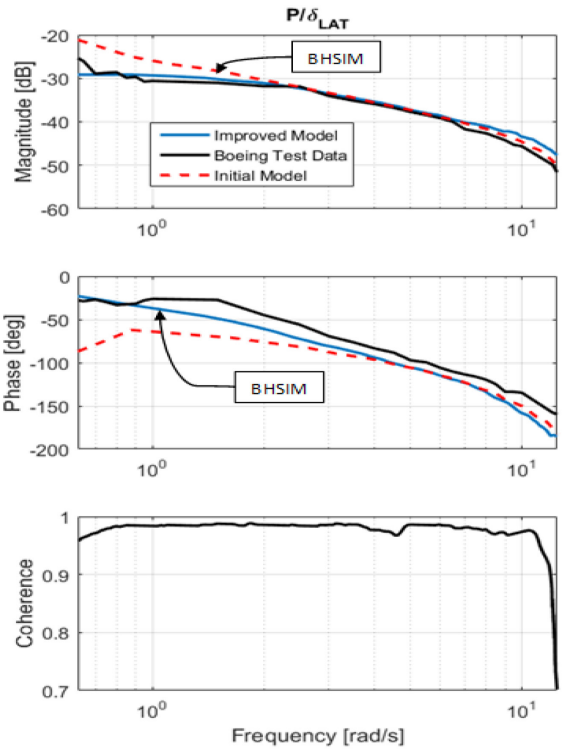

Figure 7.5-9: Improved CAE Simulation Roll Response.

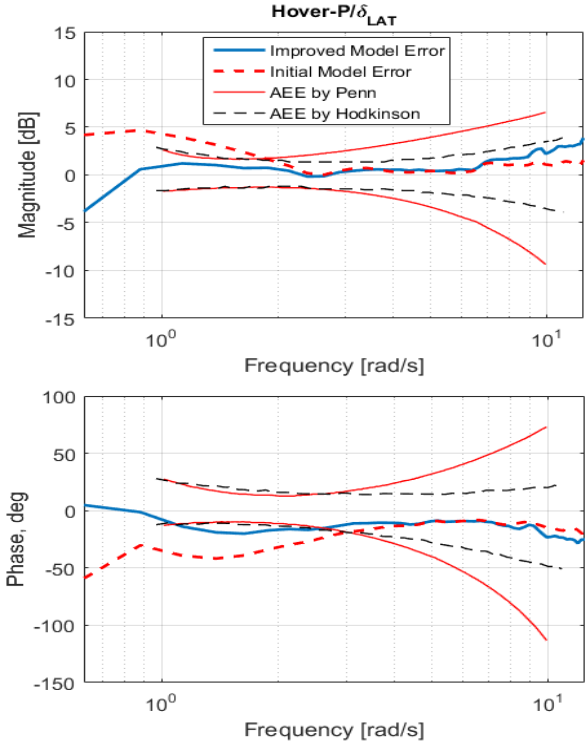

Figure 7.5-10: Improved CAE Simulation Roll MUAD.

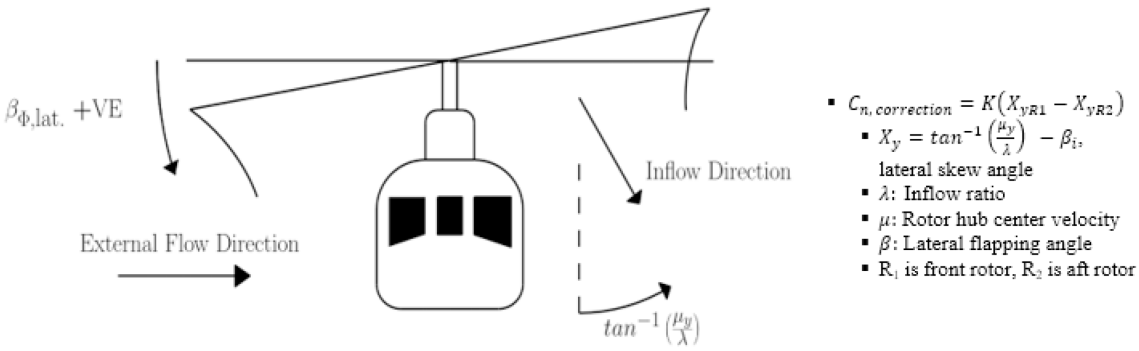

Figure 7.5-11: Description of Yaw Phase and Magnitude Adjustment.

As Figure 7.5-12 and Figure 7.5-13 show, the yaw response was noticeably improved by this quick method, especially at the low frequency ranges. It is worth noting that the development cost of this method is very low as this coefficient can be used as a tuning knob to tune the yaw control derivative of the helicopter. The Chinook CH147 frequency response has a high frequency rotor-on-rotor torque mode which adds a dip to the pitch and yaw response at frequencies above approximately 7 rad/sec. Ivler et al. [9] as well as Miller and White (1987) [15] attributed this mode to drive system flexibility in the tandem rotor Chinook, causing a lagging and leading difference between the rotors during high frequency control input. In the pitch and yaw response results below, a transfer dipole function was used to capture the response at these higher frequencies. The dipole transfer function is explained in detail in Tischler et al. [7], Section 7.2.3, on the 'Black Box' input and output filters.

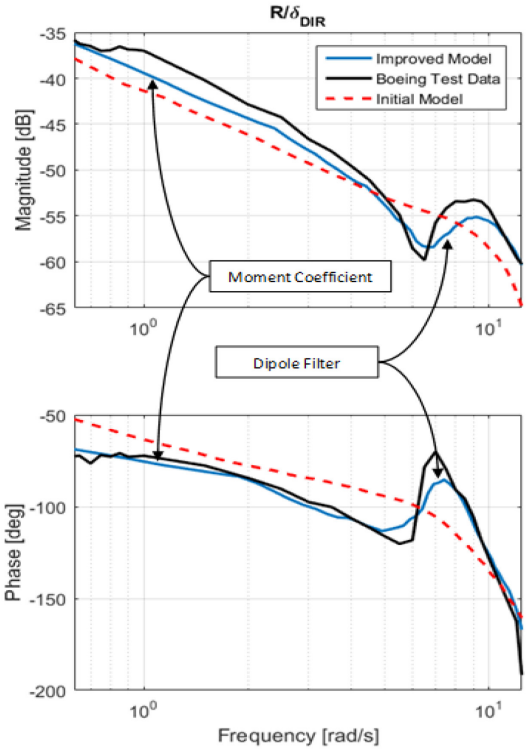

Figure 7.5-12: Improved CAE Simulation Yaw Response.

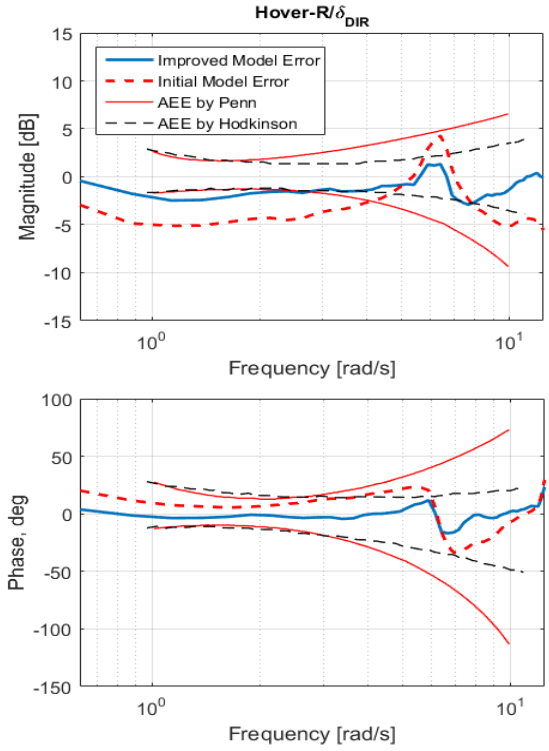

Figure 7.5-13: Improved CAE Simulation Yaw MUAD.

Table 7.5-4 below illustrates the cost function improvement resulting from using each of these methods in addition with the dipole transfer function described in Tischler et al. [7], Section 7.2.3. Note that depending on the application, it is debatable to use a cost function only to evaluate whether a model is 'good enough.' In this case, the frequency domain and MUAD plots show a better picture of the strength and limitations of the new model. The suitability of the model becomes dependent on the application.

Table 7.5-4: Model Frequency-Domain Cost Functions.

Axis	Initial Cost	New Cost
P/LAT	281.6	237.6
R/DIR	410.7	86.2

7.5.3 Australian DSTG Updates to CH-147F Model

This section discusses simulation model updates performed by the Australian Defence Science and Technology Group to improve fidelity of a FLIGHLAB simulation model of the CH-47F. Note that this aircraft is essentially the same as the CH-147F addressed in the previous section. However, this represents a separate effort using a different set of flight data and a different simulation model. The updates were conducted with reference to frequency responses generated from Australian Army flight-test activities, however, these are unable to be presented in this document. Public domain data from Lawler et. al. [16] are presented in this report as a flight test comparison.

7.5.3.1 Inertia Correction

In the baseline CH-47F FLIGHTLAB® model, a magnitude discrepancy of approximately 2.5dB was present in the longitudinal-to-pitch frequency responses with respect to flight-test data. This difference was relatively constant with frequency, behaving primarily as a gain offset. The mechanical control system linkage gains were confirmed to be correct, and in order to improve the model response the moment of inertia values was adjusted. Increasing the model inertia effectively reduces the magnitude of the control derivatives, acting primarily as a gain adjustment [17]. Shown in Figure 7.5-14(a) are the cost function results for the longitudinal frequency response (with respect to flight-test data) over a range of longitudinal inertia (I_{YY}) values. The baseline model I_{YY} value is indicated in the figure.

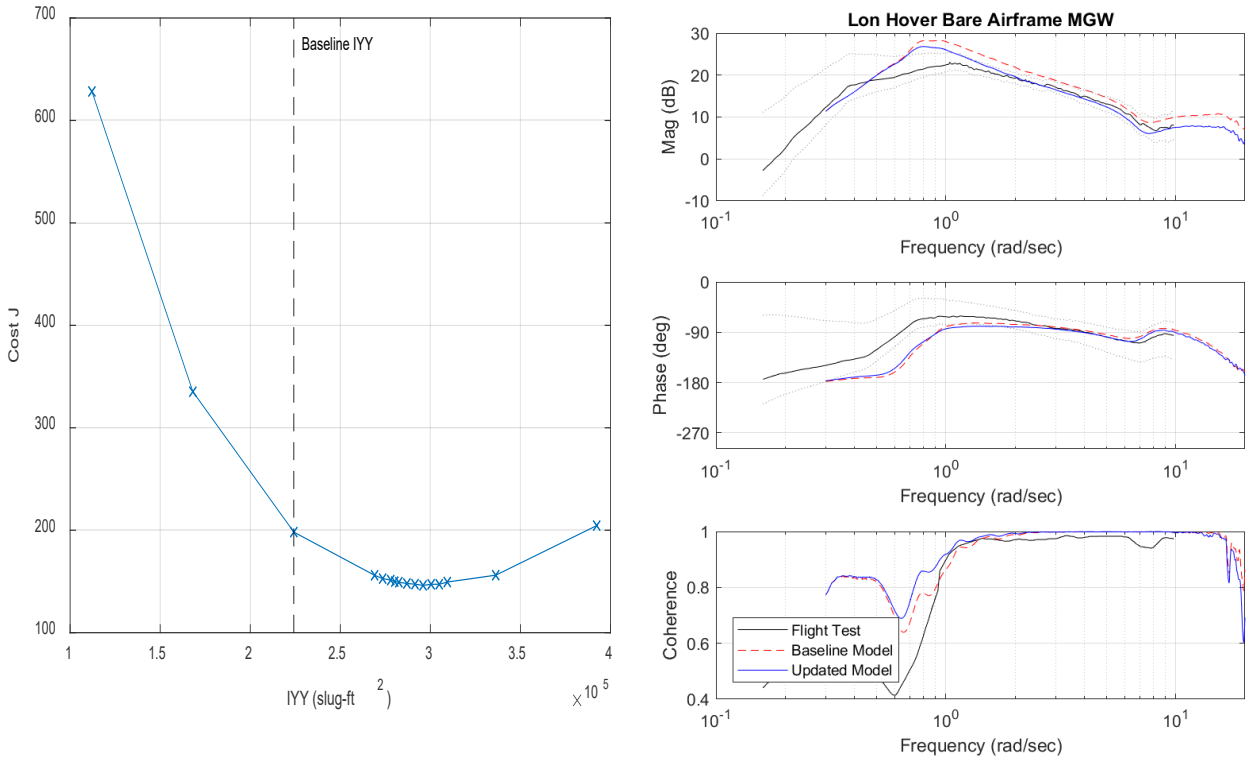

(a) Model Mismatch Cost. **(b) Frequency Response Comparison.**

Figure 7.5-14: Effect of Pitch Inertia on Longitudinal Axis Response.

The cost function can be seen to reduce in an approximately quadratic manner with increasing inertia, indicating that the model response is approaching the flight-test data response. The inertia value for the updated model was selected as the point of minimum cost function, representing the best match with the flight-test data. The baseline and updated inertia and cost function values for pitch are shown in Table 7.5-5.

Table 7.5-5: Baseline and Updated Inertia and Cost Values.

Inertia	Baseline (slug-ft^2)	Updated (slug-ft^2)	Baseline Cost	Updated Cost	Improvement (%)
I_{YY}	224206	302678	313	142	55

Hover frequency response comparisons in the longitudinal axis are shown in Figure 7.5-14(b), before and after the model update. The inertia update can be seen to reduce the magnitude of the model frequency response as desired, resulting in a 55% reduction in cost with respect to the flight-test responses.

7.5.3.2 Lag Damper Correction

In the baseline FLIGHTLAB CH-47F model, the magnitude of the dipole associated with the Rotor-on-Rotor (RoR) mode was lower than the flight-test data. The RoR mode produces differential thrust and torque between the forward and aft rotors, which results in a moderately damped coupled pitch-yaw mode. The reduced RoR dipole magnitude manifested as a smaller coupling between the longitudinal dynamics and the rotor lag modes, primarily around the 8 rad/sec range.

In order to increase the magnitude of the RoR mode dipole, the blade lag damping was reduced in the model, which directly reduced the damping of the lag modes. Shown in Figure 7.5-15(a) is longitudinal frequency response comparison for a range of lag damper values. Note the reduced frequency range of 3-15 rad/sec, utilized to enhance the effect of the RoR dipole on the overall response. As can be seen, the height of the dipole increases in both the magnitude and phase with lower lag damping. Shown in Figure 7.5-15(b) is the integrated cost function calculation for the range of lag damper values, evaluated over the reduced frequency range of 3 – 15 rad/sec. As would be expected, the cost function reduces in a quadratic fashion as the lag damping reduces with a minimum at 4500 ft-lbf-sec/rad.

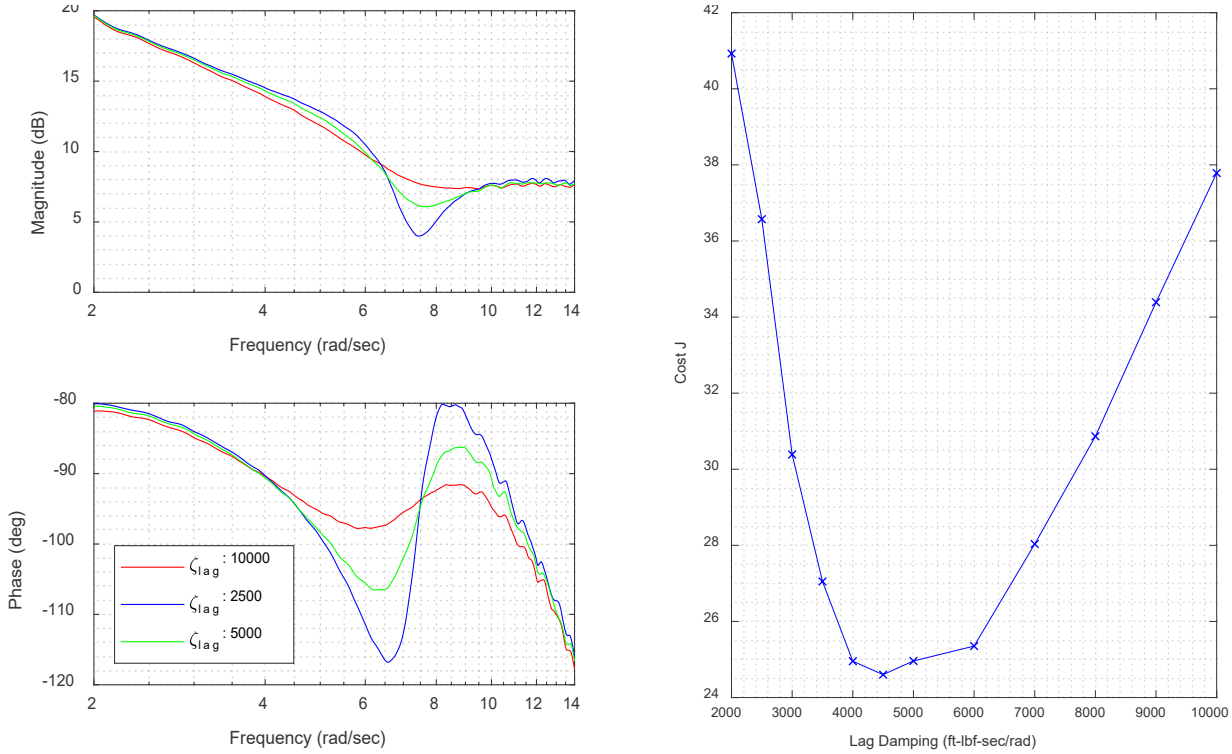

(a) Frequency Response Comparison. **(b) Cost Function Comparison.**

Figure 7.5-15: Effect of Lag Damping on Longitudinal Response.

The baseline damping value was 12,506 ft-lbf-sec/rad, which was reduced to 5,000 ft-lbf-sec/rad in the updated configuration, which resulted in a 7.3% reduction in cost in the longitudinal axis (evaluated over the 0.7 – 20 rad/s range), and a 40% cost reduction when evaluated over the limited frequency range of 3 - 15 rad/s.

7.5.4 Summary

Each of the case studies above sought to improve model fidelity via tuning of model input parameters in physics-based simulation models. Each case study focused on model parameters for which there is significant uncertainty. While some of these parameters can be measured, they often vary significantly between aircraft of the same type, and some of these properties can change during flight due to unmodeled physical effects. Thus, there is justification for tailoring these input parameters if they are known to have direct correlation with observed discrepancies between the model and flight-test data. One advantage of direct tuning of model parameters is that the simulations retain physics-based structure without relying on non-physical corrections. Furthermore, the results of parametric studies can be informative to developing better physics-based models while also providing improvements to the model in the near term while the model physics are investigated further.

The studies presented above focused on optimizations or parametric studies involving one to three input parameters, and generally similar levels of improvement were achieved in frequency- and time-domain cost functions for each of the cases:

1) The CAE improvements to the Bell 412 model reduced frequency-domain costs for the on-axis roll and pitch responses by 50 – 60 %. This was achieved by optimizing helicopter control derivatives by varying main rotor aeromechanical parameters, such as the swashplate phase angle offset, rotor blade pitch-flap coupling angle, and flap hinge offset. The off-axis roll response to longitudinal input was also significantly improved while the off-axis pitch response was degraded slightly.

2) CAE efforts to enhance the CH-147 model focused on the roll and yaw axis. The frequency-domain cost in the roll axis was reduced by 16% while the yaw axis cost was reduced by 79%. The pitch axis frequency-domain cost increased slightly.

3) Australian DST Group performed updates to their FLIGHTLAB® model of the CH-47F. Updates to the roll and pitch inertias improved frequency-domain costs by 95% and 55% respectively. Updates to the lag damper properties resulted in 7% and 21% reductions in the roll and pitch axis frequency-domain costs but increased directional axis cost by 86%.

While these studies illustrate the efficacy of improving model fidelity via parameter adjustments, the studies also illustrate some of the potential pitfalls of the approach:

1) Overall, model discrepancies can be due to multiple different discrepancies physical properties. Therefore, adjustment to parameters may be non-physical. For example, fidelity improvements achieved by adjustments to model parameter A might be overcoming for the true discrepancies that exist in model parameter B, or the adjustment might be covering for some unmodeled physics.

2) Parameter adjustments may have unintended secondary effects. For example, as was shown in two of the studies, increasing inertia to reduce control sensitivity will also lead to phase reduction via equivalent reductions in damping.

3) Corrections applied to improve one axis may degrade the performance in the other axes (e.g., the CH-47 lag damping reduction improved the longitudinal response but degraded the directional axis response).

Thus, model developers need to be cautious in applying modifications to physical input parameters, especially if the intended use of the simulation model is engineering development. These concerns may be of less importance for the development of training simulators where meeting the fidelity requirement for a specific aircraft is the foremost concern.

7.5.5 References

[1] Gubbels, A.W., Carignan, S., Ellis, K., Dillon, J., Bastian, M., Swail, C. and Wilkinson, C. (2006), "NRC Bell 412 Aircraft Fuselage Pressure and Rotor State Data Collection Flight Test", 32nd European Rotorcraft Forum, Maastricht, Netherlands, September 12 – 14.

[2] Seher-Weiß., S., Tischler, M.B., Scepanovic, J., and Gubbels, B. (2019), "Bell 412 System Identification and Model Fidelity Assessment for Hover and Forward Flight", 8th Asian/Australian Rotorcraft Forum, Ankara, Turkey, Oct. 30 – Nov. 2.

[3] Tischler, M.B., and Remple, R.K. (2012), Aircraft and Rotorcraft System Identification: Engineering Methods with Flight Test Examples, 2nd edition, Reston, VA: American Institute of Aeronautics and Astronautics.

[4] Theophanides, M., and Spira, D. (2009), "An Object-Oriented Framework for Blade Element Rotor Modelling and Scalable Flight Mechanics Simulation". Proceedings of the 35th European Rotorcraft Forum, Hamburg, Germany, September 22 – 25.

[5] Bailey, F.J. (1941), "A Simplified Theoretical Method of Determining the Characteristics of a Lifting Rotor in Forward Flight", NACA Report No. 716.

[6] Spira, D., Myrand-Lapierre, V., and Soucy, O. (2012), "Reducing Blade Element Model Configuration Data Requirements Using System Identification and Optimization", American Helicopter Society 68th Annual Forum, Fort Worth Texas, May.

[7] Tischler, M.B., White, M.D., Cameron, N., D'Agosto, S., Greiser, S., Gubbels, A., Guner, F., He, C., Horn, J., Hui., K., Jones, M., Juhasz, O., Lee, O., Lehmann, R., Miller, D., Myrand-Lapierre, V., Nadeau-Beaulieu, M., Nadell, S., Padfield, G., Pavel, M., Prasad, J., Ragazzi, A., Richard, S., Scepanovic, P., Seher-Weiß, S., Soong, J., Stroosma, O., Taghizad, A., Tobias, E., Xin, H., and Yavrucuk, I. (2021), "Rotorcraft Flight Simulation Model Fidelity Improvement and Assessment," NATO STO AVT-296 Technical Report.

[8] Keller, J.F., Hart, D.C., Shubert, M.W., and Feingold A. (1995), "Handling Qualities Specification Development for Cargo Helicopters", American Helicopter Society 51st Annual Forum.

[9] Ivler, C.M., Tischler, M.B., and Shtessel, Y. (2006), "System Identification of the Longitudinal/Heave Dynamics for a Tandem-Rotor Helicopter Including Higher-Order Dynamics", AIAA Atmospheric Flight Mechanics Conference and Exhibit, August.

[10] Gunner, F., Prasad, J.V.R., He, C., and Miller, D.G. (2019), "Tandem Rotor Inflow Modelling and its Effect on Vehicle Dynamics", Vertical Flight Society 75th Annual Forum & Technology Display, May.

[11] Hackett, W.E., Garnett, T., and Borek, B.V. (1983), "Mathematical Model of the CH-47B Helicopter Capable of Real-Time Simulation of the Full Flight Envelope", Vol.1, NASA CR-166458, July.

[12] Howlett, J. (1981), UH60A BLACK HAWK Engineering Simulation Program: Volume I Mathematical Model, NASA CR166309.

[13] Pitt, D. M. and Peters, D. A. (1983), "Rotor Dynamic Inflow Derivatives and Time Constants from Various Inflow Models", Associazione Italiana di Aeronautica ed Astronautica, September.

[14] Peters, D.A., and HaQuang, N. (1988), "Technical Note: Dynamic Inflow for Practical Applications", *Journal of the American Helicopter Society*, October.

[15] Miller, D.G., and White, F. (1987), "A Treatment of the Impact of Rotor-Fuselage Coupling on Helicopter Handling Qualities", American Helicopter Society 43rd Annual Forum, May.

[16] Lawler, M.A., Ivler, C.M., Tischler, M.B., Shtessel, Y.B. (2006), "System Identification of the Longitudinal/Heave Dynamics for a Tandem-Rotor Helicopter Including Higher-Order Dynamics", Proceedings of the AIAA Atmospheric Flight Mechanics Conference and Exhibit, Keystone, Colorado, Paper No. AIAA-2006-6147, August 21 – 24.

[17] Grauer, J.A., and Morelli, E.A. (2013), "Dynamic Modeling Accuracy Dependence on Errors in Sensor Measurements, Mass Properties, and Aircraft Geometry", Proceedings to 51st AIAA Aerospace Sciences Meeting, Grapevine TX, January 2013.

Chapter 7.6 – CASE STUDY OF PARAMETER IDENTIFICATION OF KEY SIMULATION CONSTANTS

ABSTRACT

This section presents a model fidelity update and assessment case study that uses system identification to directly determine rotorcraft physical parameters (e.g., hinge-offset, inertias, spring constants, etc.) from flight-test data. The identified physical parameters are used to update the input parameters of a physics-based model to improve model fidelity. A detailed method description can be found in Tischler et al. [1], Section 5.6, and additional detail for this method can be found in Fegely, et al. [2]. The X2TD is the aircraft used for this case study.

7.6.1 X2TD Case Study

7.6.1.1 Baseline Hover Model Identification and Comparisons

The overall bare-airframe validation based on X2TD flight-test data used the total commands (pilot + flight control) sent to the mixer for each axis. For the validation, first-order actuator dynamics, IMU filtering, and an empirical time delay to account for sensor delay were removed from the flight data.

Frequency sweeps were performed on the aircraft in hover for the lateral and longitudinal axes to capture the dynamic response of the aircraft. Roll and pitch frequency responses to on-axis commands were extracted from flight data and GenHel time histories using CIFER® [3] and numerical linearization of the HeliUM model was conducted [4]. CIFER converts the frequency sweep time histories into the frequency domain using overlapping windows of varying time lengths and a chirp-Z transform. Multi-input conditioning is then performed to remove effects of off-axis inputs from the pilots. The coaxial rotor system of the X2TD naturally gives a decoupled aircraft response, so off-axis inputs did not have large effects in the on-axis response as they do for single main rotor helicopters.

In addition to frequency response generation, the state-space model identification utility within CIFER was used to provide physical updates to HeliUM model parameters. The state-space model structure was formulated based on first principles equations of motion and constraint equations were used to identify key parameters within the equations. Initial guesses for each parameter came from the baseline HeliUM model.

Figure 7.6-1 depicts the bare-airframe frequency response in hover for pitch and roll, respectively. There is a broad frequency range of high-quality flight data, about 1-20 rad/sec for pitch and 1-30 rad/sec in roll, as seen from the high coherence. GenHel and HeliUM accurately predict the pitch response from 1.0 to 12 rad/sec. For the roll response, both models under-predict the absolute gain from 2 to 12 rad/sec. GenHel and HeliUM both correctly predict the rotor regressive flap mode at approximately 30 rad/sec as seen in the roll response.

Both models predict the frequency of the lead-lag dipole to be 20 rad/sec, which is closer to 12 rad/sec in the flight data. The models predict different frequencies for the hovering cubic, but all are at low frequency (< 1 rad/sec).

Comprehensive simulation models rely on a large quantity of input parameters for blade and aircraft properties. Many of these parameters are difficult to measure in lab tests, let alone during actual flight test. Furthermore, the analytical formulation of the model simplifies the vehicle geometry, introducing uncertainty into the definition of the input parameters. This is especially true for new/novel configurations like the X2TD that differ significantly from single main rotor helicopters. System identification is used herein to improve the correlation of the math model to flight data.

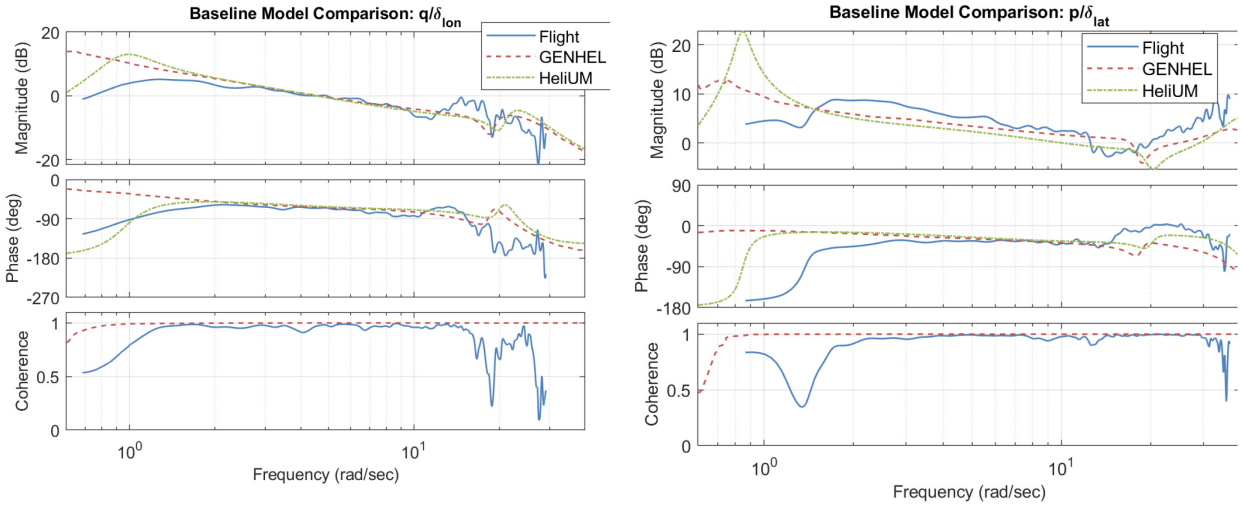

(a) Pitch Rate Response to Longitudinal Command.

(b) Roll Rate Response to Lateral Command.

Figure 7.6-1: Baseline Roll and Pitch Bare-Airframe Aircraft Responses to Total Commands.

7.6.1.2 Identification of Hover Regressive Flap / Fuselage Dynamics

Analytically derived coupled fuselage and blade flap equations of motion for the Sikorsky X2TD based on the work by Chen [5] were used to derive flight-test data-based updates to the math model. These analytical equations use a hinge-offset / flap spring to approximate the dynamics of the hingeless Sikorsky X2TD rotor. The coupled rotor-body equations of motion (for a single rotor) are:

$$\begin{Bmatrix} \dot{p} \\ \dot{q} \\ \ddot{\beta}_{1c} \\ \ddot{\beta}_{1s} \\ \dot{\beta}_{1c} \\ \dot{\beta}_{1s} \end{Bmatrix} = \Omega \begin{bmatrix} 0 & 0 & 0 & 0 & 0 & \frac{L_{\beta_{1s}}}{\Omega} \\ 0 & 0 & 0 & 0 & \frac{M_{\beta_{1c}}}{\Omega} & 0 \\ 2\left(1+\frac{eM_\beta}{I_\beta}\right) & \frac{\gamma}{2}\left(\frac{1}{4}-\frac{e}{3}\right) & -\gamma\left(\frac{1}{8}-\frac{e}{3}+\frac{e^2}{4}\right) & -2 & -\Omega(\nu_\beta^2-1) & -\gamma\Omega\left(\frac{1}{8}-\frac{e}{3}+\frac{e^2}{4}\right) \\ \frac{\gamma}{2}\left(\frac{1}{4}-\frac{e}{3}\right) & -2\left(1+\frac{eM_\beta}{I_\beta}\right) & 2 & -\gamma\left(\frac{1}{8}-\frac{e}{3}+\frac{e^2}{4}\right) & \gamma\Omega\left(\frac{1}{8}-\frac{e}{3}+\frac{e^2}{4}\right) & -\Omega(\nu_\beta^2-1) \\ 0 & 0 & \frac{1}{\Omega} & 0 & 0 & 0 \\ 0 & 0 & 0 & \frac{1}{\Omega} & 0 & 0 \end{bmatrix} \begin{Bmatrix} p \\ q \\ \dot{\beta}_{1c} \\ \dot{\beta}_{1s} \\ \beta_{1c} \\ \beta_{1s} \end{Bmatrix}$$
$$-\frac{\Omega^2\gamma}{2}\left(\frac{1}{4}-\frac{e}{3}\right)\begin{bmatrix} 0 & 0 \\ 0 & 0 \\ \theta_{\delta_{lon}}\cos(\Gamma) & \theta_{\delta_{lat}}\sin(\Gamma) \\ -\theta_{\delta_{lon}}\sin(\Gamma) & \theta_{\delta_{lat}}\cos(\Gamma) \\ 0 & 0 \\ 0 & 0 \end{bmatrix}\begin{Bmatrix} \delta_{lon} \\ \delta_{lat} \end{Bmatrix} \tag{7.6-1}$$

where Tischler and Remple [3] and Heffley et al. [6] give:

$$-L_{\beta_{1s}} = \frac{W_h h_r}{I_{xx}^*} + \frac{n_b M_\beta^* \Omega^2 e^*}{2I_{xx}^*} + \frac{n_b K_\beta^*}{2I_{xx}^*} \tag{7.6-2}$$

$$\boldsymbol{M_{\beta_{1c}} = \frac{W_h h_r}{I_{yy}^*} + \frac{n_b M_\beta^* \Omega^2 e^*}{2I_{yy}^*} + \frac{n_b K_\beta^*}{2I_{yy}^*}} \tag{7.6-3}$$

$$\nu_\beta^2 = 1 + \frac{e^* M_\beta^*}{I_\beta^*} + \frac{K_\beta^*}{I_\beta^* \Omega^2} \tag{7.6-4}$$

$$\gamma = \frac{\rho a c R^4}{I_\beta^*} \tag{7.6-5}$$

* Indicates a parameter that will be identified.

An equivalent set of equations exists for the second rotor. The key drivers of dynamics in the frequency range of the regressive flap mode are the coupling between the fuselage and rotor dynamics through $L_{\beta 1s}$ and $M_{\beta 1c}$, and the blade flap frequency, ν_β. The $L_{\beta 1s}$ term in Equation 7.6-2 is highly dependent on roll inertia, I_{xx}, and the flap frequency, ν_β, which is based on the effective hinge-offset (e) and flap spring constant, K_β, as in Equation 7.6-4. The X2TD has a very small fuselage roll inertia of $I_{xx} = 340$ slug-ft^2. Small errors in this value have a profound impact on the equations of motion and could lead to over-prediction of the coupled rotor-body flap modes. Flight-test derived values of roll inertia and flap frequency were sought to improve the model correlation to flight data.

The HeliUM model in hover was used to initialize the values above. A quasi-static reduction of the lag modes was used to remove lag dynamics from the solution, greatly simplifying the identification procedure. Inflow dynamics were held fixed at the baseline HeliUM values, and no inflow related parameters were identified. Small changes in the rotor and fuselage parameters in the equations above do not affect the dynamic inflow portion of the model.

The entire system of equations above reduces to a few unknowns, namely I_β, I_{xx}, I_{yy}, K_β, and e. These unknowns were updated using system identification. The blade first flapping moment of inertia, M_β, was constrained to be a factor of I_β, the second mass moment of inertia, which is consistent for constant mass scaling along the blade span. The lateral axis control sensitivity, $\theta_{\delta_{lat}}$, was also identified. The rest of the parameters, such as weight, number of blades, radius, etc. were held as constants. Equations 7.6-1 to 7.6-5 were implemented within CIFER®'s state-space identification utility DERIVID [3]. The equations are constrained to be functions of the unknown parameters, which are initialized using the baseline values from the HeliUM model. The parameters were then optimized to minimize a coherence weighted cost-function of the flight data responses over a broad frequency range (3 – 60 rad/sec).

The identification results give a flap frequency estimate (using a hinge-offset / flap spring approximation) of $\nu_\beta = 1.38$ / rev and fuselage roll inertia of $I_{xx} = 490$ slug-ft^2. Both values are identified with Cramer-Rao bounds (CR% < 10) and Insensitivities (I% < 2) well within the guidelines given in Tischler and Remple [3]. The 8% reduction in identified flap stiffness as compared to the finite-element approximation encompasses all components in the roll degree of freedom of the aircraft, including shaft and fuselage flexibility as well as any unmodeled flexibility in the hub (from linkages, hub/blade connections, etc.).

The state-space model identification results in an average cost function of $J_{ave} = 100$, indicating very good agreement with the test data [3].

The identification aligns the response to flight data around the rotor modes. The regressive flap mode was clearly over-predicted by HeliUM and is brought to lower frequencies in the CIFER ID result. The identified model is compared to the baseline model and flight data in Figure 7.6-2.

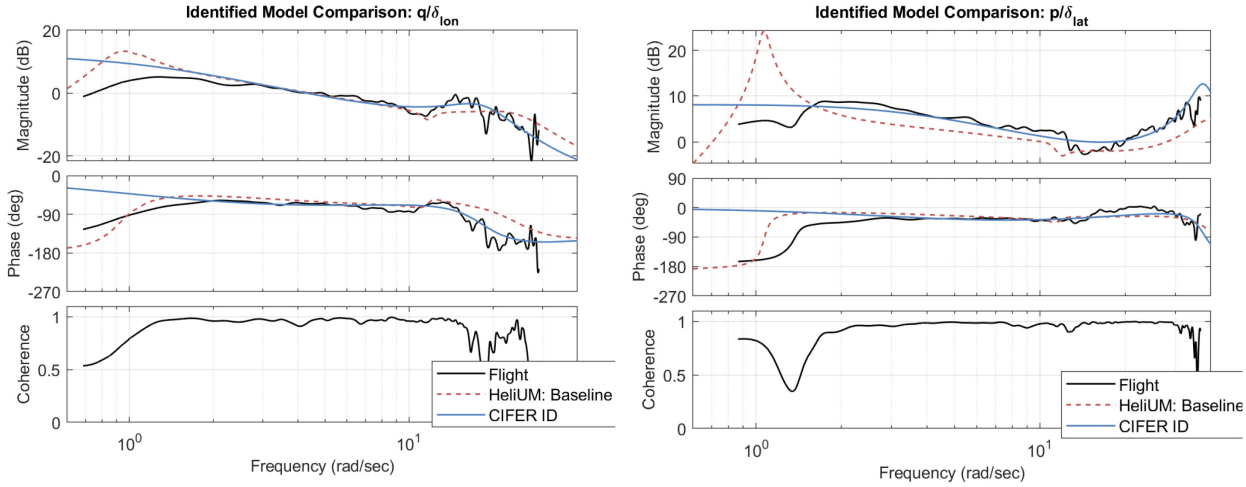

(a) Pitch Rate Response to Longitudinal Command.

(b) Roll Rate Response to Lateral Command.

Figure 7.6-2: Comparison of Roll and Pitch Bare-Airframe Aircraft Responses to Total Commands for the CIFER State-Space Identified Model, the Baseline Model, and Flight Data.

7.6.1.3 Physical Parameter Update

The flap frequency and roll inertia were then reinserted back into the HeliUM math model as necessary reductions in flap stiffness and an increase in roll inertia to match flight data. The stiffness of the innermost portion of the finite-element beam, corresponding to the hub, was reduced to align the flap frequency closer to flight data and the ID result. The fuselage roll inertia was assumed to be well estimated to within ±10% and was only increased within these allowances to $I_{xx} = 378$ slug-ft^2.

Blade stiffness in lag was also reduced to match flight data. Shaft torsional flexibility was not modeled and is the key factor in lowering lag frequency below the predicted value. The final updated HeliUM model is compared with flight in Figure 7.6-3.

The baseline models (GenHel and HeliUM) have similar and high mismatch costs ($J > 300$) relative to the flight data as shown in Table 7.6-1, indicating degraded fidelity for the baseline models [3]. With the corrections included, the updated HeliUM models have an average cost of about $J_{ave} = 120$, very close to recommended cost of $J_{ave} = 100$. The updated HeliUM model in Figure 7.6-3 now aligns well with flight data over a broad frequency range including the low frequency rigid-body and high frequency rotor dynamics. Relatively small changes in a few key physical parameters greatly improved the overall ability of the model to track flight data.

Table 7.6-1: Frequency Response Costs Between Flight Data and Math Models.

Axis	GenHel	HeliUM: Baseline	HeliUM: Updated
Roll	304	404	123
Pitch	303	324	120

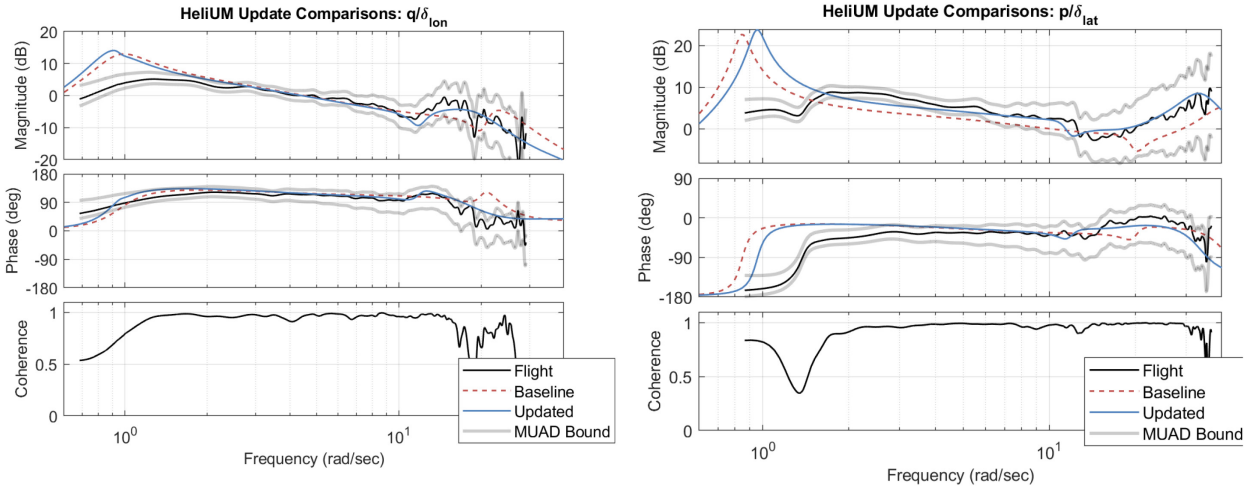

(a) Updated Pitch Rate Response to Longitudinal Command.

(b) Updated Roll Rate Response to Lateral Command.

Figure 7.6-3: Comparisons of Roll and Pitch Bare-Airframe Aircraft Responses to Total Commands for Updated HeliUM Model, the Baseline HeliUM Model, and Flight Data.

7.6.2 Summary

This case study demonstrated how updating simulation parameters can provide direct insight into sources of modeling error. To be effective, this methodology requires extensive knowledge of the underlying aircraft physics as well as system identification. Further, the identification process gives parameters that minimize the error between the model and flight data. Any physics that is not captured by the math model and identification parameters will skew the identified parameter accuracy.

The results showed that both original GenHel and HeliUM math models similarly over-predicted the frequency range of the coupled fuselage-rotor modes. The update strategy greatly improved the model fidelity within the desired frequency range and resulted in viable values of flap frequency, inertia, and control power.

7.6.3 References

[1] Tischler, M.B., White, M.D., Cameron, N., D'Agosto, S., Greiser, S., Gubbels, A., Guner, F., He, C., Horn, J., Hui., K., Jones, M., Juhasz, O., Lee, O., Lehmann, R., Miller, D., Myrand-Lapierre, V., Nadeau-Beaulieu, M., Nadell, S., Padfield, G., Pavel, M., Prasad, J., Ragazzi, A., Richard, S., Scepanovic, P., Seher-Weiß, S., Soong, J., Stroosma, O., Taghizad, A., Tobias, E., Xin, H., and Yavrucuk, I. (2021), "Rotorcraft Flight Simulation Model Fidelity Improvement and Assessment," NATO STO AVT-296 Technical Report.

[2] Fegely, C., Xin, H., Juhasz, O., and Tischler, M.B. (2016), "Flight Dynamics and Control Modeling with System Identification Validation of the Sikorsky X2 Technology Demonstrator," Presented at the 72nd Annual Forum of the American Helicopter Society, West Palm Beach, FL, May 2016.

[3] Tischler, M.B., and Remple, R.K. (2012), *Aircraft and Rotorcraft System Identification: Engineering Methods with Flight Test Examples*, AIAA, Second Edition, Reston, VA, 2012.

[4] Juhasz, O., Celi, R., Ivler, C.M., Tischler, M.B., and Berger, T. (2012), "Flight Dynamic Simulation Modeling of Large Flexible Tiltrotor Aircraft," American Helicopter Society 68th Annual Forum, FortWorth, TX, May 2012.

[5] Chen, R.T.N. (1980), "Effects of Primary Rotor Parameters on Flapping Dynamics," NASA TP-1431, January 1980.

[6] Heffley, R.K., Bourne, S.M., Curtiss, H.C., Hindson, W.S., and Hess, R.A. (1986), "Study of Helicopter Roll Control Effectiveness Criteria," NASA CR-177404, April 1986.

Chapter 7.7 – STITCHED SIMULATION FROM POINT ID MODELS AND TRIM DATA

ABSTRACT

Model stitching is the technique of combining or 'stitching' together individual linear models and trim data for discrete flight conditions to produce a continuous, full flight-envelope stitched simulation model. Four applications of the model stitching technique are presented below. In each case, a collection of discrete linear models and trim data was used to generate a stitched simulation model and was shown to adequately and accurately cover the nominal flight envelope. Additional flight-test data and extrapolation methods are shown to expand the simulation to cover edge-of-the-envelope maneuvers and off-nominal loading configurations.

7.7.1 Model Stitching Motivation and Background

Linear state-space perturbation models, which represent the dynamic response of an aircraft for a discrete reference flight condition and configuration, are accurate within some limited range of the reference condition. These discrete-point linear models are suitable for point control-system design and point handling qualities analyses; however, continuous, full-envelope simulation is desirable for full-mission simulation.

Model stitching combines linear models and trim data for discrete flight conditions with nonlinear elements to produce a continuous, quasi-nonlinear *stitched* simulation model that can replace a physics-based model for full-envelope simulation. In the model stitching technique, the stability and control derivatives and trim data for each discrete-point model are stored as a function of key parameters, such as airspeed and altitude. Applications of model stitching include the development of Level D flight simulators, hardware-in-the-loop simulation, high-accuracy simulation of off-nominal loading configurations (CG, mass, and inertia), alternate conditions (e.g., air density), and wide-envelope simulation models of unconventional aircraft. Additional nonlinear dynamics may be included to cover complex or edge-of-the-flight-envelope maneuvers, e.g., autorotation.

The key requirement for model stitching is a series of state-space point models and associated trim data of the states and controls for point flight conditions or 'anchor' points. Additional, more finely-spaced 'trim shot' data, which capture the variation in trim states and controls over the full airspeed range, are recommended. The dimensional stability and control derivatives are extracted from the anchor point models and stored in lookup tables. The trim data of the states and controls are typically first fitted with splines before being stored in lookup tables. The lookup tables are combined with the nonlinear equations of motion and other simulation elements to yield the model stitching simulation architecture.

A powerful feature of the model stitching architecture is the ability to accurately simulate off-nominal aircraft loading configurations without the need for additional data, as presented by Tobias and Tischler [1]. Simulation of off-nominal values of aircraft mass, inertia, and/or Center of Gravity (CG) that differ from the identified/baseline values is accomplished using extrapolation methods within the stitching architecture. This extrapolation capability can be used to simulate an alternate gross weight, as well as continuous, real-time simulation of fuel burn and changes in inertia/CG location due to jettisoning of external stores, for example. These extrapolation capabilities allow a stitched model to be constructed using only a small number of point models and dramatically reduce the required number of flight-test points for identified models. Flight-test data collection of an off-nominal configuration is useful for validation.

7.7.2 IRIS+ Quadcopter

This section presents the development and verification of a continuous, full-envelope stitched simulation model of the 3D Robotics IRIS+ quadcopter using flight-identified models and the TDD-developed model stitching simulation software, STITCH. Two flight-identified point models (one at hover and one at forward flight), plus some additional trim data, are shown to adequately and accurately capture the bare-airframe dynamics of the IRIS+ over its nominal flight envelope. Additionally, the off-nominal mass-, CG-, and inertia-extrapolation capabilities of STITCH are investigated, and the results are verified for a heavy loading configuration. The overall findings are considered to provide flight-test guidance for the development of stitched simulation models of small-scale multi-rotor vehicles.

7.7.2.1 STITCH Software

A comprehensive model stitching simulation architecture is presented in Section 5.7 of Tischler et al. [2], which allows continuous, full flight-envelope simulation from discrete linear models and trim data. Extrapolation methods in the stitching architecture permit accurate simulation of off-nominal aircraft loading configurations, which minimize the required number of point models for full-envelope simulation. STITCH is a software capability developed by TDD that provides a user interface front end to the model stitching simulation architecture and features anticipatory design elements to guide the user through the entire process of generating a stitched model [3]. STITCH is applicable to any flight vehicle for which point-wise linear models and trim data can be obtained and was employed herein to develop a stitched simulation model of the IRIS+ quadcopter.

7.7.2.2 Flight-Identified Point Models and Trim Data of the IRIS+ Quadcopter

Accurate bare-airframe state-space models of the vehicle, which consist of the IRIS+ airframe, mixer, and motors, in hover and forward flight were identified from flight data using CIFER®. Steady-state trim data were also collected from hover to 32 kn; six anchor trim points at a spacing of about 6 kn were collected. The flight-test process was repeated in a heavy loading configuration for verification of the extrapolation process.

The 3D Robotics IRIS+ is a quadcopter that measures 19.75 inches diagonally motor-to-motor, has a total flying weight of 3.2 lb, and a payload capacity of 0.9 lb. To verify the extrapolation capabilities of the stitched model, the aircraft was flown in two loading configurations: nominal and heavy. The heavy configuration featured a 200-gram (0.441-lb) cylinder attached to the aircraft, as shown in Figure 7.7-1.

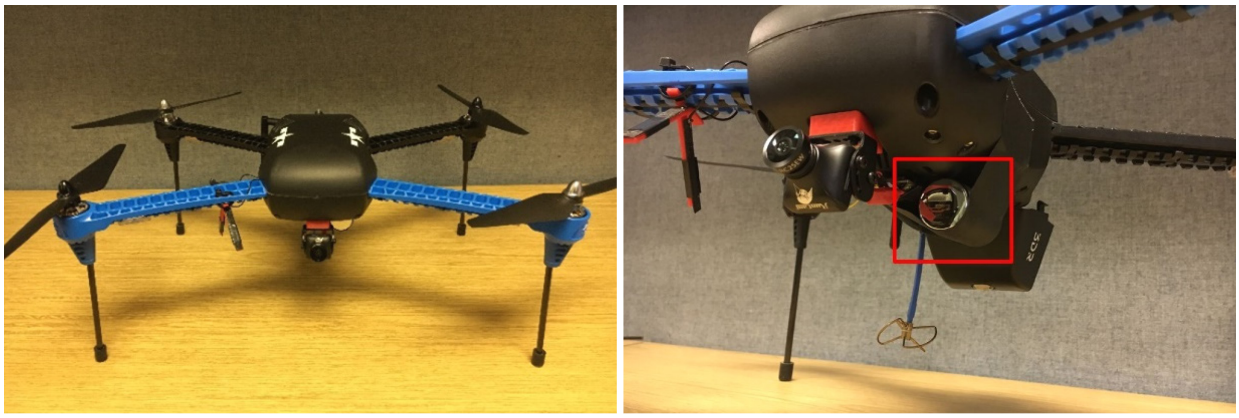

Figure 7.7-1: 3D Robotics IRIS+, Shown in Heavy Loading Configuration with 200-Gram Payload.

7.7.2.3 Quadcopter Stitched Simulation Model Using STITCH

STITCH was used to develop a full-envelope stitched simulation model of the IRIS+ using the two flight-identified point models and finely-spaced trim data of the nominal configuration. The model was configured for 'stitching in U,' which means the point model derivatives and trim data are stored and subsequently looked-up as a function of x-body airspeed U only.

7.7.2.3.1 Anchor Point Data

Anchor points are the specific flight conditions for which a linear model or trim data is included in the stitched model. For the IRIS+ stitched model, the two flight-identified point models (hover and 17 kn) were included as the anchor point models. As such, the stability and control derivatives are linearly interpolated in the stitched model between hover and 17 kn (and linearly extrapolated beyond) as a function of x-body airspeed U. The finely-spaced trim data, which capture the variation in trim states and controls for straight-and-level flight over the full airspeed range, were included as the anchor trim data. See Figure 7.7-2 for an overview of the anchor points; the two-point models and trim data of the nominal configuration are the only data included in the stitched model. The values of longitudinal trim states and controls (i.e., trim z-body airspeed, W, trim pitch attitude, Θ, trim longitudinal stick, δ_{lon}, and trim collective, δ_{col}), as captured by the trim data from flight, are shown by the markers in Figure 7.7-3. Shape-preserving piecewise cubic interpolation was performed on the anchor trim data to produce smooth, finely-spaced data for the stitched model, as shown by the dashed curves.

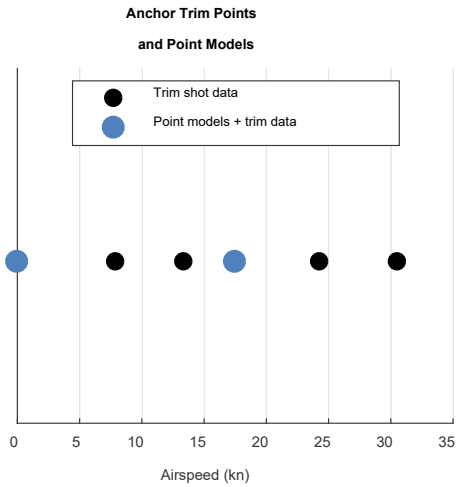

Figure 7.7-2: Anchor Points Included in the Stitched Model.

7.7.2.3.2 Stitched Model Verification

Verification of the stitched model is performed by linearizing the stitched model at the anchor point flight conditions, in this case, hover and 17 kn. This is important because it verifies the accuracy of the implicit speed derivatives (see Tischler et al. [2] Section 5.7) and their effect on the dynamic response of the stitched model. Figure 7.7-4 and Figure 7.7-5 show the error responses of the on-axis pitch frequency responses between the linearized stitched model and the anchor point models at hover and 17 kn, respectively. There is near-perfect agreement for hover ($J = 3.75$). There is very good agreement at 17 kn ($J = 51.7$); the slight disparity at low frequency is due to small differences in the values of the speed derivatives. However, the response is well within the MUAD bounds, and perfect agreement is realized around crossover frequency $\omega_c \geq 18$ rad/sec.

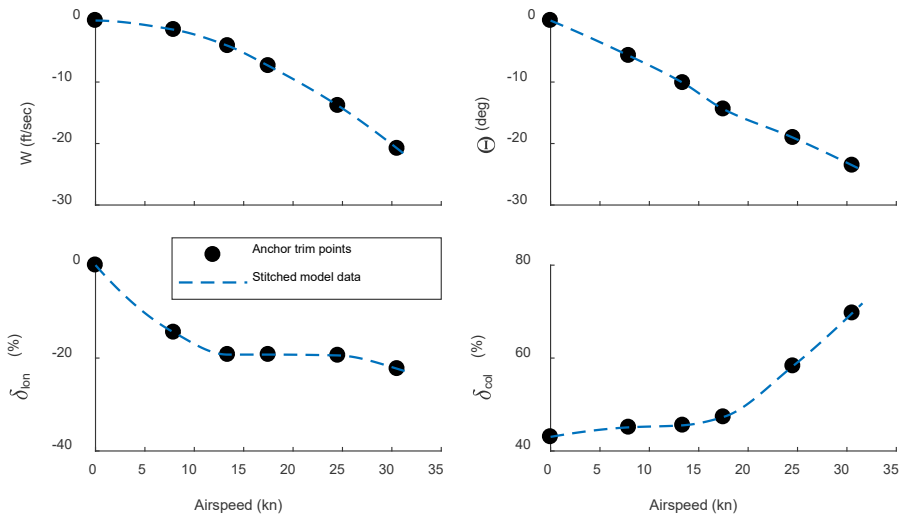

Figure 7.7-3: Variation in Trim States and Controls Over the Full Airspeed Range.

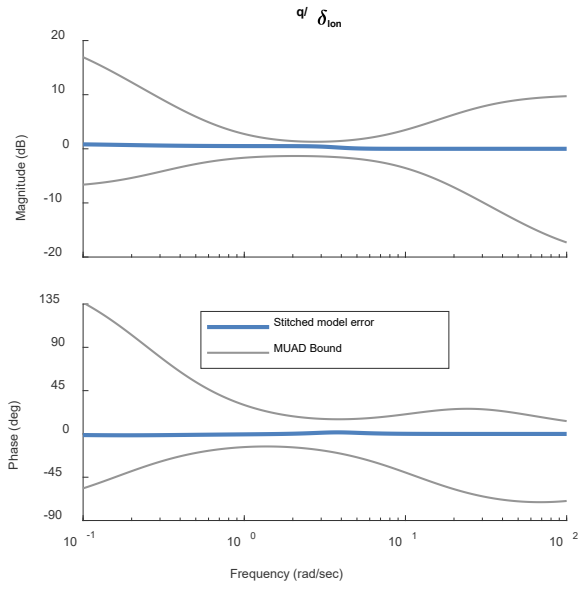

Figure 7.7-4: Dynamic Response Verification, Hover (J = 3.75).

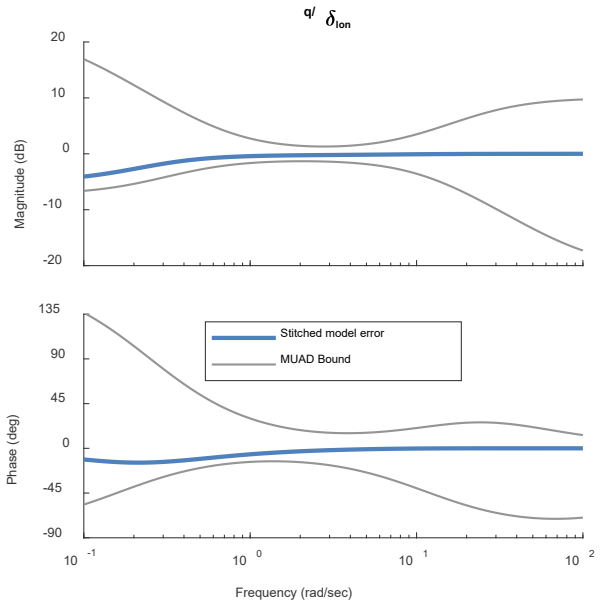

Figure 7.7-5: Dynamic Response Verification, 17 kn (J = 51.7).

7.7.2.3.3 Interpolation for Airspeed

The dynamic response of the stitched model at a mid-airspeed point of 10 kn was verified. As truth data, frequency sweeps were performed in flight at 10 kn to generate truth frequency responses. The stitched model, configured only with the two anchor point models at hover and 17 kn, was re-trimmed and re-linearized for the 10-kn flight condition in simulation; this requires interpolation of the stability and control derivatives. Figure 7.7-6 shows the pitch-rate response to longitudinal stick comparison of the stitched model for the interpolated airspeed of 10 kn (blue dashed line) against the truth 10-kn response from flight (black solid line). The responses of the anchor point models at hover and 17 kn are included in the figure for context.

Two key conclusions are obtained from these comparisons: 1) The quadcopter's dynamic responses at hover, 10 kn, and 17 kn are appreciably different; and 2) The stitched model, configured only with the anchor point models at hover and 17 kn, when linearized at 10 kn has a response that agrees with the truth 10-kn response from flight. This confirms that the IRIS+ bare-airframe dynamics are well characterized by two-point models, and that the stitched model accurately predicts the dynamics by interpolation at a mid-airspeed condition. The stitched model interpolates continuously in real-time simulation, so accurate dynamics are realized over the full airspeed range.

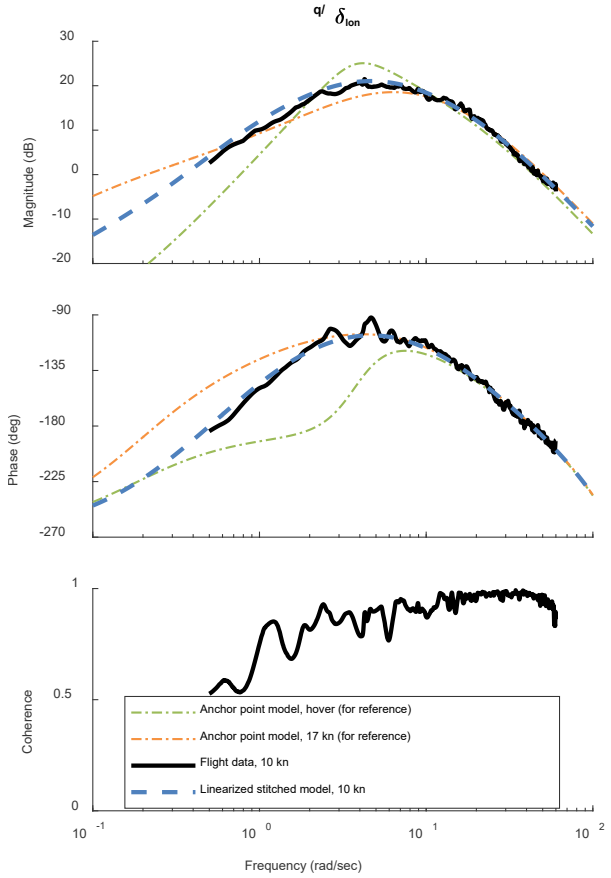

Figure 7.7-6: Interpolation for Airspeed Compared to Truth 10-kn Pitch-Rate Response from Flight.

7.7.2.3.4 Extrapolation for Loading Configuration

The effects of the quadcopter carrying an external payload on trim and dynamic response were investigated. A heavy loading configuration was arranged by attaching a 200-gram (0.441-lb) mass to the underside of the IRIS+ fuselage (see Figure 7.7-1), which increased the total weight from 3.168 to 3.609 lbs. The mass was attached 2 inches below, 1 inch left, and 0.5 inches forward of the vehicle's CG, which shifted the overall CG 0.275 inches down and slightly forward/left, based on a simple calculation of the mass center. Inertia values for a nominally configured IRIS+ (see Tischler et al. [2] Section 6.8) were used as simulation values for the nominal configuration. For the heavy configuration, the added 200-gram mass increased roll inertia I_{xx} and pitch inertia I_{yy} by 3% and 6%, respectively.

To verify the stitched model's ability to simulate for the off-nominal loading configuration, the simulation values of weight, inertia, and CG offset were set to those of the heavy loading. The stitched model,

containing only the nominal anchor point data, was then re-trimmed in simulation for the heavy loading over the full airspeed range from hover to 32 kn. Flight-test data of the heavy configuration were collected for use as truth data only. The nominal and heavy trim data comparison results are shown in Figure 7.7-7. The anchor trim points (black solid markers) and the corresponding stitched model data for the nominal loading (blue dashed lines) are repeated from those shown previously in Figure 7.7-3 for reference. The trim results of the stitched model as re-trimmed (i.e., extrapolated) to the heavy loading are shown by the magenta dashed lines. Lastly, the truth trim points for the heavy loading configuration, as obtained from flight, are shown by the red triangle markers.

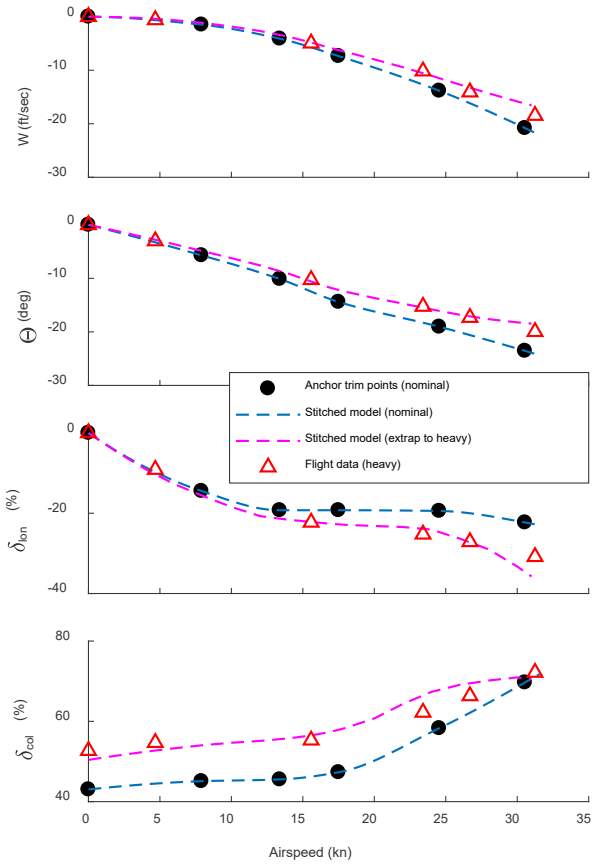

Figure 7.7-7: Extrapolation for Heavy Loading Compared to Truth Heavy Trim Data from Flight.

There is excellent agreement between the extrapolated stitched model results and truth heavy trim data. The increased trim angle of attack (analogous to W) and trim pitch attitude, Θ, in forward flight for the heavy loading are well predicted by the stitched model. Trim longitudinal stick, δ_{lon}, is also well predicted. The increased trim collective, δ_{col}, necessary for hover and level forward flight of the heavy configuration is well extrapolated. See Tobias et al. [3] for more discussion and results, including the dynamic response of the stitched model configured for the heavy loading as verified against the truth response of the heavy loading configuration from flight.

7.7.2.4 Flight-Test Implications for Development of Small-Scale Multi-Rotor Stitched Models

Flight-test recommendations for future development of stitched models involving small-scale multi-rotor vehicles are presented below, based on the IRIS+ results covered in this section.

Trim Data: Finely-spaced level trim data covering the entire airspeed envelope should be collected for use as anchor trim data in the stitched model. These trim data must include the trim values of the states and controls as a function of *x*-body airspeed *U* for 'stitching in *U*.' Due to the smooth trends in trim data over the airspeed range for the IRIS+, six trim points, spaced approximately every 6 kn, adequately covered the full airspeed range from hover to about 32 kn. A spacing of approximately 5 – 7 kn is therefore recommended for the collection of trim data.

Point Models: Frequency sweeps should be performed at hover and forward flight for the identification of state-space anchor point models. Airspeed will naturally tend to vary about the trim condition during the frequency sweep; a variation of approximately ±5 kn was observed during the frequency sweep data collection on the IRIS+. Furthermore, the identified linear point models will be accurate over some minimum range of airspeed (approximately ±10-kn accuracy was realized for the IRIS+ point models, as presented in this section). Therefore, it is recommended that the identification of anchor point models be performed at a spacing of 15 – 20 kn for small-scale multi-rotor vehicles.

In summary, two flight-identified point models were found to adequately and accurately capture the bare-airframe dynamics of the IRIS+ over its full airspeed envelope: one point model at hover, valid up to about 10 kn, and one point model at 17 kn, valid from about 10 – 30 kn (30 kn is the approximate maximum airspeed of the IRIS+). However, the spacing of the anchor point models depends on the size of the vehicle (according to the Froude scaling relationship for velocity [3], [4]) and the complexity of the rotor configuration.

7.7.2.5 Conclusions

A full-envelope stitched simulation model of a quadcopter was developed using two flight-identified models of the IRIS+ and finely-spaced trim data. The following conclusions were determined:

1) Forward-flight dynamics are appreciably different than the dynamics in hover for the IRIS+.
2) Two flight-identified point models (at hover and 17 kn), plus some finely-spaced trim data, are shown to adequately and accurately capture the IRIS+ bare-airframe dynamics over its nominal flight envelope.
3) The stitched model accurately predicts the dynamics at a mid-airspeed condition of 10 kn by interpolation of the stability and control derivatives, as verified by a truth response from flight.
4) The stitched model's extrapolation for off-nominal loading configuration is very accurate. Therefore, flight testing may be conducted with a nominally loaded UAS only.

7.7.3 Bell 412

This section presents the development and verification of a continuous, full-envelope stitched simulation model of a helicopter using discrete flight-identified models of the Bell 412 helicopter and the NRC Aerospace's process of regressing and stitching the point model stability and control derivatives from different flight conditions. Thirty-two flight-identified point models (spanning from hover to 120 kn forward flight with various climbs and descents) were used to develop the bare-airframe dynamics of the Bell 412 nominal flight envelope. The final stitched simulation model is verified against the FAA Part 60 [5] Level D standard for helicopters.

7.7.3.1 Model Stitching Process

For the development of a Level D flight simulator and simulation model, a continuous full-envelope stitched model of a helicopter is needed. The stitched model allows a smooth interpolation between available point models, so the behavior of the helicopter can be simulated even if a point model near a particular configuration or trim point is not readily available.

The helicopter's small-perturbation stability and control derivatives were determined at different helicopter configurations and trim conditions. A continuous full-envelope model was developed by regressing and stitching the point model stability and control derivatives from different configurations and trim points against the corresponding averaged trim states and flight conditions. These trim states and flight conditions were determined by averaging two to five seconds of trim data prior to the start of each 2-3-1-1 maneuver. An automatic linear interpolation software was used to combine the derivatives into a smooth function across the operating points.

7.7.3.2 Flight-Identified Point Models of the Bell 412

NRC's Advanced Systems Research Aircraft (ASRA) Bell 412 HP (Tischler et al. [2], Section 6.1), was used for this project. The database of collected flight-test data consists of test points flown in a wide variety of steady-state conditions throughout the aircraft's flight envelope, as well as low-speed dynamic maneuvers. Test points included hover, forward flight to VNE, climbs, descents, autorotative descents, coordinated turns up to 45 degrees of bank, steady sideslips, and a selection of ADS-33 maneuvers. Additionally, a set of aircraft modeling data suitable for use in system identification was collected. This included frequency sweeps and 2-3-1-1s in hover and at 30, 60, 90, and 120 kn, and 2-3-1-1s in climbs and descents.

The measured data for the linear accelerometers and air data sensors were first transformed to the position of the CG. The air data was further corrected for time delays in angle of attack, sideslip angle, and airspeed. These time delays are caused by the pitot-static system used for air data measurement. The numerical values for the delays were determined by correlation analysis. Inertial data were measured using a Honeywell IMU HG1700, which is integrated with Kalman filtering. After this combination, the unit results in a high-quality inertial Attitude and Heading Reference System (AHRS). A compatibility check performed on the inertial data showed that the rates and attitudes were fully compatible without any corrections.

For the identification, a 6-DOF model structure was implemented with the following input, state, and output variables [6]:

$$\begin{aligned} u^{\mathrm{T}} &= \left[\delta_{\mathrm{lon}}, \delta_{\mathrm{lat}}, \delta_{\mathrm{ped}}, \delta_{\mathrm{col}}, \phi, \theta\right] \\ x^{\mathrm{T}} &= \left[u, v, w, p, q, r\right] \\ y^{\mathrm{T}} &= \left[u, v, w, p, q, r, a_x, a_y, a_z\right] \end{aligned} \tag{7.7-1}$$

The method uses roll angle, ϕ, and pitch angle, θ, as pseudo-controls. The NRC Aerospace's Modified Maximum Likelihood Estimation (MMLE) technique [7] was performed for quick point model identification. With this approach, 60 stability and control derivatives were computed, and the corresponding point models were identified. The point models describe the small-perturbation dynamics of the helicopter around each specific trim flight condition and configuration.

7.7.3.3 Stitched Simulation Model of the Bell 412

The stitched model was developed to satisfy Level D requirements. The identified point models for the various flight conditions are stitched together to arrive at a full-envelope model.

7.7.3.3.1 Interpolation of the Derivatives

For the Bell 412, a linear relationship between the stability and control derivatives and advance ratio was found. Figure 7.7-8 shows the corresponding regression of one of the 60 derivatives as an example, namely the $Z_{\delta_{col}}$ derivative, versus advance ratio.

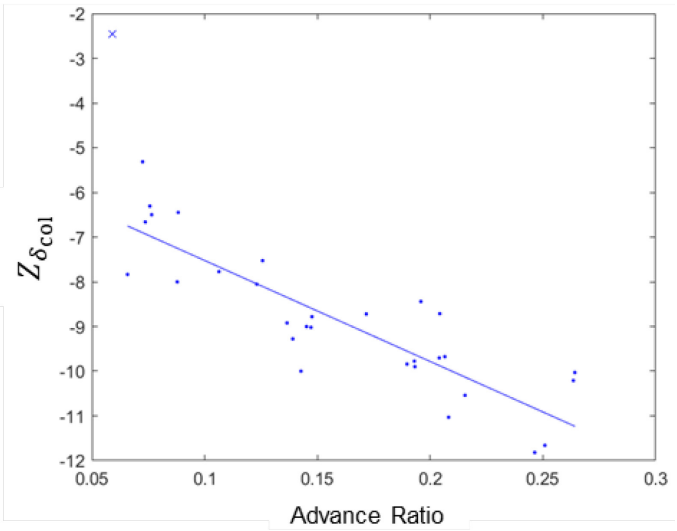

Figure 7.7-8: Regression of $Z_{\delta_{col}}$ vs Advance Ratio.

With additional flight data, machine learning can be used to identify patterns in the plots and generate additional equations. This allows for enhanced modeling accuracy during simulation and can produce better matches with respect to flight data.

7.7.3.3.2 Naught Terms Interpolation

Using trim data of the states and controls, a naught (zero) term model is developed by determining the difference between the measured and calculated values for each of the six forces and moments $(X_0, Y_0, Z_0, L_0, M_0, N_0)$. Naught terms allow the model to account for trim data measurement errors and capture any missing aircraft responses. For example, the longitudinal force naught term is determined as follows:

$$\begin{aligned} X_{\text{calculated}} &= X_u u + X_v v + X_w w + X_p p + X_q q + X_r r + X_{\delta_{\text{lon}}}\delta_{\text{lon}} + X_{\delta_{\text{lat}}}\delta_{\text{lat}} \\ &\quad + X_{\delta_{\text{col}}}\delta_{\text{col}} + X_{\delta_{\text{ped}}}\delta_{\text{ped}} \\ X_0 &= X_{\text{measured}} - X_{\text{calculated}} \end{aligned} \tag{7.7-2}$$

The measured values for the forces are determined from the linear accelerations whereas the measured values for the moments are calculated from the angular accelerations. The naught terms were determined for each flight condition to produce a continuous naught term model. For the Bell 412, the naught terms were regressed against advanced ratio only [6]; see Figure 7.7-9 for an example.

7.7.3.3.3 Higher-Order Dynamics Optimization

Higher-order dynamics optimization can be used to identify cross-axis and higher-order dynamics data. This process was shown to minimize the residual between the stitched model's calculated and measured force and moment components for unique maneuver time histories in Hui, et al. [8]. Additionally, nonlinear dynamics, including edge-of-the-flight-envelope maneuvers (e.g., run up and down the runway, autorotation, and many other large amplitude maneuvers), ground effect, etc. can be modeled and included in the stitched model. Lastly, known helicopter configuration parameters (CG, weight, longitudinal/lateral flap, altitude, etc.) can be used to identify patterns in the small-perturbation stability and control derivatives and appended to the standard flight envelope to produce a full flight model; this allows the modeling of helicopter responses outside of the small-perturbation domain.

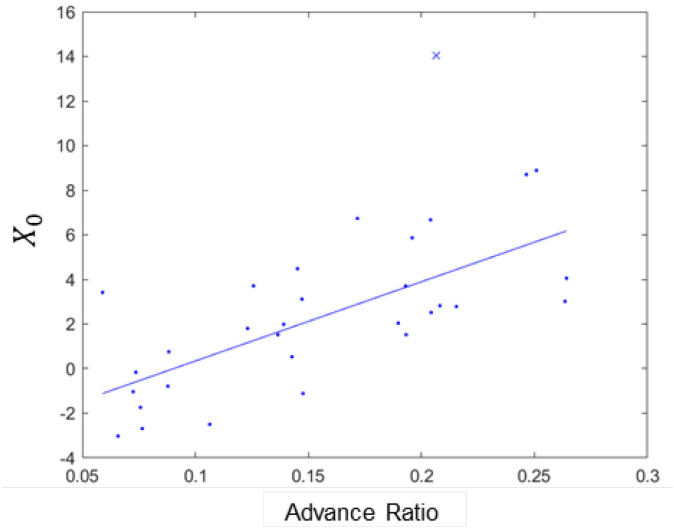

Figure 7.7-9: Regression of Longitudinal Force Naught Term.

7.7.3.3.4 Full Flight-Envelope Model Verification

The stitched model underwent a two-step verification process. For the first verification step, the preliminary stitched model was used to compute all the state and control derivatives that were fixed in MMLE to obtain the model response compared with the raw data as a quick and straightforward process. Additionally, a simulation was used to verify the stitched model by computing the state and control derivatives and the naught terms at each time step.

As the final verification step, Proof of Match (PoM) of the aerodynamic models was conducted to verify the accuracy of the stitched simulation model. This process ensures that the aerodynamic model is verified to the FAA's Part 60 Helicopter Simulator Qualification Guidelines [5]. Initial conditions for the simulation were obtained from the first trim point. A trim function is also applied, which could result in a small change to the initial conditions. Figure 7.7-10 shows an example for such a POM plot. The simulation model response (blue dashed lines) is plotted against the flight data (yellow solid lines) with FAA tolerances (red dash-dot bounds) included; if the model stays within the FAA tolerances, the model is considered verified. An optimization algorithm was developed for an automatic POM process, otherwise POM is time consuming.

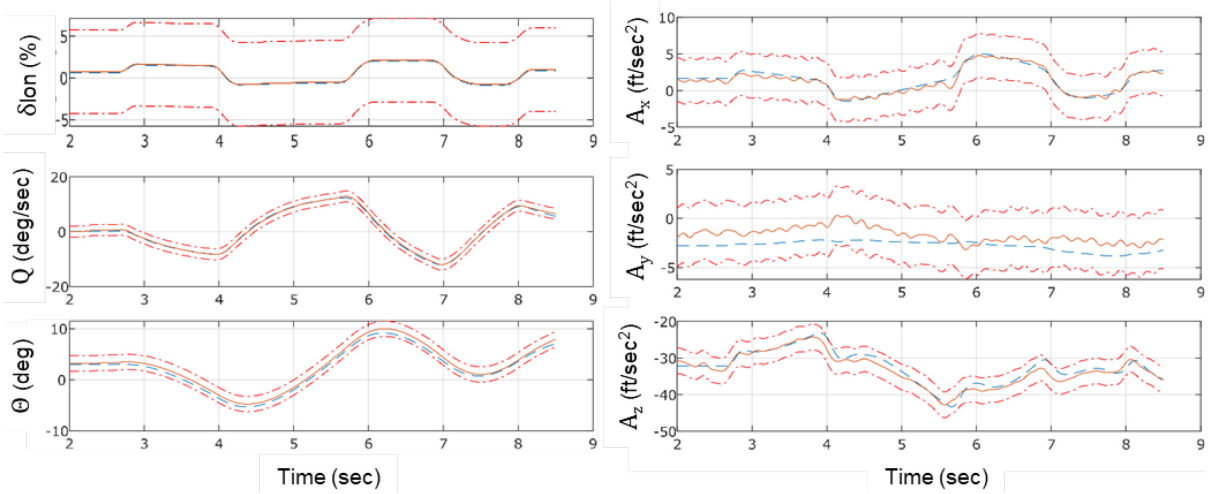

Figure 7.7-10: Proof of Match (PoM) of Stitched Model.

7.7.3.4 Conclusions

Application of the helicopter aerodynamic stitched modeling technique to develop a full-envelope mathematical model of the Bell 412 helicopter demonstrated the following:

1) The MMLE method provides quick and effective point model identification. With this approach, 60 stability and control derivatives describing the Bell 412's dynamics were determined automatically.
2) The helicopter stitched model development process is practical. A continuous aerodynamic model spanning the full flight envelope of the Bell 412 was developed.
3) The POM process ensures that the aerodynamic stitched model is verified to the FAA's Part 60 Helicopter Simulator Qualification Guidelines to satisfy Level D requirements.

7.7.4 EC135

The EC135 stitched model is based on linear operating point models derived from system identification. Stitching allows a continuous wide-envelope simulation of the EC135 based on just five anchor point models. Extrapolation of mass- and CG-variations of the ACT/FHS (Tischler et al. [2], Section 6.3) was not applied due to payload restrictions when flying with the experimental computer system. The stitched model is used for flight control design and for engineering simulators at the DLR.

7.7.4.1 Models and Data

System identification has been applied to flight-test data of the EC135 at five operating points, i.e., hover up to 120 kn in increments of 30 kn. The resulting high-order 11-DOF models have 15 states including rigid body states, regressive blade flapping, regressive lead-lag, and mean inflow. Trim curves for the roll and pitch attitudes and stick inputs, were extracted from trim flights that were conducted in addition to the system identification flights. The trim points were extracted on a fine grid to better approximate the trim gradients, as shown in Figure 7.7-11. For the EC135, trim flights are challenging for airspeeds between 20 kn and 35 kn, so the approximated trim gradients in this region are smoothed out.

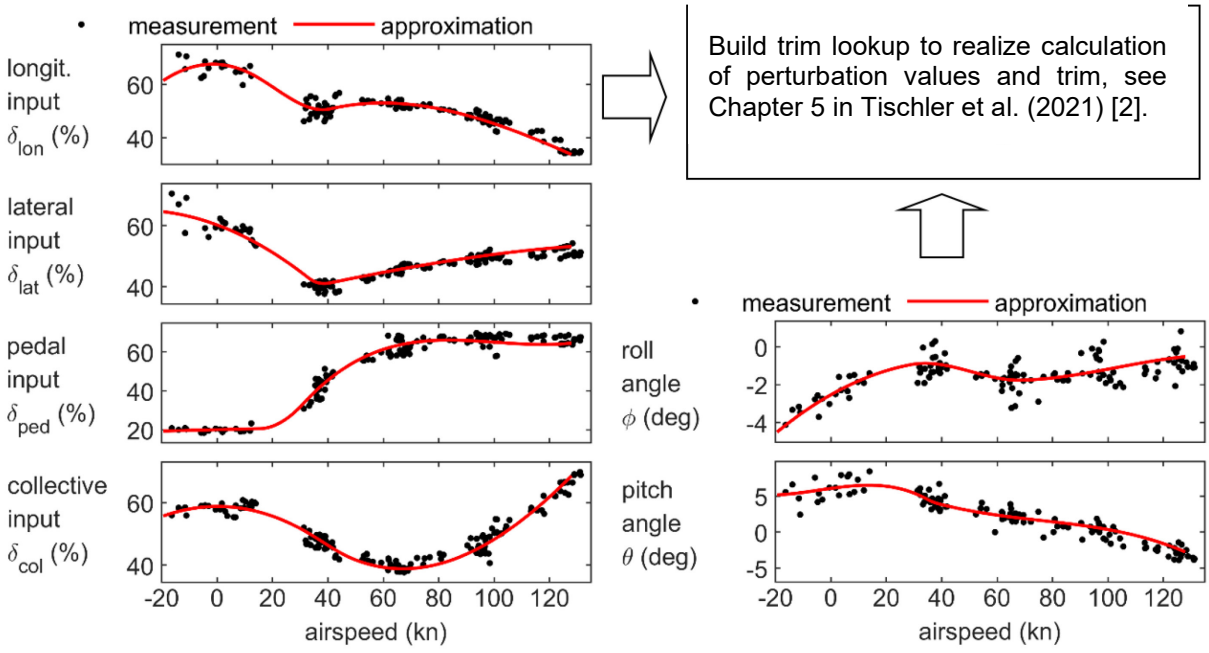

Figure 7.7-11: Trim Data of the ACT/FHS and Approximated Trim Curves.

7.7.4.2 Application of the Stitching Architecture

The model stitching architecture is applied to EC135 ACT/FHS trim data and anchor point models. The identified models for the different operating points have limited validity. If airspeed changes significantly, another operating point model is needed. As presented in Tischler et al. [2], stitching smoothly combines all given anchor point models. Known kinematic relationships such as the transformation of the gravity force into the body-fixed coordinate system, Euler attitudes, inertia, and helicopter mass are included in their nonlinear form. The vectors of trim controls and states, as well as the stability and control matrices, are interpolated smoothly with respect to the simulated forward speed.

At each of the five operating points, the linearized stitched model is identical to the original anchor point model, as shown in Figure 7.7-12. The red dashed curve shows the anchor point model, and the blue curve represents the linearized transfer function of the stitched model. Both curves are identical as the speed derivatives are preserved explicitly, and the trim state vector is low-pass filtered. Forward speed drives the table lookup for stability and control derivatives of the stitched model so that flight dynamics are interpolated between the anchor points. Small deviations of the forward speed such as those that occur during lateral stick inputs do not result in significant change in flight dynamics. The multi-step input shows that the stitched and linear operating point models are almost identical. The mean RMS between anchor point and stitched model responses for all multi-step inputs in all axes at 60 kn is 0.52 and in hover is 0.47; the integrated frequency cost is zero at the anchor points. The stitched model dynamics are indistinguishable from system identification results in the frequency domain. The verification of the multi-steps in the time domain shows good agreement and differ most if forward speed variations are present (e.g., for longitudinal inputs).

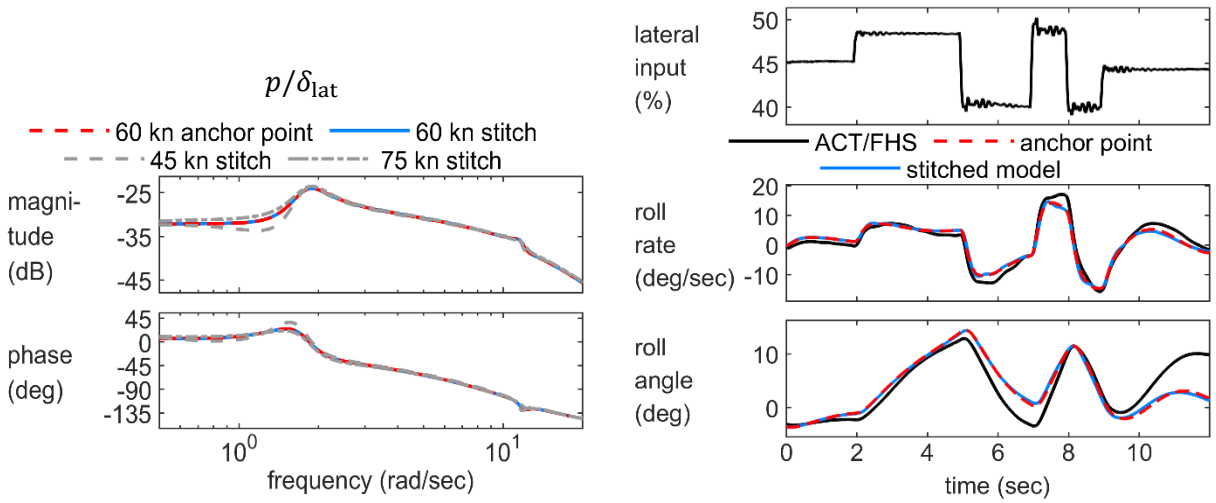

Figure 7.7-12: Comparison of Linear Point Model and Stitched Model at 60 kn for Lateral Inputs.

Another desired property of the stitched model is smooth eigenvalue transition between the operating points. It has been observed that smooth eigenvalue transition is achieved by piecewise cubic spline interpolation of the anchor point models. This means that first the derivatives of the anchor point models are interpolated, and then the linearized effect of nonlinear kinematic terms and trim gradients are subtracted from the interpolated matrices. The resulting matrices form the control and stability lookup to calculate the matrix-vector products. The respective eigenvalues and their transition are shown in Figure 7.7-13. The path of the eigenvalues looks consistent and supports the application of the stitched model for maneuvering flight.

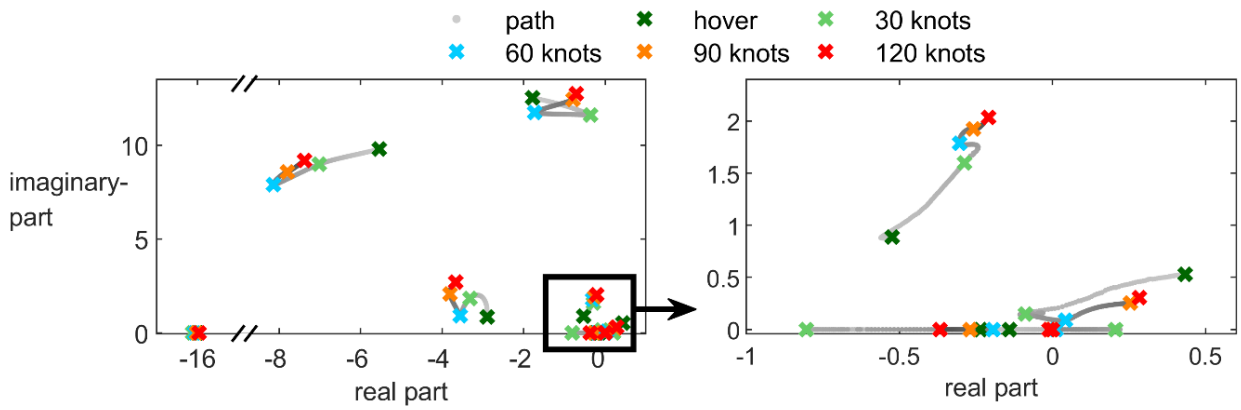

Figure 7.7-13: Eigenvalues of the ACT/FHS Models and their Transition.

7.7.4.3 Maneuvering Flight

One benefit of the stitching architecture is its ability to simulate maneuvering flight. To match the maneuver flight data as well as possible, the filter time constant (⑩ in Figure 5.7-1 in Tischler et al. [2]) should be adjusted based on the flight data. For the EC135 ACT/FHS, the filter time constant was set to $T_f = 15$ sec.

Figure 7.7-14 shows the results obtained for a deceleration-acceleration maneuver that covers a wide airspeed range. As this type of maneuver has a duration of 2 minutes, unstable modes such as the phugoid mode need to be stabilized. A flight controller minimizing attitude and speed errors is used to stabilize the simulation. The simulated control input is the sum of the measured control and the feedback signal and therefore deviates from the measured control input. The blue curve is the simulated response using the 60 kn anchor point model. For this maneuver, the stick input of the linear point model has to be adjusted significantly to obtain a good match for the attitude and forward speed. The two stick input signals deviate mainly between 50 and 80 sec where the 60 kn linear point model is used for small forward-speeds near hover. The red curves represent the responses for the stitched model. Compared to the linear model, the stitched model shows a better match of the longitudinal stick position and the pitch attitude, which originates primarily from the interpolation of the trim vectors. As expected, the stitched model achieves a good approximation of maneuvering flight data.

7.7.4.4 Combination with Update Method 2 “Black Box”

For the ACT/FHS, further improvements were achieved by augmenting the stitched model with an input filter, i.e., by combining the methods of Sections 5.2 and 5.7 in Tischler et al. [2]. As only one input filter correction for all airspeeds was determined, it is an averaged filter that corrects/mitigates major deficiencies observed at all anchor points. Using one filter for all airspeeds enables the black box input filter to be added just to the stitched model simulation. The stitched model’s dynamics are identical to those of the anchor points which further streamlines the direct application of black box transfer functions (Method 2) to stitched model results (Method 7). Figure 7.7-15 shows the result of maneuvering flight with the updated stitched model. The qualitative signal trend of the stick input is slightly improved compared to Figure 7.7-14 while the high fidelity of the states is maintained.

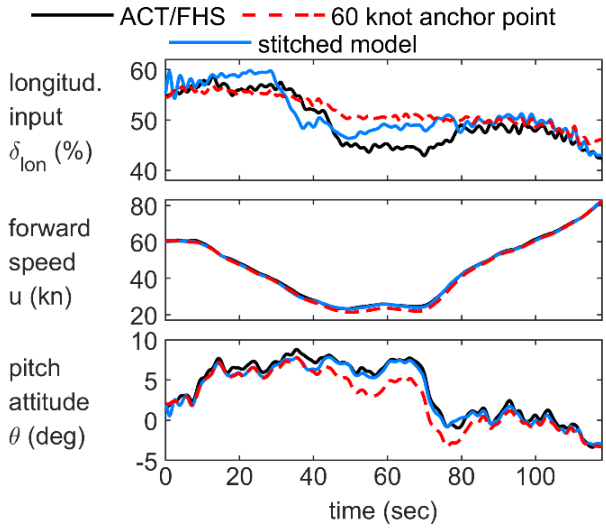

Figure 7.7-14: Comparison of Linear Point Model (60 kn) and Stitched Model for a Deceleration-Acceleration Maneuver.

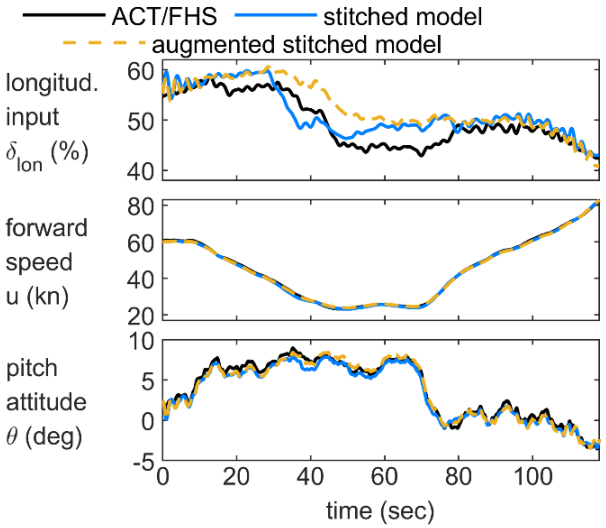

Figure 7.7-15: Comparison of the Stitched Model (with and Without Input Filter Augmentation) and Flight-Test Data.

7.7.4.5 Fidelity Metrics

Fidelity is assessed using the RMS in the time domain and by showing MUAD boundary plots for selected on-axis frequency responses. Table 7.7-1 lists the RMS values of the hover and 60 kn forward flight case. As expected, the mean RMS value of the anchor point model and stitched model is almost the same. In the case of maneuvering flight as shown in Figure 7.7-14, the stitched model achieves a much better agreement for the accel/decel maneuver; the RMS reduces from 1.08 to 0.89. In addition, the feedback controller inputs (needed for stabilization) are smaller in the case of the stitched model; the mean RMS of all four control inputs is 4.74.

Table 7.7-1: RMS Cost for Stitched Model and Augmented Model Compared to Flight-Test Data (Stitched Model Matches Almost Perfectly the Baseline Anchor Point Model).

		RMS of the Output Signals	RMS of the Control Signals
hover	anchor point model	1.47	-
	stitched model	1.46	-
	augmented stitched model	1.29	-
60 kn	anchor point model	1.78	-
	stitched model	1.70	-
	augmented stitched model	1.71	-
maneuver	anchor point model	1.08	10.99
	stitched model	0.89	4.74
	augmented stitched model	0.75	5.20

Additionally, the fidelity is assessed for the augmented stitched model. In the time domain, the input filter only achieves slightly better results. As this filter was designed to respect model deficiencies at higher frequencies between 5 to 40 rad/sec (covering the effect of engine dynamics and flexible modes), the effect of the filter on time-domain responses can hardly be revealed using the RMS. Clearly, the frequency domain is better suited to show the effect of the black box input filter. Figure 7.7-16 and Figure 7.7-17 show two Maximum Unnoticeable Added Dynamics (MUAD) boundary plots for the longitudinal and pedal on-axis in forward flight and hover, respectively. In both cases, the augmented simulation better fits the MUAD boundary. These results can be even further improved if the black box input filter is extracted for each anchor point individually.

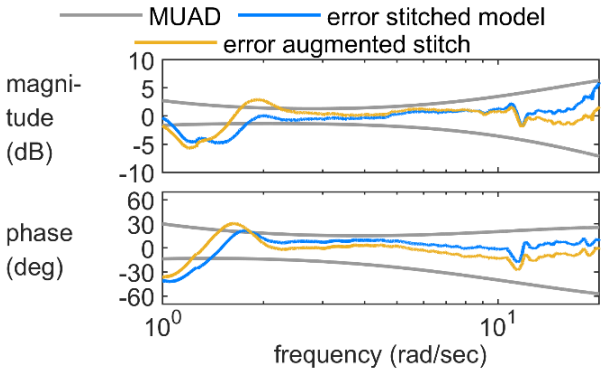

Figure 7.7-16: MUAD Plot for the Longitudinal On-Axis (q/δ_{lon}) at 60 kn Forward Flight.

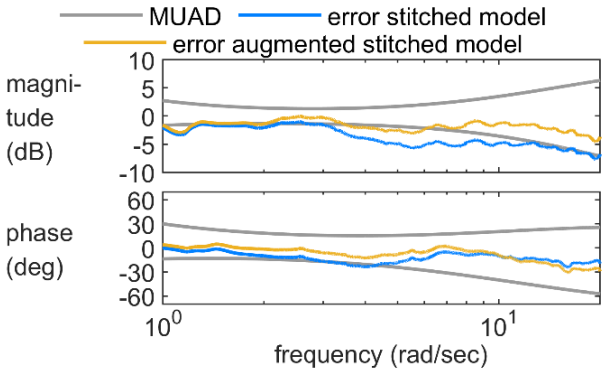

Figure 7.7-17: MUAD plot for the Directional On-Axis (r/δ_{ped}) in Hover.

7.7.4.6 Conclusions

A wide-envelope EC135 simulation model was developed based on five anchor point models and trim data. The following conclusions were determined:

1) Cubic spline interpolation of the derivatives leads to the best and smoothest eigenvalue transitions.
2) Dynamics of the anchor point models are exactly retained by the stitched model.
3) The EC135 stitched model was updated by Method 2 (Black Box) to improve its fidelity.

7.7.5 Summary and Overall Conclusions

Four applications of the model stitching technique were presented. In each case, a collection of discrete linear models and trim data were used to generate a stitched simulation model and were shown to adequately and accurately cover the nominal flight envelope. Additionally, extrapolation methods were shown to accurately simulate off-nominal loading configurations. The following overall conclusions were determined:

1) The model stitching method provides a quasi-nonlinear, time-varying simulation model from individual linear models and trim data for discrete flight conditions that is accurate for flight dynamics and control applications over the operational envelope, with good accuracy maintained in the frequency and time domains.
2) Interpolation of the anchor trim data and point model derivatives is important to capture the trends over the flight envelope of interest. Shape-preserving piecewise cubic interpolation performed on the anchor trim data produces smooth, finely-spaced data over the full flight envelope for use in the stitched model. Linear interpolation and piecewise cubic interpolation were both found to adequately capture the stability and control derivatives.

3) Accurate simulation of off-nominal loading configuration (e.g., variations in weight and CG) is accomplished by extrapolation methods in the model stitching simulation architecture. The off-nominal extrapolation necessitates only point models and trim data of the baseline aircraft loading configuration to be included in the stitched model, which significantly reduces required flight-test points and associated flight costs.

7.7.6 References

[1] Tobias, E.L., and Tischler, M.B. (2016), "A Model Stitching Architecture for Continuous Full Flight-Envelope Simulation of Fixed-Wing Aircraft and Rotorcraft from Discrete-Point Linear Models," U.S. Army AMRDEC Special Report RDMR-AF-16-01, April.

[2] Tischler, M.B., White, M.D., Cameron, N., D'Agosto, S., Greiser, S., Gubbels, A., Guner, F., He, C., Horn, J., Hui., K., Jones, M., Juhasz, O., Lee, O., Lehmann, R., Miller, D., Myrand-Lapierre, V., Nadeau-Beaulieu, M., Nadell, S., Padfield, G., Pavel, M., Prasad, J., Ragazzi, A., Richard, S., Scepanovic, P., Seher-Weiß, S., Soong, J., Stroosma, O., Taghizad, A., Tobias, E., Xin, H., and Yavrucuk, I. (2021), "Rotorcraft Flight Simulation Model Fidelity Improvement and Assessment," NATO STO AVT-296 Technical Report.

[3] Tobias, E.L., Sanders, F.C., and Tischler, M.B. (2018), "Full-Envelope Stitched Simulation Model of a Quadcopter Using STITCH," American Helicopter Society 74th Annual Forum, Phoenix, AZ, USA, May.

[4] Ivler, C.M., Rowe, E.S., Martin, J., Lopez, M.J., and Tischler, M.B. (2019), "System Identification Guidance for Multirotor Aircraft: Dynamic Scaling and Test Techniques," Vertical Flight Society 75th Annual Forum, Philadelphia, PA, USA, May.

[5] FAA (2016), "Federal Aviation Administration," National Simulator Program, 14 CFR Part 60, 2016.

[6] Seher-Weiß, S., Greiser, S., Wartmann, J., Myrand-Lapierre, V., Gubbels, A., Ricciardi, J., and Hui, K. (2019), "Bell 412 System Identification: Comparing Methods and Tools," VFS 75th Annual Forum & Technology Display, Philadelphia, PA, USA, May.

[7] Leeuw, J.H. de, and Hui, K. (1989), "The Application of Linear Maximum Likelihood Estimation of Aerodynamic Derivatives for the Bell-205 and Bell-206," *Vertica*, Vol. 13, Issue 3, pp. 403-412, January.

[8] Hui, K., Lambert, E., and Seto, J. (2006), "Bell M427 Flight Test Data Gathering and Level-D Simulator Model Development," ICAS 25th Congress, Hamburg, Germany, September.

Chapter 7.8 – PERCEPTUAL FIDELITY ASSESSMENT BASED ON THE SFR SCALE: BELL 412

ABSTRACT

Previous research has highlighted the need to develop new objective and subjective metrics for fidelity assessments of rotorcraft flight training simulators. This Chapter provides an overview of the development of such metrics and their application to the fidelity assessment of the University of Liverpool's flight simulator which was configured to be representative of the National Research Council's (Canada) Bell 412 helicopter.

7.8.1 Simulator Fidelity Rating Scale Background

The Group for Aeronautical Research and Technology in Europe (GARTEUR) Action Group (AG) HC/AG-12 was formed to conduct a critical examination of the simulator standard, JAR-STD 1H [1], (replaced by EASA CS-FSTD(H) [2] in 2012). One of AG12's recommendations [3] was that additional research was required to bridge the gap between pilot subjective opinion and the quantified metrics, and it highlighted the importance of developing an objective means for assessing overall fidelity.

Research addressing the AG-12 recommendations to develop a method for the subjective assessment of simulator fidelity and the formulation of new objective metrics was undertaken at the University of Liverpool. Working in collaboration with the National Research Council's (NRC) Flight Research Laboratory, the Simulator Fidelity Rating (SFR) scale (Figure 7.8-1) was developed to provide a method for an evaluating pilot to rate the suitability of the overall simulation for a specified task [4]. The pilot is asked to compare the level of performance attained in flight and simulator, and to judge the level of 'adaptation' of task control strategy used in flight compared with simulation. New objective fidelity metrics [5] were also developed in the AG-12 follow-on research, based on ADS-33E-PRF HQ parameters [6].

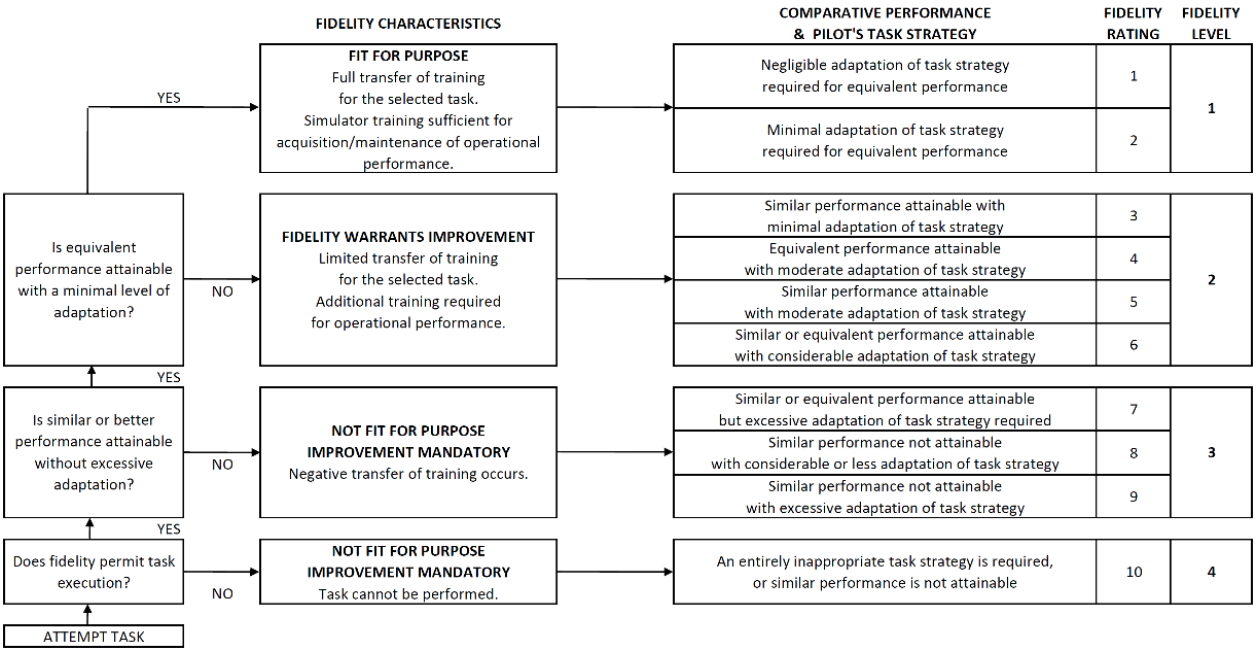

Figure 7.8-1: Simulator Fidelity Rating Scale.

The SFR scale has been designed to evaluate a simulator on a task-by-task basis. Consequently, where fidelity defines fitness for purpose, a collection of ratings for various Mission Task Elements (MTE) would define the boundaries of positive training transfer for a given simulator.

The first definition that must be made prior to the commencement of fidelity assessment with the SFR scale is that of the purpose of the simulator. The purpose describes the range of tasks to be flown using the simulator and hence, the scope of the SFR evaluations. Each task identified in this step would be assessed on an individual basis; the results for each task would then be used to create a 'usage envelope,' within which the simulator may be effectively (and safely) employed.

The SFR scale employs several key concepts that are considered fundamental to the utility of a simulation device. They are as follows:

- Transfer of Training (ToT) – the degree to which behaviors learned in a simulator are appropriate to flight.
- Comparative Task Performance (CTP) – comparison of the precision with which a task is completed in flight and simulator.
- Task Strategy Adaptation (TSA) – the degree to which the pilot is required to modify their behaviors when transferring from simulator to flight and vice versa.

In the context of a training simulator, the definition of the levels of fidelity has been made relative to the Transfer of Training (ToT) that occurs when a pilot transitions between the simulator and the aircraft. It should be noted that in assigning the level of fidelity, the evaluating pilot is being asked to make a subjective judgement on the degree of ToT that is likely to take place. For the SFR scale, the definition of the four levels of fidelity depends on the objective of the training. Three types of simulation training have been defined – skills acquisition, skills development, and skills assessment, where acquisition and development would correspond to the processes of initial training and recurrent training, respectively. For skills acquisition, the levels have been defined as follows:

- Level 1 fidelity: Simulation training is sufficient to allow operational performance to be attained with minimal pilot adaptation. There is complete ToT from the simulator to the aircraft in this task.
- Level 2 fidelity: Additional training in the aircraft would be required in order to achieve an operational level of performance. There is limited positive ToT from the simulator to the aircraft in this task but no negative ToT.
- Level 3 fidelity: Negative ToT occurs (i.e., the pilot learns an inappropriate technique), and the simulator is not suitable for training to fly the aircraft in this task.

Similarly, the levels for skills development have been defined as:

- Level 1 fidelity: Simulation training is sufficient to restore previous performance capabilities.
- Level 2 fidelity: Simulation training provides limited improved performance capability. Additional training is required.
- Level 3 fidelity: No positive ToT occurs. The simulator is unsuitable for training.

And the levels for skills assessment are defined as:

- Level 1 fidelity: Simulation is sufficient to comprehensively demonstrate skills associated with qualified performance.
- Level 2 fidelity: Performance in the simulator demonstrates limited elements of the required skills.
- Level 3 fidelity: Performance in the simulator does not serve to demonstrate the required skills.

Please note that in each of these cases, a Level 4 fidelity rating indicates that it is not even possible to complete the task using the simulator.

The task may be defined as the training maneuver/procedure, accompanied by a set of performance requirements and environmental conditions. In an HQR evaluation, an MTE specification consists of the target maneuver profile alongside a set of 'desired' and 'adequate' performance tolerances for each element of the maneuver profile (height, airspeed, heading, etc.), where the achievement of a certain category of performance assists the pilot with determining the level of handling qualities of the aircraft. The same style of task definition is adopted for an SFR evaluation. The comparison of the achieved level of performance between flight and simulator assists the evaluating pilot with the judgement of comparative performance. The three levels of comparative performance have been defined as follows:

- Equivalent performance: The same level of task performance (desired, adequate, etc.) is achieved for all defined parameters in simulator and flight. Any variations in performance are small.
- Similar performance: There are no large single variations in task performance, or there are no combinations of multiple moderate variations across the defined parameters.
- Not similar performance: Any large single variation in task performance or multiple moderate variations will put the comparison of performance into this category.

Definition of 'moderate' and 'large' variations has proven to be a complex process. Initially, the test pilots were instructed to consider these as being a deviation from desired to adequate or adequate to beyond adequate for a moderate variation and from desired to beyond adequate and vice versa for a large variation. However, this proved to be too restrictive: the pilots commented that with certain test configurations, desired performance may be just achievable on one side of the flight-simulator comparison but marginally unachievable on the other, forcing the pilot to degrade the fidelity rating to Level 2 despite a very small change in the actual task experience. In the final implementation of the SFR scale, the pilots have been allowed a greater degree of flexibility in making decisions regarding whether a deviation is small, moderate, or large. This approach allows the pilots to ensure that they rate the simulation in the level that they consider to be appropriate rather than being driven by the task performance.

A second area where the pilots are asked to make a qualitative distinction is for strategy adaptation. This is intended to capture all aspects of a pilot's behavior, and would include:

- Control strategy – differences in the size, shape, and frequency of the applied control inputs.
- Cueing – differences in the way in which task cues are presented to the pilot.
- Workload – including differences in the physical effort of moving the controls; scanning of the available task cues; and the mental work associated with interpreting cues and determining the required control inputs.
- Vehicle response – differences in the perceived response of the vehicle.

Any other aspects of the task, other than the achieved level of performance that are perceived to be different between the simulation and flight test, should also be included within the level of adaptation required. Five levels of strategy adaptation are defined – negligible, minimal, moderate, considerable, and excessive. These terms have deliberately been selected to be familiar in name and meaning to pilots who have used the HQR scale and have, thus, rated compensation/workload during a task.

7.8.2 Bell 412 SFR Assessment

Flight trials using the National Research Council's (NRC) Bell 412 Advanced Systems Research Aircraft (ASRA) (Figure 7.8-2) were conducted flying a range of MTEs. The trials were then repeated using the University of Liverpool's HELIFLIGHT-R simulator [7] (Figure 7.8-3) as part of the SFR development

process. It should be noted that HELIFLIGHT-R is not a training simulator but had been configured with a flight model and pilot instrument panel to be representative of the ASRA. Flight testing was conducted using two aircraft configurations – 'bare airframe' with no control augmentation, and a configuration with an Attitude Command/Attitude Hold (ACAH) system, implemented using the ASRA Fly-by-Wire system architecture.

Figure 7.8-2: NRC's ASRA.

Figure 7.8-3: HELIFLIGHT-R Simulator.

The Mission Task Elements (MTEs) chosen for the fidelity assessment focused on the hover and low speed flight regime with the precision hover, pirouette, acceleration-deceleration, and lateral reposition ADS-33E-PRF MTEs being performed. The approach is presented in detail in Perfect et al. [5] and an example of the precision hover MTE (Figure 7.8-4) is presented here for illustration.

The task performance and pilot control activity in the precision hover MTE are shown in Figure 7.8-5 and Figure 7.8-6.

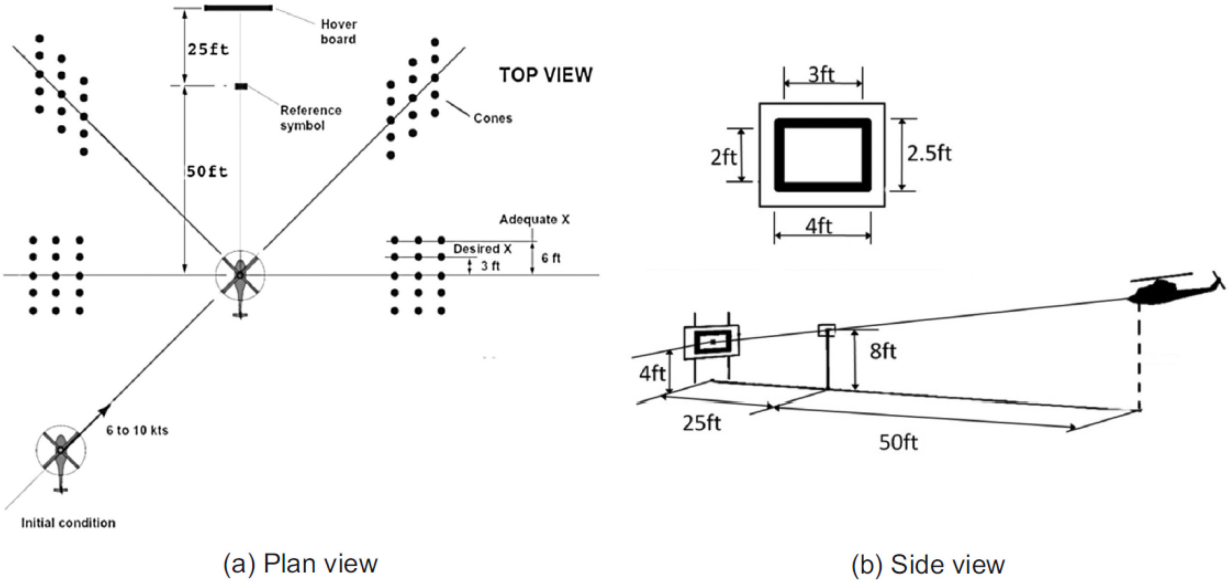

Figure 7.8-4: Precision Hover MTE [6].

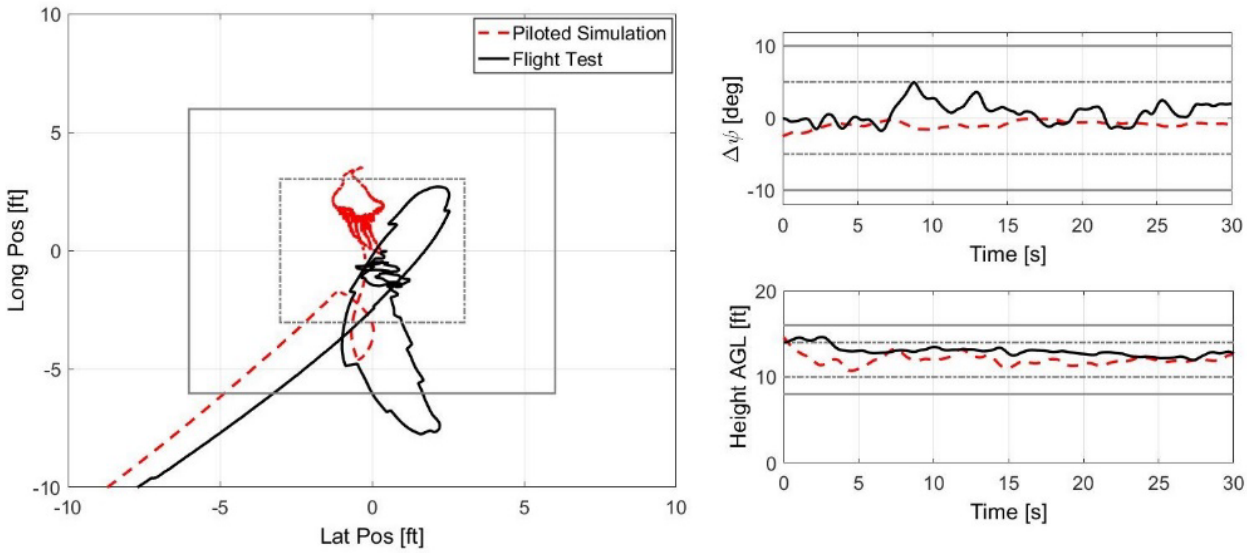

Figure 7.8-5: Precision Hover MTE Task Performance.

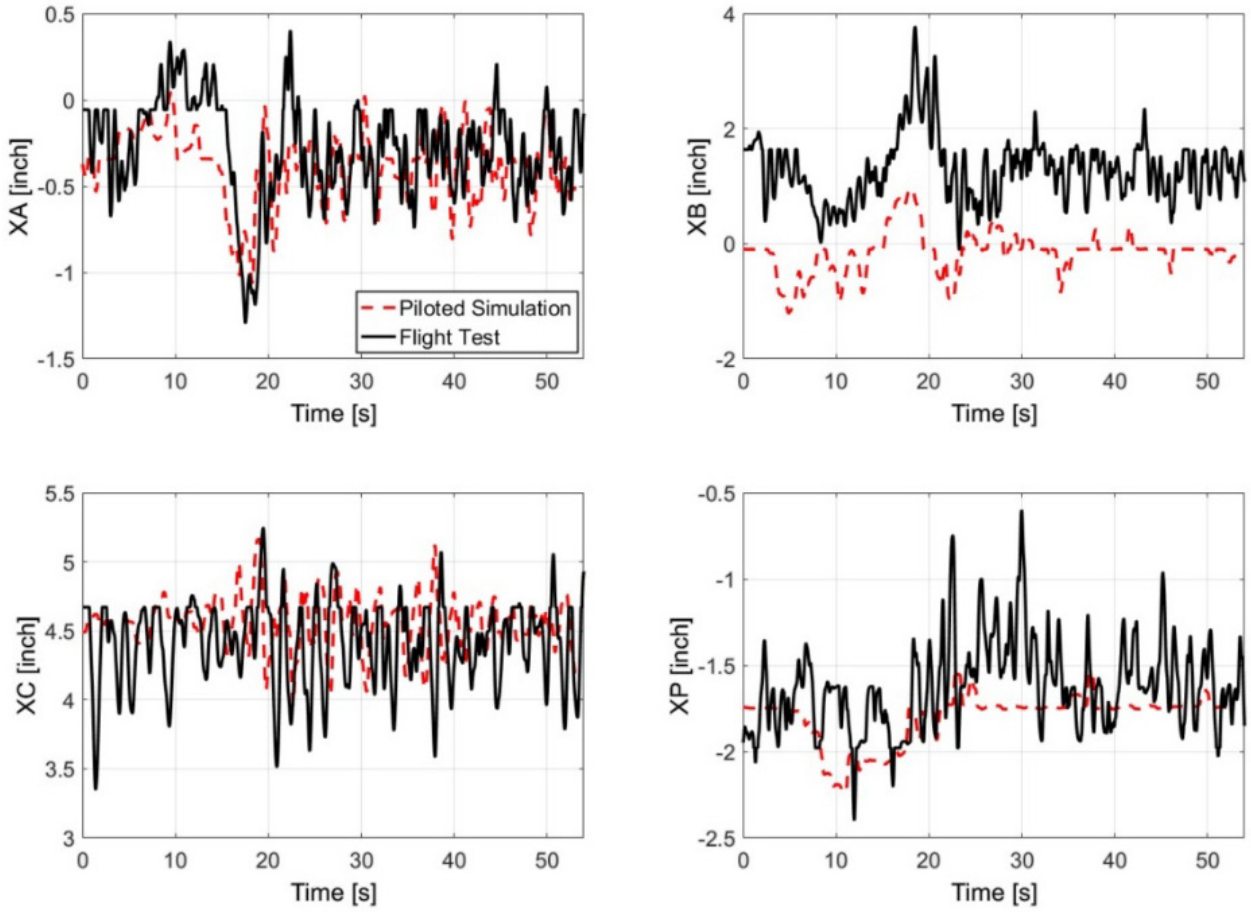

Figure 7.8-6: Precision Hover MTE Control Activity.

To aid in understanding pilot's control compensation, the control attack parameter proposed by Padfield et al. [8] has been used. The attack parameter measures the size and rapidity of a pilot's control inputs, is defined as

$$\text{attack} = \left| \frac{\dot{\eta}_{pk}}{\Delta\eta} \right|$$

where η is the pilot's control deflection (Figure 7.8-7). The attack analysis is shown in Figure 7.8-8 for lateral (*xa*), longitudinal (*xb*), collective (*xc*), and pedal (*xp*) channels. The longitudinal fidelity metrics are presented in Table 7.8-1; full metrics are given in Perfect et al. [5].

The HQR 5 to 4 comparison (flight vs simulator) is contrasted by the UCE 1 to 2 comparison. In flight, the excursion into the adequate region and beyond (12% of time) for longitudinal position during the initial capture of the hover, led the pilot to award an HQR of 5. Apart from this excursion, the pilot-maintained position within the desired region for nearly 80% of the time and held the desired vertical and lateral position, and heading (ψ), for more than 90% of the time (see Perfect et al. [4] for full results). In simulation, task performance was improved, which resulted in the pilot awarding an HQR of 4. By examining the attack parameters, the control attack, η, shows the pilot using an increased number of cyclic inputs in flight compared with the simulator. The combination of changes in task performance and adaptation of control strategy led to an SFR of 3, indicating 'fidelity warrants improvement' and that 'additional training is required' on the aircraft.

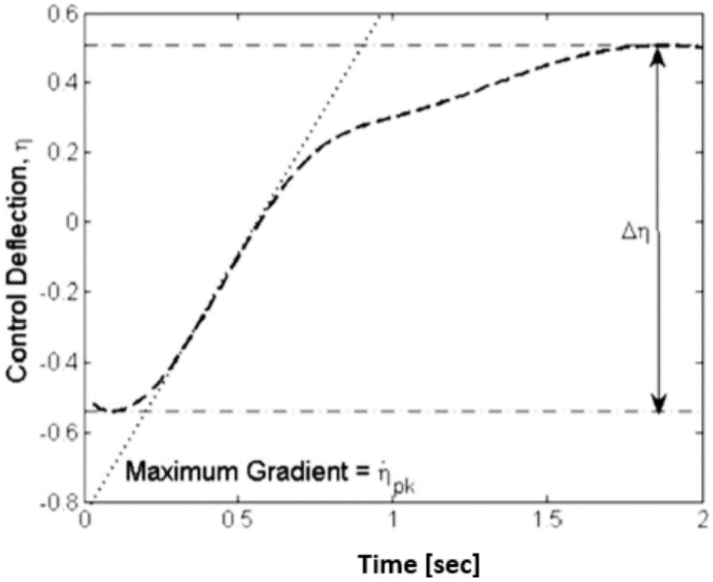

Figure 7.8-7: Attack Point Parameters [5].

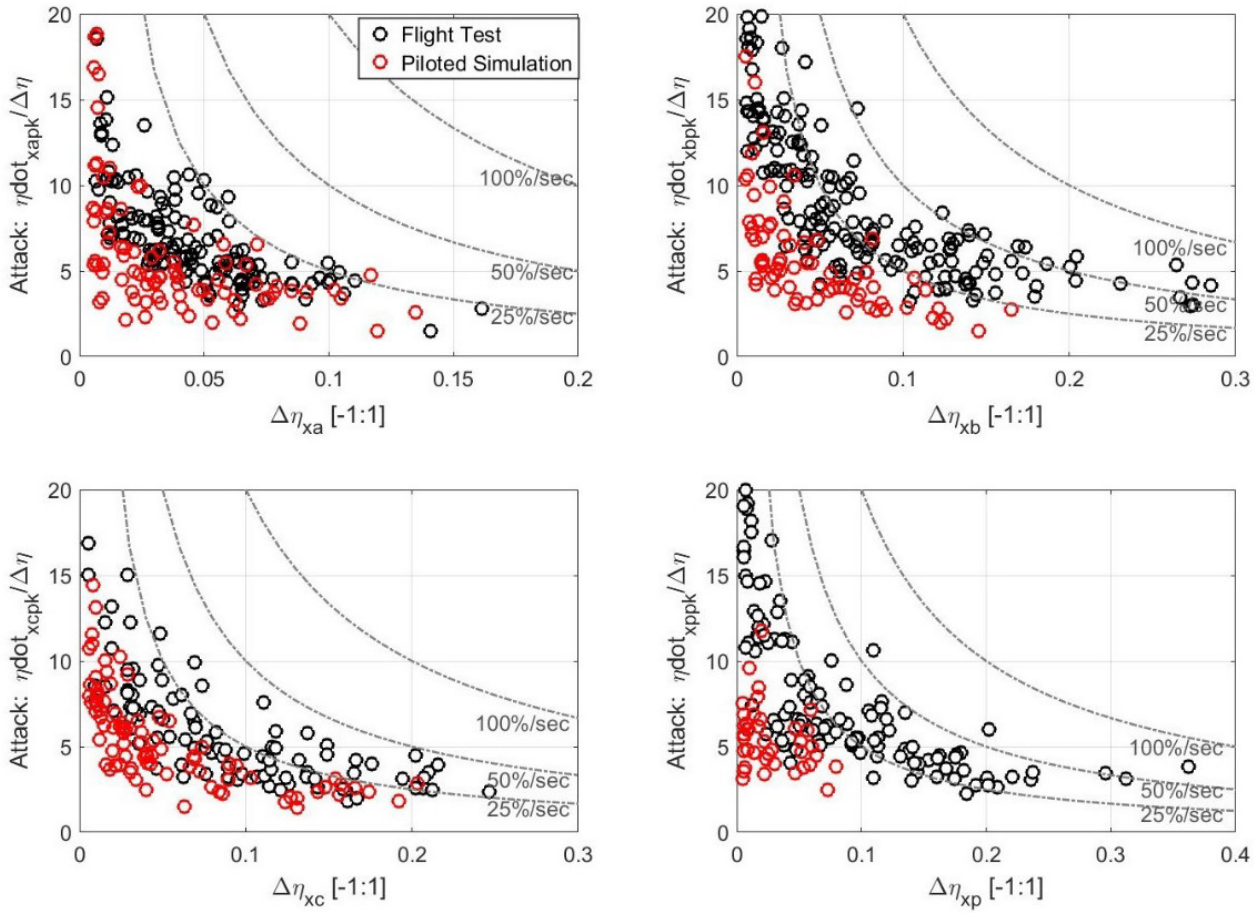

Figure 7.8-8: Precision Hover MTE Attack Analysis.

The control attack shows the pilot using more than double the number of cyclic inputs in flight compared with the simulator, at an average rate of 1.60/1.25 Hz (pitch/roll) compared with 0·7/0·8 Hz. By comparison, the cut-off frequencies are only about 20% greater in flight.

The metrics discussed have been shown to provide effective methods to quantify the difference between a pilot's control strategy in flight and that adopted in the simulator. However, the exact tolerances required to match flight behavior and enable qualification of a flight simulator have not yet been determined. This process has begun at UoL [4], in conjunction with the development and validation of the new Simulator Fidelity Rating scale and will be used to identify pilot sensitivity to fidelity tolerances.

Table 7.8-1: Precision Hover Perceptual Metrics.

Fidelity Parameter	Flight	Simulator	Δ%
HQR	5	4	
SFR		3	
UCE	1	2	
VCR(TR)	3.0	3.0	0
VCR(A)	1.5	2.0	
Total task time	30	30	0
Longitudinal			
Position % time			
Inside desired	79.2	76.2	-3
Inside adequate	88.5	100	12
Outside adequate	11.5	0	-12
Attack number	172	72	-58
Attack number per sec (/s)	3.21	1.36	-58
Mean attack rate (%/s)	25	10	-60
Mean control displ (%)	7.8	4.7	-40
No. of quickness points	32	18	-44
Quickness points per sec (/s)	0.59	0.34	-42
Mean quickness (/s)	2.45	0.81	-67
PSD RMS	0.050	0.022	-56
Cut-off frequency (Hz)	0.705	0.340	-52

7.8.3 References

[1] JAR-STD 1H (2001), "Helicopter Flight Simulators," April 2001, Joint Aviation Authorities.

[2] EASA CS-FSTD(H) (2012), "Certification Specifications for Helicopter Flight Simulation Training Devices," European Aviation Safety Agency EASA CS-FSTD(H), June.

[3] Pavel, M.D., White, M.D., Padfield, M.D., Roth, G., Hamers, M., and Taghizad, A. (2013), "Validation of Mathematical Models for Helicopter Flight Simulators Current and Future Challenges," *The Aeronautical Journal*, 117(1190), pp. 343-388, April.

[4] Perfect, P., Timson E., White, M.D., Padfield, G.D., Erdos, R., and Gubbels, A.W. (2014), "A Rating Scale for the Subjective Assessment of Simulation Fidelity," *The Aeronautical Journal*, August, 118(1206), pp. 953-974.

[5] Perfect, P., White, M.D., Padfield, G.D., and Gubbels, A.W. (2013), "Rotorcraft Simulation Fidelity: New Methods for Quantification and Assessment," *The Aeronautical Journal*, March, 117(1189), pp. 235-282.

[6] ADS-33E (2000), "Aeronautical Design Standard, Performance Specification, Handling Qualities Requirements for Military Rotorcraft," US Army, ADS-33E-PRF.

[7] White M.D., Perfect P., Padfield G.D., Gubbels A.W., and Berryman A.C. (2013), "Acceptance Testing and Commissioning of a Flight Simulator for Rotorcraft Simulation Fidelity Research," Proceedings of the Institution of Mechanical Engineers, *Part G: Journal of Aerospace Engineering*, Volume 227 Issue 4, pp. 663-686, April.

[8] Padfield, G.D., Charlton, M.T., Jones, J.P., and Bradley, R. (1994), "Where Does the Workload Go When Pilots Attack Manoeuvres? An Analysis of Results from Flying Qualities Theory and Experient," Paper 83, 20th European Rotorcraft Forum, Amsterdam, The Netherlands, Sept 1994.

Chapter 7.9 – SUMMARY OF UPDATE METHODS: PRINCIPLE, APPLICATIONS, EFFORT, ADVANTAGES, LIMITATIONS

ABSTRACT

Seven different identification methods of different complexity for improving a baseline rotorcraft simulation model have been presented and multiple case studies related to the Bell 412, UH-60, EC135, CH-47, AW139, AW109, and X2 helicopters assessed. This documented experience has been invaluable for gaining a better understanding of the advantages and limitations of each method and for comparing and coordinating analysis of a common rotorcraft database. It has been shown that different methods have many distinct and important advantages, such as improving model accuracy and providing particular types of physical insight. The methods also demonstrate applicability to control-system design methods and handling qualities design and assessment, including useful viewpoints for both the data analysis and the modeling. This section will summarize the key aspects of the methods, highlighting their main applications, assumptions, and ease/difficulty in applications.

7.9.1 Introduction

Seven different update methods have been presented and comprehensive case studies have been analyzed in the NATO STO-TR-AVT-296 on 'Rotorcraft Flight Simulation Model Fidelity and Improvement' [1] using a comprehensive flight-test database (see Figure 7.9-1). This section presents the summary of most important conclusions and lessons learned from using these update methods to improve a baseline simulation model for rotorcraft.

Flight Simulation Model Update Methods

- Method 1: Gain/Time Delay Corrections for Key Responses
- Method 2: "Black Box" Input and Output Filters
- Method 3: Force and Moment Increments Based on Stability Derivatives
- Method 4: Reduced Order Models and Physics-Based Corrections
- Method 5: Simulation Model Parameter Adjustment
- Method 6: Parameter Identification of Key Simulation Constants
- Method 7: Stitched Simulation from Point ID Models and Trim Data

Flight Test Database	Method 1 (Section 7.1)	Method 2 (Section 7.2)	Method 3 (Section 7.3)	Method 4 (Section 7.4)	Method 5 (Section 7.5)	Method 6 (Section 7.6)	Method 7 (Section 7.7)	Quantitative Fidelity	Perceptual Fidelity
412 (NRC)		DLR	UoL, CAE		CAE		NRC	X	UoL
UH-60 (USNA)	USNA			ART, GT, SAC	PSU		TDD	X	
EC135 (DLR)		DLR	METU		Thales/ONERA		DLR	X	
CH-47 (Boeing/DSTG)	DSTG	CAE		GT, Boeing, DSTG	DSTG, CAE			X	
AW139 (Thales/ONERA)			Thales/ONERA					X	
AW109 (LH)				LH				X	
X2 (SAC)				SAC, USNA		USNA		X	
Iris+ (TDD)							TDD	X	

Figure 7.9-1: AVT-296 – Flight Simulation Model Update Methods and Flight-Test Databases.

Identification Method	Method 1 Gain/Time Delay Corrections for Rotorcraft Key Responses	Method 2 "Black Box" Input and Output Filters	Method 3 Force and Moment Increments Based on Stability Derivatives	Method 4 Reduced Order Models and Physics-Based Corrections	Method 5 Model Parameter Adjustment for Physics-Based Simulations	Method 6 Parameter Identification of Key Simulation Constants	Method 7 Stitched Simulation from Point ID Models and Trim Data
Method Principle	The method applies gain/time delay corrections to a flight simulation model based on frequency responses collected from flight-test data. The method does not modify the physical structure of a baseline model.	The method aims at improving the fidelity of an existing baseline model by appending low-order correction models in transfer function or state-space form. The method does not modify the physical structure of the baseline model.	The method modifies the baseline nonlinear simulation model. It uses a comparison of stability and control derivatives from flight-test data and from the baseline model to derive force and moment increments that are then added to the baseline nonlinear model to improve it.	The method modifies the baseline simulation model. It improves the baseline model by adding physics-based reduced order models and corrections for complicated phenomenon such as stall, inflow dynamics, aerodynamic interference, engine/drivetrain dynamics and sensor/actuator dynamics.	The method modifies the baseline simulation model by adjusting aeromechanical parameters (e.g., moments of inertia or hinge offsets) through matching stability and control derivatives or minimizing frequency response errors.	The method modifies the baseline simulation model using system identification to directly determine rotorcraft parameters e.g., inertias or flapping frequency from flight-test data.	The method replaces the baseline simulation model by stitching together linear point models and trim data at different flight conditions into a real-time, full flight-envelope model. Nonlinear components are included to re-establish and enhance the physical reliability of the linear models, which produces a quasi-nonlinear stitched simulation model.
Main Technical Applications	Applying small adjustments to high fidelity models to correct for unknown elements in the simulation model.	Provides a reduction of the model dynamic errors across a broad frequency range.	For enhancing the model capacity to capture the rotorcraft dynamics and improving the flight simulator model fidelity.	The method can be used for both engineering and training simulators.	The cases focus on input parameters that were uncertain and that had known correlation with the observed discrepancies between the simulation models and flight-test data.	Improvement of engineering simulation model fidelity for control design and flight dynamics analysis.	Creation of a real-time, quasi-nonlinear model for full-mission and hardware-in-the-loop simulation, control design, and flight dynamics analysis.

Identification Method	Method 1 Gain/Time Delay Corrections for Rotorcraft Key Responses	Method 2 "Black Box" Input and Output Filters	Method 3 Force and Moment Increments Based on Stability Derivatives	Method 4 Reduced Order Models and Physics-Based Corrections	Method 5 Model Parameter Adjustment for Physics-Based Simulations	Method 6 Parameter Identification of Key Simulation Constants	Method 7 Stitched Simulation from Point ID Models and Trim Data
Main Technical Applications (cont'd)	Applying corrections to lower order models to account for unmodeled higher order dynamics. Accounting for additional delays introduced by the simulation environment.		Particular application to training simulators where detailed physical enhancements are not required.	The cases focus on ground effect, rotor and fuselage aerodynamic interference, fuselage drag, elastic driveshaft dynamics, engine dynamics and fuel control, sensor and actuator dynamics.			
Main Assumptions	The underlying physics of the system being modeled needs to be well captured by the baseline model structure for the frequency range of interest.	The correction models are not physics-based. Corrections can be added at the input side (input filter) in parallel to the baseline simulation model, and/or at the output side.	The assumed model structure should capture the vehicle dynamics sufficiently well that reduced order approximations remain valid. This method provides insight into model deficiencies through the 'delta' derivatives but may not directly identify the root causes of the model's deficiency.	Physics-based methods are based on physical laws. The applications of physics-based approaches require good understanding of rotorcraft aerodynamics, dynamics, propulsion, and flight controls for identifying the root cause of the modeling discrepancies and applying the corrections accordingly.	Depending on the application considered, the simulation model needs to cover the proper range of dynamics e.g., low-medium frequency dynamics for handling qualities and pilot perception applications and higher frequency dynamics associated with rotor blade and inflow modes for high bandwidth control design and structural load predictions.	This model update strategy is best utilized when there is uncertainty in the input design data for a rotorcraft.	The stitched model is a quasi-nonlinear simulation model with linear, time-varying aerodynamics. The process is applicable to any flight vehicle for which point-wise linear models and trim data can be obtained. Trim data trends over the flight envelope should vary smoothly or first be processed with piecewise cubic interpolation.

Identification Method	Method 1 Gain/Time Delay Corrections for Rotorcraft Key Responses	Method 2 "Black Box" Input and Output Filters	Method 3 Force and Moment Increments Based on Stability Derivatives	Method 4 Reduced Order Models and Physics-Based Corrections	Method 5 Model Parameter Adjustment for Physics-Based Simulations	Method 6 Parameter Identification of Key Simulation Constants	Method 7 Stitched Simulation from Point ID Models and Trim Data
Ease/Difficulty in Application	Rapid and easy to apply, implementing corrections without delving into the underlying model physics. However, the method is not physics-based, and therefore, it does not allow for extrapolation to other flight conditions.	Relatively fast and easy to apply, allowing easily implemented corrections. However, as a limitation, the method is not physics-based, and therefore, it does not allow for extrapolation to other flight conditions.	Moderately difficult. The force and moment 'increments' can correct nonlinear model shortfalls very effectively. However, this method requires the selection of an adequate set of derivatives. This depends on the nature of the model shortfall. The selection of derivatives can be guided by sensitivity analysis or through a physics-based study.	Difficult. Good understandings of simulation model assumptions and input parameters are required. The method is a physics-based correction, so it allows general improvement that may allow for extrapolation to other flight conditions and even other configurations.	Moderately difficult to Difficult. The level of difficulty would depend on the specific problem to solve and the parameters that are used. The method requires conducting parametric studies on the simulation model and performing optimization of the selected parameters.	Difficult. Flight-identified linear models are compared to a linearized math model. Once updated, the math model will have e.g., the correct rigid-body and rotor modes, enabling analysis of the flight dynamics and control-system design and analysis.	Moderately difficult. The key requirement for model stitching is a series of state-space point models and associated trim data of the states and controls for point flight conditions. A model stitching simulation architecture, including lookups of the stability and control derivatives and trim data, gravity forces, and nonlinear equations of motion, is required for continuous, full-envelope simulation.

Identification Method	Method 1 Gain/Time Delay Corrections for Rotorcraft Key Responses	Method 2 "Black Box" Input and Output Filters	Method 3 Force and Moment Increments Based on Stability Derivatives	Method 4 Reduced Order Models and Physics-Based Corrections	Method 5 Model Parameter Adjustment for Physics-Based Simulations	Method 6 Parameter Identification of Key Simulation Constants	Method 7 Stitched Simulation from Point ID Models and Trim Data
Level of Specialized Knowledge Needed	The corrections introduced are not necessarily physically representative, so little specialized knowledge is required for application.	Moderate level required for SISO case. MIMO case requires extensive knowledge of inverse simulation and update filter realization. The filters can be combined in such a way that an input filter is first designed to correct the main deficits of the baseline model, and any remaining deficits are then corrected by output filters.	Moderately high. The System Identification processes require specialist knowledge. Concerning the simulation model, the assumed model should capture the vehicle dynamics sufficiently well that the reduced order approximations remain valid.	High to Very high. Good understanding of baseline simulation model and flight dynamics are required. In addition, a good understanding of the fine details of the system is required (detailed aerodynamic inflow model, very detailed aeromechanical characteristics, etc.)	High. Good understanding of the baseline simulation model and flight-test dynamics are required. While Method 5 requires an understanding of how changing a parameter will change the model behavior, Method 4 requires an in-depth physical calculation of the actual physical parameter.	High. e.g., the physical equations of motion such as of the rotor/inflow dynamics are needed to properly capture the rotorcraft flight dynamics response.	Moderately high to ensure the correct selection of the set of anchor point models and trim data, as identified from flight testing or derived from a non-real-time model. Trim data may require processing to ensure smooth data trends over the flight envelope of interest.
Primary Inputs and Measurements for Simulation	Flight test and baseline model bare-airframe frequency responses.	Two steps need to be followed: 1) Modified inputs must be determined so that the baseline simulation model yields the correct (measured) outputs; and	The stability and control derivatives derived from frequency-sweep or multi-step control inputs from flight-test data and the baseline simulation model are needed.	Properly derived reduced order models and physics-based corrections of the modeling parameters can retain the simulation accuracy needed for both engineering and real-time flight simulation.	Examples of simulation model parameters uncertain to the model developer: • Rotorcraft moments of inertia as these affect control sensitivity.	Assuming measurements are available, this method allows any parameters for which there is uncertainly to be identified while other more reliable parameters may be fixed.	A collection of pointwise linear models and associated values of the trim states and controls for discrete flight conditions are required.

Identification Method	Method 1 Gain/Time Delay Corrections for Rotorcraft Key Responses	Method 2 "Black Box" Input and Output Filters	Method 3 Force and Moment Increments Based on Stability Derivatives	Method 4 Reduced Order Models and Physics-Based Corrections	Method 5 Model Parameter Adjustment for Physics-Based Simulations	Method 6 Parameter Identification of Key Simulation Constants	Method 7 Stitched Simulation from Point ID Models and Trim Data
Primary Inputs and Measurements for Simulation (cont'd)		2) The input correction model is determined from the measured input data and the modified inputs from Step 1.			• Variations in the rotor blade mass properties as these affect the control sensitivity. • Longitudinal and lateral control linkage gains. • Swashplate phase angle, rotor blade pitch-flap coupling angle and flap hinge offset.	For example, blade properties may be held fixed and only inertias identified. Caution must be used to not over-parameterize the identification. Further, proper use of this method can shed light onto areas where further model refinement is needed.	
Contributions of the Method. Advantages and Limitations	Relatively fast and easy to apply to improve fidelity of model control sensitivities and high frequency response phase. However, it is not physical, and therefore, it does not allow for extrapolation to other flight conditions.	Relatively fast and easy to apply for SISO systems. Black box updates for MIMO systems mostly require an extensive evaluation compared to SISO systems. The corrections do not by default allow for extrapolation to other flight conditions.	The method is applicable for both engineering simulation for supporting design and development and real-time flight-models for training simulator applications.	The method is applicable for both engineering simulation in supporting design and analysis and for real-time flight simulation in training simulator applications.	The method is applicable for both engineering simulation in supporting design and analysis and for real-time flight simulation in training simulator applications. It allows moderate extrapolation beyond the flight envelope.	As limitation, this update methodology identifies changes in physical design parameters that are required to improve a model fit with flight data.	A powerful feature of the model stitching architecture is the ability to accurately simulate off-nominal aircraft loading configurations without the need for additional data. Simulation of off-nominal values of aircraft mass, inertia, and/or center of gravity that differ from the identified/baseline values is accomplished using extrapolation methods.

Identification Method	Method 1 Gain/Time Delay Corrections for Rotorcraft Key Responses	Method 2 "Black Box" Input and Output Filters	Method 3 Force and Moment Increments Based on Stability Derivatives	Method 4 Reduced Order Models and Physics-Based Corrections	Method 5 Model Parameter Adjustment for Physics-Based Simulations	Method 6 Parameter Identification of Key Simulation Constants	Method 7 Stitched Simulation from Point ID Models and Trim Data
Contributions of the Method. Advantages and Limitations (cont'd)			Care must be taken when extrapolating results to flight conditions outside the range considered. Concerning the quality of the flight-test data, the control inputs should excite the vehicle dynamics sufficiently well that the force and moment contributions from the states and controls are 'strong' enough to be identifiable.	A limitation can stem from the reduced order model not being effective at capturing the physics; this emphasizes the skill and knowledge required in applications.			within the stitching architecture. The stitched model is accurate over the nominal flight envelope, but does not by default include certain nonlinearities or edge-of-the-envelope dynamics, such as stall or autorotation. Nonlinear components can be incorporated into the stitched model but require additional flight-test data and modeling efforts.

Identification Method	Method 1 Gain/Time Delay Corrections for Rotorcraft Key Responses	Method 2 "Black Box" Input and Output Filters	Method 3 Force and Moment Increments Based on Stability Derivatives	Method 4 Reduced Order Models and Physics-Based Corrections	Method 5 Model Parameter Adjustment for Physics-Based Simulations	Method 6 Parameter Identification of Key Simulation Constants	Method 7 Stitched Simulation from Point ID Models and Trim Data
Key Lessons Learned from Case Studies	Method is highly effective when used for the right application. More precisely, where the underlying physics is well captured in the baseline model, this method produces good corrections; however, this method will be not suitable where the dynamics is poorly modeled across a range of frequencies.	Care must be taken if the filters have unstable modes – the time-to-double should not exceed 1.5 sec so that a pilot can still stabilize the simulation. If the correction model is in parallel or on the output side, care must be taken to retain consistency between the outputs. To avoid this problem, the use of a correction model at the input side is usually preferred.	The force and moment increments applied to a nonlinear simulation model in the form of 'delta' stability and control derivatives can indeed improve the simulation model fidelity. For example, model improvements were achieved by renovating the weathercock and dihedral effects, and yaw damping, pointing to missing aerodynamic interference from the fuselage and main rotor wake on the tail surfaces.	The method requires good understanding of rotorcraft aerodynamics, dynamics, propulsion, and flight controls for identifying the root cause of the modeling discrepancies and applying the corrections accordingly. Physics-based modeling of rotor-on-rotor interference interactions between both cyclic and collective rotor inflow distributions improves simulation fidelity significantly for multi-rotor vehicle configurations.	The suitability of the method is dependent on the application. Simulation model developers need to be cautious in applying modifications to physical input parameters, especially if the intended use of the simulation model is engineering development. These concerns may be of less importance for the development of training simulators where meeting the fidelity requirement for a specific aircraft is the foremost concern, not necessarily with physics-based corrections.	If poor choices of parameters to be identified are made, the identification procedure is likely to produce physically implausible results. Also, if the model is missing key dynamics that show up in the flight data; this method will combine the net impact of those dynamics into the identified parameters.	Smooth eigenvalue transition between the operating points is best achieved by piecewise cubic spline interpolation of the original anchor point models. For higher order point models, trim data of the higher order states must be included. The predictive accuracy of the stitched model for a realistic maneuvering scenario is very accurate compared to a truth nonlinear simulation. The stitched model's extrapolation for off-nominal loading configuration is very accurate, which necessitates only point models and trim data of the baseline aircraft loading configuration to be included in the stitched model.

Identification Method	Method 1 Gain/Time Delay Corrections for Rotorcraft Key Responses	Method 2 "Black Box" Input and Output Filters	Method 3 Force and Moment Increments Based on Stability Derivatives	Method 4 Reduced Order Models and Physics-Based Corrections	Method 5 Model Parameter Adjustment for Physics-Based Simulations	Method 6 Parameter Identification of Key Simulation Constants	Method 7 Stitched Simulation from Point ID Models and Trim Data
Estimated Time to Use Method and Improvement Accuracy	Minimal. The method requires minimal work effort, and hence, it may be considered as a first approach in many circumstances. Care should be exercised when applying this method to cases where a physically representative system is required.	Moderate. As with Method 1, this method may be considered as a first approach leading to good model improvements. Balancing the input-output filters can be a time-consuming activity.	Considerable. Data preparation and conducting the system identification can be time-consuming. The method is an efficient approach to correcting some shortfalls in the baseline nonlinear model.	Considerable, but the payoff is that the corrections implemented for ground effect, rotor and fuselage aerodynamic interference, fuselage drag, elastic driveshaft dynamics, engine dynamics and fuel control, sensor and actuator dynamics showed remarkable improvements in the model.	Considerable. Improvements of system responses were demonstrated. However, in some cases, this method can be a time-consuming process as the sheer number of uncertain model parameters can be high.	Considerable. The method demonstrated that relatively small changes in a few model key physical parameters can greatly improve the overall ability of the updated simulation model to track flight-test data.	Considerable. Stitched models can adequately and accurately cover the nominal helicopter flight envelope. Extrapolation can be performed to simulate off-nominal loading configurations. This proves to significantly reduce required flight-test points and associated flight costs.

Chapter 8 – SIMULATION APPLICATION ORIENTED DISCUSSION ON MODEL DEVELOPMENT/UPDATE METHODS

ABSTRACT

This lecture discusses the challenges faced in rotorcraft flight simulation model development, fidelity assessment, and update for various simulation applications. The different end-uses of flight simulation drive the necessary model update strategies. Engineering simulations are usually developed with the primary purpose to support design and development of aircraft systems and equipment. Engineering simulation model development and updates are discussed in Section 8.1. Another major application of an engineering simulation is to support design of flight control system and evaluation of Handling Qualities (HQ). This application and the model development and update methods suitable for this application are discussed in Section 8.2. Sections 8.3 and 8.4 discuss the use of flight dynamic models in helicopter training simulators, how they are validated today, and what possible improvements there could be made. Flight Simulators are currently validated by FAA or EASA using published qualification standards. Most of the validation is done in the time domain. A flight model in a Level D qualified simulator is compared in time domain against a large number of flight-test data. Flight regimes not included in the flight-test data are handled through expert opinion. In this section, it is argued that the number of time-domain comparisons can be reduced and perhaps an even better validation can be achieved using data comparison in the frequency domain, such as the MUAD criteria.

8.1 ENGINEERING SIMULATION FOR SUPPORTING DESIGN AND TEST

An engineering simulation can be used to support aircraft conceptual, preliminary, and detailed design, design modification, control laws design and analysis, handling-qualities evaluation, flight loads development and analysis, flight testing, test pilot training, accident investigation, etc. The predictive capability of an engineering model is critical for design trade studies and flight envelop expansion tests. On the other hand, a version of the model needs to be capable of operating in real time for pilot-in-the-loop simulation. These requirements determined that an engineering simulation must be developed using a physics-based math model and applying proper simplifications/approximations to maintain the computational efficiency. The development and validation of an engineering model for supporting design and flight test are discussed in this section as well as the proper methods for improving the model correlation with test data.

8.1.1 Model Development and Validation

An engineering simulation should faithfully reflect the flight characteristics of the aircraft modeled. Although an engineering simulation does not need to meet FAA Level D trainer criteria, the model must demonstrate good correlation with test data; the trending for the trim states, the dynamic responses in both time and frequency domain, and the flight loads must be correct compared to the test data. Therefore, rotorcraft Original Equipment Manufacturers (OEM) have placed significant emphasis and efforts on developing high-fidelity flight dynamics models.

8.1.1.1 Model Update During a New Design

As the new design becomes progressively mature, the simulation model data are continuously updated from various sources, mainly including but not limited to:

- **Design change**: aerodynamic configuration, geometry, structure properties, mass/inertia and CG, flight controls, etc.
- **Analysis using higher-fidelity models**: free-wake, vortex-lattice, CFD, finite-element structure, etc.

- **Component test**: wind-tunnel tests for airfoil, airframe, and rotor(s), blade rap test, etc.
- **Lessons learned** from existing aircraft simulation model validation effort.

In recent years, high-fidelity analytical tools have become more mature and practical, and thus, more routinely applied to supporting the rotorcraft design. Although they are still computationally expensive and usually specialized at certain component levels, these tools can be very useful in generating flight simulation model input data.

8.1.1.2 Model Verification and Validation

Model verification and validation are critical to ensure the quality of the baseline model. The simulation model should be verified every time any input data are updated. Before test data become available, some of the model input data are generated from different analytical tools which are usually specialized for certain components. The verification process during this phase mainly involves comparison between the simulation model and other analytical tools. For example, the rotor modal frequencies can be compared with a finite-element model to ensure the geometry (e.g., hinge offset), stiffness of hinge (and blade if elastic), and blade inertia data are correct and accurate. This model 'leveling' process is to ensure the same model data are correctly interpreted among different models.

When the aircraft design becomes mature and component test data becomes available, the simulation model input data can be updated and validated in a timely manner. The validation process usually requires a carefully designed comparison between the updated simulation model and source of the input data, either component test data or higher-fidelity model results. Two examples are discussed below.

8.2 CORRELATION WITH FLIGHT-TEST DATA AND MODEL IMPROVEMENT

When flight-test data become available, the simulation model needs to be thoroughly validated against a comprehensive set of flight-test data from both steady trim and dynamic response tests that cover a broad range of vehicle configurations and flight conditions.

8.2.1 Test Data Collection

The quality of the flight-test data is very important for supporting the simulation model validation. The test data for model correlation need to be selected through various consistency checks. In general, the following should be considered when preparing the test data for model correlation:

- Careful setting up of flight conditions is very important to achieve quality data. Flight performance and handling data are preferred than data from load survey tests due to tighter trim tolerances and better monitored wind conditions.
- Frequency-domain data (i.e., time domain properly designed and processed) are better than generic time histories due to proper removal of initial conditions dependence and external disturbance effects. However, for validation of aggressive maneuvers, time response data are the only options.

8.2.2 Model Update Methods for Improving Correlation with Test Data

During model correlation with test data, discrepancies are usually observed in rotor performance, trim control positions and attitude angles, control power and control phase, stability and control derivatives, and dynamic responses in the time domain and frequency domain. To improve the model-test data correlation for an engineering simulation, efforts should first be made on improving the model data accuracy using high-fidelity tools and component test data. After the model-data accuracy is examined/improved, the model-data discrepancy analysis should be started with a revisit of the simulation model assumptions and

limitations. Once a model-data discrepancy can be related with some missing physics or assumptions/approximations made in the model, a physics-based or physics-inspired correction method can be developed to improve the model-data correlation. It is important to keep in mind that non-physical corrections could compromise the model's predictive capability.

In some well-developed engineering simulation tools such as GenHel [1] and FLIGHTLAB, a series of physics-based semi-empirical or empirical corrections have been developed based on extensive model validation/correlation efforts over several decades. In Tischler et al. [2], many of these corrections belong to Method 4, 'Reduced-order models and physics-based corrections', described in Section 5.4 and demonstrated in Section 7.4. Some can be categorized as Method 5, 'Model Parameter Adjustment' of which examples can be found in Section 7.5 [2]. These physics-based corrections are clearly preferred methods to improve the predictive capability of engineering simulation models for supporting new aircraft design and flight tests.

The parameters in many of these corrections can be derived from higher-fidelity analytical tools. Details can be found in Method 4 discussion in Section 5.4 [2]. Most of these corrections can also be empirically derived by matching certain test data. Various examples from the model update case studies can be found in Sections 7.4 and 7.5 [2].

As examples, some commonly applied correction methods are listed in Table 8-1, although some can appear in different forms in different simulation tools. In the table, the first column lists the model-data discrepancies often observed from the correlation. The 2nd column lists the possible causes of the discrepancies, most of which are complicated physical phenomenon that are not modeled rigorously in an engineering simulation. Some of the discrepancies could also be caused by model data uncertainty. The 3rd column lists the potential corrections/adjustments, mainly including reduced-order models and semi-empirical and empirical corrections. The 4th column lists the higher-fidelity analytical tools that could be used to derive the parameter values for these corrections. The 5th column lists the test data that could be used to derive the correction parameters empirically.

As shown in Table 8-1 some the discrepancies seen, for example, in rotor performance and collective control position could be caused by modeling simplifications in rotor airloads, inflow, ground effect, and rotor-fuselage aerodynamics interaction. Application examples for ground effect model adjustment can be found in Section 7.4.1.2 [3].

Some discrepancies seen in handling-qualities characteristics, such as quickness, bandwidth and phase delay, and cross coupling, are often related to modeling simplifications in rotor inflow dynamics and wake interference. Wake curvature effect corrections and reduced-order rotor interference models are frequently used to improve the model-data correlation [4]. These corrections can be derived from higher-fidelity wake models such as free vortex wake or viscous Vortex Particle Method (VPM); see Tischler et al. [2], Section 5.4 for details. Several application examples can be found in Section 7.4.1.3 [3] and Section 7.4.1.7 [5] for rotor wake distortion corrections, in Section 7.4.2 for tandem rotor mutual interference models [6], and in Section 7.4.4 for coaxial rotor mutual interference models [7], [8].

The model-data discrepancies in trim attitude angles and control positions are often related to rotor and/or fuselage interference on empennage, especially in the low-to-mid speed range. This relationship can be confirmed if the empennage loads are measured in the flight test. Various reduced-order interference models have been developed and implemented in flight dynamics simulation tools such GenHel and FLIGHTLAB. These models can be augmented by using high-fidelity tools such as free-wake model or VPM. There are also semi-empirical corrections, such effective wake skew and viscous decay, that can be used to compensate the simplification in the interference models. An example of model improvement with the rotor-on-empennage interference correction is presented in Section 7.4.1.4 [3]. At high angle of attack and/or high sideslip angle conditions, the fuselage-on-empennage interference becomes important and could significantly impact the model correlation with test data. An example in Section 7.4.1.5 demonstrates the model improvement with the fuselage on vertical fin interference corrections [9].

Table 8-1: Examples of Model Corrections/Adjustments.

Model-Data Discrepancy	Possible Causes	Possible Corrections and Adjustments	High-Fidelity Tools	Test Data
Rotor performance and collective control position	3D effect near the blade tip	Tip loss factor	Free-wake model VPM CFD	Whirl-stand test, wind-tunnel test, flight-test hover, level flight, climb and descent
	Additional skin-friction drag on blade	Delta drag coef. Correction		
	Nonuniform inflow distribution	Wake contraction factor; radial variation		
	Ground effect	Ground effect coef.		
	Rotor downwash on fuselage	Empirical fuselage interference on rotor		
Handling qualities (e.g., bandwidth, cross coupling)	Wake distortion effect on inflow	Wake curvature correction factor/map	Free-wake model VPM	Frequency sweeps, pulse/doublet responses
	Rotor mutual interference	Rotor interference coef. and time delay		
Trim attitude and control position and empennage loads	Rotor-on-empennage interference	Effective wake skew		Wind-tunnel test, low speed flight, level flight trim, climb and descent
		Viscous decay		
		Wake contraction and expansion		
		Wake geometry change and time delay		
	Fuselage interference	Blockage effect	CFD	
		Penal methods		
	3D effect on empennage airloads	Sideslip correction		
		Lift deficiency correction		
	Empennage stall	Stall characteristics		
Control power and control phase	Bending flexibility of hub and/or blade	Effective hinge offset/spring stiffness	Finite-element models such as RCAS, ANSYS, NASTRAN	Rap test, whirl-stand test; wind-tunnel test, trim flight test
	Flap-pitch elastic/ geometry coupling	Effective δ_3 angle		
	Control system flexibility	Root torsional spring		
Frequency response near rotor lag mode	Damper nonlinearity	Effective damping		Frequency-sweep (chirp) flight test
	Drivetrain dynamics	Drivetrain flexibility		
Frequency response in high frequency range	Rotor Shaft bending flexibility	Simplified shaft bending model		
	Fuselage flexibility and structure damping	Modal elastic fuselage		

In summary, for engineering simulation models used to support the design and testing for an aircraft under development or modification, the model development, validation, and improvement is a progressive process through the entire design and testing cycle. The model needs to be continuously updated/enhanced to improve the correlation with test data in order to gain a level of confidence in the model fidelity. Physics-based methods must be used to preserve the model's predictive capability which is critical for design trade studies and flight envelop expansion tests.

8.3 HANDLING QUALITIES AND FLIGHT CONTROL

Model-based design for flight control development holds the 'promise' of achieving good Handling Qualities (HQ) and flight control performance with much reduced time/cost in flight testing. This is only possible when the key frequency/time responses and associated metrics of the integrated bare-airframe/flight control system simulation are validated through each step in the development process. Tischler et al. [10] gives additional background on the validation methods/metrics presented in this section.

8.3.1 Simplified Flight Control Development Roadmap and the Role of Validated Models

A simplified roadmap of the flight control development process and the associated central roles of a validated math model are shown in Figure 8-1. While this report has focused primarily on update/assessment of the bare-airframe model, this section considers the update and assessment of an *integrated airframe/actuators/control system* as depicted in Figure 8-2 to support the flight control development process. An accurate integrated simulation model ensures that predicted handling qualities and closed-loop flight dynamics translate from desktop design to real-time simulation and eventually to flight with a minimum of costly retuning. The five steps in the roadmap are referred to in the following discussion with bold font and are summarized:

- Specifications: ADS-33 [11], SAE AS 94900 [12], FAR, etc.
- Design: definition of architecture, continuous s-plane block diagram, linearization validation vs. off-line sweeps.
- Simulation: real-time piloted simulation, initial handling-qualities ratings.
- Development: digital implementation of control laws, Hardware-In-the-Loop (HIL) testing, flight-test rehearsals.
- Flight testing: frequency-sweep testing to validate system performance and update models.

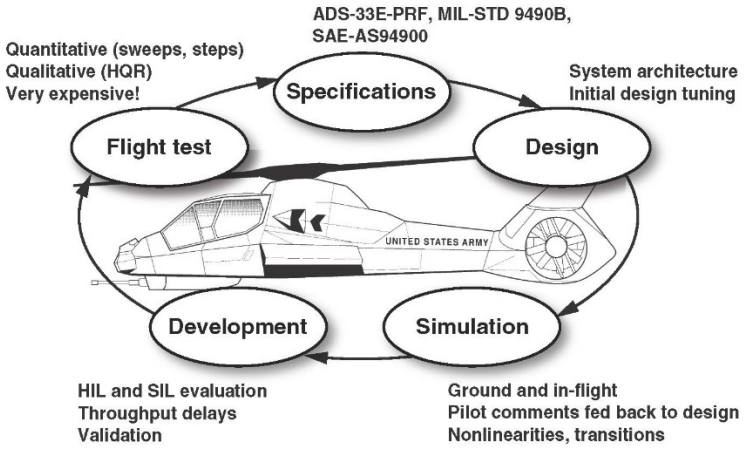

Figure 8-1: Flight Control System Development Roadmap. (Reproduced from Ref. [10], Figure 1.4.)

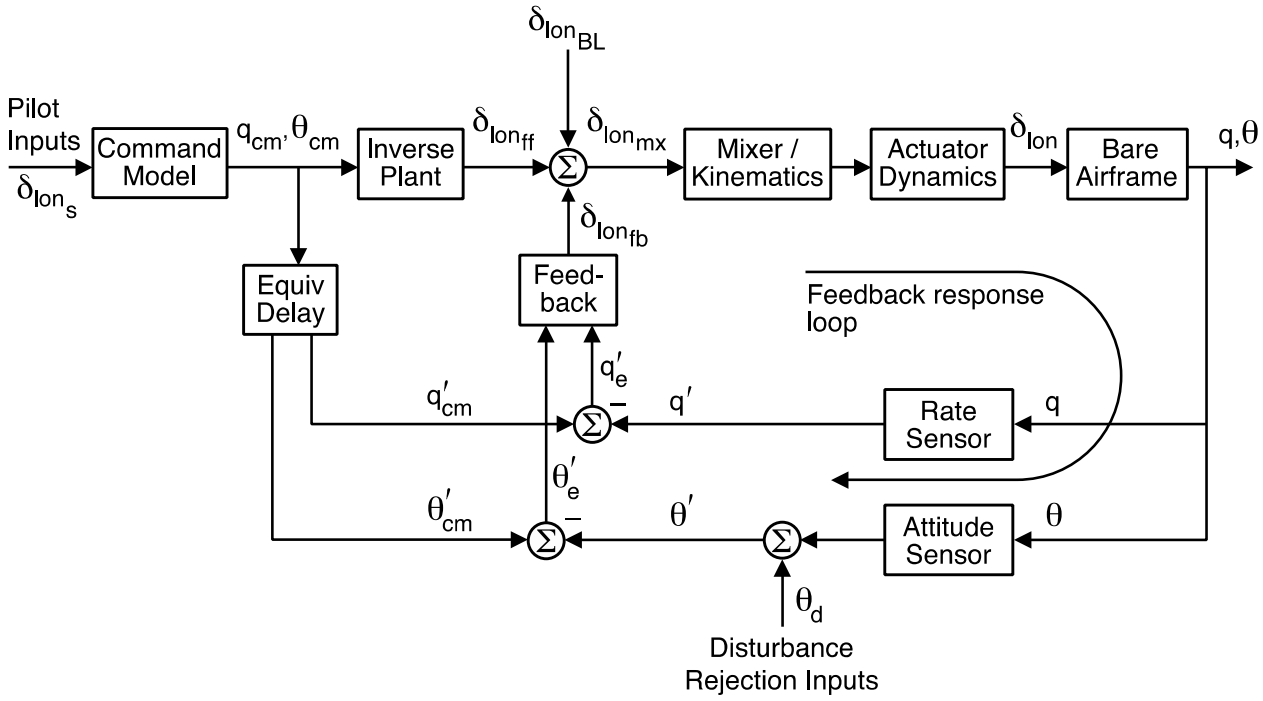

Figure 8-2: Model-Following Architecture (Pitch).

8.3.2 Explicit Model-Following Control System Architecture Example (Inner-Loop)

An Explicit Model-Following (EMF) architecture is used as an example of control system validation methods in the discussion that follows, although the methods and metrics would be the same for other architectures. A typical top-level schematic for attitude (inner-loop) control in the longitudinal axis is shown in Figure 8-2. The EMF control system architecture has become a widely used standard for rotorcraft, both on many partial-authority upgrade systems and on new-build fly-by-wire rotorcraft systems. This 'two degree-of-freedom' architecture allows independent design of the feedback (gust rejection and stability) from pilot response characteristics. Also, the single input/single output (SISO) architecture allows for transparent design and flight validation/development for each channel. The key elements of the architecture are described briefly herein and in a detailed treatment given by Tischler et al. [10].

The *command model* is a lower-order (first- or second-order) transfer function, providing a simple pilot-selectable or automatic implementation of various required response types (e.g., attitude-command / attitude-hold, rate-command/attitude-hold) as required in ADS-33 [11]. A lower-order (first-order) *inverse plant* ensures that the aircraft short-term response will closely follow the command model, but will not overdrive the actuators and rotor. Placing the inverse in the forward path and outside of the feedback loop ensures that errors in the lower-order inverse will not compromise stability. The *equivalent delay* synchronizes the commanded and feedback signals to avoid overdriving the higher-order dynamics (i.e., rotor system) or causing actuator saturation. The equivalent delay also improves the model-following performance without introducing additional delay to pilot input. The feedback compensation is typically a classical PID system and may include some lead-lag shaping. Finally, the *mixer* distributes the channel commands to the control effectors (i.e., rotor push rods, aerodynamic surfaces, etc.). In the full multi-channel system, the *mixer* contains a crossfeed matrix, derived from the bare-airframe model to decouple the MIMO system into effectively distinct SISO loops. Therefore, achieving a high-fidelity bare-airframe model (using the methods presented in this report) will improve the decoupling. This will improve the accuracy with which the closed-loop system will track the command model for good handling qualities and improve gust rejection.

8.3.3 Integrated Simulation Validation and Key Metrics

This section presents the methods and metrics for quantitative validation of the integrated model for each step of the flight control development process, using system identification techniques. The frequency responses and associated metrics used for validation are the same at each step of the development cycle. As more flight hardware and modeling detail is introduced, fidelity and confidence in the integrated simulation improves. A good practice followed by industry is to keep and update a 'smart book' that contains the frequency responses and metrics (presented in this section) and a log of model changes throughout the development process. Then, if there is a significant change in flight control system behavior from one step to the next, sources of possible errors/corrections are more easily traced. Validation examples in this section are based on flight-test data for hover from the RASCAL fly-by-wire UH-60 helicopter, as presented in detail in Mansur and Tischler [13] and summarized in Tischler et al. [10].

Broken-loop response validation. The broken-loop response, $\delta_{lon_{fb}}/\delta_{lon_{mx}}$, is central to the performance of the control system, dictating the speed of the feedback response (crossover frequency, ω_c), stability margins for robustness to modeling uncertainty, command response tracking precision, and closed-loop response damping. Close agreement of the broken-loop response and associated metrics (crossover frequency, phase margin, and gain margin) with flight-test data is essential in model-based control system development for effectively guiding needed flight control system improvements. The nature of feedback itself is to suppress the effects of errors/uncertainties in the constituent bare-airframe and control system models that make up the overall closed-loop response [10]. Therefore, considerable errors in the key broken-loop metrics will not be very apparent in the closed-loop response validation. This makes the validation and update of the simulation response for precise broken-loop response fidelity the key step for model-based control system development.

The broken-loop response is comprised of the product of the bare-airframe response, $q'/\delta_{lon_{mx}}$, and the feedback compensation response, $\delta_{lon_{fb}}/q'$. These responses can be independently determined and verified using the same broken-loop frequency-sweep data for the $\delta_{lon_{BL}}$ input as well as by linearization perturbation. The methods for bare-airframe model update and fidelity assessment to ensure good agreement have been addressed at length in this report, thus at this point we assume that the $q'/\delta_{lon_{mx}}$ frequency responses from frequency sweeps of the nonlinear simulation and linearization perturbation meet the fidelity criteria of Section 7.1 and Section 7.2. The q' and $\delta_{lon_{fb}}$ signals as recorded in the broken-loop frequency-sweep tests, provide an accurate feedback system frequency response, $\delta_{lon_{fb}}/q'$. This system identification result will include both the q' and θ' feedback shown in Figure 8-2. The perturbation linearization result for the feedback response in the SIMULINK analysis model is determined as shown in Figure 8-3 for the pitch axis and must agree very closely with the frequency-sweep results.

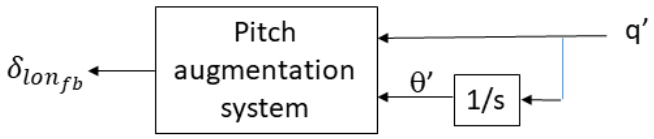

Figure 8-3: Perturbation and Sweep Method for Determining the Feedback Response from a SIMLINK Block Diagram.

A test example in Figure 8-4 shows close agreement of $\delta_{lon_{fb}}/q'$ using the method Figure 8-3 for the 1) Perturbation linearized SIMLINK simulation model vs; 2) Sweeps of the SIL; and 3) Test results obtained from manual angular oscillation of the vehicle on the ground.

These results validate the analysis model and the pictures-to-code implementation of the control laws in the flight processor.

Small errors in the feedback response simulation model may be due to digitalization and nonlinear effects and can be corrected with a simple gain (magnitude errors) and time delay (phase errors) applied to the output of the feedback signal $\delta_{lon_{fb}}$ (Figure 8-2).

Errors in the broken-loop response are associated with residual discrepancies in the corrected bare-airframe model and uncertainties in sensor and actuator dynamic modeling. The comparison of flight and simulation broken-loop responses provides final gain and time delay corrections that are inserted just ahead of the *mixer*. The key metrics of interest for this response are the crossover frequency (ω_c), Phase Margin (PM), and Gain Margin (GM) as defined in Figure 8-5(a). The simulation and flight values of these metrics should all agree closely, and the Gain/Phase Margin point (PM, GM) must be in the same region of the SAE AS949000 specification of Figure 8-5(b) (e.g., both in the unshaded Level 1 region). An example of the pitch response validation for the UH-60 RASCAL aircraft is given in Figure 8-6, which shows very close agreement of the linear simulation (CONDUIT®) and flight responses.

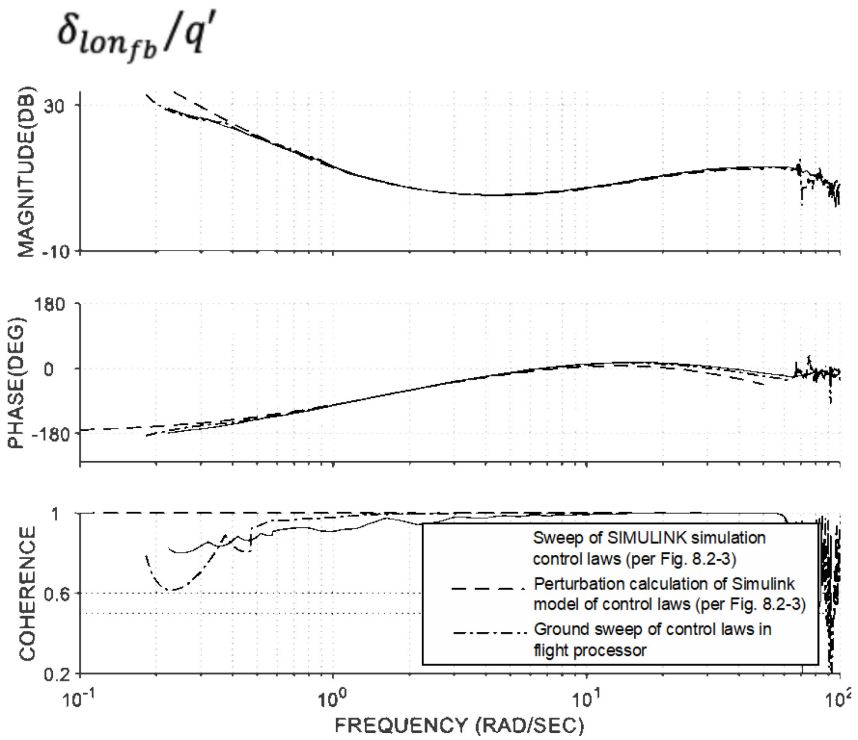

Figure 8-4: Perturbation Linearization of the SIMULINK Feedback Response, Frequency-Sweep Determination of the SIMULINK Control Laws, and Ground-Sweep Validation (By Hand) of the Real-Time Control Laws (In the Flight Processor).

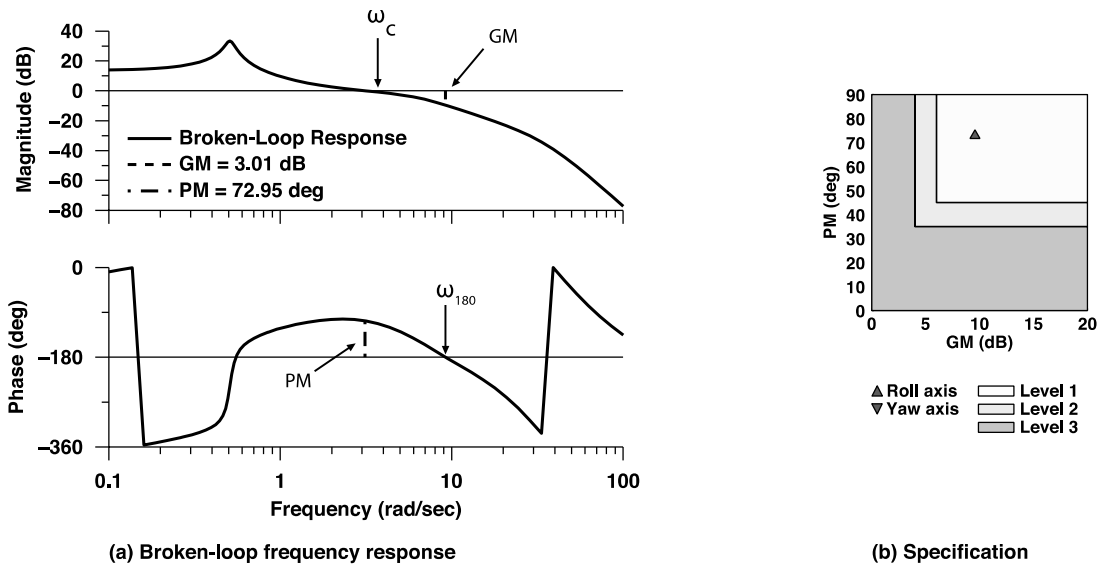

(a) Broken-loop frequency response

(b) Specification

Figure 8-5: (a) Definition of Broken-Loop Response Metrics; (b) SAE AS94000 Stability Margin Specification.

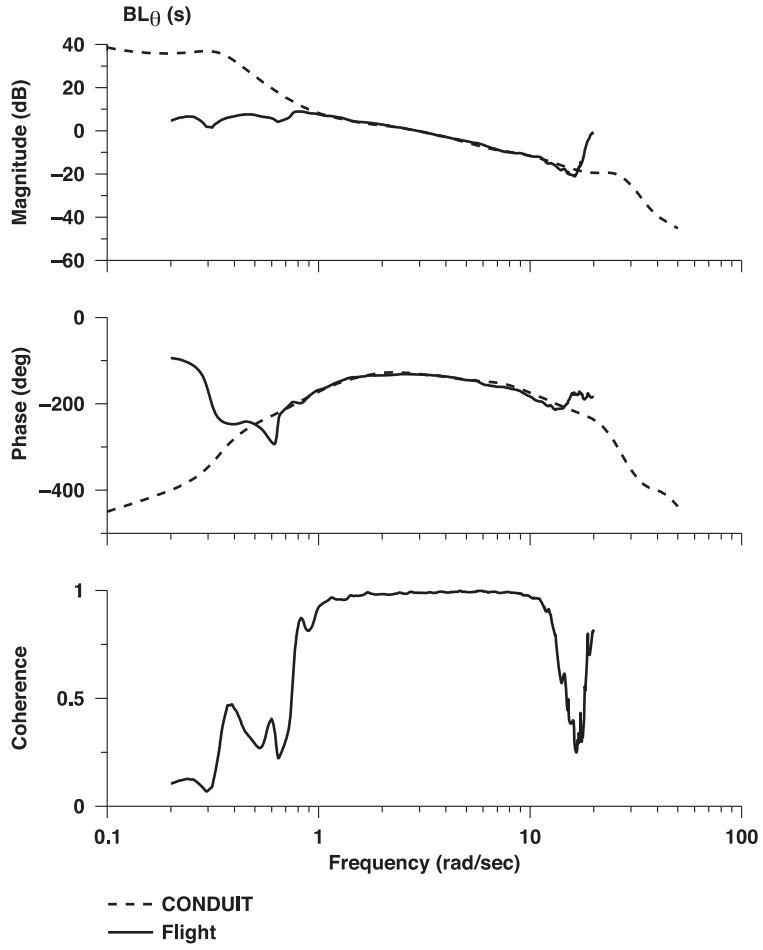

Figure 8-6: Analysis Model Validation for Broken-Loop Pitch Response (UH-60 RASCAL, Hover).

Closed-loop response validation. The closed-loop response, θ/δ_{lon_s} is determined from a piloted (or automated) sweep injected at the stick input, δ_{lon_s}, with the inner (attitude) loops closed. Key closed-loop HQ metrics are the bandwidth frequency and phase delay (ω_{BW}, τ_p), as defined in Figure 8-7(a).

The simulation point, (ω_{BW}, τ_p), must be in the same region of the ADS-33 specification as the flight response. For example, both should be in the same region of the HQ specification of Figure 8-7(b) (e.g., Level 1 is the unshaded region). Time-domain validation criteria for the closed-loop forced response are given via the QTG criteria ([2] (Section 4.6)). Another important time-domain criterion is the closed-loop damping ratio ζ, that can be obtained from a log decrement analysis for stick pulse response. An example of the closed-loop pitch response validation for the UH-60 RASCAL is given in Figure 8-8, showing very good agreement of the linear simulation (CONDUIT) and flight responses.

Disturbance rejection response validation. Finally, the disturbance rejection response θ'/θ_d is obtained by injecting an automated frequency sweep θ_d as shown in Figure 8-2, with the inner (attitude) loops closed. The key metrics are the Disturbance Rejection Bandwidth (DRB) and Disturbance Rejection Peak (DRP), as defined in Figure 8-9. The simulation values of these disturbance response metrics must be in the same region of the ADS-33 specification as the flight response (e.g., Level 1 is the unshaded region in the specifications of Figure 8-10). An example of the yaw disturbance rejection response validation for the UH-60 RASCAL is given in Figure 8-11.

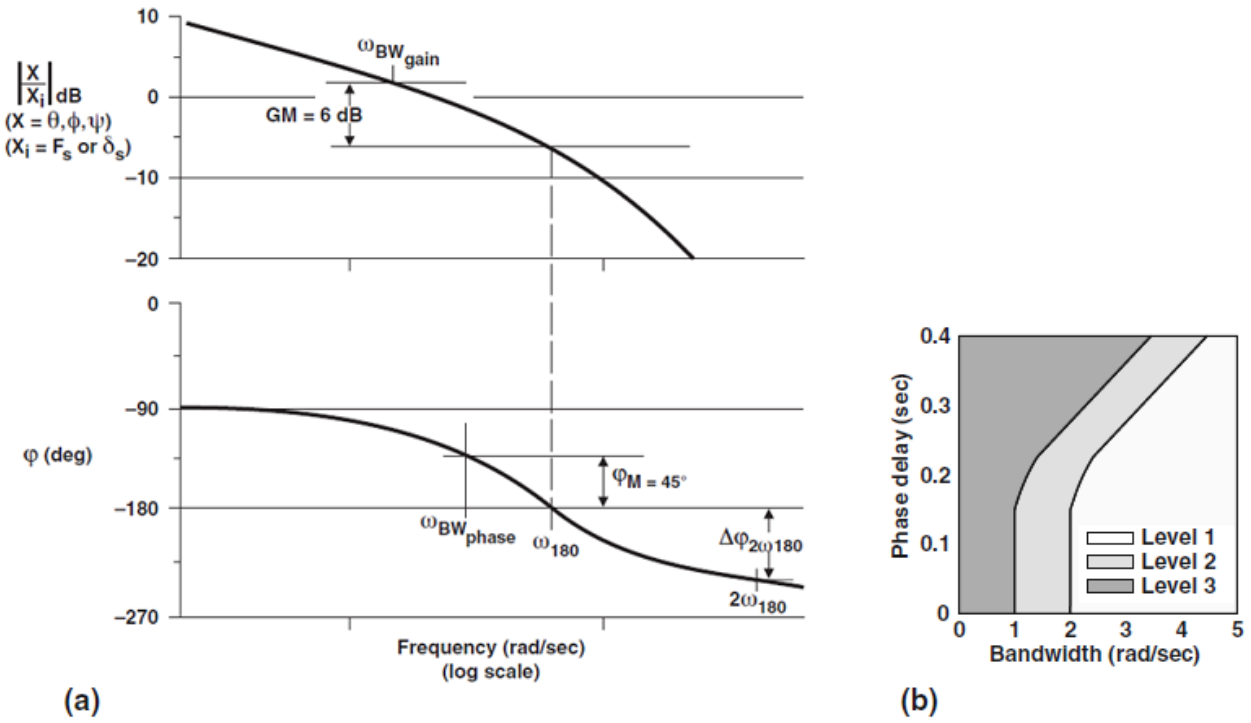

Figure 8-7: (a) Definition of the ADS-33 Bandwidth and Phase Delay Metrics, (b) ADS-33F Criteria for Pitch Axis (All Other MTE and/or Divided Attention).

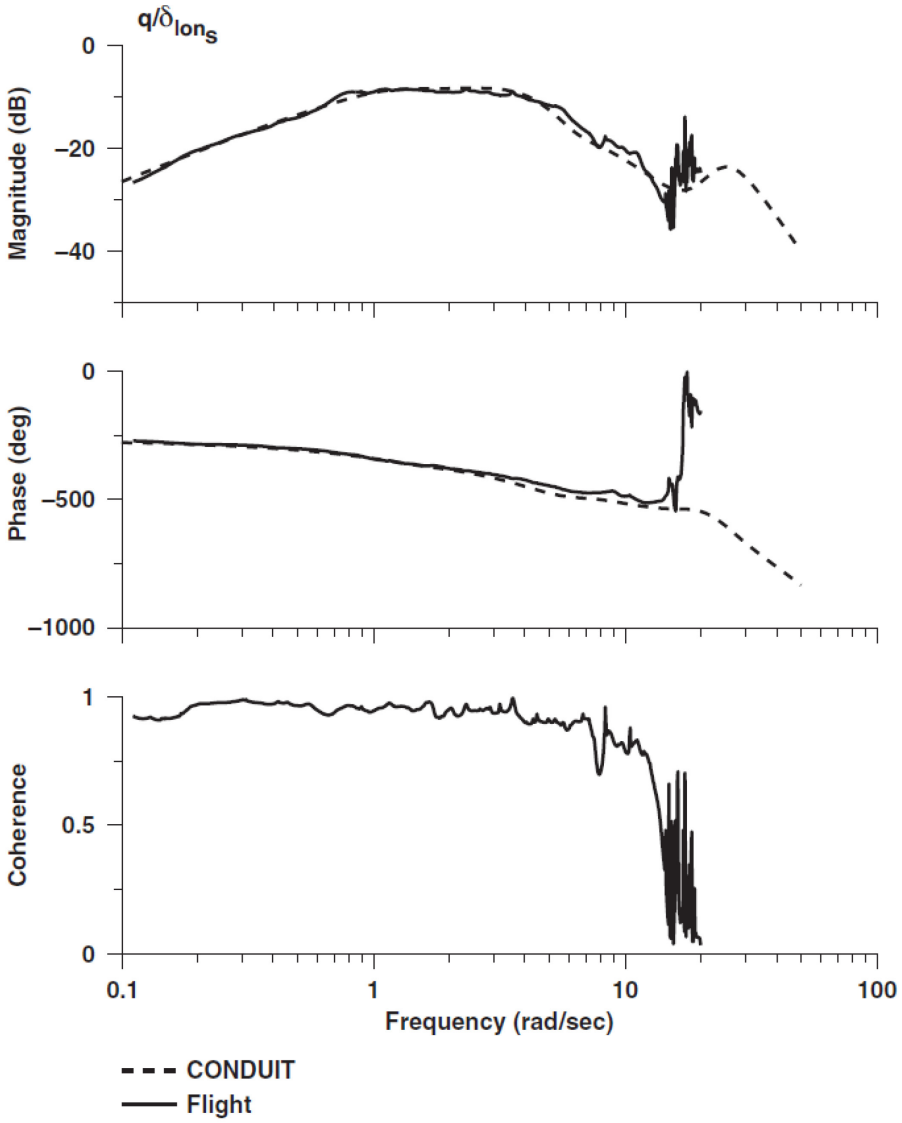

Figure 8-8: Analysis Model Validation for Closed-Loop Pitch Response (UH-60 RASCAL, Hover).

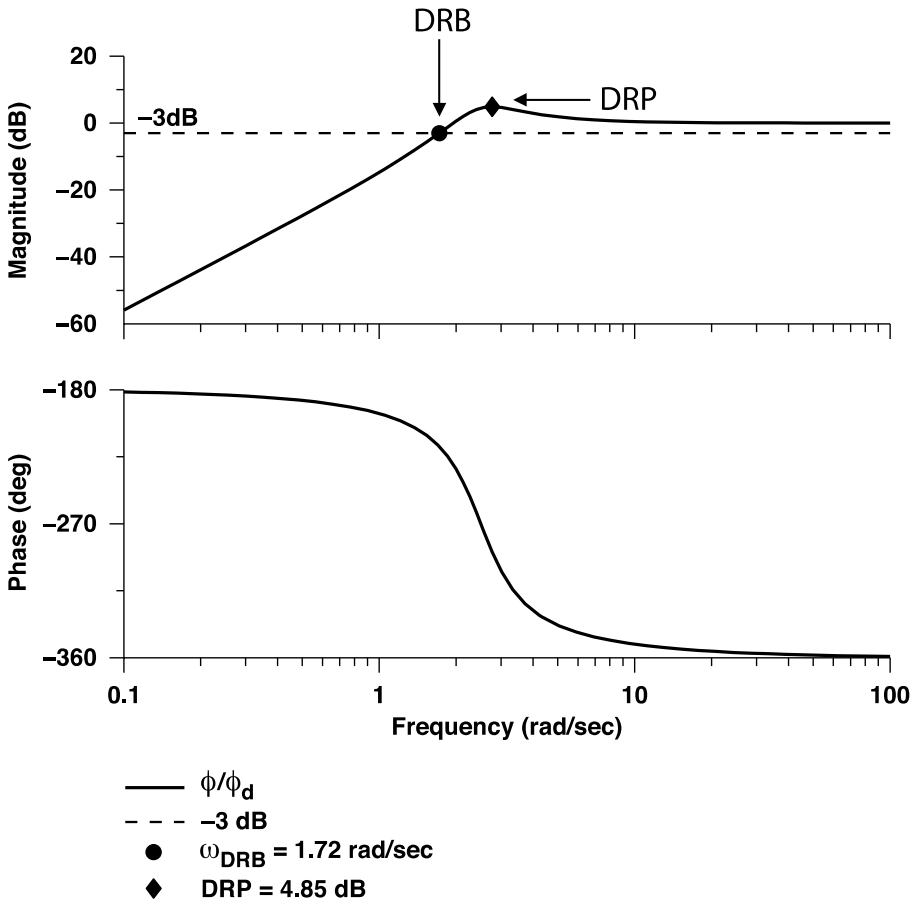

Figure 8-9: Definition of ADS-33 Disturbance Rejection Specification Metrics.

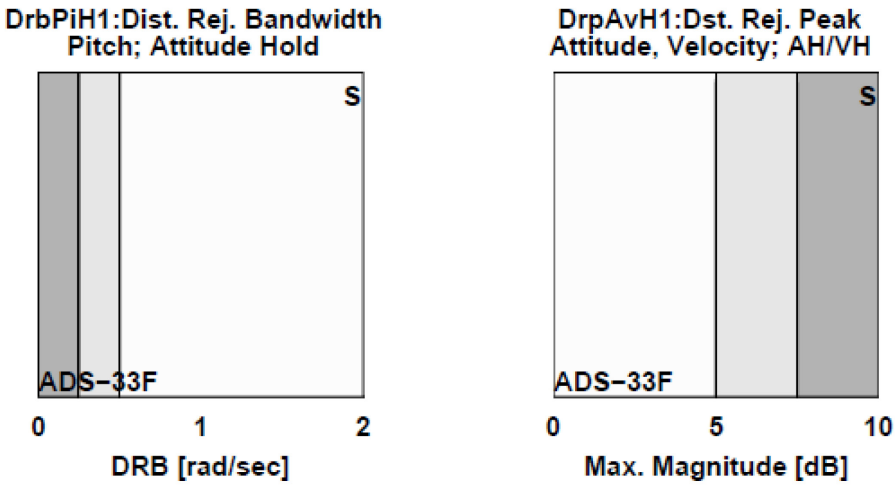

Figure 8-10: ADS-33 Disturbance Rejection Specifications for Pitch: (a) DRB; (b) DRP.

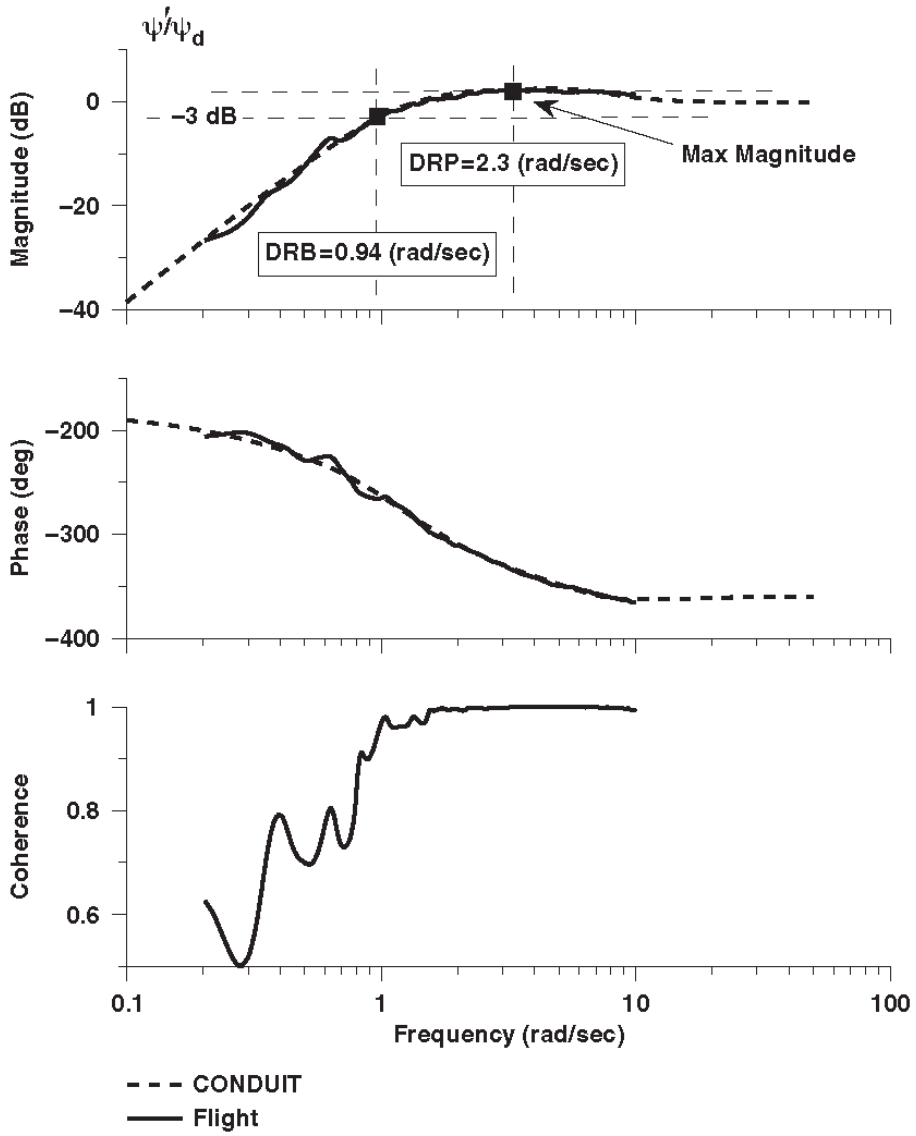

Figure 8-11: Analysis Model Validation for Disturbance Rejection Yaw Response (UH-60 RASCAL, Hover).

8.3.4 Outer-Loop Control System Architecture and Validation

The discussion so far in this section has concentrated on the inner (attitude) loop control system. Typically, a nested-loop architecture closes velocity and position 'outer loops' around this inner-loop system as required by ADS-33 for the Degraded Visibility Environment (DVE) and shown schematically in Figure 8-12. The same three frequency responses and associated metrics, as discussed in the previous sections, are validated for both the velocity and position loops. The outer-loop broken-loop response break points are denoted as 'Point 1,' 'Point 2,' and 'Point 3.' More detail on the outer-loop architecture and associated responses and metrics are given by Tischler et al. [10].

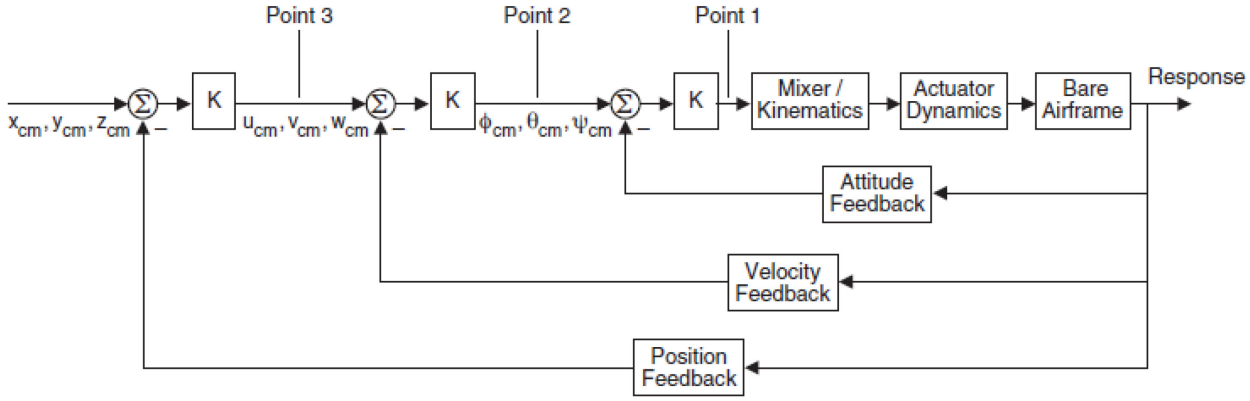

Figure 8-12: Typical Outer-Loop Schematic for Explicit Model-Following System.

8.3.4.1 Flight-Test Validation Results for UH-60 RASCAL

A summary of the validation results for the UH-60 RASCAL aircraft is given in example of the pitch response validation for the UH-60 RASCAL aircraft is given in Table 8-2, which shows very close agreement of the linear simulation (CONDUIT®) and flight responses. The broken-loop metrics for the simulation and flight-test results (ω_c, PM, GM) all agree closely, as is shown for the UH-60 in Table 8-2, and both are in the Level 1 region of Figure 8-5(b). The closed-loop metrics for the simulation and flight-test results (ω_{BW}, τ_p) agree closely, as is shown for the UH-60 in Table 8-2, and both are in the Level 1 region of Figure 8-7(b). The disturbance response metrics all agree closely as is shown for the UH-60 in Table 8-2, and both are within the Level 1 region for the yaw DRB ADS-33F requirement of Figure 8-10.

Table 8-2: Comparison of Fidelity Metrics for Analysis vs Flight (UH-60 RASCAL, Hover).

Engineering Name	Engineering Symbol	Analysis Value	Flight-Test Value
Crossover Frequency, Pitch	$\overline{\omega_c}$	2.87 rad/sec	2.94 rad/sec
Phase Margin, Pitch	PM	49.8 deg	49.3 deg
Gain Margin, Pitch	GM	12.3 dB	11.1 dB
Bandwidth, Pitch	ω_{BW}	2.72 rad/sec	3.10 rad/sec
Phase Delay, Pitch	τ_p	0.06 sec	0.12 sec
Disturbance Rejection Bandwidth, Yaw	ω_{DRB}	0.96 rad/sec	0.96 rad/sec
Disturbance Rejection Peak, Yaw	DRP	2.61 dB	2.42 dB

Once the control system architecture is fixed, the integrated bare-airframe/flight control model needs only to be validated against the flight data for *any single gain set,* and then the model will be valid for all future gain adjustments. In the Armed Reconnaissance Helicopter (ARH) flight control development program, Bell Helicopter engineers used a flight identified bare-airframe model of the prototype and the various response metrics were validated for the initial gain set, providing an accurate basis for final flight control tuning. They credit this process with enabling them to 'clear the ARH-70A in less than one third of the flight-test time that had been originally planned for AFCS development' [14].

The summary of this section is as follows:

1) Model-based flight control design requires an accurate model that is validated at each step of the development process, based on three key frequency responses (broken-loop, closed-loop, and disturbance rejection) and associated metrics.
2) With a validated/corrected bare-airframe model, the feedback and broken-loop responses are then corrected with a gain and time delay to provide excellent fidelity.
3) Once the control system architecture is fixed, the integrated bare-airframe/flight control model needs only to be validated against the flight data for a single (any) gain set. Then, the model will be valid for all future gain adjustments as needed to guide flight control and handling qualities improvements.
4) Experience from many flight control development programs demonstrates that using a flight-validated model-based approach can achieve good Handling Qualities (HQ) and flight control performance with much reduced time/cost in flight testing.

8.4 RAINING SIMULATION

Helicopter training simulators need to provide high-fidelity immersive environments for pilots in order to obtain a Level D qualification, which is the highest level of simulator qualification defined by the Federal Aviation Administration (FAA) [15], the European Union Aviation Safety Agency (EASA) [16] and the International Civil Aviation Organization (ICAO) [17]. A Level D qualification allows the replacement of most of the flight hours required for a pilot's type rating or recurrent training with simulator hours. A Level D simulator is made of many subsystem models related to the vehicle dynamics (flight dynamics, flight controls, engines, and autopilot), vehicles systems (avionics, ancillaries, etc.) and simulator immersive cueing environments (motion, sound, visual, weather, airport environment, etc.). Each of these subsystems must meet qualitative and quantitative validation criteria for the specific aircraft type to meet Level D simulator requirements.

8.4.1 Level D Data Package Requirement

A flight-test data package must contain measured data for more than one hundred flight-test maneuvers to meet Level D validation requirements [18]. The signals are filtered and outputted to a network. Unfiltered parameters include digital, discrete, air-data, and time-data parameters. Engine data are collected to the same network consisting of over 100 data channels and recorded typically around 100 Hz. The measurements include sound and vibration at higher frequencies, such as 1000 Hz.

In all, over 1000 test points and Qualification Test Guide (QTG) maneuvers s are typically collected for simulator model generation and validation. The maneuvers range from those near the ground (hover and low speed, takeoff, and landing) to cruise flight performance, static stability, dynamic maneuvers, and autorotation. The flight-test time can be over 100 hours collected over a period of months. The total number of sorties is about 40.

8.4.2 Blade-Element Rotor Models

While no model structure can give a complete representation of the physics related to helicopter simulation, blade-element rotor models for rotorcraft dynamics are typically used to meet the fidelity requirements for the Level D training simulator classification. Physics-based models such as the blade-element rotor models have some advantages compared to their strictly parametric counterparts, because of their predictability and their capability to extend the flight envelope. Capturing the full flight envelope requires including multiple configurations of gross weight and Center of Gravity (CG), maximum rearward/sideward speeds up to VNE, low speed azimuths, In-Ground Effect (IGE), climb/descent/autorotation, and high bank turn (maneuvering stability and coordinated turns). In addition to providing a full continuous envelope and accurate performance and handling qualities, pilots can observe and train for various special flight conditions in

training simulators: vortex ring state, retreating blade stall, loss of tail rotor effectiveness, engine malfunctions, autorotation entry, icing, etc. Subject Matter Expert (SME) pilots can also request subjective corrections, which are usually stated in 'pilot's language', for aircraft stability, workload, unexpected behaviors, etc. These comments often offer valuable clues to the engineer about deficiencies in the model.

Blade-element rotor models can easily integrate main rotor inflow models that are determined from reduced-order models and physics-based corrections (Method 4). More precisely, they may come from basic momentum theory or possibly more complete inflow models (e.g., Pitt Peters, harmonic inflow components). If the inflow model from theory is insufficient for agreement between simulation model and flight-test data, it can be augmented by various simulator model parameters adjustments (Method 5). Force and moment increments can also be calculated to complete the updated blade-element rotor model (Method 3). Corrections by adding filters (Method 2) can be used when the blade-element rotor model has reached its limitation or special effects are required. While physics-based models are still most commonly used for engineering and real-time trainer simulations, when flight data exists or can be collected for an existing rotorcraft (manned or UAV), some organizations are using stitched models obtained through system identification are being used entirely for trainer applications in some organizations or as a means to update physics-based models (Method 7).

8.4.3 Flight Simulator Model Development

A major challenge of flight simulator model development is the requirement that helicopter training simulations are executed in real time. This requires high levels of computational efficiency, which effectively limit increases in model complexity associated with improving physical accuracy.

Another major challenge for flight simulator model development is data availability. Simulator manufacturers often do not have full access to the complete set of aircraft data required to generate accurate physics-based models. To meet the Level D simulator requirements despite the model's limitations or lack of data, the discrepancies between the trainer models and flight-test data can be compensated for using the model update techniques discussed in Chapters 5 and 7.

The flight dynamics modeling effort is treated in various ways by different simulator companies. The majority use dynamics models well established in literature and try to adjust the model to match discrepancies relative to the flight-test data. Common practice is to tune a model based on one set of data and validate the model with an independent set of data.

System identification methods can help to systematically compensate for the missing dynamics. Therefore, often a separate system identification effort is put into place to help identify the dynamics missing from the physics-based models. Many companies make use of the techniques reported in Tischler et al. [2] (Chapter 5).

8.4.4 Simulator Qualification Requirements Today

The level of effort to obtain the required data package and model fidelity can be adapted depending on the qualification level sought. Level D is the highest standard sought for full flight simulators and requires the highest level of fidelity. Levels A, B, and C require relatively lower levels of fidelity. A thorough definition of these standards is given in FAA Part 60 [15] and CS-FTD (H) [16].

The flight dynamics model is an important part of the qualification of a Level D full flight simulator. The standard requires comparison of the model with flight-test data using metrics such as flight parameters in trimmed flight conditions (e.g., control positions, Euler angles, torque readings, etc.) and responses to pilot inputs. Nearly 50% of the flight tests are simple hands-off control input tests where the pilot performs a step input or doublet in one axis and keeps his hands off of the controls to evaluate the helicopter short-term response. The majority of handling-qualities tests include those associated with the longitudinal long-term response (phugoid), lateral-directional oscillations (Dutch roll), spiral stability, and adverse-proverse yaw.

In addition, long flight maneuvers, such as take-off and landing, are compared with the response of the flight model in the simulator. Altogether, more than 100 flight maneuvers are compared. This is the so-called 'objective' part of the qualification procedure related to flight dynamics and is presented to the authorities via documentation. The tolerances required for these comparisons are quite small such that very small violations not even noticeable by a pilot could result in failing certification for the whole simulator. For flight model developers, this results in a very tedious tuning effort, which sometimes results in over-tuned models, i.e., flight model tuning for behavior not noticeable by pilots. The 'subjective' part of certification includes assessment of the general 'feel' of the simulator by a subject matter expert pilot, including in flight regimes that were not included in the objective assessment.

The 'subjective' part of certification includes assessment of the general 'feel' of the simulator by a subject matter expert pilot and flight regimes that were not included in the objective assessment. A common issue arises when a pilot's subjective opinion does not agree with the objective assessment of the handling qualities.

Reasons for such conflicts can be various and some may be credited to the lack of accurate data. For example, some of the flight-test maneuvers may be sensitive to initial conditions or environmental conditions. It is also not always possible to accurately measure the magnitude and direction of the wind at the time and location that the flight-test data are recorded. Moreover, it is not entirely clear that the set of validation tests as described in FAA Part 60 [15] and CS-FTD (H) [16] cover the entire frequency range in which the vehicle will operate. The models used may only be valid in parts of the flight envelope for which data are available and less accurate in parts of the flight envelope for which data were not available. As a result, a compromise is often reached between a model that satisfies the objective part of the validation and the opinion of the subject matter expert pilot.

QTG runs provide full documentation of comparisons of the simulator responses with flight-test data (more details in Tischler et al. [2], Chapter 4.5). QTG runs are executed in the simulator during every cycle of its life: flight model development, initial qualification, and every recurrent qualification. QTG runs will be performed by a simulator technician periodically, typically every 6 months. This testing involves running the complete QTG test package, which contains typically about 100 time history and static cases, in real time. The goal of these recurring tests is to determine if any of the results have degraded since the initial simulator qualification for results that were accepted by the civil regulatory authorities. Degradation of the QTG results when the simulator is in operation can occur for the following reasons:

- A model change required to resolve a valid subjective concern raised by a pilot after the official qualification. This may lead to slight degradation where the results are still in tolerance but lean more towards the pilot needs.
- Unexpected degradation resulting from a change that was not supposed to affect simulator handling or hardware issue that has gone undetected.

Whether before or after qualification, once the QTG batch is run, the results have to be printed and analyzed. Running a QTG batch itself involves using around 6 hours of simulator time (for which the simulator cannot generate revenue) and involves at least 4 hours of manual review and overlay plots to ensure that the match of the time histories is exactly the same as before. These tests are very sensitive to minor setup or hardware issues (friction, flight control hysteresis, etc.), which may result in a case being falsely out of tolerance. When this happens, simply re-running the case usually solves the problem; however, this uses more of the simulator's and technician's time.

Reducing the number of QTG test cases related to flight dynamics would result in a smaller number of flight tests, reduced cost, and faster evaluation of the simulators. Moreover, the recurrent evaluation runs would provide a more exhaustive analysis and recurrent cost would be reduced. This could be achieved by carefully selecting maneuvers that could replace a number of the current QTGs. By doing so, the new maneuvers should still preserve data content that was covered by the existing QTGs and that are deemed to be important

to the pilot. In the case of military projects, QTG runs are usually a requirement to be met, but it is possible that the models will diverge from the flight-test data. This sometimes happens because a required training task to be performed is in contradiction with the flight-test data. In this case, a rational would be provided by the military regulatory authority.

One way to reduce the number of QTG runs could be the inclusion of frequency-domain based tests. This could help the developer evaluate the model at the frequency bands the pilots primarily operate at. In fact, a pilot rarely flies with 'step-type' inputs used in the QTG validation. Validation of training simulator fidelity for pilot-in-the-loop tasks (e.g., tracking tasks, high bandwith slope and run-on landing), is best accomplished from the simulator vs flight frequency responses and associated metrics of key input-output pairs.

To validate a model using frequency-domain analysis, the Maximum Unnoticeable Added Dynamics (MUAD) criteria could be applied to the resulting frequency plots in order to evaluate whether or not the change would be noticeable by a pilot. Frequency-domain runs, however, would not replace all QTG runs in time-domain validation, especially tests related to performance and maneuvers related to actual aircraft operation (takeoff, landings, autorotation entry, etc.). Section 8.5.2 will show the QTG tolerance bands in the frequency domain. A suggested replacement to reduce the number of QTG tests using frequency-sweep tests is given in Table 8-3. Frequency response tests are usually easier to generate inside a simulator, as they don't rely on initial condition adjustments. The Table suggests a possible reduction by a factor of 6 in the simulation and flight tests with the inclusion of frequency-sweep tests in the overall text matrix.

Table 8-3: Summary of the Reduction in QTG Test Cases Using Frequency Sweeps.

Flight Regime	Current QTG Cases	Recommended Frequency-Sweep Tests that Could Replace the Current QTG Tests
Hover	Longitudinal Control Response, SAS OFF & SAS ON Lateral Control Response, SAS OFF & SAS ON Directional Control Response, SAS OFF & SAS ON Vertical Control Response, SAS OFF & SAS ON Total: 8 cases	Frequency responses, SAS OFF & SAS ON Total: 2 tests
Mid Speed Cruise	Longitudinal Long-Term Response, SAS OFF or SAS ON Longitudinal Short-Term Response, SAS OFF & SAS ON Lateral Control Response, SAS OFF & SAS ON Directional Control Response, SAS OFF & SAS ON Lateral-Directional Oscillations, SAS OFF & SAS ON Spiral Stability, Left & Right, SAS OFF or SAS ON Adverse/Proverse Yaw, SAS OFF & SAS ON Total: 18 cases	Frequency responses, SAS OFF & SAS ON Total: 2 tests

Flight Regime	Current QTG Cases	Recommended Frequency-Sweep Tests that Could Replace the Current QTG Tests
High Speed Cruise	Longitudinal Short-Term Response, SAS OFF & SAS ON Lateral Control Response, SAS OFF & SAS ON Directional Control Response, SAS OFF & SAS ON Lateral-Directional Oscillations, SAS OFF & SAS ON Spiral Stability, Left & Right, SAS OFF or SAS ON Adverse/Proverse Yaw, SAS OFF & SAS ON Total: 12 cases	Frequency responses, SAS OFF & SAS ON Total: 2 tests
Total Number of Handing-Related Dynamics Cases	Total: 38 cases	Total: 6 tests

8.5 FIDELITY METRICS REVISITED

As discussed in the previous section, a revisit to the exiting fidelity metrics is sought. Section 8.5.1 will describe the fidelity metrics applicable to a flight simulator in the time domain and Section 8.5.2 will demonstrate how frequency-domain metrics may be beneficial in replacing some of the time-domain metrics.

8.5.1 Time-Domain Metrics

The timed-domain metrics currently used in flight simulators are described in detail in the various advisory circulars such as FAA Part 60 [15] and EASA [16]. The tolerance bands are expressed in terms of percentage of allowable error. An example of the tolerance requirements in the FAA Part 60 circular is found in Figure 8-13 below for longitudinal handling qualities, which shows a representative sample of the typical time history tolerances that are found in a circular.

A joint research program between Bell Helicopter Textron Canada (BHTC), NRC Aerospace, and several universities in Montreal (École de technologie Supérieure and École Polytechnique de Montréal) was initiated and addressed various challenges associated with modeling high-fidelity helicopter aerodynamics from a flight-test-generated database.

A parameter estimation technique is routinely used to determine the helicopter's small perturbation stability and control derivatives at numerous trim conditions, which are associated with the helicopter's motion for specific speeds and maneuvers. For a continuous simulation, the discrete derivatives are equated using the helicopter states and configuration to produce a preliminary global model that covered the majority flight envelope of the helicopter; flight data based on the FAA Helicopter Simulator Qualification Test Guide (Level D) maneuvers are used to validate the aerodynamic model. Model stitching is used to combine the three components: 1) Preliminary global model; 2) Trim curves that are generated from the trim model and equations; and 3) Nonlinear gravitational force equations to produce a continuous, quasi-nonlinear, stitched global model.

The process ultimately results in a global model able to accurately capture the higher-order dynamics of the helicopter. To see details concerning use of the stitched global model for Level D application please see Section 8.4.1 and Chapter 7.7.1 in Tischler et al. [2].

QPS requirements								Information
Test		Tolerance(s)	Flight condition	Test details	Simulator level			Notes
Entry No.	Title				B	C	D	
2.b.3.b.	Lateral	Roll Rate—±10% or ±3°/sec., Roll Attitude Change—±10% or ±3°.	Hover Augmentation On and Off.	Record results for a step control input. The Off-axis response must show correct trend for unaugmented cases.		X	X	This is a "short time" test conducted in a hover, in ground effect, without entering translational flight, to provide better visual reference.
2.b.3.c.	Directional	Yaw Rate—±10% or ±2°/sec., Heading Change—±10% or ±2°.	Hover Augmentation On and Off.	Record results for a step control input. The Off-axis response must show correct trend for unaugmented cases.		X	X	This is a "short time" test conducted in a hover, in ground effect, without entering translational flight, to provide better visual reference.
2.b.3.d.	Vertical	Normal Acceleration—±0.1 g.	Hover Augmentation On and Off.	Record results for a step control input. The Off-axis response must show correct trend for unaugmented cases.		X	X	
2.c.	Longitudinal Handling Qualities							
2.c.1.	Control Response	Pitch Rate—±10% or ±2°/sec., Pitch Attitude Change—±10% or ±1.5°.	Cruise Augmentation On and Off.	Results must be recorded for two cruise airspeeds to include minimum power required speed. Record data for a step control input. The Off-axis response must show correct trend for unaugmented cases.	X	X	X	
2.c.2.	Static Stability	Longitudinal Control Position: ±10% of change from trim or ±0.25 in. (6.3 mm) or Longitudinal Control Force : ±0.5 lb. (0.223 daN) or ±10%.	Cruise or Climb. Autorotation. Augmentation On and Off.	Record results for a minimum of two speeds on each side of the trim speed. May be a series of snapshot tests.	X	X	X	
2.c.3.	Dynamic Stability							

Figure 8-13: Typical Time-Domain Metrics Required in a QTG Package.

The stitching technique has been successfully applied in the development of many aircraft simulations in the last two decades. For fixed-wing aircraft, the technique has been used during the development of flight simulators for the Cessna Citation CJ1 aircraft [19], Beechjet [20] and King Air [21]. Due to this NATO group's interest in high-fidelity helicopter modeling work, the Bell 427 [22], [23] Level D simulator mathematical model development utilized the stitching technique. Furthermore, higher-order dynamics were used to model main rotor speed and torque during autorotation. Notably, autorotation maneuvers involve complex non-linear dynamics and are described below. Also, an aerodynamic model was developed using flight data to support use of a Commercial Off-The-Shelf (COTS) autopilot for the TRex helicopter [24] and Aphid UAV [25].

In summary, time-domain metrics are in widespread use in the flight simulator industry primarily because the advisory circulars that qualify flight simulators use them. Since these time-domain metrics are using error tolerance bands instead of a more quantitative approach (such as an RMS cost function), the evaluation of whether a simulation result is 'good enough' is subject to a wide range of interpretations. Meeting these time-domain criteria also does not guarantee that the simulation response will have a high fidelity across all frequencies that may be of interest to a pilot. The next section will cover the frequency-domain metrics.

8.5.2 Frequency-Domain Metrics

In the frequency domain, one metric that can be used to measure the fidelity of a simulation model is the Maximum Unnoticeable Added Dynamics (MUAD) envelope. The MUAD boundaries were first proposed by Hodgkinson [26] to assess lower-order model accuracy for fixed-wing handling-qualities applications. Being within the MUADs boundaries means that the model mismatch error will remain unnoticed to a SME pilot and therefore the added dynamics should be acceptable. The same analysis approach was first proposed by Tischler [27] for model fidelity assessment.

As shown in Figure 8-14, the shape of MUAD envelopes is like an hourglass. Pilots are more sensitive to the added dynamics at mid-frequencies (around 1-3 rad/sec), which are characteristic of the pilot operating frequencies. As a result, the MUAD allowable mismatch boundaries are most narrow in this range. At either end of the envelopes, their shape becomes wider. This means that pilots are less sensitive to the added dynamics beyond and below these frequencies.

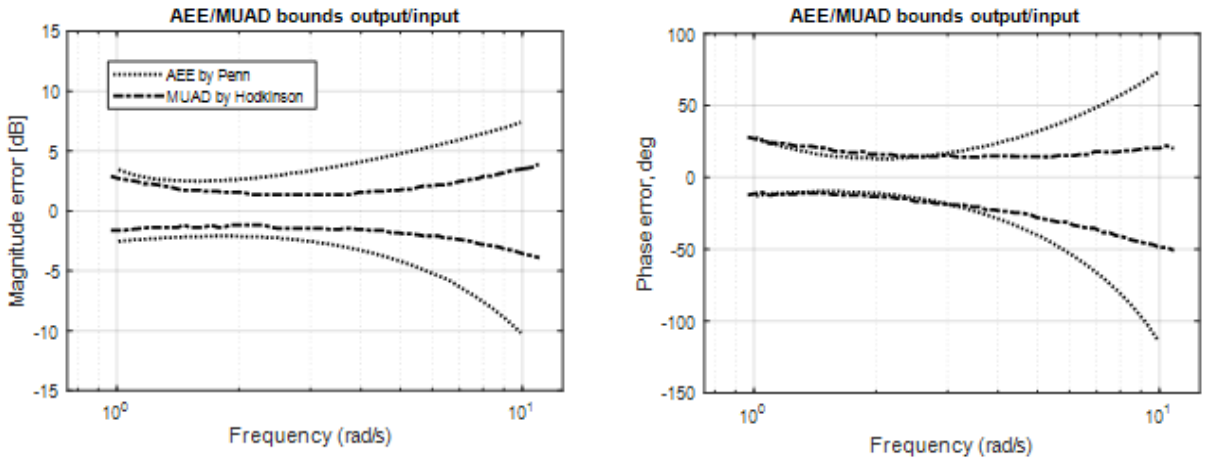

Figure 8-14: AEE/MUAD Error Bounds in Frequency Domain.

The most important characteristic of MUADs envelopes is that the boundaries are defined by a perceived change in the handling qualities. Mitchell et al. [28] proposed an experiment to study the pilot sensitivity on the variations in the helicopter dynamics. Instead of determining the critical added dynamics by degrading handling qualities, the boundaries were found by SME pilots' rating the noticeability of the added dynamics in the so-called Allowable Error Envelops (AEE). The boundaries on MUAD show the envelopes based on handling quality, the AEE boundaries show the envelopes based on pilot's opinion on the task performance. Figure 8-14 shows the AEE/MUAD bounds for the CAE's OO-BERM compared to flight-test data. Also, for frequency domain, an equivalence to the time-domain QTG tolerance bands can be expressed in the frequency domain were added in for each axis responses:

$$|QTG_{band}(j\omega)|_{dB} = \pm 20\log_{10}(\max(abs, rel)))$$
$$\angle QTG_{band}(j\omega) = \pm \Delta t \frac{\omega}{2\pi} * 360 \text{ deg} \quad (8\text{-}1)$$

where |…|_dB is the QTG magnitude tolerance band, ∠(…) is the QTG phase tolerance band, abs is the absolute QTG tolerance band, rel is the QTG relative tolerance band and Δt is the delay introduced by the simulation. It should be noted that the magnitude tolerance is constant for every frequency (gain), whereas the phase tolerance will increase with the frequency.

For the frequency domain tolerance bands, both FAA ([15] (Paragraph 15)) and EASA ([16] (Appendix 5)) define the maximum permissible delay to be 100 ms. This delay can be measured through the 'Transport delay' test. 'Transport delay' defines the total training simulator system processing time required for an input signal from a pilot primary flight control until the motion system, visual system, or instrument response. It is the overall time delay incurred from signal input until output response perceptible by the pilots. In the case where only the vehicle dynamics loop is analyzed (flight dynamics, flight controls, engines, and autopilot), it is reasonable to reduce this maximum delay to 50 ms.

In Figure 8-15, the sequence to measure the transport delay from control inputs through the interface is shown. In a typical training simulator configuration, there will be up to one iteration between flight controls input and the simulator flight control interface, which calculates the main rotor blade angles from the flight control measured position. This is because a flight controls input can occur at any time in the iteration, but it will not be processed before the start of the new iteration. There is at least one iteration between the simulator flight control interface and the Host where helicopter aerodynamics is calculated and integrated. This adds up to up to 2 iteration delays that are completely independent from the model itself. If a training simulator is running at 60 Hz, 3 iterations will mean a reasonable delay of 50 ms while allowing for a very small model error in terms of delay.

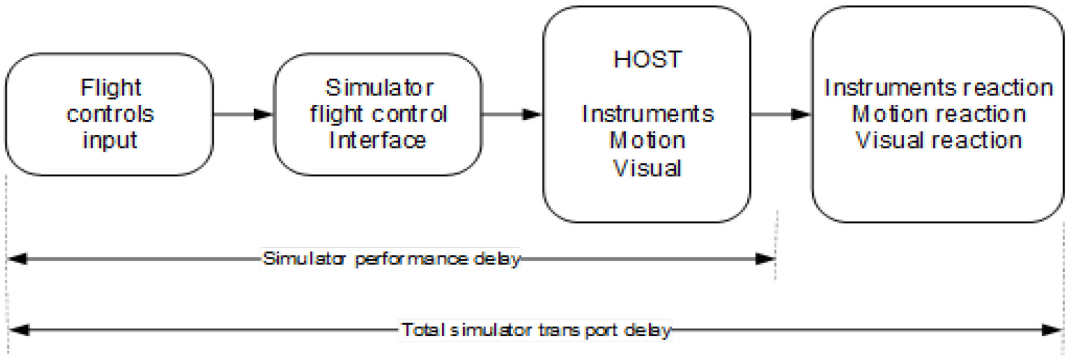

Figure 8-15: Transport Delay for Training Simulator.

Finally, in Figure 8-15, the Model Error is determined from

$$\text{Model Error} = \text{OO-BERM response} / \text{flight-test response} \tag{8-2}$$

As can be seen in Figure 8-16, which shows the time-domain validation of the hover model OO-BERM against flight data (top: lateral cyclic input; bottom: longitudinal cyclic input) for a B412 helicopter, the MUAD boundaries are consistent with the QTG boundaries, especially at mid frequencies, allowing both fidelity assessment methods to be used with a common implied level of fidelity. When comparing the QTG tolerance band to the MUAD, in Figure 8-16, it can be seen that the magnitude QTG tolerance band is more restrictive at lower and higher frequency. The phase tolerance of the QTG band is very restrictive at lower frequency when compared to the MUAD boundary. If we assume that the MUAD boundaries are correct, it may indicate that the QTG criteria are sometimes more restrictive than what a pilot would notice at very low and high frequencies. From Figure 8-16, the updated OO-BERM frequency-domain errors are within the FAA and EASA tolerance bands for the on-axis responses and off-axis responses are reasonably within 2 x the tolerance bands. As expected, the Baseline OO-BERM frequency-domain errors show poor results.

From Figure 8-17 (B412 case study), off-axis roll time response to longitudinal cyclic input seems to show reasonable behavior, but when we look at p/δ-lon Baseline OO-BERM model error from Figure 8-16, the match is not within the MUAD & QTG boundaries throughout the whole range of frequencies. Similar observation can be applied to off-axis pitch time response to lateral cyclic input q/δ-lat. This indicates that the while a model result may be in tolerance in time domain, it may still present discrepancies that can be noticed by a pilot when analyzing the results against the MUAD boundaries. In this case, the MUAD may therefore be a more restrictive guidance than a correct trend and magnitude criteria defined in time domain.

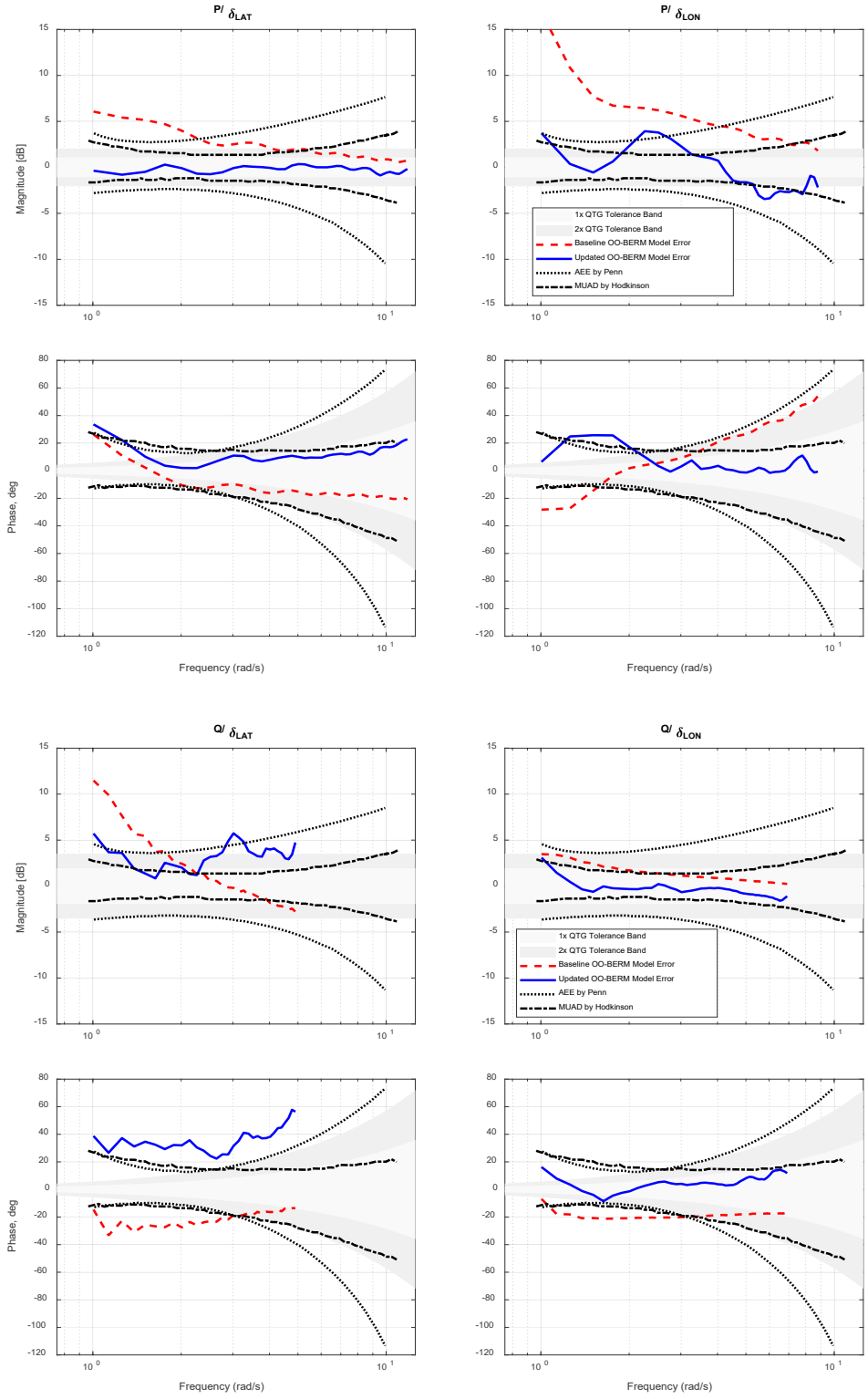

Figure 8-16: Frequency-Domain Validation of the Hover Model OO-BERM Against Flight Data (Top: Lateral Cyclic Input, Bottom: Longitudinal Cyclic Input).

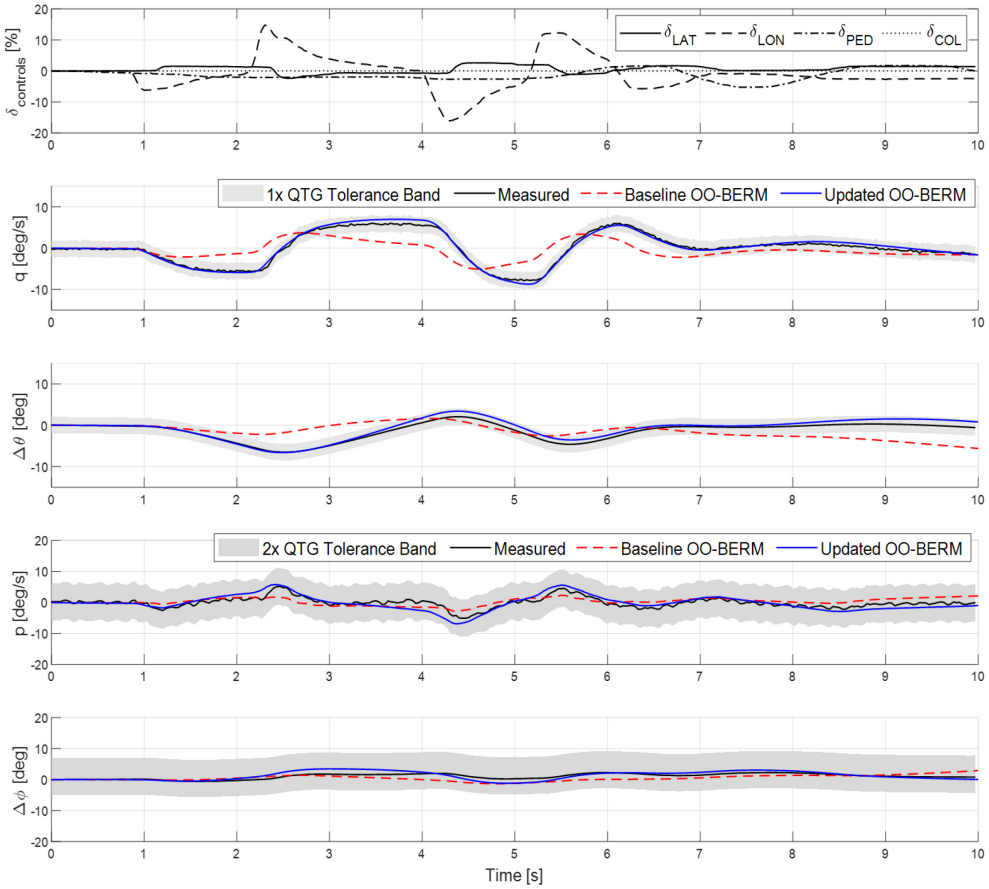

Figure 8-17: Time Domain Validation of the Hover Model OO-BERM Against Flight Data (Top: Lateral Cyclic Input, Bottom: Longitudinal Cyclic Input).

The QTG TD metrics are not based on what the pilot might or might not notice. Tests usually represent a fairly broad-brush measure of the accuracy/fidelity of a model to step inputs over the short term; the short-term character means that low frequency behavior (lower end of MUAD chart) are not captured. However, as it is shown in the MUAD plots in Figure 8-16, using the frequency-domain criterion gives a quantifiable measure of how much a pilot would notice a discrepancy between the simulator and flight-test data for both the on-axis and off-axis response. For this reason, it would be advisable to consider the suitability of a frequency-domain qualification for simulator qualifications.

Frequency-domain metrics could also be used to reduce the time spent in the recurrent evaluation of a flight model in a simulator. Currently, a flight model is objectively evaluated by running what is known as a QTG run. A QTG run provides a full validation of the simulator against the flight-test data for all the test cases defined by the advisory circular (Figure 8-13). QTG runs are executed in the simulator at every cycle of its live: during the flight model development, at the initial qualification and at every recurrent qualification. In the recurrent qualifications, QTG runs will be performed by a simulator technician periodically typically every 6 months. This testing involves running in real time the complete QTG test package, which contains around one hundred time history cases and static cases. The goal of these recurring tests is to determine if any of the results have degraded since the initial simulator qualification where results were accepted by the civil regulatory authorities. This is explained in greater details in Section 8.4.4 of these notes.

8.6 REFERENCES

[1] Howlett, J.J. (1981), "UH-60A Black Hawk Engineering Simulation Program: Volume I – Mathematical Model," NASA CR-166309, Dec.

[2] Tischler, M.B., White, M.D., Cameron, N., D'Agosto, S., Greiser, S., Gubbels, A., Guner, F., He, C., Horn, J., Hui., K., Jones, M., Juhasz, O., Lee, O., Lehmann, R., Miller, D., Myrand-Lapierre, V., Nadeau-Beaulieu, M., Nadell, S., Padfield, G., Pavel, M., Prasad, J., Ragazzi, A., Richard, S., Scepanovic, P., Seher-Weiß, S., Soong, J., Stroosma, O., Taghizad, A., Tobias, E., Xin, H., and Yavrucuk, I. (2021), "Rotorcraft Flight Simulation Model Fidelity Improvement and Assessment," NATO STO AVT-296 Technical Report.

[3] Zhang, C., Xin, H., and Driscoll, J. (2017), "Development and Validation of an Engineering Simulation Model in FLIGHTLAB with Customized Modeling Enhancements," AHS 73rd Annual Forum, Fort Worth, Texas, May.

[4] He, C., Xin, H., and Bhagwat, M. (2004), "Advanced Rotor Wake Interference Modeling for Multiple Aircraft Shipboard Landing Simulation," AHS 59th Annual Forum, Baltimore, MD.

[5] Zhao, J., Prasad, J.V.R., and Peters, D.A. (2004), "Rotor Dynamic Wake Distortion Model for Helicopter Maneuvering Flight," *Journal of the American Helicopter Society*, Vol. 49, No. 4, October, pp. 414-424.

[6] Guner, F., Miller, D.G., and Prasad, J.V.R. (2020), "Understanding the Effect of Rotor-to-Rotor Interference on CH-47D Helicopter Lateral Axis Dynamics in Hover," VFS 76th Annual Forum, October.

[7] Fegely, C., Xin, H., Juhasz, O., and Tischler, M.B. (2016), "Flight Dynamics and Control Modeling with System Identification Validation of the Sikorsky X2 Technology Demonstrator," American Helicopter Society 72nd Annual Forum Proceedings, May, West Palm Beach, FL.

[8] Juhasz, O., Xin, H., and Tischler, M.B. (2020), "Inflow Based Flight Dynamics Modeling Improvements for the Sikorsky X2 Technology™ Demonstrator," VFS 76th Annual Forum, October.

[9] Xin, H., Zhang, C., and Driscoll, J. (2019), "Enhancement of an Engineering Simulation Model to Improve the Correlation with Flight Test Data in Climb/Descent and Autorotation," AHS 75th Annual Forum, Philadelphia, PA, May.

[10] Tischler, M.B., Berger, T., Ivler, C.M., Mansur, M.H., Cheung, K.K., and Soong, J.Y. (2017), Practical Methods for Aircraft and Rotorcraft Flight Control Design: An Optimization-Based Approach, AIAA, April.

[11] ADS-33E (2000), "Aeronautical Design Standard, Handling Qualities Requirements for Military Rotorcraft," USAAMCOM ADS-33E-PRF, US Army Aviation and Missile Command, Huntsville, AL, March.

[12] SAE (2007), "Aerospace – Flight Control Systems – Design, Installation and Test of Piloted Military Aircraft, General Specification for," SAE-AS94900, July.

[13] Mansur, M.H., and Tischler, M.B. (2013), "Flight Test Comparison of Alternate Strategies for Multi-Loop Control Law Optimization," American Helicopter Society 69th Annual Forum, Phoenix, Arizona, May 21 – 23.

[14] Christensen, K.T., Campbell, K.G., Griffith, C.D., Ivler, C.M., Tischler, M.B., and Harding, J.W. (2007), "Flight Control Development for the ARH-70 Armed Reconnaissance Helicopter Program," American Helicopter Society 63rd Annual Forum, Virginia Beach, VA, May.

[15] FAA (2016), "Federal Aviation Administration," National Simulator Program, 14 CFR Part 60, 2016.

[16] EASA (2012), European Union Aviation Safety Agency, CS-FSTD(H), Certification Specifications for Helicopter Flight Simulation Training Devices, *Initial Issue*, June 2012.

[17] ICAO (2012), ICAO 9625 Manual of Criteria for the Qualification of Flight Simulation Training Devices, Volume II – Helicopters, 1st edition, 2012.

[18] SAE (2019), ARINC 450-1 Flight Simulator Design and Performance Data Requirements, 2019.

[19] Hui, K., Auriti, L., and Ricciardi, J., (2008), "Cessna Citation CJ1 Flight-Test Data Gathering and Level-C Simulator Aerodynamic Model Development," International Council of the Aeronautical Sciences (ICAS), Sept. 14-19, 2008, Anchorage, Alaska USA.

[20] Hui, K., Ricciardi, J., Ellis, K., and Tuomey, D. (2001), "Beechjet Flight Data Gathering and Level D Simulator Aerodynamic Mathematical Model Development," AIAA ADM conference in August 2001, Montreal, Quebec.

[21] Hui, K., Srinivasan, R., Auriti, L., Ricciardi, J., Blair, K., and Pokhariyal, D. (2002), "King Air Flight-Test Data Gathering and Level-D Simulator Model Development," ICAS 2002 Conference from September 8 – 13, 2002, Toronto, Ontario.

[22] Hui, K., Shives, M., Morbi A., Swartz, M., Robinson, J., and McTavish S. (2007), "Bell 427 Helicopter Level D Full Flight Simulator Mathematical Model Development Technique," National Research Council of Canada, February 2007, Ottawa, Canada.

[23] Hui, K., Lambert, E., and Seto, J. (2006), "Bell M427 Flight Test Data Gathering and Level-D Simulator Model Development," ICAS 2006 International Congress of the Aeronautical Sciences, Sept. 3 – 8, 2006, Hamburg, Germany.

[24] Hui, K., Crain, A., Gorman, J., Ellis, K., Cheung, S., and Giardino, F. (2015a), "Design and Development of a TRex 700E UAV Helicopter for Flight Test Data Gathering and Hover Model Development," LTR-FRL-2015-0033, 11/6/2015

[25] Hui, K., Crain, A., and Grymonpre, D. (2015b), "Instrumentation, Flight Testing and Aerodynamic Hover Modeling of the Aphid Unmanned Ultralight Helicopter," LTR-FRL-2015-0037, 8/5/2015

[26] Hodgkinson, J. (1998), Aircraft Handling Qualities, AIAA Education Series, American Institute of Aeronautics and Astronautics, Reston, VA.

[27] Tischler, M.B., (1996), *Advances in Aircraft Flight Control*, Taylor & Francis Ltd, London, U.K., 1996, pp. 52-54.

[28] Mitchell, D.G., Doman D.B., Key, D.L., Klyde, D.H., Leggett D.B., Moorhouse D.J., Mason D.H., Raney D.L., and Schmidt D.K., (2004), "Evolution, Revolution, and Challenges of Handling Qualities," Journal of Guidance, Control, And Dynamics, Vol. 27, No. 1, January–February 2004, pp. 12-28.

7.9.2 References

[1] Tischler, M.B., White, M.D., Cameron, N., D'Agosto, S., Greiser, S., Gubbels, A., Guner, F., He, C., Horn, J., Hui., K., Jones, M., Juhasz, O., Lee, O., Lehmann, R., Miller, D., Myrand-Lapierre, V., Nadeau-Beaulieu, M., Nadell, S., Padfield, G., Pavel, M., Prasad, J., Ragazzi, A., Richard, S., Scepanovic, P., Seher-Weiß, S., Soong, J., Stroosma, O., Taghizad, A., Tobias, E., Xin, H., and Yavrucuk, I. (2021), "Rotorcraft Flight Simulation Model Fidelity Improvement and Assessment," NATO STO AVT-296 Technical Report.

Chapter 9 – DISCUSSION AND SUMMARY

ABSTRACT

This final Chapter first recaps the goals and objectives of NATO Working Group AVT-296. Advancements in system identification over the past 30 years allow the extraction of accurate linear-time invariant 'truth models' in the form of frequency responses and stability and control derivative matrices from flight-test data. The use of these truth models to update and validate the fidelity of the rotorcraft flight simulation in the context of the overall flight vehicle development and flight-test processes is emphasized. Then, the key findings and recommendations of AVT-296 are summarized.

9.1 DISCUSSION

NATO Working Group AVT-296 have engaged in the task to 'apply and compare rotorcraft flight simulation model update and fidelity assessment methods based on flight-test case studies' and to 'document best practices for application to rotorcraft design, certification, and pilot training.' An ambition of the group was 'to align control design and simulation certification standards between the nations.' Industry and government laboratories in NATO nations can derive considerable benefit from a coherent exposition of best practices as planned by the group. The use of System IDentification (SID) methods in flight model updating has been advancing over the decades since AGARD Working Group 18 and associate Lecture Series (AR-280, [1]) and now form a rational and systematic approach to the exploration of model fidelity improvements (see Chapter 4). AVT-296 took on the task of reviewing and reporting these advancements as part of their work. Before summarizing the findings and recommended practices from AVT-296, it is useful to remind the reader of the different contexts of flight model developments.

Flight simulation modeling and fidelity assessment is an activity within the larger *Virtual Engineering* discipline, which spans the life-cycle of a rotorcraft [2]. There is strong motivation to have the highest possible fidelity in the early design phase to avoid costly re-design during the development phase. Without flight-test data on the actual aircraft, early fidelity assessment is often based on existing baseline configurations, e.g., an earlier version of the aircraft type. Flight models are used to support decision making in this design phase and to provide critical support through to design freeze, to first flight and throughout the development phase. The life-cycle continues through into operation where flight models feature at the heart of crew training devices, including the highest fidelity, Level D pilot training simulators.

As flight-test data become available during the development phase, the fidelity can be improved through rotorcraft flight model updating processes. During this fidelity evolution, it is expected that fidelity metrics and quality standards (e.g., for performance and handling qualities) are used to judge fitness for purpose of the flight model (see Chapter 7 of Tischler et al. [3]). An important aspect of the process during the design and development phases is that the models need to be 'physics-based.' There is no scope here for updating or repairing model deficiencies with non-physical attributes and parameter adjustments. There may also be different variants (levels of complexity) of the same physics-based model in these phases. For example, as discussed in Ries [4], coupled CFD and flight mechanics models are used in the critical design review, but some reduced order forms of these are required, for example, in piloted simulation assessments of handling qualities and associated control law design. Fidelity degradation as the physics-complexity decreases must be quantified here as it will impact confidence in decision making. There is considerable scope for SID methods in the development of these reduced-complexity models, for example, replacing the complex wake dynamics with finite-state inflow models (see e.g., Chapter 7.4 of Tischler et al. [3]). The derivation of the parameters in these reduced-complexity models is fertile ground for the methods presented in this AVT Report.

Flight models used to support qualification and certification processes need to be, arguably, at the highest level of fidelity in the life-cycle. This is particularly true when the flight model is being used to demonstrate

compliance with airworthiness standards [5]. In the example provided in Ragazzi, [5], the flight model in question was part of a piloted flight simulator, so reduced-complexity was necessary to achieve the real-time operation. Also, the other aspects of the flight simulator, including the vestibular/visual motion cueing, become part of the fidelity assessment (see e.g., Chapter 7.8 of Tischler et al. [3]). There are no international/NATO standards for flight model fidelity in this critical airworthiness area, and the AVT-296 activity was scoped to provide guidance. The issues here revolve around how to preserve the physics-based fidelity while reducing the model complexity; so, strictly, the process is not so much model 'updating' as reduced-complexity modeling and the impact on fidelity.

Flight model updating and fidelity assessment play strong roles in the development of flight training simulators. Here, the flight model is often developed by the simulator manufacturer with limited support from the aircraft manufacturer, hence, relying extensively on measurements made on the aircraft including dedicated flight tests. Certification standards (e.g., FSTD H [6]) are defined in terms of fidelity metrics and tolerances in this phase for both the flight model and the components of the flight simulator (e.g., motion, visual, and feel systems). The standards also require comparisons between flight test and simulation maneuvers with acceptability tolerances defined. However, there is nothing in the standards requiring the flight models to be physics-based. Typical practices to achieve compliance with the fidelity standards therefore often involve adjusting simulation model parameters without strict adherence to a physics-based justification, typically within a low-medium complexity model (see e.g., Chapter 7.6 of Tischler et al. [3]).

9.2 CONCLUSIONS AND RECOMMENDATIONS

Within the final report, past research on math model update strategies from each participating organization was first summarized. This included work at various government research labs, academia, rotorcraft Original Equipment Manufacturers (OEM), and simulator developers. Fidelity, or the ability of the flight model to predict rotorcraft behavior, is a central theme in rotorcraft model development and was featured across the work of AVT-296. Model fidelity metrics were presented and discussed. The discussion then focused on model fidelity improvement methods and gave several case studies per method with the aim of highlighting the applicability and limitations for each model update method. Common to all fidelity assessment and update methods in this report is the extensive use of rotorcraft SID that has been considerably advanced in the past 30 years, starting under the landmark report of NATO AGARD Working Group 18 [1]. System identification provides 'truth models,' nonparametric frequency responses, or parametric transfer function, and state-space models empirically extracted from flight-test data. In the current work, comprehensive flight-test case studies have demonstrated the approach, effectiveness, and shortfalls of each of the model update and fidelity assessment methods. Eight rotorcraft, varying greatly in size and configuration, showed the flexibility and robustness of the methods. Chapter 8.5 discussed the applicability of each flight model update method for rotorcraft engineering development, control law design, and piloted training simulation [3]. The individual chapters and sections contain extensive summary/comparison tables and conclusions whereas this final chapter draws overall conclusions and recommendations from the effort as follows:

1) Recent activities comparing and updating rotorcraft flight dynamics models with flight data show that each organization's flight dynamics simulation capabilities are continually improving, and the various flight dynamics models used by each organization are comprised of common modeling elements (e.g., blade element main rotors and look-up tables for fuselage aerodynamics). There is still, however, a strong need to update flight dynamics models after the initial predicted responses are compared with flight-test data. The update method(s) used within each organization have generally been developed 'in-house' and specifically to each organization's need with limited collaboration between various organizations. The AVT-296 team meetings and collaborative research provided a unique opportunity for Subject Matter Experts (SMEs) in flight simulation to compare, learn, discuss, and explore a range of model update and fidelity assessment methods, as well as document the advantages, limitations, and roles of each.

2) Quantitative fidelity assessment methods and metrics consider the agreement or 'match' of the trim and dynamic response of the flight model and test data in the time and frequency domains. Time-domain fidelity assessment is established by comparing time histories of the flight simulation model and aircraft response for various dynamic maneuvers. For piloted training simulator application, regulatory agencies within the US and Europe make extensive use of Qualification Test Guide (QTG) inputs and associated tolerance standards to define an acceptable level of match between flight and simulation data. In this AVT report, additional fidelity assessment methods and standards in the time and frequency domains, drawn from the SID literature, were found to be robust for the wide range of aircraft configurations considered in this RTG and provided important insight for flight simulation updates. Analogous to the QTG assessment method is a comparison of simulation vs flight frequency responses. An important advantage is the clear distinction of magnitude and phase errors, and the ability to visualize fidelity as a function of frequency. When simulation model and flight responses are plotted as error functions, the Maximum Unnoticeable Added Dynamics, or 'MUAD' boundaries, originally developed for fixed-wing model fidelity assessment and later adapted for rotorcraft provide mismatch envelopes that emphasize fidelity in the mid-frequency range (1 – 10 rad/sec), most important for flight control design and pilot training applications. If a single metric is desired, an integrated frequency cost function has been widely validated in the rotorcraft SID literature and is useful for overall model assessment. An analogous integrated time-domain cost function, also from rotorcraft SID, is a useful overall metric in the time-domain. Statistically based time- and frequency-domain metrics allow an assessment of the relative (statistical) significance of errors between two models.

3) The pilot's perception of simulator fidelity combines the quantitative flight model fidelity discussed above with the fidelity of the simulator facility environment, predominantly the visual and motion cueing and stick force/feel dynamics. Guidelines for simulator facility fidelity assessment and tuning have been the subject of several prior AGARD (NATO) activities and reports. Some key results for simulator motion fidelity are summarized in Tischler et al. Chapter 4 [3]. In recent years, the Simulator Fidelity Rating (SFR) scale has been used to assess the overall suitability of rotorcraft training simulators from a transfer of training perspective. Additional useful metrics to quantify, for example, simulation vs flight pilot control stick activity, have been proposed as a measure of fidelity. A flight-test study based on the Bell 412, summarized in Tischler et al. [3], examines these metrics.

4) Eight rotorcraft data sets were made available for analysis by this working group, giving opportunities for a large breadth of case studies. While the update methods vary greatly in their implementation, evaluating each update method against the same set of flight data and fidelity assessment metrics was useful in determining improvements in model fidelity for each method. Each aircraft database included time and frequency responses from which stability and control derivatives obtained using SID could be derived to characterize key on- and off-axis responses as the basis for flight model update and fidelity assessment. The update method results are well summarized in Section 7.9, each demonstrating the ability to greatly improve the model fidelity compared with baseline model behavior [3]. Key conclusions and recommendations for using the methods are:

   i) Gain and time delay corrections (or in their more generally form, black box filters determined from frequency response error functions) work well to improve an already well-developed flight dynamics model. These methods were shown to ensure adequate prediction of control system and handling qualities metrics at higher frequencies and are recommended as a last step in the model update process or if the model is not able to be adjusted for further improvement in quantitative fidelity, e.g., using higher-order dynamics. These methods do not give physical insight into sources of modeling error.

ii) Comparing state-space model stability derivatives estimated from SID of flight-test data with perturbation models numerically extracted from the nonlinear simulation can provide insight into sources of missing dynamics in the simulation model. The key discrepancies in the stability and control derivatives provide incremental forces and moments that can be used to augment or 'renovate' the nonlinear flight model for a further improvement in fidelity. Establishing the derivatives that provide the greatest fidelity improvements provides a route to identifying the physical source of poor model fidelity.

iii) If the physical sources of model deficiencies are known, using reduced order models and physics-based corrections to improve model fidelity can give broad improvements in the model and will have the largest benefit when extrapolating to other flight conditions or different rotorcraft. However, this method requires extensive knowledge of physics within the rotorcraft simulation and requires detailed flight-test data, which may not be available to some organizations. Furthermore, higher-order modeling tools, such as various computational fluid dynamics rotor wake and finite-element structural modeling software are required. This method may work well when teaming with various SMEs is possible, e.g., in academia/research labs.

iv) Where there is uncertainty in model input data, individual model input parameters can be adjusted based on engineering insight or directly identified using system identification. In-depth understanding of rotorcraft simulation and frequency response analysis, particularly rotor system modes and their interaction with the rigid-body dynamics is required. These update methods are time consuming but give insight into sources of modeling errors.

v) When an instrumented test aircraft is available, system identification can provide accurate point models that can span the flight envelope with relatively few test points. Then, linear stability and control derivatives, as obtained from SID, can be combined (stitched) with the trim data and analytic expressions for the nonlinear gravity/kinematics to rapidly achieve an accurate full-flight envelope model, which extrapolates for changes in inertial characteristics and interpolated airspeed/altitude. The same approach can be used to create a real-time pilot simulation, from Linear Time Invariant (LTI) point models extracted numerically from a non-real-time physics-based model. This method produces highly accurate models since trim and dynamic response flight data are directly used in the simulation development. However, no extrapolation is possible to different aircraft configuration or aerodynamic changes, and limited extrapolation outside of the speed/altitude envelope where the 'anchor-point' state-space models were developed. A stitched model obtained from flight-test SID results can be rapidly produced, but, obviously, this is not a good approach in the early stages of aircraft development before an extensive flight-test database is available.

5) The different model update methods described have their unique strengths and weaknesses and give improvements to the model fidelity in different ways. There is no one method that is preferable to others, and the choice of method will be based on many factors, including model input data availability, SME availability, time/financial resources, and the ultimate end-use of the model. These topics are discussed in depth in Chapter 8 and summarized in Table 8.5-1 [3]. Key conclusions and recommendations from this chapter are:

i) No matter the update method or flight dynamics model end-use, model validation with flight-test data is essential and widely conducted in rotorcraft development. An accurate flight simulation model, able to predict behavior with high fidelity, can greatly enhance design confidence and reduce flight-test development time and cost.

ii) For OEM simulations, since the models are used in design trade studies and for a large variety of aircraft, model predictive capability is paramount. This drives a strong need for physics-based update methods with validation in time and frequency domains. Trim, stability, and dynamic maneuver validation are all important for handling qualities, flight control, and pilot training simulation applications.

iii) For flight control purposes, it is recommended that the validation with flight test be conducted not just for the bare-airframe aircraft response, but also the broken-loop, disturbance rejection, and closed-loop responses. In this context, the use of frequency-domain model design and assessment methods and metrics, as used in the case studies, has evolved into a very mature approach complementing SID flight model fidelity assessment.

iv) Model validation for training simulations using the existing QTG criteria is found to be restrictive and can lead to 'over-tuning' the model. Furthermore, evaluating and tuning against the QTG is time/effort intensive. It is recommended that frequency-domain validation methods and time-domain handling qualities based metrics be investigated for simulator qualification. These methods/metrics could lead to improved simulator fidelity without degrading validation efforts.

6) Flight model updating and fidelity assessment is an activity done throughout the rotorcraft life-cycle. The AVT Group comprised engineers from the aircraft manufacturing and flight simulator manufacturing industries, as well as their supply chains, government research laboratories, and academia. Generally, the emphasis in the work of the latter two is research to develop methods in support the activities of industry and government acquisition, as well as furthering the knowledge base. The AVT Group has thus been able to assess the status of fidelity assessment and update methods from both developer and user perspectives, linking methods classification with application in the rotorcraft life-cycle. The teaming accomplished between industry, academia, and government labs during this research activity was highly effective for data analysis and tech transfer between the various groups and should be maintained moving forward to continue developing the technical knowledge base in the field and pushing forward relevant technical work.

9.3 FINAL CONCLUDING REMARKS

This AVT-296 Report has gathered a wide range of, hitherto disparate, knowledge and experience on the theme of rotorcraft flight model fidelity assessment and improvement. It is intended as a lasting and comprehensive reference on a topic of major importance in the design and development of conventional helicopters, advanced high-speed rotorcrafts, and the growing novel urban air mobility configurations. As these industries strive to achieve greater efficiency and safety in their products, the fidelity of simulation should match commercial aspirations to ensure that the 'right first time' ethos is fully embedded into the virtual engineering dimension of industrial practice.

9.4 REFERENCES

[1] Hamel, P. G., (1991), "Rotorcraft System Identification," AGARD AR 280/ LS 178.

[2] Padfield, G.D. (2016), "Rotorcraft Virtual Engineering; Supporting Life-Cycle Engineering through Design and Development, Test and Certification and Operations," *Aeronautical Journal of the RAeS*, March 2018, doi: 10.1017/aer.2018.47 (also keynote at the RAeS conference on Rotorcraft Virtual Engineering, Liverpool, November).

[3] Tischler, M.B., White, M.D., Cameron, N., D'Agosto, S., Greiser, S., Gubbels, A., Guner, F., He, C., Horn, J., Hui., K., Jones, M., Juhasz, O., Lee, O., Lehmann, R., Miller, D., Myrand-Lapierre, V., Nadeau-Beaulieu, M., Nadell, S., Padfield, G., Pavel, M., Prasad, J., Ragazzi, A., Richard, S., Scepanovic, P., Seher-Weiß, S., Soong, J., Stroosma, O., Taghizad, A., Tobias, E., Xin, H., and Yavrucuk, I. (2021), "Rotorcraft Flight Simulation Model Fidelity Improvement and Assessment," NATO STO AVT-296 Technical Report.

[4] Ries, T. (2016), “Industrial Prediction of Helicopters in Flight; Interlinking Simulation Capabilities and Tools of Different Complexity,” RAeS conference on Rotorcraft Virtual Engineering, Liverpool, November.

[5] Ragazzi, A. (2016), “AW189 Engine-Off Landing Certification by Simulation,” RAeS Conference on Rotorcraft Virtual Engineering, Liverpool, November.

[6] CS-FSTD H (2012), “Certification Specifications for Helicopter Flight Simulation Training Devices,” (initial issue), EASA, June.

REPORT DOCUMENTATION PAGE

1. Recipient's Reference	2. Originator's References	3. Further Reference	4. Security Classification of Document
	STO-EN-AVT-365 AC/323(AVT-365)TP/1037	ISBN 978-92-837-2356-1	PUBLIC RELEASE

5. Originator

Science and Technology Organization
North Atlantic Treaty Organization
BP 25, F-92201 Neuilly-sur-Seine Cedex, France

6. Title

Rotorcraft Flight Simulation Model Fidelity Improvement and Assessment

7. Presented at/Sponsored by

Educational Notes for the AVT-365 Lecture Series.

8. Author(s)/Editor(s)	9. Date
Multiple	October 2021
10. Author's/Editor's Address	**11. Pages**
Multiple	270

12. Distribution Statement

There are no restrictions on the distribution of this document. Information about the availability of this and other STO unclassified publications is given on the back cover.

13. Keywords/Descriptors

Fidelity metrics; Flight dynamics; Flight simulation; Flight simulation model update; Inverse simulation; Perceptual fidelity; Rotorcraft; System identification

14. Abstract

Rotorcraft flight simulation models require high levels of fidelity to be suitable for use in support of life cycle practices, particularly vehicle and control design/development, system certification, and training qualification. More rigorous and systematic practices for fidelity assessments and enhancements could pay significant dividends in reducing life cycle costs for both military and civil rotorcraft. The AVT-296 Research Task Group concluded in 2020 and produced a technical report examining a range of rotorcraft simulation fidelity improvement methods and assessment metrics. The proposal of this follow-on Research Lecture Series is to disseminate the results based on the conclusion of the effort from AVT-296, with the intention to train NATO member nations in these best practices. Seven different model update methods, from simple to more complex, for improving the fidelity of a flight simulation model have been presented using eight comprehensive flight test databases made available through this working group. Fidelity assessment metrics in the time- and frequency-domains are considered, including those in current use by simulator qualification authorities (Qualification Test Guide, QTG) and others widely used in the research community for specific applications such as vehicle design improvement, development of handling-qualities requirements, and flight control design/evaluation. The benefits and limitations of the various methods/metrics for different engineering applications have been reported and recommendations made for future activities. The methods and metrics presented herein will find use in military and civilian applications to set criteria that will underpin the use of modeling and simulation in certification to accelerate development and acquisition and reduce the cost of new rotorcraft systems and legacy system upgrades. The criteria may also set standards for training devices to support the expansion of synthetic environments for training to offset the high costs of flying hours.

NORTH ATLANTIC TREATY ORGANIZATION

BP 25
F-92201 NEUILLY-SUR-SEINE CEDEX • FRANCE
Télécopie 0(1)55.61.22.99 • E-mail mailbox@cso.nato.int

SCIENCE AND TECHNOLOGY ORGANIZATION

DIFFUSION DES PUBLICATIONS
STO NON CLASSIFIEES

Les publications de l'AGARD, de la RTO et de la STO peuvent parfois être obtenues auprès des centres nationaux de distribution indiqués ci-dessous. Si vous souhaitez recevoir toutes les publications de la STO, ou simplement celles qui concernent certains Panels, vous pouvez demander d'être inclus soit à titre personnel, soit au nom de votre organisation, sur la liste d'envoi.

Les publications de la STO, de la RTO et de l'AGARD sont également en vente auprès des agences de vente indiquées ci-dessous.

Les demandes de documents STO, RTO ou AGARD doivent comporter la dénomination « STO », « RTO » ou « AGARD » selon le cas, suivi du numéro de série. Des informations analogues, telles que le titre est la date de publication sont souhaitables.

Si vous souhaitez recevoir une notification électronique de la disponibilité des rapports de la STO au fur et à mesure de leur publication, vous pouvez consulter notre site Web (http://www.sto.nato.int/) et vous abonner à ce service.

CENTRES DE DIFFUSION NATIONAUX

ALLEMAGNE
Streitkräfteamt / Abteilung III
Fachinformationszentrum der Bundeswehr (FIZBw)
Gorch-Fock-Straße 7, D-53229 Bonn

BELGIQUE
Royal High Institute for Defence – KHID/IRSD/RHID
Management of Scientific & Technological Research
for Defence, National STO Coordinator
Royal Military Academy – Campus Renaissance
Renaissancelaan 30, 1000 Bruxelles

BULGARIE
Ministry of Defence
Defence Institute "Prof. Tsvetan Lazarov"
"Tsvetan Lazarov" bul no.2
1592 Sofia

CANADA
DGSIST 2
Recherche et développement pour la défense Canada
60 Moodie Drive (7N-1-F20)
Ottawa, Ontario K1A 0K2

DANEMARK
Danish Acquisition and Logistics Organization
(DALO)
Lautrupbjerg 1-5
2750 Ballerup

ESPAGNE
Área de Cooperación Internacional en I+D
SDGPLATIN (DGAM)
C/ Arturo Soria 289
28033 Madrid

ESTONIE
Estonian National Defence College
Centre for Applied Research
Riia str 12
Tartu 51013

ETATS-UNIS
Defense Technical Information Center
8725 John J. Kingman Road
Fort Belvoir, VA 22060-6218

FRANCE
O.N.E.R.A. (ISP)
29, Avenue de la Division Leclerc
BP 72
92322 Châtillon Cedex

GRECE (Correspondant)
Defence Industry & Research General
Directorate, Research Directorate
Fakinos Base Camp, S.T.G. 1020
Holargos, Athens

HONGRIE
Hungarian Ministry of Defence
Development and Logistics Agency
P.O.B. 25
H-1885 Budapest

ITALIE
Ten Col Renato NARO
Capo servizio Gestione della Conoscenza
F. Baracca Military Airport "Comparto A"
Via di Centocelle, 301
00175, Rome

LUXEMBOURG
Voir Belgique

NORVEGE
Norwegian Defence Research
Establishment
Attn: Biblioteket
P.O. Box 25
NO-2007 Kjeller

PAYS-BAS
Royal Netherlands Military
Academy Library
P.O. Box 90.002
4800 PA Breda

POLOGNE
Centralna Biblioteka Wojskowa
ul. Ostrobramska 109
04-041 Warszawa

PORTUGAL
Estado Maior da Força Aérea
SDFA – Centro de Documentação
Alfragide
P-2720 Amadora

REPUBLIQUE TCHEQUE
Vojenský technický ústav s.p.
CZ Distribution Information Centre
Mladoboleslavská 944
PO Box 18
197 06 Praha 9

ROUMANIE
Romanian National Distribution
Centre
Armaments Department
9-11, Drumul Taberei Street
Sector 6
061353 Bucharest

ROYAUME-UNI
Dstl Records Centre
Rm G02, ISAT F, Building 5
Dstl Porton Down
Salisbury SP4 0JQ

SLOVAQUIE
Akadémia ozbrojených síl gen.
M.R. Štefánika, Distribučné a
informačné stredisko STO
Demänová 393
031 01 Liptovský Mikuláš 1

SLOVENIE
Ministry of Defence
Central Registry for EU & NATO
Vojkova 55
1000 Ljubljana

TURQUIE
Milli Savunma Bakanlığı (MSB)
ARGE ve Teknoloji Dairesi
Başkanlığı
06650 Bakanliklar – Ankara

AGENCES DE VENTE

The British Library Document
Supply Centre
Boston Spa, Wetherby
West Yorkshire LS23 7BQ
ROYAUME-UNI

Canada Institute for Scientific and
Technical Information (CISTI)
National Research Council Acquisitions
Montreal Road, Building M-55
Ottawa, Ontario K1A 0S2
CANADA

Les demandes de documents STO, RTO ou AGARD doivent comporter la dénomination « STO », « RTO » ou « AGARD » selon le cas, suivie du numéro de série (par exemple AGARD-AG-315). Des informations analogues, telles que le titre et la date de publication sont souhaitables. Des références bibliographiques complètes ainsi que des résumés des publications STO, RTO et AGARD figurent dans le « NTIS Publications Database » (http://www.ntis.gov).

NORTH ATLANTIC TREATY ORGANIZATION

BP 25
F-92201 NEUILLY-SUR-SEINE CEDEX • FRANCE
Télécopie 0(1)55.61.22.99 • E-mail mailbox@cso.nato.int

SCIENCE AND TECHNOLOGY ORGANIZATION

DISTRIBUTION OF UNCLASSIFIED STO PUBLICATIONS

AGARD, RTO & STO publications are sometimes available from the National Distribution Centres listed below. If you wish to receive all STO reports, or just those relating to one or more specific STO Panels, they may be willing to include you (or your Organisation) in their distribution.

STO, RTO and AGARD reports may also be purchased from the Sales Agencies listed below.

Requests for STO, RTO or AGARD documents should include the word 'STO', 'RTO' or 'AGARD', as appropriate, followed by the serial number. Collateral information such as title and publication date is desirable.

If you wish to receive electronic notification of STO reports as they are published, please visit our website (http://www.sto.nato.int/) from where you can register for this service.

NATIONAL DISTRIBUTION CENTRES

BELGIUM
Royal High Institute for Defence – KHID/IRSD/RHID
Management of Scientific & Technological Research for Defence, National STO Coordinator
Royal Military Academy – Campus Renaissance
Renaissancelaan 30
1000 Brussels

BULGARIA
Ministry of Defence
Defence Institute "Prof. Tsvetan Lazarov"
"Tsvetan Lazarov" bul no.2
1592 Sofia

CANADA
DSTKIM 2
Defence Research and Development Canada
60 Moodie Drive (7N-1-F20)
Ottawa, Ontario K1A 0K2

CZECH REPUBLIC
Vojenský technický ústav s.p.
CZ Distribution Information Centre
Mladoboleslavská 944
PO Box 18
197 06 Praha 9

DENMARK
Danish Acquisition and Logistics Organization (DALO)
Lautrupbjerg 1-5
2750 Ballerup

ESTONIA
Estonian National Defence College
Centre for Applied Research
Riia str 12
Tartu 51013

FRANCE
O.N.E.R.A. (ISP)
29, Avenue de la Division Leclerc – BP 72
92322 Châtillon Cedex

GERMANY
Streitkräfteamt / Abteilung III
Fachinformationszentrum der Bundeswehr (FIZBw)
Gorch-Fock-Straße 7
D-53229 Bonn

GREECE (Point of Contact)
Defence Industry & Research General Directorate, Research Directorate
Fakinos Base Camp, S.T.G. 1020
Holargos, Athens

HUNGARY
Hungarian Ministry of Defence
Development and Logistics Agency
P.O.B. 25
H-1885 Budapest

ITALY
Ten Col Renato NARO
Capo servizio Gestione della Conoscenza
F. Baracca Military Airport "Comparto A"
Via di Centocelle, 301
00175, Rome

LUXEMBOURG
See Belgium

NETHERLANDS
Royal Netherlands Military Academy Library
P.O. Box 90.002
4800 PA Breda

NORWAY
Norwegian Defence Research Establishment, Attn: Biblioteket
P.O. Box 25
NO-2007 Kjeller

POLAND
Centralna Biblioteka Wojskowa
ul. Ostrobramska 109
04-041 Warszawa

PORTUGAL
Estado Maior da Força Aérea
SDFA – Centro de Documentação
Alfragide
P-2720 Amadora

ROMANIA
Romanian National Distribution Centre
Armaments Department
9-11, Drumul Taberei Street
Sector 6
061353 Bucharest

SLOVAKIA
Akadémia ozbrojených síl gen M.R. Štefánika, Distribučné a informačné stredisko STO
Demänová 393
031 01 Liptovský Mikuláš 1

SLOVENIA
Ministry of Defence
Central Registry for EU & NATO
Vojkova 55
1000 Ljubljana

SPAIN
Área de Cooperación Internacional en I+D
SDGPLATIN (DGAM)
C/ Arturo Soria 289
28033 Madrid

TURKEY
Milli Savunma Bakanlığı (MSB)
ARGE ve Teknoloji Dairesi Başkanlığı
06650 Bakanliklar – Ankara

UNITED KINGDOM
Dstl Records Centre
Rm G02, ISAT F, Building 5
Dstl Porton Down, Salisbury SP4 0JQ

UNITED STATES
Defense Technical Information Center
8725 John J. Kingman Road
Fort Belvoir, VA 22060-6218

SALES AGENCIES

The British Library Document Supply Centre
Boston Spa, Wetherby
West Yorkshire LS23 7BQ
UNITED KINGDOM

Canada Institute for Scientific and Technical Information (CISTI)
National Research Council Acquisitions
Montreal Road, Building M-55
Ottawa, Ontario K1A 0S2
CANADA

Requests for STO, RTO or AGARD documents should include the word 'STO', 'RTO' or 'AGARD', as appropriate, followed by the serial number (for example AGARD-AG-315). Collateral information such as title and publication date is desirable. Full bibliographical references and abstracts of STO, RTO and AGARD publications are given in "NTIS Publications Database" (http://www.ntis.gov).

ISBN 978-92-837-2356-1